1-1-2020

# Nonstandard Interactions And B-Hadron Decays

Saeed Kamali

# NONSTANDARD INTERACTIONS AND $b$-HADRON DECAYS

A Dissertation
presented in partial fulfillment of requirements
for the degree of Doctor of Philosophy
in the Department of Physics and Astronomy
The University of Mississippi

by

SAEED KAMALI

MAY 2020

ABSTRACT

In this work, we study the decays of heavy hadrons that contain the $b$ quark. We study the decay modes $B \to D^{(*)}\tau^-\bar{\nu}_\tau$, $\Lambda_b \to \Lambda_c\tau^-\bar{\nu}_\tau$ and $B \to X_c\tau^-\bar{\nu}_\tau$ and analyze the effects of beyond the standard model new physics in various observables of these decay modes. This is important since the measurements of the decay $B \to D^{(*)}\tau^-\bar{\nu}_\tau$ deviate from the standard model predictions and this points to physics beyond the standard model. We also study CP violation in the angular distribution of the decay $B \to D^*(\to D\pi)\mu^-\bar{\nu}_\mu$ and use it as a way to differentiate various new physics scenarios. Finally we focus on the muon $(g-2)$ anomaly and study a solution to this anomaly that relates it to all other $B$-meson anomalies. This leads to a lot of interesting signals that can be probed in the current and future experiments.

DEDICATION

To my lovely parents, my wonderful sisters, Gilnaz, Fariba,

Fahimeh, and my awesome brothers, Farzad and Masoud.

ACKNOWLEDGEMENTS

I would like to thank every one who helped me during my journey of my graduate studies. First, I would like to thank my advisor Alakabha Datta who has always been supportive and helpful. His constant encouragement and guidance was very helpful during all ups and downs of my studies and research works. I would like to thank my committee members Luca Bombelli, Lucien Cremaldi, Richard Gordon and Donald Summers for their insight and helpful comments.

I would like to specially thank Luca Bombelli and Emanuele Berti who have always been supportive of me during all steps of my studies. I want to thank the Department of Physics and Astronomy at the University of Mississippi for supporting me and also the Graduate School and the College of Liberal Arts at the University of Mississippi for partially supporting my research. I also want to thank all the faculty and nonfaculty members of the physics department at the University of Mississippi who made my life and work here, joyful.

I had the opportunity to work with great collaborators. I would like to thank Jonathan Feng for his collaboration and support. I would also like to thank David London, Bhubanjyoti Bhattacharya, Stefan Meinel and Ahmed Rashed for their collaborations.

This work was in part supported by the National Science Foundation under Grant No. PHY-1414345. I would like to acknowledge the hospitality of the Department of Physics and Astronomy at the University of California, Irvine; and the Lawrence Technological University where part of the work was done.

TABLE OF CONTENTS

LIST OF FIGURES

3.10 The effects of the $U_1$ leptoquark model on the differential decay rates $(1/\Gamma_0)d\Gamma/dq^2$, $(1/\Gamma_0)d\Gamma/dE_\tau$; the ratio of differential rates $B$; and the forward-backward asymmetry $(A_{FB})$ of $B \to X_c\tau^-\bar{\nu}_\tau$. Each plot shows the observable in the Standard Model and for two allowed values of the NP couplings. The red curves correspond to $h_{1L}^{23}h_{1R}^{33*} = -0.127 - 0.395i$, $h_{1L}^{22}h_{1R}^{33*} = 0.077 + 0.043i$, $h_{1L}^{21}h_{1R}^{33*} = -0.040 + 0.034i$, $h_{1L}^{23}h_{1L}^{33*} = -1.523 - 0.394i$, $h_{1L}^{22}h_{1L}^{33*} = 0.247 + 0.473i$, $h_{1L}^{21}h_{1L}^{33*} = 0.226 + 1.261i$, and the blue curves correspond to $h_{1L}^{23}h_{1R}^{33*} = 0.017 - 0.028i$, $h_{1L}^{22}h_{1R}^{33*} = -0.115 + 0.017i$, $h_{1L}^{21}h_{1R}^{33*} = -0.238 - 0.041i$, $h_{1L}^{23}h_{1L}^{33*} = -1.22 + 0.301i$, $h_{1L}^{22}h_{1L}^{33*} = 0.730 - 0.039i$, $h_{1L}^{21}h_{1L}^{33*} = -1.327 + 0.357i$, respectively, while the green curves correspond to the Standard Model. . . . . 60

3.11 The effects of the $S_3$ leptoquark model on the differential decay rates $(1/\Gamma_0)d\Gamma/dq^2$, $(1/\Gamma_0)d\Gamma/dE_\tau$; the ratio of differential rates $B$; and the forward-backward asymmetry $(A_{FB})$ of $B \to X_c\tau^-\bar{\nu}_\tau$. Each plot shows the observable in the Standard Model and for two allowed values of the NP couplings. The red curves correspond to $g_{3L}^{33}g_{3L}^{23*} = -0.062 - 0.028i$, $g_{3L}^{32}g_{3L}^{23*} = 0.031 - 0.005i$, $g_{3L}^{31}g_{3L}^{23*} = 0.013 - 0.003i$, and the blue curves correspond to $g_{3L}^{33}g_{3L}^{23*} = -0.062 - 0.028i$, $g_{3L}^{32}g_{3L}^{23*} = 0.003 - 0.031i$, $g_{3L}^{31}g_{3L}^{23*} = 0.052 - 0.054i$, respectively, while the green curves correspond to the Standard Model. . . . . 61

LIST OF TABLES

# CHAPTER 1

# INTRODUCTION

Laws of nature are governed by four fundamental forces: gravity, electromagnetic, weak and strong. We have been able to quantize the electromagnetic, weak and strong forces and give a consistent description of their behavior at the quantum level. This is formulated in the Standard Model (SM) of particle physics where the three forces are described by the $SU(3) \times SU(2) \times U(1)$ gauge group. The elementary particles of the SM are fermions (spin $1/2$ particles), gauge bosons (spin 1 particles) and the Higgs boson (a fundamental spin zero particle). In the SM, the gauge bosons are described as force carriers that make the interactions between various fermions, possible. The Higgs boson is the only spin zero elementary particle in the SM and is responsible for the non-zero mass of other elementary particles.

Despite its many great successes, there are several reasons to believe that SM is incomplete and we need to add more structure to it. Here we name some of the main problems that we still do not have any answer to. One of the most important and fundamental ones is that the SM does not describe gravity. There are still intense efforts to build a quantum theory of gravity with many fundamentally different approaches. This includes loop quantum gravity and spin foam formalism, causal sets and string theory. Another important reason for looking for beyond the SM physics is the huge gap between the weak scale and the Planck scale. This problem, which is known as the hierarchy problem, is explicitly seen in quantum corrections to the Higgs mass which are quadratically divergent. Generically, it is expected that new physics (NP) will show up at the TeV scale to remedy this behavior and in some models, such as supersymmetry, there are extra, beyond the SM particles that compensate for the large corrections to the Higgs mass in the Standard Model. Any new physics that might be present at this scale, can affect the phenomena at lower energy

processes. This can most easily be seen in the framework of an effective field theory where the effect of particles at a particular scale can be seen at a much lower scale through operators of higher dimensions (dimension $\geq 4$). This is one of the main motivations to study low energy processes and make precision measurements. By comparing these measurements with SM predictions, we can see if any significant deviation shows up and if this is the case, we may have indirect evidence for physics beyond the SM.

Recently, there have been some anomalies in the measurements of the $B$-meson decays and this has caused a lot of interest and activity in the particles physics community. These anomalies are related to the semileptonic decays of the $B$-meson, $B \to K^{(*)}\ell^+\ell^-$ and $B \to D^{(*)}\ell\nu_\ell$. The decay $B \to K^{(*)}\ell^+\ell^-$ is an example of a Flavor Changing Neutral Current (FCNC) transition where the flavor of the quark changes but its charge remains the same. The underlying quark level transition in this decay mode is $b \to s$. In the SM, FCNC transitions can not happen at tree level, but they can happen via higher order loops such as penguin or box diagrams, so they are highly suppressed. Consequently, it is expected that we see the effects of beyond the SM physics in FCNC processes where particles in higher mass scales can compete with the SM contributions. This fact makes the anomaly in $B \to K^{(*)}\ell^+\ell^-$ quite interesting. On the other hand, the decay $B \to D^{(*)}\ell\nu_\ell$, is a charged current transition that can happen in the SM at tree level. The quark level transition of this decay mode is $b \to c$ where the bottom quark decays to a charm quark and a $W$ boson. Any new physics (NP) that is supposed to contribute to this decay mode should have a large contribution in order to be able to compete with the tree level contribution from the SM. In this work, our main focus is on the anomalies in these $B$ decays. Before we present the details of our work, in the following, we describe briefly the outline of this dissertation.

Regarding the $B \to D^{(*)}$ transitions, the measured observable that we are interested in, is $R(D^{(*)})$ which is defined as

$$R(D^{(*)}) = \frac{\mathcal{B}(B \to D^{(*)}\tau\nu)}{\mathcal{B}(B \to D^{(*)}\ell\nu)}\,, \tag{1.1}$$

where $\ell = \mu, e$.

These ratios have several advantages over the absolute branching fractions. They are relatively less sensitive to form factor variations since the uncertainties in the form factors cancel largely in the ratio. Besides, most of the experimental uncertainties as well as the dependence on the value of $|V_{cb}|$ cancel in the ratio. On the other hand, we may view these observables as lepton flavor universality observables since in the numerator we have the much heavier lepton, the $\tau$, and in the denominator we have the light leptons, $e$ and $\mu$. We can view the probes of these observables as tests of lepton flavor universality in the SM. In the SM, the gauge interactions are universal for all lepton generations. This means that the gauge bosons couple to all leptons with the same strength irrespective of their generations. So, the experimental deviations of the above observables from the SM predictions are signs of lepton flavor nonuniversality which requires NP beyond the SM.

These obsevables have been measured by BaBar [2, 3], Belle [4, 5, 6] and LHCb [7, 8] collaborations. By averaging these measurements, the Heavy Flavour Averaging Group (HFLAV) finds [9],

$$R(D)^{\rm exp} = 0.407 \pm 0.039 \pm 0.024 \tag{1.2}$$

$$R(D^*)^{\rm exp} = 0.306 \pm 0.013 \pm 0.007\,, \tag{1.3}$$

where the first uncertainty is statistical and the second is systematic. The SM predictions are [10, 11, 12, 13],

$$R(D)^{\rm SM} = \ 0.299 \pm 0.003 \tag{1.4}$$

$$R(D^*)^{\rm SM} = \ 0.258 \pm 0.005. \tag{1.5}$$

Combining the two measurements with their correlations, the deviation from SM predictions becomes $\sim 4\,\sigma$ [9]. Recently, a new measurement by the Belle collaboration [14], using semileptonic tagging, has been reported,

$$R(D)^{\text{Belle}} = 0.307 \pm 0.037 \pm 0.016 \tag{1.6}$$

$$R(D^*)^{\text{Belle}} = 0.283 \pm 0.018 \pm 0.014\ . \tag{1.7}$$

Including this measurement, HFLAV finds

$$R(D)^{\text{exp,new}} = 0.340 \pm 0.027 \pm 0.013 \tag{1.8}$$

$$R(D^*)^{\text{exp,new}} = 0.295 \pm 0.011 \pm 0.008\ , \tag{1.9}$$

which reduces the deviation from the SM predictions to $\sim 3.1\sigma$ [9] [1] . This discrepancy is very interesting and it is worth a detailed study.

In the next three chapters of this dissertation, we probe the $R(D^{(*)})$ anomalies in other decay modes that are related to the $B \to D^{(*)}$ via the same quark level transition. These decay modes are the semileptonic decay, $\Lambda_b \to \Lambda_c \tau \nu_\tau$ and the inclusive semileptonic decay $B \to X_c \tau \nu_\tau$. In the numerical calculations, we use the ratio of the experimental results to their corresponding SM predictions,

$$R(D)^{\text{Ratio}} = \frac{R(D)^{\text{exp}}}{R(D)^{\text{SM}}}\ , \tag{1.10}$$

$$R(D^*)^{\text{Ratio}} = \frac{R(D^*)^{\text{exp}}}{R(D^*)^{\text{SM}}}\ . \tag{1.11}$$

Since we are interested in Lepton Flavor Universality Violation (LFUV) and in view of the fact that the mass of the $\tau$ lepton is much larger than the electron or muon, we usually consider NP to be present in the $b \to c\tau\nu$ decay only. Here we follow the same approach and consider NP only in the $\tau$ mode.

[1] There has been new measurements of $R(D^{(*)})$ at the time of writing the dissertation. Since our results and phenomenology do not change by including these new measurements, we will use the published results in presenting our works.

Next, we present a study of the charge-parity (CP) violation in the decay $B \to D^* \mu\nu$ and show its usefulness in distinguishing different NP models that are capable of explaining the $R(D^{(*)})$ anomalies. For this purpose, we calculate the full angular distribution of the decay $B \to D^*(\to D\pi)\mu\nu$ and extract the CP violating triple product terms. Since these CP violating terms are absent in the SM, any measurement of these terms, will be a clear sign of physics beyond the SM. We will elaborate more on this in chapter 5.

Finally we move on to a study of the longstanding anomaly, the muon $(g-2)$. We will discuss a solution to this anomaly and its possible relation to the $B$-meson anomalies. These $B$-meson anomalies include $R(D^{(*)})$ (as we discussed above) and the anomalies in the FCNC decay $B \to K^{(*)}\ell^+\ell^-$. For this decay mode, we can define a similar observable,

$$R(K^{(*)}) = \frac{\mathcal{B}(B \to K^{(*)}\mu^+\mu^-)}{\mathcal{B}(B \to K^{(*)}e^+e^-)}\,, \tag{1.12}$$

where like in the $R(D^{(*)})$ case, we can view $R(K^{(*)})$ as a lepton flavor universality observable. Generally, it is very desirable to have a minimal, simplified model, in which all anomalies are resolved. In chapter 6, we present a model which addresses the muon $(g-2)$ and all $B$ anomalies, simultaneously. As we will see, this model has very interesting signals that can be probed in current and future experiments.

In summary, the dissertation is organized as follows. In chapter 2, we present our study on the semileptonic $\Lambda_b \to \Lambda_c$ transition. In chapters 3 and 4, we present our study on the inclusive $B$ decay and in chapter 5, we present our study of CP violation in the angular distribution of the decay $B \to D^*(\to D\pi)\mu\nu_\mu$. In chapter 6, we present our study of the muon $(g-2)$ anomaly and its relation to all other $B$ anomalies. Finally, in chapter 7, we present our conclusion.

# CHAPTER 2

# NEW PHYSICS IN $\Lambda_b \to \Lambda_c \tau \bar{\nu}_\tau$ USING LATTICE QCD CALCULATIONS

## 2.1 Introduction

In this chapter we present our study of the decay mode $\Lambda_b \to \Lambda_c \tau \bar{\nu}$ as was done in Ref. [15]. This decay mode is useful in addressing the $R(D^{(*)})$ anomalies since it has the same quark level transition as in $R(D^{(*)})$, which is $b \to c$. In the SM, this transition can happen at tree level where the bottom quark decays to a charm quark and a $W$ boson which subsequently decays to a charged lepton and a neutrino as shown in Fig. 2.1. Generically, we can have new physics (NP) contributions to this decay: a new particle that can effectively play the role of the $W$ boson in the SM as shown in Fig. 2.1. At quark level, the exact same transition happens in the $B \to D^{(*)} \tau \nu$ decay mode and the only difference with the baryonic mode is the hadronization effects. Therefore, any new physics that is required to explain the $R(D^{(*)})$ anomalies, can affect the $\Lambda_b \to \Lambda_c \tau \nu_\tau$ decay as well. So, the $\Lambda_b \to \Lambda_c$ transition is very useful in exploring $R(D^{(*)})$ anomalies and as we will see later in this chapter, it can help differentiate various NP models.

In this chapter we study the effects of NP operators with different Lorentz structures on the semileptonic decay $\Lambda_b \to \Lambda_c \tau \bar{\nu}$. We consider both model-independent NP and specific classes of models that are proposed to address the $R(D^{(*)})$ anomalies. For the model-independent analysis, we consider the most general dimension-6 NP operators that contribute to this decay mode. Then, we constrain the parameters of each operator by $R(D^{(*)})$ measurements and use the allowed parameter space to make predictions for the semileptonic $\Lambda_b \to \Lambda_c$ decay mode. The decay $\Lambda_b \to \Lambda_c \tau \bar{\nu}$ in the

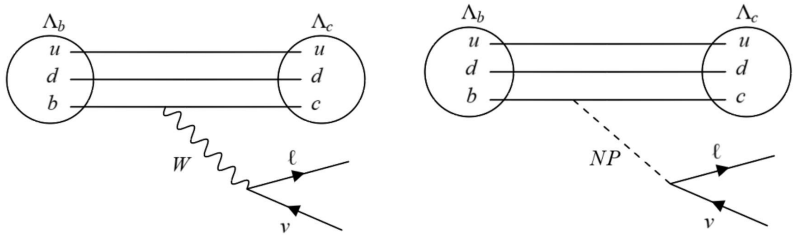


**Figure 2.1:** The semileptonic decay $\Lambda_b \to \Lambda_c \ell \nu$

SM and with NP, has been discussed in various works [16, 17, 18, 19, 20, 21, 22, 23, 24, 25, 26, 27]. Similar to the definition for $R(D^{(*)})$, we calculate the lepton flavor universality observable in our analysis, $R(\Lambda_c) = \frac{BR[\Lambda_b \to \Lambda_c \tau \bar{\nu}]}{BR[\Lambda_b \to \Lambda_c \ell \bar{\nu}]}$ where $\ell = e, \mu$. We also present the results for the differential and angular observables. We calculate the $q^2$ distribution $d\Gamma/dq^2$, the ratio of differential distributions,

$$B_{\Lambda_c}(q^2) = \frac{d\Gamma[\Lambda_b \to \Lambda_c \tau \bar{\nu}]/dq^2}{d\Gamma[\Lambda_b \to \Lambda_c \ell \bar{\nu}]/dq^2}, \tag{2.1}$$

and the forward-backward asymmetry defined as

$$A_{FB}(q^2) = \frac{\int_0^1 (d^2\Gamma/dq^2 d\cos\theta_\tau)\, d\cos\theta_\tau - \int_{-1}^0 (d^2\Gamma/dq^2 d\cos\theta_\tau)\, d\cos\theta_\tau}{d\Gamma/dq^2}. \tag{2.2}$$

Here $q^2$ is the momentum transfer $q^2 = p_{\Lambda_b} - p_{\Lambda_c}$, $\ell = \mu, e$ and $\theta_\tau$ is the angle between the momenta of the $\tau$ lepton and $\Lambda_c$ baryon in the dilepton rest frame, as shown in Fig. 2.2.

For the numerical calculations, we use the phenomenological SM predictions for $R(D)$ [28] and $R(D^*)$ [29],

$$\begin{aligned} R(D)^{\rm SM} &= 0.305 \pm 0.012\,, \\ R(D^*)^{\rm SM} &= 0.252 \pm 0.003\,, \end{aligned} \tag{2.3}$$

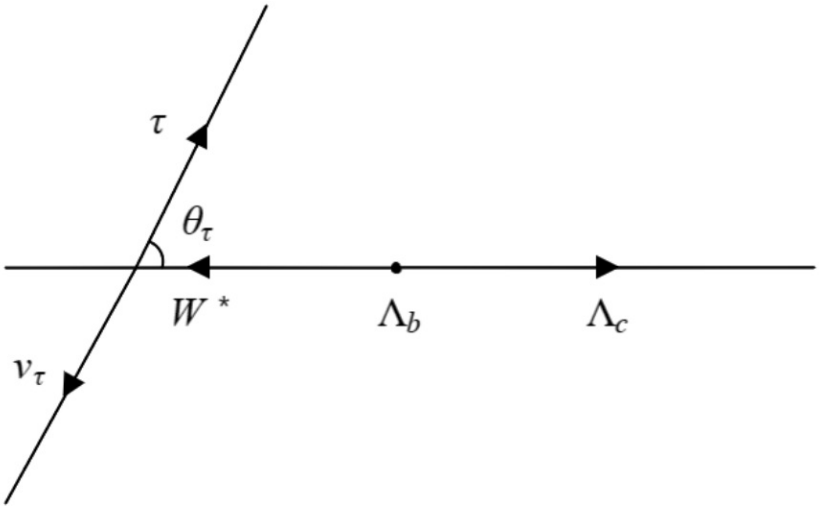


**Figure 2.2:** Definition of the angle $\theta_\tau$ in the decay $\Lambda_b \to \Lambda_c \tau \nu_\tau$

which are based on form factors extracted from the experimental data for the $B \to D^{(*)} \ell \bar{\nu}_\ell$ decay distributions using heavy-quark effective theory.

The averages of $R(D)$ and $R(D^*)$ measurements evaluated by the Heavy-Flavor Averaging Group, are

$$\begin{aligned} R(D)^{\text{exp}} &= 0.397 \pm 0.040 \pm 0.028, \\ R(D^*)^{\text{exp}} &= 0.316 \pm 0.016 \pm 0.010, \end{aligned} \tag{2.4}$$

where the first uncertainty is statistical and the second is systematic. $R(D)$ and $R(D^*)$ exceed the SM predictions by $3.3\,\sigma$ and $1.9\,\sigma$, respectively and the combined analysis of $R(D)$ and $R(D^*)$, taking into account measurement correlations, finds that the deviation from the SM prediction is $\approx 4\,\sigma$ [30]. We also construct the ratios of the experimental results (2.4) to the phenomenological

SM predictions (2.3):

$$R_D^{\text{Ratio}} = \frac{R(D)^{\text{exp}}}{R(D)^{\text{SM}}} = 1.30 \pm 0.17, \tag{2.5}$$

$$R_{D^*}^{\text{Ratio}} = \frac{R(D^*)^{\text{exp}}}{R(D^*)^{\text{SM}}} = 1.25 \pm 0.08\ . \tag{2.6}$$

We use these ratios to put constraints on the NP parameters and find their allowed parameter space.

This chapter is organized in the following manner: In Sec. 2.2, we introduce the effective Lagrangian to parameterize the NP operators and give the expressions for the decay distribution in terms of helicity amplitudes. The model-independent phenomenological analysis of individual new-physics couplings is discussed in Sec. 2.3, while explicit models are considered in Sec. 2.4. We conclude in Sec. 2.5.

## 2.2 Formalism

### 2.2.1 Effective Hamiltonian

In the presence of NP, the effective Hamiltonian for the quark-level transition $b \to c\tau^-\bar{\nu}_\tau$ can be written in the form [31, 32]

$$\begin{aligned}\mathcal{H}_{eff} \;=\; & \frac{G_F V_{cb}}{\sqrt{2}} \Big\{ \Big[ \bar{c}\gamma_\mu(1-\gamma_5)b + g_L \bar{c}\gamma_\mu(1-\gamma_5)b + g_R \bar{c}\gamma_\mu(1+\gamma_5)b \Big] \bar{\tau}\gamma^\mu(1-\gamma_5)\nu_\tau \\ & + \Big[ g_S \bar{c}b + g_P \bar{c}\gamma_5 b \Big] \bar{\tau}(1-\gamma_5)\nu_\tau + \Big[ g_T \bar{c}\sigma^{\mu\nu}(1-\gamma_5)b \Big] \bar{\tau}\sigma_{\mu\nu}(1-\gamma_5)\nu_\tau + h.c \Big\}\ , \end{aligned} \tag{2.7}$$

where $G_F$ is the Fermi constant, $V_{cb}$ is the Cabibbo-Kobayashi-Maskawa (CKM) matrix element, and we use $\sigma_{\mu\nu} = i[\gamma_\mu, \gamma_\nu]/2$. The SM effective Hamiltonian corresponds to $g_L = g_R = g_S = g_P = g_T = 0$. In Eq. (2.7), we have assumed the neutrinos to be always left chiral. In general, with NP, the neutrino associated with the $\tau$ lepton does not have to carry the same flavor. In the model-independent analysis of individual couplings (Sec. 2.3) we will not consider this possibility. But, in the leptoquark models, we consider all neutrino flavors that may couple to the $\tau$ lepton.

### 2.2.2 Decay process

The process under consideration is $\Lambda_b(p_{\Lambda_b}) \to \Lambda_c(p_{\Lambda_c})+\tau^-(p_\tau)+\bar{\nu}_\tau(p_{\bar{\nu}_\tau})$. We calculate the decay rate using the helicity method [33] where one builds the helicity amplitudes by contracting the hadronic and leptonic currents with the polarization of the intermediate particles. The differential decay rate for this process can be represented as

$$\frac{d\Gamma}{dq^2 d\cos\theta_\tau} = \frac{G_F^2|V_{cb}|^2}{2048\pi^3}\left(1-\frac{m_\tau^2}{q^2}\right)\frac{\sqrt{Q_+Q_-}}{m_{\Lambda_b}^3}\sum_{\lambda_{\Lambda_c}}\sum_{\lambda_\tau}|\mathcal{M}^{\lambda_\tau}_{\lambda_{\Lambda_c}}|^2, \tag{2.8}$$

where

$$q = p_{\Lambda_b} - p_{\Lambda_c}, \tag{2.9}$$

$$Q_\pm = (m_{\Lambda_b} \pm m_{\Lambda_c})^2 - q^2\,, \tag{2.10}$$

and the helicity amplitude $\mathcal{M}^{\lambda_\tau}_{\lambda_{\Lambda_c}}$ is written as

$$\mathcal{M}^{\lambda_\tau}_{\lambda_{\Lambda_c}} = H^{SP}_{\lambda_{\Lambda_c},\lambda_\tau=0} + \sum_\lambda \eta_\lambda H^{VA}_{\lambda_{\Lambda_c},\lambda} L^{\lambda_\tau}_\lambda + \sum_{\lambda,\lambda'}\eta_\lambda\eta_{\lambda'} H^{(T)\lambda_{\Lambda_b}}_{\lambda_{\Lambda_c},\lambda,\lambda'} L^{\lambda_\tau}_{\lambda,\lambda'}. \tag{2.11}$$

Here, $(\lambda, \lambda')$ indicate the helicity of the virtual vector boson (see Appendix A), $\lambda_{\Lambda_c}$ and $\lambda_\tau$ are the helicities of the $\Lambda_c$ baryon and $\tau$ lepton, respectively, and $\eta_\lambda = 1$ for $\lambda = t$ and $\eta_\lambda = -1$ for $\lambda = 0, \pm 1$.

The scalar-type, vector/axial-vector-type, and tensor-type hadronic helicity amplitudes are defined as

$$\begin{aligned} H^{SP}_{\lambda_{\Lambda_c},\lambda=0} &= H^{S}_{\lambda_{\Lambda_c},\lambda=0} + H^{P}_{\lambda_{\Lambda_c},\lambda=0}, \\ H^{S}_{\lambda_{\Lambda_c},\lambda=0} &= g_S\,\langle\Lambda_c|\,\bar{c}b\,|\Lambda_b\rangle\,, \\ H^{P}_{\lambda_{\Lambda_c},\lambda=0} &= g_P\,\langle\Lambda_c|\,\bar{c}\gamma_5 b\,|\Lambda_b\rangle\,, \end{aligned} \tag{2.12}$$

$$
\begin{aligned}
H^{VA}_{\lambda_{\Lambda_c},\lambda} &= H^{V}_{\lambda_{\Lambda_c},\lambda} - H^{A}_{\lambda_{\Lambda_c},\lambda}, \\
H^{V}_{\lambda_{\Lambda_c},\lambda} &= (1 + g_L + g_R)\, \epsilon^{*\mu}(\lambda)\, \langle \Lambda_c |\, \bar{c}\gamma_\mu b\, | \Lambda_b \rangle\,, \\
H^{A}_{\lambda_{\Lambda_c},\lambda} &= (1 + g_L - g_R)\, \epsilon^{*\mu}(\lambda)\, \langle \Lambda_c |\, \bar{c}\gamma_\mu\gamma_5 b\, | \Lambda_b \rangle\,,
\end{aligned} \tag{2.13}
$$

and

$$
\begin{aligned}
H^{(T)\lambda_{\Lambda_b}}_{\lambda_{\Lambda_c},\lambda,\lambda'} &= H^{(T1)\lambda_{\Lambda_b}}_{\lambda_{\Lambda_c},\lambda,\lambda'} - H^{(T2)\lambda_{\Lambda_b}}_{\lambda_{\Lambda_c},\lambda,\lambda'}, \\
H^{(T1)\lambda_{\Lambda_b}}_{\lambda_{\Lambda_c},\lambda,\lambda'} &= g_T\, \epsilon^{*\mu}(\lambda)\epsilon^{*\nu}(\lambda')\, \langle \Lambda_c |\, \bar{c} i\sigma_{\mu\nu} b\, | \Lambda_b \rangle\,, \\
H^{(T2)\lambda_{\Lambda_b}}_{\lambda_{\Lambda_c},\lambda,\lambda'} &= g_T\, \epsilon^{*\mu}(\lambda)\epsilon^{*\nu}(\lambda')\, \langle \Lambda_c |\, \bar{c} i\sigma_{\mu\nu}\gamma_5 b\, | \Lambda_b \rangle\,.
\end{aligned} \tag{2.14}
$$

The leptonic amplitudes are defined as

$$
\begin{aligned}
L^{\lambda_\tau} &= \langle \tau \bar{\nu}_\tau |\, \bar{\tau}(1 - \gamma_5)\nu_\tau\, | 0 \rangle\,, \\
L^{\lambda_\tau}_{\lambda} &= \epsilon^{\mu}(\lambda)\, \langle \tau \bar{\nu}_\tau |\, \bar{\tau}\gamma_\mu(1 - \gamma_5)\nu_\tau\, | 0 \rangle\,, \\
L^{\lambda_\tau}_{\lambda,\lambda'} &= -i\epsilon^{\mu}(\lambda)\epsilon^{\nu}(\lambda')\, \langle \tau \bar{\nu}_\tau |\, \bar{\tau}\sigma_{\mu\nu}(1 - \gamma_5)\nu_\tau\, | 0 \rangle\,.
\end{aligned} \tag{2.15}
$$

Above, $\epsilon^\mu$ are the polarization vectors of the virtual vector boson (see Appendix A). The explicit expressions for the hadronic and leptonic helicity amplitudes are presented in the following.

#### 2.2.2.1 Hadronic helicity amplitudes

Here, we use the helicity-based definition of the $\Lambda_b \to \Lambda_c$ form factors, which was introduced in [34]. The matrix elements of the vector and axial vector currents can be written in terms

of six helicity form factors $F_+$, $F_\perp$, $F_0$, $G_+$, $G_\perp$, and $G_0$ as follows:

$$\begin{aligned}
\langle \Lambda_c | \, \bar{c}\gamma^\mu b \, | \Lambda_b \rangle &= \bar{u}_{\Lambda_c} \Big[ F_0(q^2)(m_{\Lambda_b} - m_{\Lambda_c}) \frac{q^\mu}{q^2} \\
&\quad + F_+(q^2) \frac{m_{\Lambda_b} + m_{\Lambda_c}}{Q_+} (p^\mu_{\Lambda_b} + p^\mu_{\Lambda_c} - (m^2_{\Lambda_b} - m^2_{\Lambda_c}) \frac{q^\mu}{q^2}) \\
&\quad + F_\perp(q^2)(\gamma^\mu - \frac{2m_{\Lambda_c}}{Q_+} p^\mu_{\Lambda_b} - \frac{2m_{\Lambda_b}}{Q_+} p^\mu_{\Lambda_c}) \Big] u_{\Lambda_b}, \qquad (2.16) \\
\langle \Lambda_c | \, \bar{c}\gamma^\mu\gamma_5 b \, | \Lambda_b \rangle &= -\bar{u}_{\Lambda_c}\gamma_5 \Big[ G_0(q^2)(m_{\Lambda_b} + m_{\Lambda_c}) \frac{q^\mu}{q^2} \\
&\quad + G_+(q^2) \frac{m_{\Lambda_b} - m_{\Lambda_c}}{Q_-} (p^\mu_{\Lambda_b} + p^\mu_{\Lambda_c} - (m^2_{\Lambda_b} - m^2_{\Lambda_c}) \frac{q^\mu}{q^2}) \\
&\quad + G_\perp(q^2)(\gamma^\mu + \frac{2m_{\Lambda_c}}{Q_-} p^\mu_{\Lambda_b} - \frac{2m_{\Lambda_b}}{Q_-} p^\mu_{\Lambda_c}) \Big] u_{\Lambda_b}. \qquad (2.17)
\end{aligned}$$

The matrix elements of the scalar and pseudoscalar currents can be obtained from the vector and axial vector matrix elements using the equations of motion:

$$\begin{aligned}
\langle \Lambda_c | \, \bar{c} b \, | \Lambda_b \rangle &= \frac{q_\mu}{m_b - m_c} \langle \Lambda_c | \, \bar{c}\gamma^\mu b \, | \Lambda_b \rangle \\
&= F_0(q^2) \frac{m_{\Lambda_b} - m_{\Lambda_c}}{m_b - m_c} \bar{u}_{\Lambda_c} u_{\Lambda_b}, \qquad (2.18) \\
\langle \Lambda_c | \, \bar{c}\gamma_5 b \, | \Lambda_b \rangle &= \frac{q_\mu}{m_b + m_c} \langle \Lambda_c | \, \bar{c}\gamma^\mu\gamma_5 b \, | \Lambda_b \rangle \\
&= G_0(q^2) \frac{m_{\Lambda_b} + m_{\Lambda_c}}{m_b + m_c} \bar{u}_{\Lambda_c}\gamma_5 u_{\Lambda_b}. \qquad (2.19)
\end{aligned}$$

In our numerical analysis, we use $m_b = 4.18(3)$ GeV, $m_c = 1.27(2)$ GeV [35]. The matrix elements of the tensor currents can be written in terms of four form factors $h_+$, $h_\perp$, $\widetilde{h}_+$, $\widetilde{h}_\perp$ [15],

$$\begin{aligned}
&\langle\Lambda_c|\,\bar{c}i\sigma^{\mu\nu}b\,|\Lambda_b\rangle = \bar{u}_{\Lambda_c}\Big[2h_+(q^2)\frac{p^\mu_{\Lambda_b}p^\nu_{\Lambda_c} - p^\nu_{\Lambda_b}p^\mu_{\Lambda_c}}{Q_+}\\
&+h_\perp(q^2)\Big(\frac{m_{\Lambda_b}+m_{\Lambda_c}}{q^2}(q^\mu\gamma^\nu - q^\nu\gamma^\mu) - 2(\frac{1}{q^2}+\frac{1}{Q_+})(p^\mu_{\Lambda_b}p^\nu_{\Lambda_c} - p^\nu_{\Lambda_b}p^\mu_{\Lambda_c})\Big)\\
&+\widetilde{h}_+(q^2)\Big(i\sigma^{\mu\nu} - \frac{2}{Q_-}(m_{\Lambda_b}(p^\mu_{\Lambda_c}\gamma^\nu - p^\nu_{\Lambda_c}\gamma^\mu)\\
&-m_{\Lambda_c}(p^\mu_{\Lambda_b}\gamma^\nu - p^\nu_{\Lambda_b}\gamma^\mu) + p^\mu_{\Lambda_b}p^\nu_{\Lambda_c} - p^\nu_{\Lambda_b}p^\mu_{\Lambda_c})\Big)\\
&+\widetilde{h}_\perp(q^2)\frac{m_{\Lambda_b}-m_{\Lambda_c}}{q^2Q_-}\Big((m^2_{\Lambda_b} - m^2_{\Lambda_c} - q^2)(\gamma^\mu p^\nu_{\Lambda_b} - \gamma^\nu p^\mu_{\Lambda_b})\\
&-(m^2_{\Lambda_b} - m^2_{\Lambda_c} + q^2)(\gamma^\mu p^\nu_{\Lambda_c} - \gamma^\nu p^\mu_{\Lambda_c}) + 2(m_{\Lambda_b} - m_{\Lambda_c})(p^\mu_{\Lambda_b}p^\nu_{\Lambda_c} - p^\nu_{\Lambda_b}p^\mu_{\Lambda_c})\Big)\Big]u_{\Lambda_b}.
\end{aligned} \tag{2.20}$$

The matrix elements of the current $\bar{c}i\sigma^{\mu\nu}\gamma_5 b$ can be obtained from the above equation by using the identity

$$\sigma^{\mu\nu}\gamma_5 = -\frac{i}{2}\epsilon^{\mu\nu\alpha\beta}\sigma_{\alpha\beta}. \tag{2.21}$$

In the following, only the non-vanishing helicity amplitudes are given. The scalar and pseudo-scalar helicity amplitudes associated with the new physics scalar and pseudo-scalar interactions are

$$H^{SP}_{1/2,0} = F_0 g_S\frac{\sqrt{Q_+}}{m_b - m_c}(m_{\Lambda_b} - m_{\Lambda_c}) - G_0 g_P\frac{\sqrt{Q_-}}{m_b + m_c}(m_{\Lambda_b} + m_{\Lambda_c}), \tag{2.22}$$

$$H^{SP}_{-1/2,0} = F_0 g_S\frac{\sqrt{Q_+}}{m_b - m_c}(m_{\Lambda_b} - m_{\Lambda_c}) + G_0 g_P\frac{\sqrt{Q_-}}{m_b + m_c}(m_{\Lambda_b} + m_{\Lambda_c}). \tag{2.23}$$

The parity-related amplitudes are

$$\begin{aligned} H^S_{\lambda_{\Lambda_c},\lambda_{NP}} &= H^S_{-\lambda_{\Lambda_c},-\lambda_{NP}}, \\ H^P_{\lambda_{\Lambda_c},\lambda_{NP}} &= -H^P_{-\lambda_{\Lambda_c},-\lambda_{NP}}. \end{aligned} \tag{2.24}$$

For the vector and axial-vector helicity amplitudes, we find

$$\begin{aligned} H^{VA}_{1/2,0} &= F_+(1+g_L+g_R)\frac{\sqrt{Q_-}}{\sqrt{q^2}}(m_{\Lambda_b}+m_{\Lambda_c}) \\ &\quad -G_+(1+g_L-g_R)\frac{\sqrt{Q_+}}{\sqrt{q^2}}(m_{\Lambda_b}-m_{\Lambda_c}), \end{aligned} \tag{2.25}$$

$$H^{VA}_{1/2,+1} = -F_\perp(1+g_L+g_R)\sqrt{2Q_-}+G_\perp(1+g_L-g_R)\sqrt{2Q_+}, \tag{2.26}$$

$$\begin{aligned} H^{VA}_{1/2,t} &= F_0(1+g_L+g_R)\frac{\sqrt{Q_+}}{\sqrt{q^2}}(m_{\Lambda_b}-m_{\Lambda_c}) \\ &\quad -G_0(1+g_L-g_R)\frac{\sqrt{Q_-}}{\sqrt{q^2}}(m_{\Lambda_b}+m_{\Lambda_c}), \end{aligned} \tag{2.27}$$

$$\begin{aligned} H^{VA}_{-1/2,0} &= F_+(1+g_L+g_R)\frac{\sqrt{Q_-}}{\sqrt{q^2}}(m_{\Lambda_b}+m_{\Lambda_c}) \\ &\quad +G_+(1+g_L-g_R)\frac{\sqrt{Q_+}}{\sqrt{q^2}}(m_{\Lambda_b}-m_{\Lambda_c}), \end{aligned} \tag{2.28}$$

$$H^{VA}_{-1/2,-1} = -F_\perp(1+g_L+g_R)\sqrt{2Q_-}-G_\perp(1+g_L-g_R)\sqrt{2Q_+}, \tag{2.29}$$

$$\begin{aligned} H^{VA}_{-1/2,t} &= F_0(1+g_L+g_R)\frac{\sqrt{Q_+}}{\sqrt{q^2}}(m_{\Lambda_b}-m_{\Lambda_c}) \\ &\quad +G_0(1+g_L-g_R)\frac{\sqrt{Q_-}}{\sqrt{q^2}}(m_{\Lambda_b}+m_{\Lambda_c}). \end{aligned} \tag{2.30}$$

We also have the relations

$$\begin{aligned} H^V_{\lambda_{\Lambda_c},\lambda_w} &= H^V_{-\lambda_{\Lambda_c},-\lambda_w}, \\ H^A_{\lambda_{\Lambda_c},\lambda_w} &= -H^A_{-\lambda_{\Lambda_c},-\lambda_w}. \end{aligned} \tag{2.31}$$

The tensor helicity amplitudes are

$$H^{(T)-1/2}_{-1/2,t,0} = -g_T\Big[-h_+\sqrt{Q_-}+\widetilde{h}_+\sqrt{Q_+}\Big], \tag{2.32}$$

$$H^{(T)+1/2}_{+1/2,t,0} = g_T\Big[h_+\sqrt{Q_-}+\widetilde{h}_+\sqrt{Q_+}\Big], \tag{2.33}$$

$$H^{(T)-1/2}_{+1/2,t,+1} = -g_T\frac{\sqrt{2}}{\sqrt{q^2}}\Big[h_\perp(m_{\Lambda_b}+m_{\Lambda_c})\sqrt{Q_-}+\widetilde{h}_\perp(m_{\Lambda_b}-m_{\Lambda_c})\sqrt{Q_+}\Big], \tag{2.34}$$

$$H^{(T)+1/2}_{-1/2,t,-1} = -g_T\frac{\sqrt{2}}{\sqrt{q^2}}\Big[h_\perp(m_{\Lambda_b}+m_{\Lambda_c})\sqrt{Q_-}-\widetilde{h}_\perp(m_{\Lambda_b}-m_{\Lambda_c})\sqrt{Q_+}\Big], \tag{2.35}$$

$$H^{(T)-1/2}_{+1/2,0,+1} = -g_T\frac{\sqrt{2}}{\sqrt{q^2}}\Big[h_\perp(m_{\Lambda_b}+m_{\Lambda_c})\sqrt{Q_-}+\widetilde{h}_\perp(m_{\Lambda_b}-m_{\Lambda_c})\sqrt{Q_+}\Big], \tag{2.36}$$

$$H^{(T)+1/2}_{-1/2,0,-1} = g_T\frac{\sqrt{2}}{\sqrt{q^2}}\Big[h_\perp(m_{\Lambda_b}+m_{\Lambda_c})\sqrt{Q_-}-\widetilde{h}_\perp(m_{\Lambda_b}-m_{\Lambda_c})\sqrt{Q_+}\Big], \tag{2.37}$$

$$H^{(T)+1/2}_{+1/2,+1,-1} = -g_T\Big[h_+\sqrt{Q_-}+\widetilde{h}_+\sqrt{Q_+}\Big], \tag{2.38}$$

$$H^{(T)-1/2}_{-1/2,+1,-1} = -g_T\Big[h_+\sqrt{Q_-}-\widetilde{h}_+\sqrt{Q_+}\Big]. \tag{2.39}$$

The other non-vanishing helicity amplitudes of tensor type are related to the above by

$$H^{(T)\lambda_{\Lambda_b}}_{\lambda_{\Lambda_c},\lambda,\lambda'} = -H^{(T)\lambda_{\Lambda_b}}_{\lambda_{\Lambda_c},\lambda',\lambda}. \tag{2.40}$$

#### 2.2.2.2 Leptonic helicity amplitudes

In the following, we define

$$v = \sqrt{1-\frac{m_\tau^2}{q^2}}. \tag{2.41}$$

The scalar and pseudoscalar leptonic helicity amplitudes are

$$L^{+1/2} = \quad 2\sqrt{q^2}v, \tag{2.42}$$

$$L^{-1/2} = \qquad 0, \tag{2.43}$$

the vector and axial-vector amplitudes are

$$L^{+1/2}_{\pm 1} = \pm\sqrt{2}m_\tau v \ \sin(\theta_\tau), \tag{2.44}$$

$$L^{+1/2}_{0} = -2m_\tau v \ \cos(\theta_\tau), \tag{2.45}$$

$$L^{+1/2}_{t} = 2m_\tau v, \tag{2.46}$$

$$L^{-1/2}_{\pm 1} = \sqrt{2q^2}v \ (1 \pm \cos(\theta_\tau)), \tag{2.47}$$

$$L^{-1/2}_{0} = 2\sqrt{q^2}v \ \sin(\theta_\tau), \tag{2.48}$$

$$L^{-1/2}_{t} = 0, \tag{2.49}$$

and the tensor amplitudes are

$$L^{+1/2}_{0,\pm 1} = -\sqrt{2q^2}v \ \sin(\theta_\tau), \tag{2.50}$$

$$L^{+1/2}_{\pm 1,t} = \mp\sqrt{2q^2}v \ \sin(\theta_\tau), \tag{2.51}$$

$$L^{+1/2}_{t,0} = L^{+1/2}_{+1,-1} = -2\sqrt{q^2}v \ \cos(\theta_\tau), \tag{2.52}$$

$$L^{-1/2}_{0,\pm 1} = \mp\sqrt{2}m_\tau v \ (1 \pm \cos(\theta_\tau)), \tag{2.53}$$

$$L^{-1/2}_{\pm 1,t} = -\sqrt{2}m_\tau v \ (1 \pm \cos(\theta_\tau)), \tag{2.54}$$

$$L^{-1/2}_{t,0} = L^{-1/2}_{+1,-1} = 2m_\tau v \ \sin(\theta_\tau). \tag{2.55}$$

Here—as in the hadronic case—for the leptonic tensor amplitudes, we have the relation

$$L^{\lambda_\tau}_{\lambda,\lambda'} = -L^{\lambda_\tau}_{\lambda',\lambda}. \tag{2.56}$$

The angle $\theta_\tau$ is defined as the angle between the momenta of the $\tau$ lepton and $\Lambda_c$ baryon in the dilepton rest frame as shown in Fig. 2.2.

### 2.2.3 Differential decay rate and forward-backward asymmetry

From the twofold decay distribution (2.8), we obtain the following expression for the differential decay rate by integrating over $\cos\theta_\tau$ [15]:

$$\begin{aligned}\frac{d\Gamma(\Lambda_b \to \Lambda_c \tau \bar{\nu}_\tau)}{dq^2} &= \frac{G_F^2 |V_{cb}|^2}{384\pi^3} \frac{q^2\sqrt{Q_+Q_-}}{m_{\Lambda_b}^3}\left(1-\frac{m_\tau^2}{q^2}\right)^2\Bigg[A_1^{VA} + \frac{m_\tau^2}{2q^2}A_2^{VA} + \frac{3}{2}A_3^{SP} \\ &\quad +2\left(1+\frac{2m_\tau^2}{q^2}\right)A_4^T + \frac{3m_\tau}{\sqrt{q^2}}A_5^{VA-SP} + \frac{6m_\tau}{\sqrt{q^2}}A_6^{VA-T}\Bigg], \end{aligned} \tag{2.57}$$

where

$$\begin{aligned}
A_1^{VA} &= |H_{1/2,1}^{VA}|^2 + |H_{1/2,0}^{VA}|^2 + |H_{-1/2,0}^{VA}|^2 + |H_{-1/2,-1}^{VA}|^2, \\
A_2^{VA} &= |H_{1/2,1}^{VA}|^2 + |H_{1/2,0}^{VA}|^2 + |H_{-1/2,0}^{VA}|^2 + |H_{-1/2,-1}^{VA}|^2 + 3|H_{1/2,t}^{VA}|^2 + 3|H_{-1/2,t}^{VA}|^2, \\
A_3^{SP} &= |H_{1/2,0}^{SP}|^2 + |H_{-1/2,0}^{SP}|^2, \\
A_4^T &= |H_{1/2,t,0}^{(T)1/2} + H_{1/2,-1,1}^{(T)1/2}|^2 + |H_{-1/2,t,-1}^{(T)1/2} + H_{-1/2,-1,0}^{(T)1/2}|^2 + |H_{1/2,0,1}^{(T)-1/2} + H_{1/2,t,1}^{(T)-1/2}|^2 \\
&\quad + |H_{-1/2,-1,1}^{(T)-1/2} + H_{-1/2,t,0}^{(T)-1/2}|^2, \\
A_5^{VA-SP} &= \mathrm{Re}(H_{1/2,0}^{SP*}\, H_{1/2,t}^{VA} + H_{-1/2,0}^{SP*}\, H_{-1/2,t}^{VA}), \\
A_6^{VA-T} &= \mathrm{Re}[H_{1/2,0}^{VA*}(H_{1/2,-1,1}^{(T)1/2} + H_{1/2,t,0}^{(T)1/2})] + \mathrm{Re}[H_{1/2,1}^{VA*}(H_{1/2,0,1}^{(T)-1/2} + H_{1/2,t,1}^{(T)-1/2})] + \\
&\quad \mathrm{Re}[H_{-1/2,0}^{VA*}(H_{-1/2,-1,1}^{(T)-1/2} + H_{-1/2,t,0}^{(T)-1/2})] + \mathrm{Re}[H_{-1/2,-1}^{VA*}(H_{-1/2,-1,0}^{(T)1/2} + H_{-1/2,t,-1}^{(T)1/2})].
\end{aligned} \tag{2.58}$$

Here, $A_1^{VA}$ and $A_2^{VA}$ are the (axial-)vector non-spin-flip and spin-flip terms respectively, $A_3^{SP}$ and $A_4^T$ are the pure (pseudo-)scalar and tensor terms respectively; and $A_5^{VA-SP}$ and $A_6^{VA-T}$ are interference

terms. The scalar-tensor interference term is proportional to $\cos\theta_\tau$ and vanishes after integration over $\cos\theta_\tau$. For the forward-backward asymmetry (2.2), we have [15]

$$A_{FB}(q^2) = \left(\frac{d\Gamma}{dq^2}\right)^{-1} \frac{G_F^2 V_{cb}^2}{512\pi^3} \frac{q^2\sqrt{Q_+Q_-}}{m_{\Lambda_b}^3}\left(1-\frac{m_\tau^2}{q^2}\right)^2\Bigg[B_1^{VA} + \frac{2m_\tau^2}{q^2}B_2^{VA} + \frac{4m_\tau^2}{q^2}B_3^T + \frac{2m_\tau}{\sqrt{q^2}}B_4^{VA-SP} + \frac{4m_\tau}{\sqrt{q^2}}B_5^{VA-T} + 4B_6^{SP-T}\Bigg], \tag{2.59}$$

where

$$\begin{aligned}
B_1^{VA} &= |H_{1/2,1}^{VA}|^2 - |H_{-1/2,-1}^{VA}|^2,\\
B_2^{VA} &= \mathrm{Re}[H_{1/2,t}^{VA*}H_{1/2,0}^{VA} + H_{-1/2,t}^{VA*}H_{-1/2,0}^{VA}],\\
B_3^T &= |H_{1/2,0,1}^{(T)-1/2} + H_{1/2,t,1}^{(T)-1/2}|^2 - |H_{-1/2,-1,0}^{(T)1/2} + H_{-1/2,t,-1}^{(T)1/2}|^2,\\
B_4^{VA-SP} &= \mathrm{Re}[H_{1/2,0}^{SP*}H_{1/2,0}^{VA} + H_{-1/2,0}^{SP*}H_{-1/2,0}^{VA}],\\
B_5^{VA-T} &= \mathrm{Re}[H_{1/2,t}^{VA*}(H_{1/2,-1,1}^{(T)1/2} + H_{1/2,t,0}^{(T)1/2})] + \mathrm{Re}[H_{1/2,1}^{VA*}(H_{1/2,0,1}^{(T)-1/2} + H_{1/2,t,1}^{(T)-1/2})]\\
&\quad + \mathrm{Re}[H_{-1/2,t}^{VA*}(H_{-1/2,-1,1}^{(T)-1/2} + H_{-1/2,t,0}^{(T)-1/2})] - \mathrm{Re}[H_{-1/2,-1}^{VA*}(H_{-1/2,-1,0}^{(T)1/2} + H_{-1/2,t,-1}^{(T)1/2})],\\
B_6^{SP-T} &= \mathrm{Re}[H_{1/2,0}^{SP*}(H_{1/2,-1,1}^{(T)1/2} + H_{1/2,t,0}^{(T)1/2})] + \mathrm{Re}[H_{-1/2,0}^{SP*}(H_{-1/2,-1,1}^{(T)-1/2} + H_{-1/2,t,0}^{(T)-1/2})].
\end{aligned} \tag{2.60}$$

There is no contribution from pure (pseudo-)scalar operators to the forward-backward asymmetry, but all possible interference terms are present.

In this work we use $\Lambda_b \to \Lambda_c$ form factors computed in lattice QCD. For a detailed discussion of the computation of the vector and axial-vector form factors for the transition $\Lambda_b \to \Lambda_c$ in lattice QCD, see [1]. The tensor form factors for this process in lattice QCD are discussed in [15].

## 2.3 Model-independent analysis of individual new-physics couplings

In this section we consider one new-physics coupling at a time. We first compute the constraints from the existing measurements with mesons, and then study the impact of a future measurement of $R(\Lambda_c)$.

### 2.3.1 Constraints from the existing measurements of $R(D)$, $R(D^*)$, and $\tau_{B_c}$

We require the NP couplings to reproduce the measurements (2.5 and 2.6 ) of $R_D^{Ratio}$ and $R_{D^*}^{Ratio}$ within the $3\sigma$ range. The coupling $g_S(g_P)$ only contributes to $R_D^{Ratio}(R_{D^*}^{Ratio})$ while the other couplings contribute to both channels. If only $g_L$ is nonzero, the SM contribution gets rescaled by an overall factor $|1+g_L|^2$, so that

$$R_D^{Ratio} = R_{D^*}^{Ratio} = R_{\Lambda_c}^{Ratio} = |1+g_L|^2. \tag{2.61}$$

Note that in the $g_L$-only scenario the forward-backward asymmetry (2.2) is unmodified, $A_{FB} = A_{FB}^{\rm SM}$.

The measured lifetime of the $B_c$ meson, $\tau_{B_c} = 0.510(9)$ ps [35], provides an upper bound on the $B_c \to \tau^- \bar{\nu}_\tau$ decay rate, which yields a strong constraint on the $g_P$ coupling [36, 37, 38]. According to SM calculations using an operator product expansion [39], only about 5% (for the central value) of the total width of the $B_c$, $\Gamma_{B_c} = 1/\tau_{B_c}$, can be attributed to purely tauonic and semi-tauonic modes. This can be relaxed as the parameters in the calculations are varied. In our analysis, we use an upper limit of $B_c \to \tau\bar{\nu}_\tau \leq 30\%$ to put constraints on the new-physics couplings. Obviously stronger bounds can be considered but here we consider the conservative bound of 30%. For the decay constant of $B_c$ we use $f_{B_c} = 0.434(15)$ GeV from lattice QCD calculations [40].

In Fig. 2.3, we present the constraints on the new-physics couplings coming from the measurements of $R_D^{Ratio}$, $R_{D^*}^{Ratio}$, and $\tau_{B_c}$. We see that $\tau_{B_c}$ puts a strong constraint on the coupling $g_P$. It does not have any significant effect on the other couplings. The $g_T$ coupling is strongly

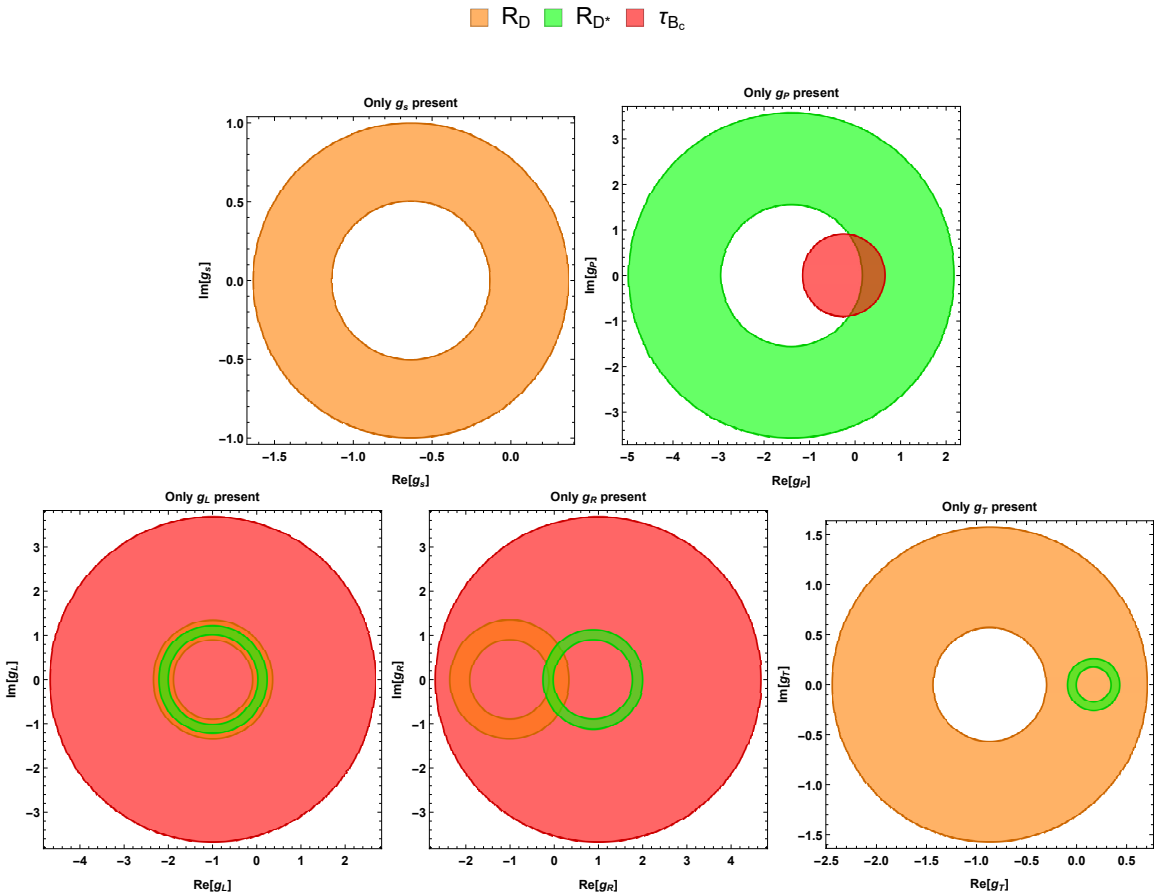


**Figure 2.3:** Constraints on the individual new-physics couplings from the measurements of $R_D^{Ratio}$, $R_{D^*}^{Ratio}$, and $\tau_{B_c}$. We require that the couplings reproduce the measurements of $R_D^{Ratio}$ and $R_{D^*}^{Ratio}$ in Eqs. 2.5 and 2.6 within $3\sigma$, and satisfy $\mathcal{B}(B_c \to \tau^- \bar{\nu}_\tau) \leq 30\%$.

constrained by $R_{D^*}^{Ratio}$ and only weakly constrained by $R_D^{Ratio}$.

Example values of the ratios $R(\Lambda_c)$ and $R_{\Lambda_c}^{Ratio} = R(\Lambda_c)/R(\Lambda_c)^{\rm SM}$ for representative allowed values of the NP couplings are given in Table 2.1. The standard-model prediction for $R(\Lambda_c)$ is $0.333 \pm 0.010$ [1]. We find that large deviations from this value are possible with the present mesonic constraints. In Table 2.2, we present the maximum and minimum allowed values of $R_{\Lambda_c}^{Ratio} = R(\Lambda_c)/R(\Lambda_c)^{\rm SM}$ in the presence of each individual new-physics coupling, and the corresponding values of the coupling at which these occur.

Figure 2.4 shows the effect of representative values of the individual NP couplings on the $\Lambda_b \to \Lambda_c \tau \bar{\nu}_\tau$ differential decay rate (evaluated assuming $|V_{cb}| = 0.041$) as well as $B_{\Lambda_c}(q^2)$ [defined in Eq. (2.1)] and $A_{FB}(q^2)$. In all cases, except for the strongly constrained pure $g_P$ coupling,

| | $g_S$ only | $g_P$ only | $g_L$ only | $g_R$ only | $g_T$ only |
|---|---|---|---|---|---|
| | $-0.4$ | $0.3$ | $-2.2$ | $-0.044$ | $0.4$ |
| $R(\Lambda_c)$ | $0.290 \pm 0.009$ | $0.342 \pm 0.010$ | $0.479 \pm 0.014$ | $0.344 \pm 0.011$ | $0.475 \pm 0.037$ |
| $R_{\Lambda_c}^{Ratio}$ | $0.872 \pm 0.007$ | $1.026 \pm 0.001$ | $1.44$ | $1.033 \pm 0.003$ | $1.426 \pm 0.100$ |
| | $-1.5 - 0.3i$ | $0.4 - 0.4i$ | $0.15 - 0.3i$ | $0.08 - 0.67i$ | $0.2 - 0.2i$ |
| $R(\Lambda_c)$ | $0.384 \pm 0.013$ | $0.346 \pm 0.011$ | $0.470 \pm 0.014$ | $0.465 \pm 0.014$ | $0.404 \pm 0.021$ |
| $R_{\Lambda_c}^{Ratio}$ | $1.154 \pm 0.008$ | $1.040 \pm 0.002$ | $1.412$ | $1.397 \pm 0.005$ | $1.213 \pm 0.050$ |

**Table 2.1:** The values of $R(\Lambda_c)$ and $R_{\Lambda_c}^{Ratio}$ for two example choices (real-valued and complex-valued) of the new-physics couplings. The standard-model value of $R(\Lambda_c)$ is $0.333 \pm 0.010$ [1]. The uncertainties given are due to the form factor uncertainties.

| Coupling | $R(\Lambda_c)_{max}$ | $R_{\Lambda_c,max}^{Ratio}$ | coupling value | $R(\Lambda_c)_{min}$ | $R_{\Lambda_c,min}^{Ratio}$ | coupling value |
|---|---|---|---|---|---|---|
| $g_S$ only | $0.405$ | $1.217$ | $0.363$ | $0.314$ | $0.942$ | $-1.14$ |
| $g_P$ only | $0.354$ | $1.062$ | $0.658$ | $0.337$ | $1.014$ | $0.168$ |
| $g_L$ only | $0.495$ | $1.486$ | $0.094 + 0.538i$ | $0.340$ | $1.022$ | $-0.070 + 0.395i$ |
| $g_R$ only | $0.525$ | $1.576$ | $0.085 + 0.793i$ | $0.336$ | $1.009$ | $-0.012$ |
| $g_T$ only | $0.526$ | $1.581$ | $0.428$ | $0.338$ | $1.015$ | $-0.005$ |

**Table 2.2:** The maximum and minimum values of $R(\Lambda_c)$ and $R_{\Lambda_c}^{Ratio}$ allowed by the mesonic constraints for each new-physics coupling, and the coupling values at which these extrema are reached.

substantial deviations from the SM predictions are allowed. We notice that $A_{FB}$ is typically above the SM prediction in the presence of $g_R$ or $g_T$, while it is typically below the SM prediction in the presence of $g_S$. Hence, it is possible to use $A_{FB}$ to distinguish between the different couplings.

### 2.3.2 Impact of a future $R(\Lambda_c)$ measurement

In this subsection, we present the effect of possible future measurements of $R(\Lambda_c)$ on the NP couplings constraints. We consider two cases, one in which the measured value is near the SM prediction and one with the measured value far from the SM. For the first case we take $R_{\Lambda_c}^{Ratio} = 1 \pm 3 \times 0.05$, and for the second case $R_{\Lambda_c}^{Ratio} = 1.3 \pm 3 \times 0.05$ (the same central values as $R_D^{Ratio}$). Note that we take the $1\sigma$ uncertainty as 0.05. Figures 2.5 and 2.6 show the allowed regions of the parameter space for the first and second case, respectively. We observe the following when adding the $R_{\Lambda_c}^{Ratio}$ constraints to the mesonic constraints:

- For $R(\Lambda_c)$ near the SM (Fig. 2.5), the allowed regions for $(g_L,\ g_R,\ g_T)$ are reduced significantly, the allowed region for $g_S$ shrinks only slightly, and the allowed region for $g_P$ remains the same (as it is dominantly constrained by $\tau_{B_c}$).

- For $R(\Lambda_c)$ far from the SM (Fig. 2.6), most of the previously allowed region for $g_S$ becomes excluded by $R(\Lambda_c)$. Even more importantly, the $g_P$-only scenario becomes ruled out. In this case, $R(\Lambda_c)$ also provides strong constraints on $(g_L,\ g_R,\ g_T)$, but these constraints still overlap with the mesonic constraints.

## 2.4 Leptoquarks as Models of New Physics

Many beyond the SM models, motivated by unifying matter, predict existence of new particles that decay into a lepton and a quark. These particles, known as leptoquarks (LQ), carry both baryon and lepton number. There are ten models in which the LQ couples to SM particles through dimension $\leq 4$ operators [35]. These include five scalar and five vector LQs. Six of these can contribute to $b \to c\tau^-\bar{\nu}_\tau$ [28]. Three have fermion-number-conserving couplings and three

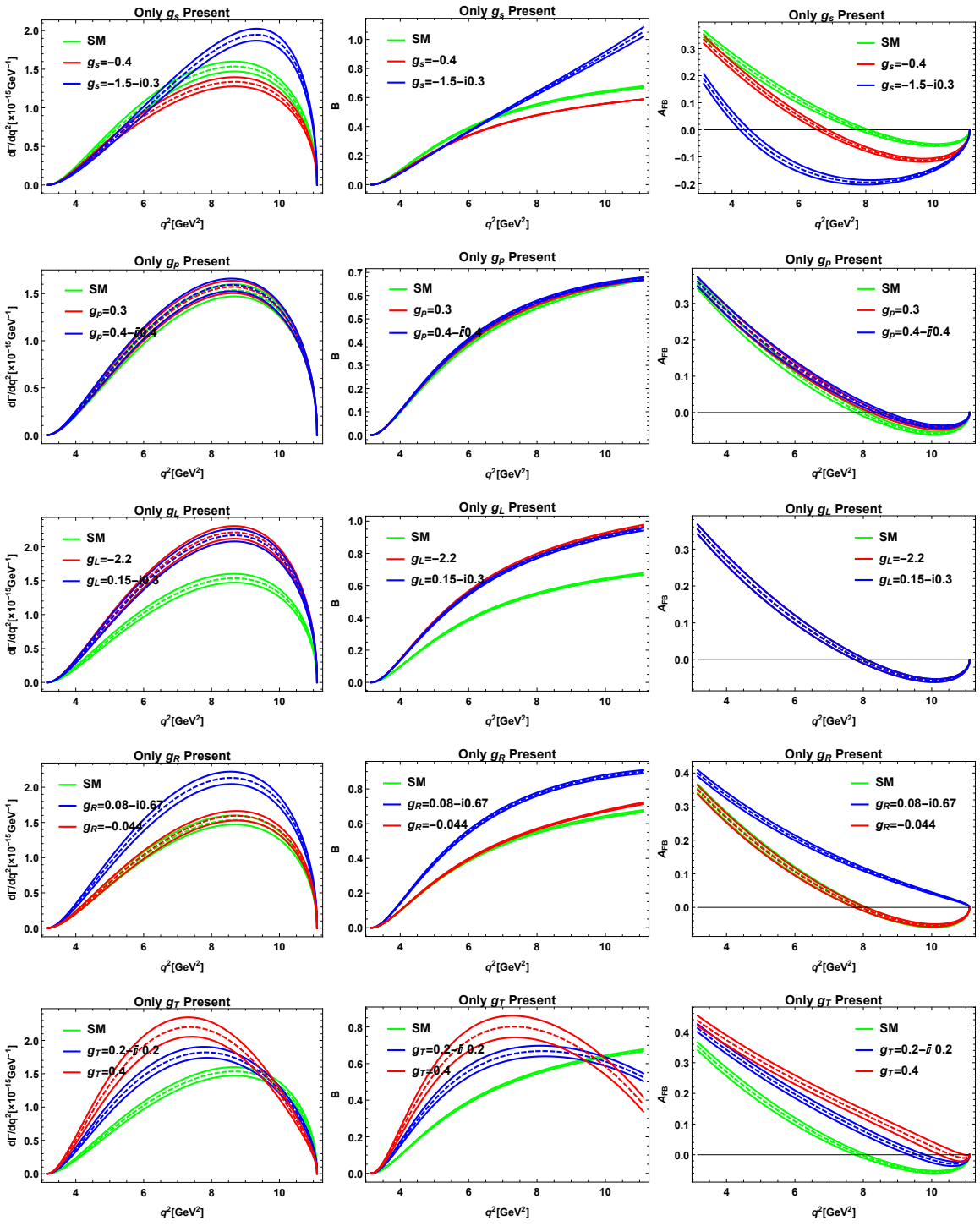


**Figure 2.4:** The effect of individual new-physics couplings on the $\Lambda_b \to \Lambda_c \tau \bar{\nu}_\tau$ differential decay rate (left), the ratio of the $\Lambda_b \to \Lambda_c \tau \bar{\nu}_\tau$ and $\Lambda_b \to \Lambda_c \ell \bar{\nu}_\ell$ differential decay rates (middle), and the $\Lambda_b \to \Lambda_c \tau \bar{\nu}_\tau$ forward-backward asymmetry (right). Each plot shows the observable in the Standard Model and for two representative values of the new-physics coupling (one real-valued choice and one complex-valued choice). The bands indicate the $1\sigma$ uncertainties originating from the $\Lambda_b \to \Lambda_c$ form factors.

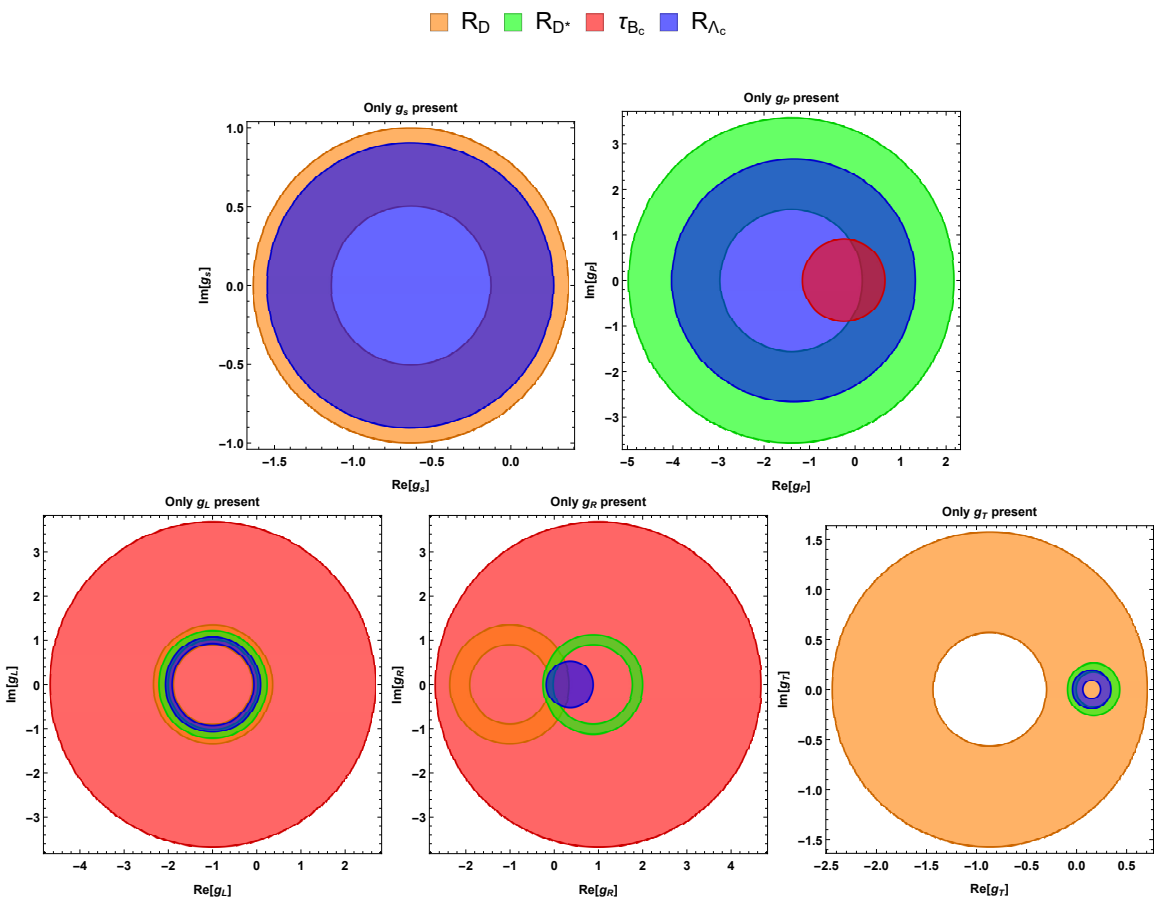


**Figure 2.5:** Constraints on individual new-physics couplings from a possible $R(\Lambda_c)$ measurement (shown in blue), assuming that $R^{Ratio}_{\Lambda_c} = 1 \pm 3 \times 0.05$ where the $1\sigma$ uncertainty is 0.05. Also shown are the mesonic constraints as in Fig. 2.3.

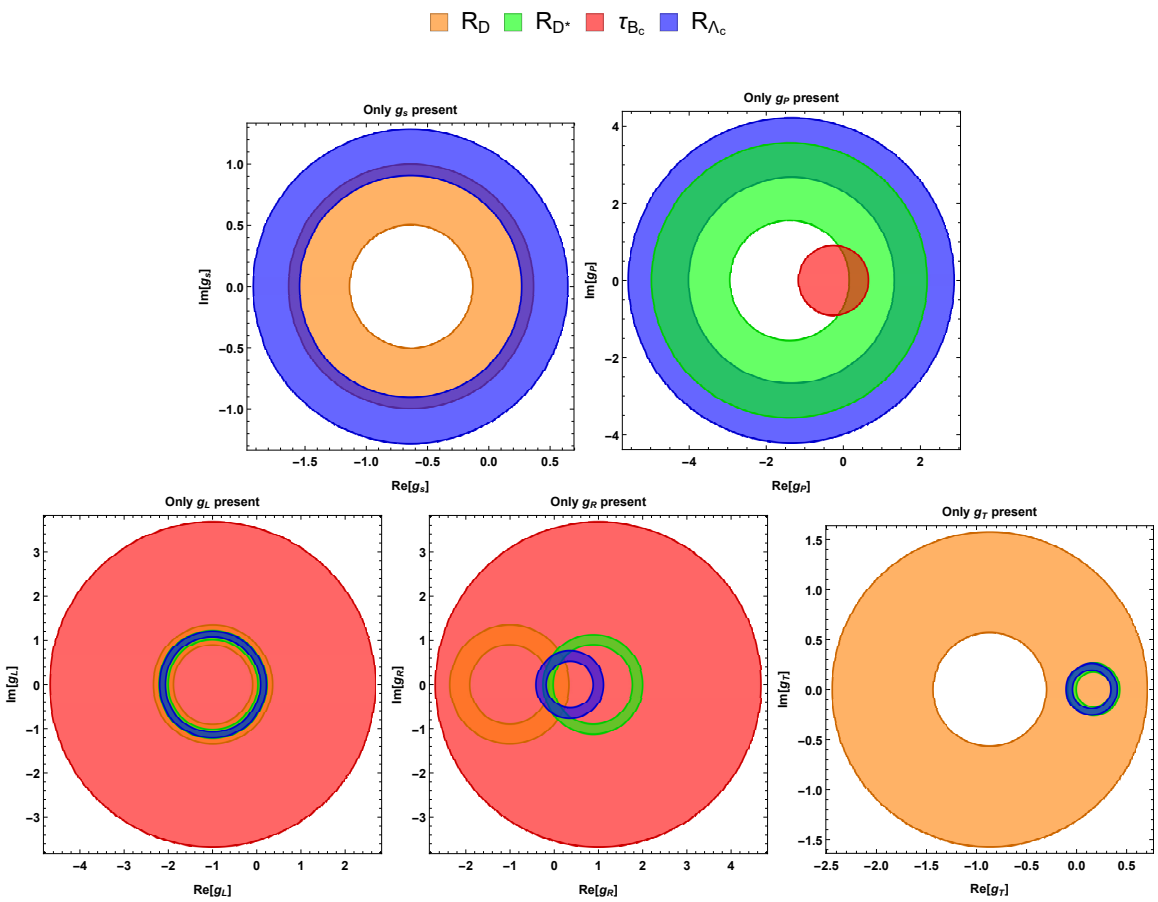


**Figure 2.6:** Constraints on individual new-physics couplings from a possible $R(\Lambda_c)$ measurement (shown in blue), assuming that $R_{\Lambda_c}^{Ratio} = 1.3 \pm 3 \times 0.05$ where the $1\sigma$ uncertainty is 0.05. Also shown are the mesonic constraints as in Fig. 2.3.

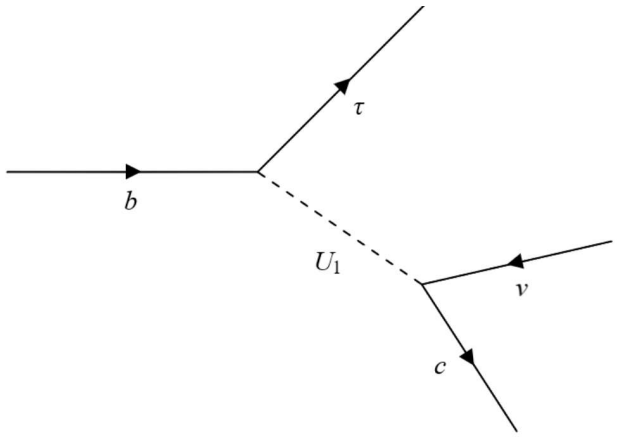


**Figure 2.7:** An example of $U_1$ leptoquark contribution to $b \to c\tau\bar{\nu}_\tau$

have fermion-number-violating couplings. An example of a LQ contribution to the $b \to c\tau^-\bar{\nu}_\tau$ mode is given in Fig. 2.7. The Lagrangian that generates the contributions to $b \to c\tau^-\bar{\nu}_\tau$ is given by

$$\begin{aligned}
\mathcal{L}^{\rm LQ} &= \mathcal{L}^{\rm LQ}_{F=0} + \mathcal{L}^{\rm LQ}_{F=-2}\,, \\
\mathcal{L}^{\rm LQ}_{F=0} &= (h^{ij}_{1L}\bar{Q}_{iL}\gamma^\mu L_{jL} + h^{ij}_{1R}\bar{d}_{iR}\gamma^\mu \ell_{jR})U_{1\mu} + h^{ij}_{3L}\bar{Q}_{iL}\vec{\sigma}\gamma^\mu L_{jL}\cdot\vec{U}_{3\mu} \\
&\quad + (h^{ij}_{2L}\bar{u}_{iR}L_{jL} + h^{ij}_{2R}\bar{Q}_{iL}i\sigma_2\ell_{jR})R_2 + h.c., \\
\mathcal{L}^{\rm LQ}_{F=-2} &= (g^{ij}_{1L}\bar{Q}^c_{iL}i\sigma_2 L_{jL} + g^{ij}_{1R}\bar{u}^c_{iR}\ell_{jR})S_1 + (g^{ij}_{3L}\bar{Q}^c_{iL}i\sigma_2\vec{\sigma}L_{jL})\cdot\vec{S}_3 \\
&\quad + (g^{ij}_{2L}\bar{d}^c_{iR}\gamma_\mu L_{jL} + g^{ij}_{2R}\bar{Q}^c_{iL}\gamma_\mu\ell_{jR})V^\mu_2 + h.c.
\end{aligned} \tag{2.62}$$

Here $Q$ and $L$ represent left-handed quark and lepton $SU(2)_L$ doublets, respectively; $u$, $d$ and $\ell$ represent right-handed up-type quark, down-type quark and charged lepton $SU(2)_L$ singlets, respectively. The indices $i$ and $j$ are the quark and lepton generations and $\psi^c = C\bar{\psi}^T$ is a charge-conjugated field. The $SU(3) \times SU(2) \times U(1)$ quantum numbers of these LQs are summarized in Table 2.3.

| | spin | $SU(3)_c$ | $SU(2)_L$ | $U(1)_{Y=Q-T_3}$ |
|---|---|---|---|---|
| $S_1$ | 0 | $3^*$ | 1 | 1/3 |
| $\boldsymbol{S}_3$ | 0 | $3^*$ | 3 | 1/3 |
| $R_2$ | 0 | 3 | 2 | 7/6 |
| $V_2$ | 1 | $3^*$ | 2 | 5/6 |
| $U_1$ | 1 | 3 | 1 | 2/3 |
| $\boldsymbol{U}_3$ | 1 | 3 | 3 | 2/3 |

**Table 2.3:** Quantum numbers of scalar and vector leptoquarks.

The interaction Lagrangian (Eq. 2.62) generates the following couplings in Eq. (2.7):

$$g_S(\mu_b) = \frac{\sqrt{2}}{4G_F V_{cb}} \left(C_{\mathcal{S}_1}(\mu_b) + C_{\mathcal{S}_2}(\mu_b)\right), \tag{2.63}$$

$$g_P(\mu_b) = \frac{\sqrt{2}}{4G_F V_{cb}} \left(C_{\mathcal{S}_1}(\mu_b) - C_{\mathcal{S}_2}(\mu_b)\right), \tag{2.64}$$

$$g_L = \frac{\sqrt{2}}{4G_F V_{cb}} C^l_{\mathcal{V}_1}, \tag{2.65}$$

$$g_R = \frac{\sqrt{2}}{4G_F V_{cb}} C^l_{\mathcal{V}_2}, \tag{2.66}$$

$$g_T(\mu_b) = \frac{\sqrt{2}}{4G_F V_{cb}} C_{\mathcal{T}}(\mu_b), \tag{2.67}$$

where the Wilson coefficients in the leptoquark models are given by

$$C_{\rm SM} = 2\sqrt{2} G_F V_{cb}\,, \tag{2.68}$$

$$C^l_{\mathcal{V}_1} = \sum_{k=1}^{3} V_{k3} \left[ \frac{g^{kl}_{1L} g^{23*}_{1L}}{2M^2_{S_1}} - \frac{g^{kl}_{3L} g^{23*}_{3L}}{2M^2_{\boldsymbol{S}_3}} + \frac{h^{2l}_{1L} h^{k3*}_{1L}}{M^2_{U_1}} - \frac{h^{2l}_{3L} h^{k3*}_{3L}}{M^2_{\boldsymbol{U}_3}} \right], \tag{2.69}$$

$$C^l_{\mathcal{V}_2} = 0\,, \tag{2.70}$$

$$C^l_{\mathcal{S}_1} = \sum_{k=1}^{3} V_{k3} \left[ -\frac{2 g^{kl}_{2L} g^{23*}_{2R}}{M^2_{V_2}} - \frac{2 h^{2l}_{1L} h^{k3*}_{1R}}{M^2_{U_1}} \right], \tag{2.71}$$

$$C^l_{\mathcal{S}_2} = \sum_{k=1}^{3} V_{k3} \left[ -\frac{g^{kl}_{1L} g^{23*}_{1R}}{2M^2_{S_1}} - \frac{h^{2l}_{2L} h^{k3*}_{2R}}{2M^2_{R_2}} \right], \tag{2.72}$$

$$C^l_{\mathcal{T}} = \sum_{k=1}^{3} V_{k3} \left[ \frac{g^{kl}_{1L} g^{23*}_{1R}}{8M^2_{S_1}} - \frac{h^{2l}_{2L} h^{k3*}_{2R}}{8M^2_{R_2}} \right]. \tag{2.73}$$

These Wilson coefficients are defined at the energy scale $\mu = M_X$, where $X$ represents a leptoquark. Above, $V_{k3}$ denotes the relevant CKM matrix element, where the 3 corresponds to the bottom quark. In the following, we neglect the CKM-suppressed contributions from $k = 1$ and $k = 2$ in the sums. Because the neutrino is not observed, we have $l = 1, 2, 3$. Note that there is a Standard-Model contribution for $l = 3$ but not for $l = 1, 2$; hence, the constraints for different $l$ will be different.

The renormalization-group running of the scalar and tensor Wilson coefficients from $\mu = M_X$ to $\mu = \mu_b$, where $\mu_b$ is the mass scale of the bottom quark, is given by

$$C_{\mathcal{S}_{1,2}}(\mu_b) = \left[\frac{\alpha_s(m_t)}{\alpha_s(\mu_b)}\right]^{-\frac{12}{23}} \left[\frac{\alpha_s(m_{\rm LQ})}{\alpha_s(m_t)}\right]^{-\frac{4}{7}} C_{\mathcal{S}_{1,2}}(m_{\rm LQ})\,, \tag{2.74}$$

$$C_{\mathcal{T}}(\mu_b) = \left[\frac{\alpha_s(m_t)}{\alpha_s(\mu_b)}\right]^{\frac{4}{23}} \left[\frac{\alpha_s(m_{\rm LQ})}{\alpha_s(m_t)}\right]^{\frac{4}{21}} C_{\mathcal{T}}(m_{\rm LQ})\,, \tag{2.75}$$

where $\alpha_s(\mu)$ is the QCD coupling at scale $\mu$. Because the anomalous dimensions of the vector and axial-vector currents are zero, the Wilson coefficients for $\mathcal{V}_{1,2}$ are scale-independent. The different leptoquarks produce different effective operators as summarized below:

- The $S_1$ leptoquark with nonzero $(g_{1L}, g_{1R}^*)$ generates $C^l_{\mathcal{V}_1}$, $C^l_{\mathcal{S}_2}$, and $C^l_{\mathcal{T}}$, with the relation $C^l_{\mathcal{S}_2} = -4C^l_{\mathcal{T}}$.
- The $R_2$ leptoquark with $(h_{2L}, h_{2R}^*)$ generates $C^l_{\mathcal{S}_2}$ and $C^l_{\mathcal{T}}$ with the relation $C^l_{\mathcal{S}_2} = 4C^l_{\mathcal{T}}$.
- The $V_2$ leptoquark generates $C^l_{\mathcal{S}_1}$ and is tightly constrained, so we do not consider this model.
- The $U_1$ leptoquark with nonzero $(g_{2L}, g_{2R}^*)$ generates $C^l_{\mathcal{S}_1}$ and $C^l_{\mathcal{V}_1}$.
- The $\boldsymbol{S}_3$ and $\boldsymbol{U}_3$ leptoquarks with nonzero values of $(g_{3L}, g_{3L}^*)$ and $(h_{3L}, h_{3L}^*)$ generate $C^l_{\mathcal{V}_1}$.

The leptoquark couplings can also be constrained using $b \to s\nu\bar{\nu}$ decays. As pointed out in Ref. [41], the exclusive decays $\bar{B} \to K\nu\bar{\nu}$ and $\bar{B} \to K^*\nu\bar{\nu}$ provide more stringent bounds than the inclusive mode $B \to X_s\nu\bar{\nu}$. The $U_1$ and $R_2$ leptoquarks do not contribute to $b \to s\nu\bar{\nu}$, while the left-handed couplings of $S_1$, $\boldsymbol{S}_3$, and $\boldsymbol{U}_3$ do. (The $V_2$ leptoquark also contributes to $b \to s\nu\bar{\nu}$, but

we do not consider this model.) The BaBar and Belle Collaborations give the following 90% C.L. upper limits [42, 43]:

$$\begin{aligned}
\mathcal{B}(B^+ \to K^+ \nu\bar{\nu}) &\leq 1.7 \times 10^{-5} \,, \\
\mathcal{B}(B^+ \to K^{*+} \nu\bar{\nu}) &\leq 4.0 \times 10^{-5} \,, \\
\mathcal{B}(B^0 \to K^{*0} \nu\bar{\nu}) &\leq 5.5 \times 10^{-5} \,.
\end{aligned} \tag{2.76}$$

In Ref. [44], these are compared with the SM predictions

$$\begin{aligned}
\mathcal{B}_K^{\rm SM} &\equiv \mathcal{B}(B \to K \nu\bar{\nu})_{\rm SM} = (3.98 \pm 0.43 \pm 0.19) \times 10^{-6} \,, \\
\mathcal{B}_{K^*}^{\rm SM} &\equiv \mathcal{B}(B \to K^* \nu\bar{\nu})_{\rm SM} = (9.19 \pm 0.86 \pm 0.50) \times 10^{-6} \,.
\end{aligned} \tag{2.77}$$

Taking into account the theoretical uncertainties [44], the 90% C.L. upper bounds on the NP contributions are

$$\frac{\mathcal{B}_K^{\rm SM+NP}}{\mathcal{B}_K^{\rm SM}} \leq 4.8 \,, \quad \frac{\mathcal{B}_{K^*}^{\rm SM+NP}}{\mathcal{B}_{K^*}^{\rm SM}} \leq 4.9 \,. \tag{2.78}$$

Following Ref. [28], the $b \to s \nu_j \bar{\nu}_i$ process can be described by the effective Hamiltonian

$$H_{eff} = \frac{4 G_F}{\sqrt{2}} V_{tb} V_{ts}^* \left[ \left( \delta_{ij} C_L^{\rm (SM)} + C_L^{ij} \right) O_L^{ij} + C_R^{ij} O_R^{ij} \right] \,, \tag{2.79}$$

where the left-handed and right-handed operators are defined as

$$\begin{aligned}
O_L^{ij} &= (\bar{s}_L \gamma^\mu b_L)(\bar{\nu}_{jL} \gamma_\mu \nu_{iL}) \,, \\
O_R^{ij} &= (\bar{s}_R \gamma^\mu b_R)(\bar{\nu}_{jL} \gamma_\mu \nu_{iL}) \,.
\end{aligned} \tag{2.80}$$

The SM Wilson coefficient $C_L^{\rm (SM)}$ receives contributions from box and $Z$-penguin diagrams, which yield

$$C_L^{\rm (SM)} = \frac{\alpha}{2\pi \sin^2 \theta_W} X(m_t^2 / M_W^2) \,, \tag{2.81}$$

where the loop function $X(x_t)$ can be found e.g. in Ref. [45]. The leptoquarks that we consider produce contributions to $C_L^{ij}$ which, to leading order, are equal to [28]

$$C_L^{ij} = -\frac{1}{2\sqrt{2}G_F V_{tb}V_{ts}^*}\left[\frac{g_{1L}^{3i}g_{1L}^{2j*}}{2M_{S_1^{1/3}}^2} + \frac{g_{3L}^{3i}g_{3L}^{2j*}}{2M_{S_3^{1/3}}^2} - \frac{2h_{3L}^{2i}h_{3L}^{3j*}}{M_{U_3^{-1/3}}^2}\right]. \tag{2.82a}$$

We obtain common coefficients for $b \to c\tau\bar{\nu}_l$ and $b \to s\nu_\tau\bar{\nu}_l$ processes,

$$C_L^{l3} = -\frac{1}{2\sqrt{2}G_F V_{tb}V_{ts}^*}\left[\frac{g_{1L}^{3l}g_{1L}^{23*}}{2M_{S_1^{1/3}}^2} + \frac{g_{3L}^{3l}g_{3L}^{23*}}{2M_{S_3^{1/3}}^2} - \frac{2h_{3L}^{2l}h_{3L}^{33*}}{M_{U_3^{-1/3}}^2}\right]. \tag{2.83a}$$

Hence, for $l = 3$ we obtain

$$\frac{\mathcal{B}_K^{\text{SM+NP}}}{\mathcal{B}_K^{\text{SM}}} = \frac{\mathcal{B}_{K^*}^{\text{SM+NP}}}{\mathcal{B}_{K^*}^{\text{SM}}} = \left|\frac{3C_L^{(\text{SM})} + C_L^{33}}{3C_L^{(\text{SM})}}\right|^2, \tag{2.84}$$

while for $l = 1, 2$ we have

$$\frac{\mathcal{B}_K^{\text{SM+NP}}}{\mathcal{B}_K^{\text{SM}}} = \frac{\mathcal{B}_{K^*}^{\text{SM+NP}}}{\mathcal{B}_{K^*}^{\text{SM}}} = \left|\frac{C_L^{l3}}{3C_L^{(\text{SM})}}\right|^2. \tag{2.85}$$

When considering nonzero values only for one coupling at a time ($l = 1, 2, 3$), the experimental measurements of $R_D^{Ratio}$, $R_{D^*}^{Ratio}$, $\tau_{B_c}$, and $\mathcal{B}(B \to K^{(*)}\nu\bar{\nu})$ yield the constraints shown in Figures 2.8, 2.9, and 2.10. The cases with $g_{3L}^{3i}g_{3L}^{23*}$ in the $\boldsymbol{S}_3$ model, $g_{1L}^{3i}g_{1L}^{23*}$ in the $S_1$ model, and $h_{3L}^{2i}h_{3L}^{23*}$ in the $\boldsymbol{U}_3$ model are ruled out for $i = 1, 2$.

Allowing all relevant couplings in each model to be nonzero simultaneously, we obtain the coupling regions sampled by the random points in Figs. 2.11 and 2.12. The corresponding allowed regions in the $R_{\Lambda_c}^{Ratio} - R_D^{Ratio}$ and $R_{\Lambda_c}^{Ratio} - R_{D^*}^{Ratio}$ planes are shown in Fig. 2.13. Since the $\boldsymbol{S}_3$ and $\boldsymbol{U}_3$ leptoquarks produce only the vector coupling $g_L$, all ratios get rescaled by the common factor of $|1 + g_L|^2$. The $\boldsymbol{S}_3$ and $\boldsymbol{U}_3$ models are tightly constrained and only small effects are allowed. The other leptoquark models can produce substantial effects in $R_{\Lambda_c}^{Ratio}$, with varying degrees of

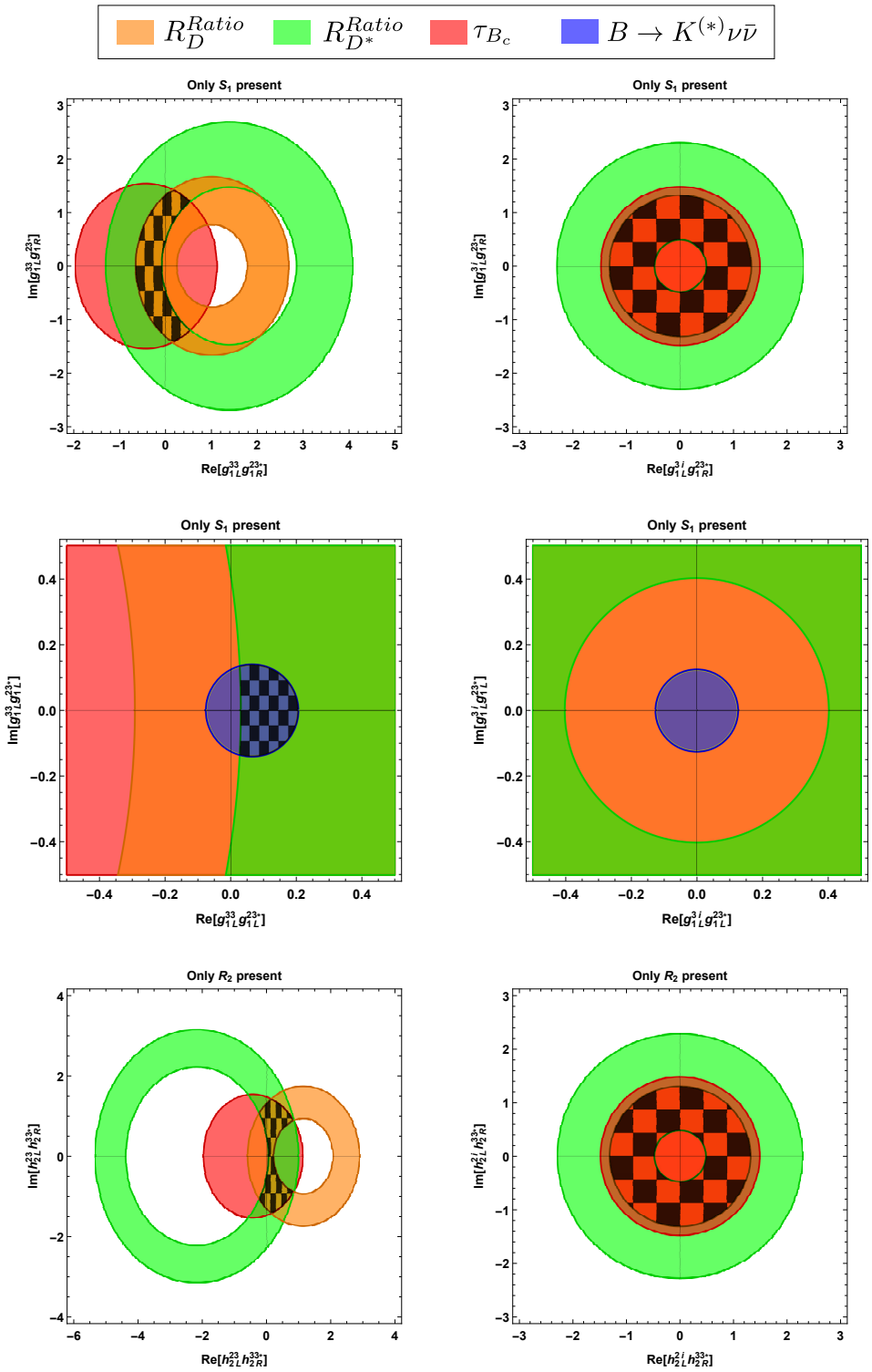


**Figure 2.8:** Constraints on the $S_1$ and $R_2$ leptoquark models when considering one coupling at a time. Here, $i = 1, 2$ denotes the electron and muon neutrinos. We require that the couplings reproduce the measurements of $R_D^{Ratio}$ and $R_{D^*}^{Ratio}$ in Eqs. (2.5) and (2.6) within $3\sigma$, satisfy $\mathcal{B}(B_c \to \tau^- \bar{\nu}_\tau) \leq 30\%$, and are consistent with the upper bounds on $\mathcal{B}(B \to K^{(*)}\nu\bar{\nu})$ at 90% C.L. The allowed regions of the parameter space when combining all constraints are highlighted with a black mesh.

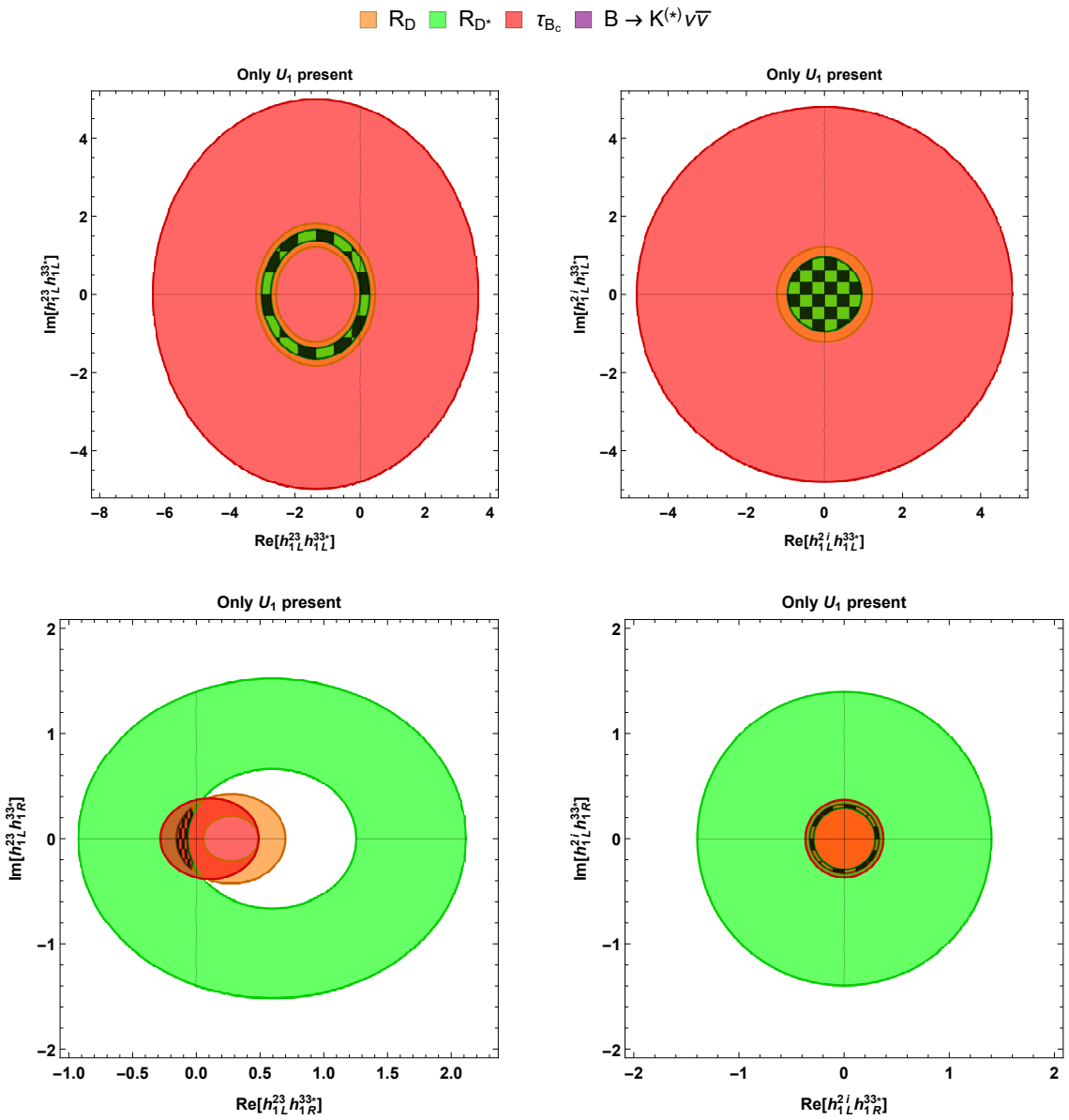


**Figure 2.9:** Constraints on the $U_1$ leptoquark model when considering one coupling at a time. Here, $i = 1, 2$ denotes the electron and muon neutrinos. We require that the couplings reproduce the measurements of $R_D^{Ratio}$ and $R_{D^*}^{Ratio}$ in Eqs. (2.5) and (2.6) within $3\sigma$ and satisfy $\mathcal{B}(B_c \to \tau^- \bar{\nu}_\tau) \leq 30\%$. The allowed regions of the parameter space when combining all constraints are highlighted with a black mesh.

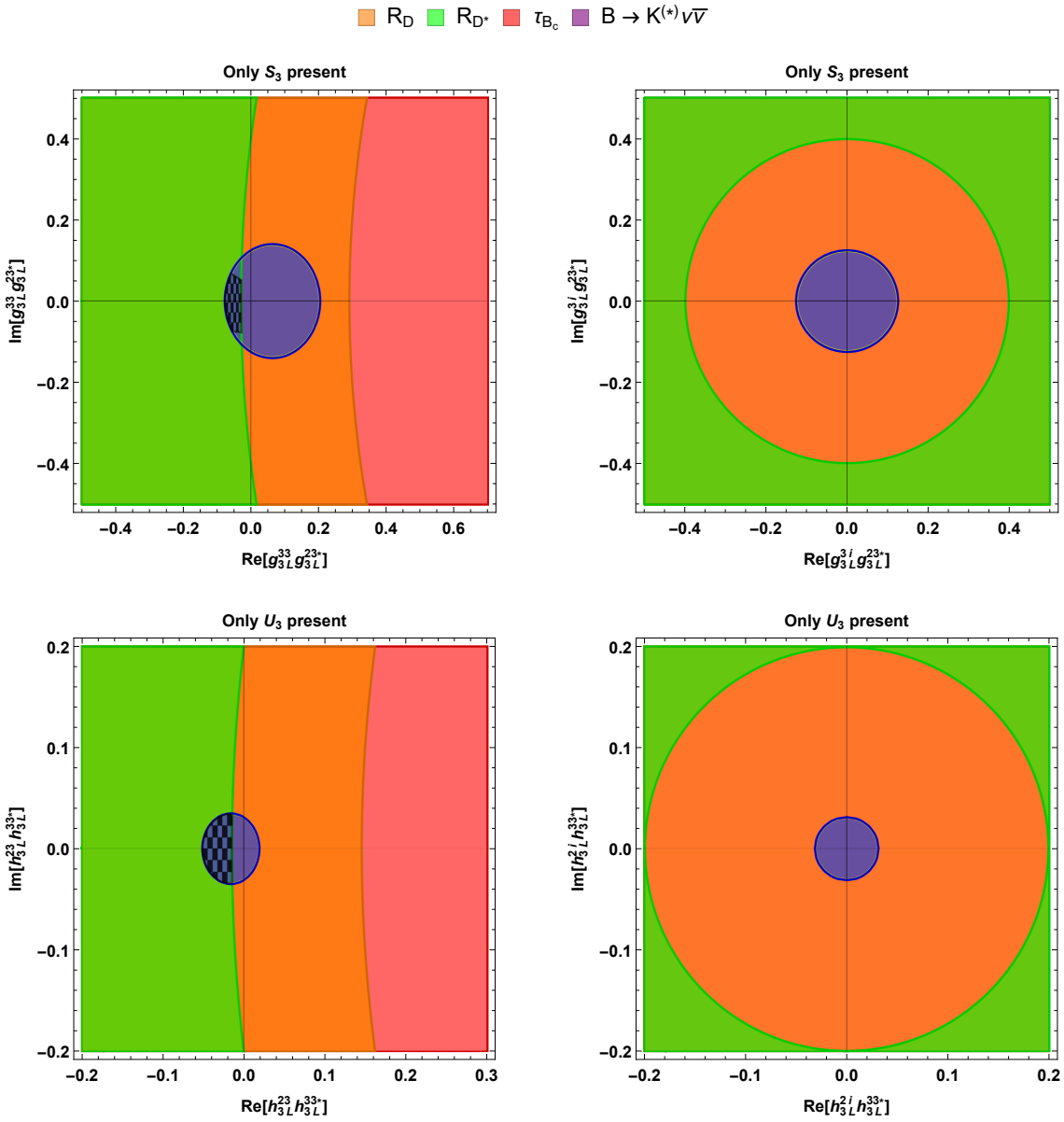


**Figure 2.10:** Constraints on the $S_3$ and $U_3$ leptoquark models when considering one coupling at a time. Here, $i = 1, 2$ denotes the electron and muon neutrinos. We require that the couplings reproduce the measurements of $R_D^{Ratio}$ and $R_{D^*}^{Ratio}$ in Eqs. (2.5) and (2.6) within $3\sigma$, satisfy $\mathcal{B}(B_c \to \tau^- \bar{\nu}_\tau) \leq 30\%$, and are consistent with the upper bounds on $\mathcal{B}(B \to K^{(*)} \nu \bar{\nu})$ at 90% C.L. The allowed regions of the parameter space when combining all constraints are highlighted with a black mesh.

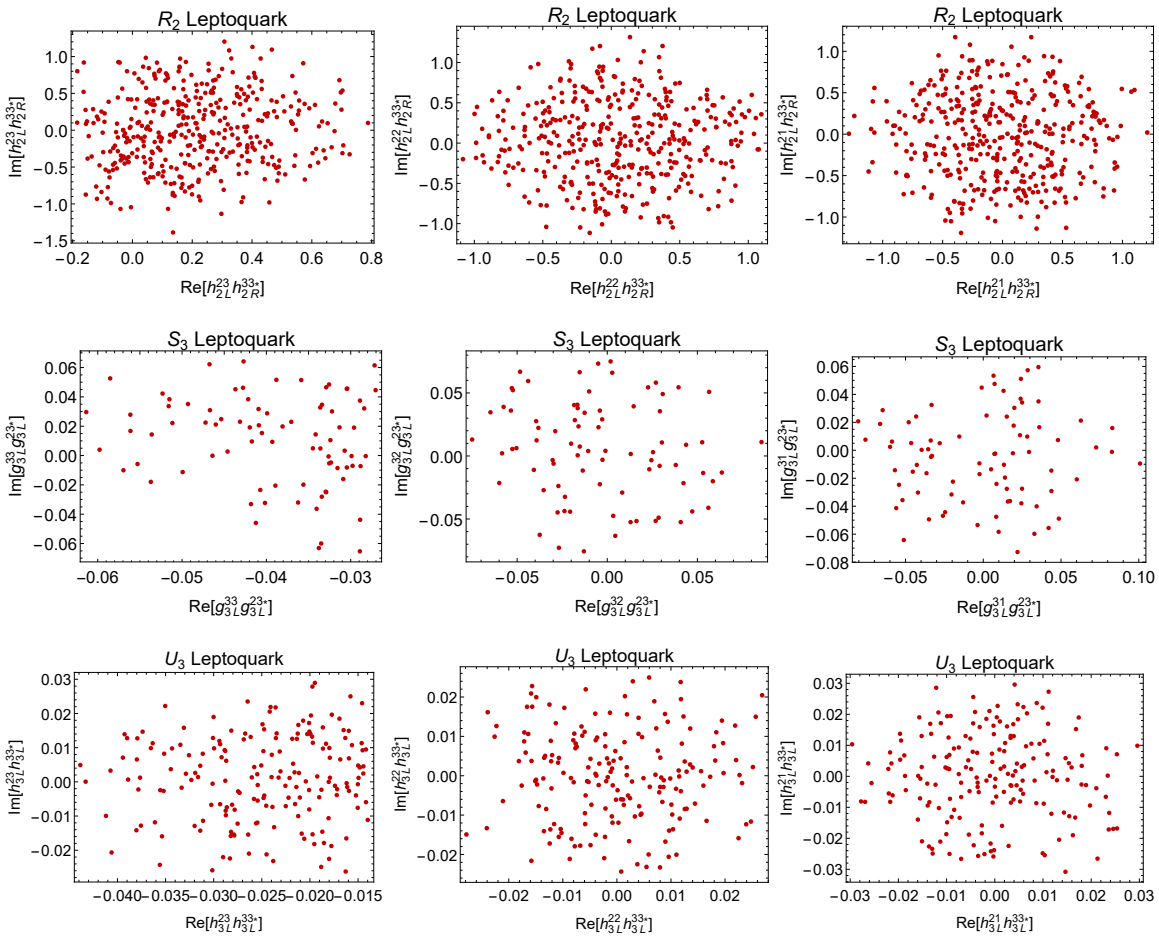


**Figure 2.11:** Allowed regions for the couplings of the $R_2$, $\boldsymbol{S}_3$, and $\boldsymbol{U}_3$ leptoquark models in the case that all relevant couplings in each model are included simultaneously. We require that the couplings reproduce the measurements of $R_D^{Ratio}$ and $R_{D^*}^{Ratio}$ in Eqs. (2.5) and (2.6) within $3\sigma$, satisfy $\mathcal{B}(B_c \to \tau^- \bar{\nu}_\tau) \leq 30\%$, and are consistent with the upper bounds on $\mathcal{B}(B \to K^{(*)} \nu \bar{\nu})$ at 90% C.L (the latter is only relevant for the left-handed couplings in the $\boldsymbol{S}_3$ and $\boldsymbol{U}_3$ models).

correlation between the mesonic and baryonic observables.

The values of $R(\Lambda_c)$ and $R_{\Lambda_c}^{Ratio}$ for two typical allowed combinations of the couplings in each model are given in Table 2.4. In Fig. 2.14, we present plots of the observables $(d\Gamma/dq^2,\ B_{\Lambda_c},\ A_{FB})$ for the same values of the couplings.

## 2.5 Conclusions

The baryonic decay $\Lambda_b \to \Lambda_c \tau \bar{\nu}_\tau$ has the potential to shed new light on the $R(D^{(*)})$ puzzle. In this chapter, we studied the phenomenology of $\Lambda_b \to \Lambda_c \tau \bar{\nu}_\tau$ in the presence of new-physics

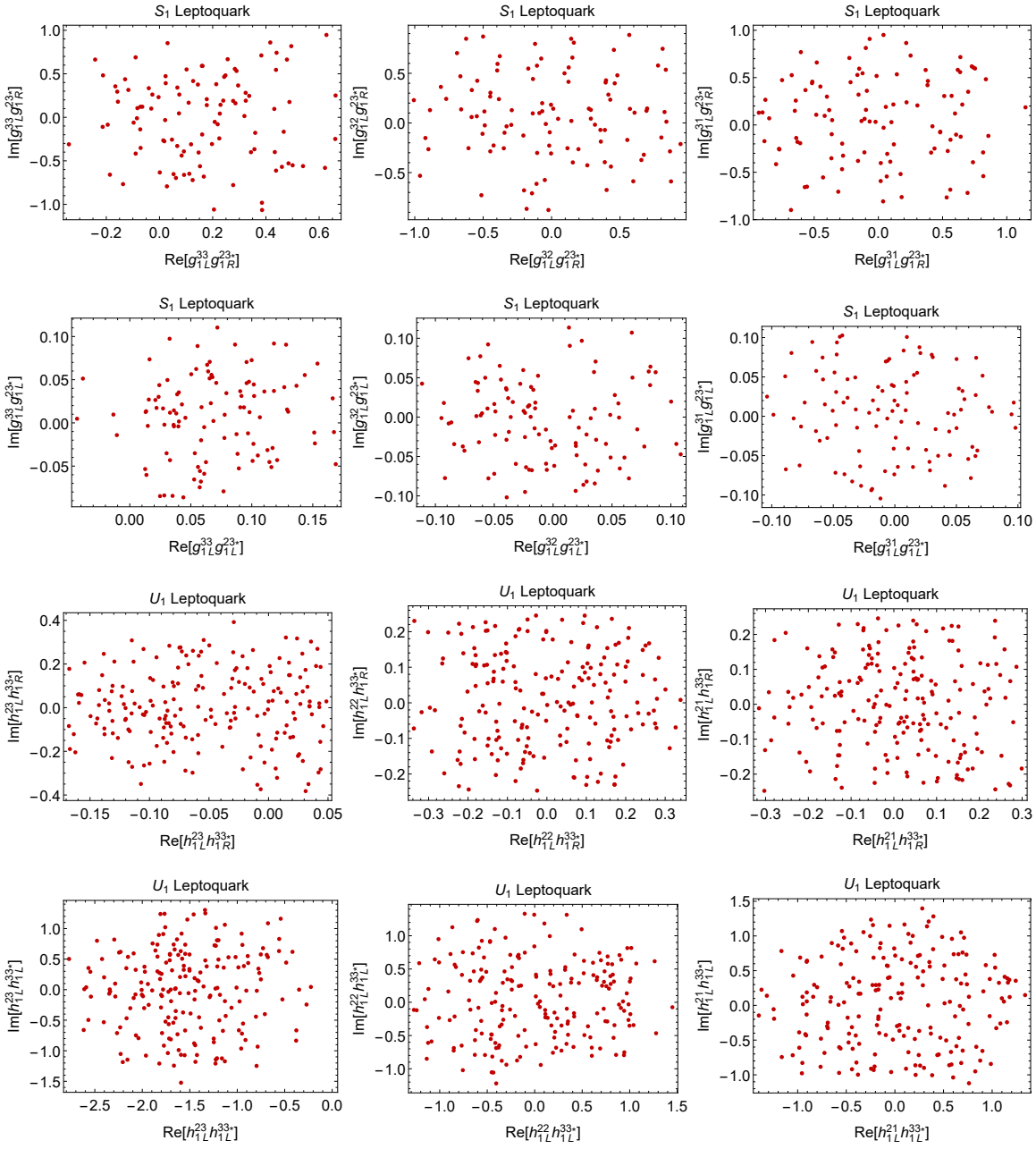


**Figure 2.12:** Allowed regions for the couplings of the $S_1$ and $U_1$ leptoquark models in the case that all relevant couplings in each model are included simultaneously. We require that the couplings reproduce the measurements of $R_D^{Ratio}$ and $R_{D^*}^{Ratio}$ in Eqs. (2.5) and (2.6) within $3\sigma$, satisfy $\mathcal{B}(B_c \to \tau^- \bar{\nu}_\tau) \leq 30\%$, and are consistent with the upper bounds on $\mathcal{B}(B \to K^{(*)} \nu \bar{\nu})$ at 90% C.L (the latter is only relevant for the left-handed couplings in the $S_1$ model).

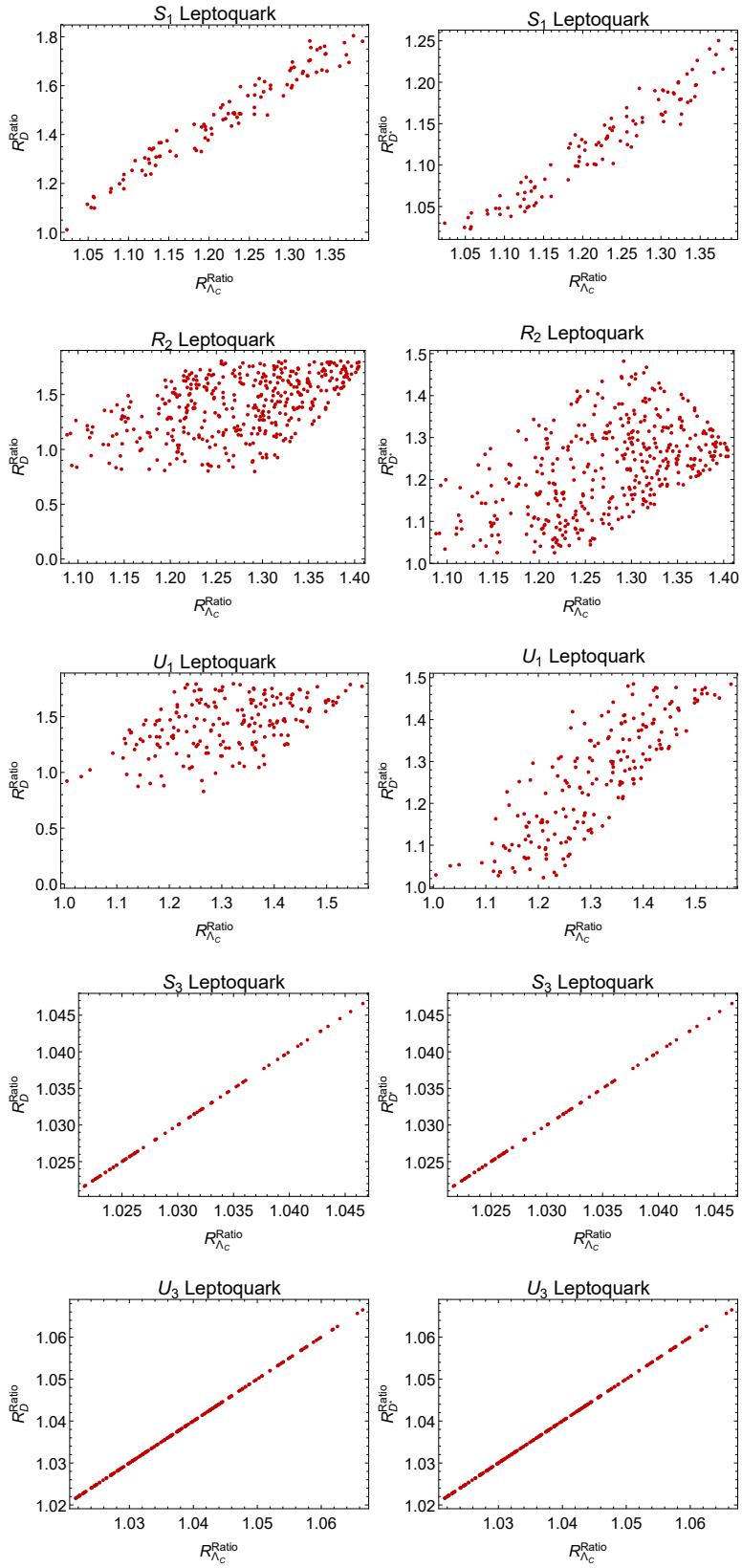


**Figure 2.13:** The allowed regions in the $R_{\Lambda_c}^{Ratio} - R_D^{Ratio}$ and $R_{\Lambda_c}^{Ratio} - R_{D^*}^{Ratio}$ planes for each leptoquark model, given the allowed regions for the couplings from Figs. 2.11 and 2.12.

| Model | Case | Couplings | $R(\Lambda_c)$ | $R_{\Lambda_c}^{Ratio}$ |
|---|---|---|---|---|
| $S_1$ | 1 | $g_{1L}^{33}g_{1R}^{23*} = 0.332 + 0.403i$, $g_{1L}^{3i}g_{1R}^{23*} = 0.417 - 0.311i$, $g_{1L}^{33}g_{1L}^{23*} = 0.015 - 0.037i$, $g_{1L}^{3i}g_{1L}^{23*} = -0.079 - 0.002i$ | $0.343 \pm 0.011$ | $1.032 \pm 0.004$ |
| $S_1$ | 2 | $g_{1L}^{33}g_{1R}^{23*} = 0.064 - 0.142i$, $g_{1L}^{3i}g_{1R}^{23*} = -1.05 + 0.638i$, $g_{1L}^{33}g_{1L}^{23*} = 0.116 - 0.043i$, $g_{1L}^{3i}g_{1L}^{23*} = 0.018 + 0.104i$ | $0.549 \pm 0.020$ | $1.648 \pm 0.025$ |
| $R_2$ | 1 | $h_{2L}^{23}h_{2R}^{33*} = 0.373 - 0.118i$, $h_{2L}^{2i}h_{2R}^{33*} = -0.846 - 0.191i$ | $0.445 \pm 0.016$ | $1.337 \pm 0.016$ |
| $R_2$ | 2 | $h_{2L}^{23}h_{2R}^{33*} = 0.753 - 0.199i$, $h_{2L}^{2i}h_{2R}^{33*} = 0.897 - 0.031i$ | $0.485 \pm 0.018$ | $1.455 \pm 0.025$ |
| $U_1$ | 1 | $h_{1L}^{23}h_{1R}^{33*} = -0.115 - 0.021i$, $h_{1L}^{2i}h_{1R}^{33*} = 0.049 + 0.159i$, $h_{1L}^{23}h_{1L}^{33*} = -1.468 + 0.271i$, $h_{1L}^{2i}h_{1L}^{33*} = 1.116 + 0.744i$ | $0.605 \pm 0.019$ | $1.818 \pm 0.008$ |
| $U_1$ | 2 | $h_{1L}^{23}h_{1R}^{33*} = -0.059 + 0.236i$, $h_{1L}^{2i}h_{1R}^{33*} = 0.234 + 0.105i$, $h_{1L}^{23}h_{1L}^{33*} = -2.002 + 0.854i$, $h_{1L}^{2i}h_{1L}^{33*} = -0.135 + 0.940i$ | $0.553 \pm 0.018$ | $1.663 \pm 0.005$ |
| $\boldsymbol{S}_3$ | 1 | $g_{3L}^{33}g_{3L}^{23*} = -0.035 + 0.032i$, $g_{3L}^{3i}g_{3L}^{23*} = 0.061 + 0.041i$ | $0.342 \pm 0.010$ | 1.027 |
| $\boldsymbol{S}_3$ | 2 | $g_{3L}^{33}g_{3L}^{23*} = -0.049 - 0.038i$, $g_{3L}^{3i}g_{3L}^{23*} = -0.01 - 0.019i$ | $0.345 \pm 0.011$ | 1.037 |
| $\boldsymbol{U}_3$ | 1 | $h_{3L}^{23}h_{3L}^{33*} = -0.032 - 0.014i$, $h_{3L}^{2i}h_{3L}^{33*} = 0.003 + 0.002i$ | $0.349 \pm 0.011$ | 1.047 |
| $\boldsymbol{U}_3$ | 2 | $h_{3L}^{23}h_{3L}^{33*} = -0.014 - 0.006i$, $h_{3L}^{2i}h_{3L}^{33*} = 0.017 - 0.007i$ | $0.340 \pm 0.010$ | 1.022 |

**Table 2.4:** The values of the $R(\Lambda_c)$ and $R_{\Lambda_c}^{Ratio}$ ratios for two representative cases of the couplings of the different leptoquark models. Above, the index $i = 1, 2$ denotes the electron and muon neutrinos. The Standard-model value of the ratio is $R(\Lambda_c) = 0.333 \pm 0.010$ [1]. The uncertainties given are due to the $\Lambda_b \to \Lambda_c$ form factor uncertainties.

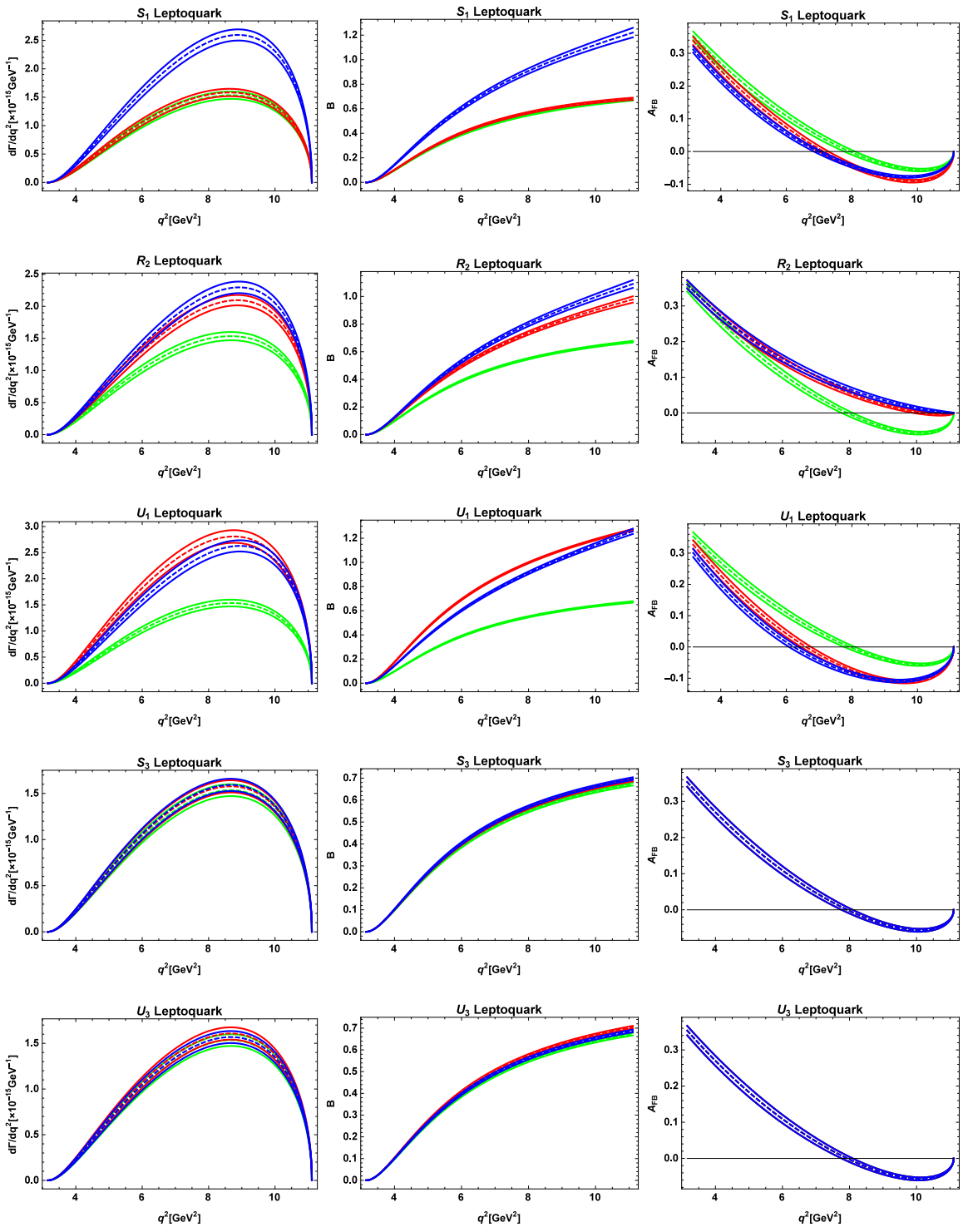


**Figure 2.14:** The effects of the different leptoquark models on the $\Lambda_b \to \Lambda_c \tau \bar{\nu}_\tau$ differential decay rate (left), the ratio of the $\Lambda_b \to \Lambda_c \tau \bar{\nu}_\tau$ and $\Lambda_b \to \Lambda_c \ell \bar{\nu}_\ell$ differential decay rates (middle), and the $\Lambda_b \to \Lambda_c \tau \bar{\nu}_\tau$ forward-backward asymmetry (right), for two representative choices of the couplings. The red and blue curves correspond to the couplings from Cases 1 and 2 in Table 2.4, respectively, while the green curves correspond to the Standard Model. Because the $\boldsymbol{S}_3$ and $\boldsymbol{U}_3$ leptoquarks produce only the vector coupling $g_L$, the forward-backward asymmetry remains equal to the Standard Model in those cases. The bands indicate the $1\sigma$ uncertainties originating from the $\Lambda_b \to \Lambda_c$ form factors.

couplings with all relevant Dirac structures where we used lattice QCD results for the $\Lambda_b \to \Lambda_c$ form factors for all possible currents.

In the first part of our phenomenological analysis, we considered individual new-physics couplings in the effective Hamiltonian in a model-independent way. After constraining these couplings using the $R(D^{(*)})$ measurements and the $B_c$ lifetime, we calculated the effects of the NP couplings in $\Lambda_b \to \Lambda_c \tau \bar{\nu}_\tau$ decays, focusing on the observables $R(\Lambda_c)$, $B_{\Lambda_c}(q^2)$, and $A_{FB}(q^2)$. Measurements of these observables can help in distinguishing among the different NP operators. For instance, the forward-backward asymmetry $A_{FB}(q^2)$ tends to be mostly above the SM value in the presence of right-handed ($g_R$) or tensor ($g_T$) couplings, but is lower than the SM value for most allowed values of the scalar ($g_S$) coupling. To illustrate the impact of a future $R(\Lambda_c)$ measurement, we presented the constraints on all couplings resulting from two possible ranges of $R(\Lambda_c)$. The baryonic decay can tightly constrain all of the couplings $g_L$, $g_R$, $g_S$, $g_P$, and $g_T$. For example, we have shown that if $R_{\Lambda_c}^{Ratio} = R(\Lambda_c)/R(\Lambda_c)^{SM}$ is observed to have a value around 1.3, the scenario with only $g_P$ becomes ruled out by the combined constraints from $R(\Lambda_c)$ and $\tau_{B_c}$.

In the second part of our phenomenological analysis, we considered the leptoquark models in which multiple NP operators are present.

We have demonstrated that some of the leptoquark models can produce large effects in the $\Lambda_b \to \Lambda_c \tau \bar{\nu}_\tau$ observables, in particular through scalar and tensor couplings. We have presented correlation plots of $R_D^{Ratio}$ and $R_{D^*}^{Ratio}$ versus $R_{\Lambda_c}^{Ratio}$, which may be helpful in discriminating among the various models.

# CHAPTER 3

# NEW PHYSICS IN INCLUSIVE $B \to X_c \tau \bar{\nu}_\tau$ DECAY IN LIGHT OF $R(D^{(*)})$ MEASUREMENTS

## 3.1 Introduction

In this chapter we study new physics (NP) effects in the inclusive $B \to X_c \tau \bar{\nu}$ decay. As we mentioned in the introduction, this decay mode is interesting since it has the same quark-level transition as in $R(D)$ and $R(D^*)$. Assuming that NP is present only in $b \to c\tau\bar{\nu}_\tau$, we make predictions for the ratio of total decay rates $R(X_c) = \frac{\Gamma(B\to X_c \tau \bar{\nu}_\tau)}{\Gamma(B\to X_c \ell \bar{\nu}_\ell)}$, with $\ell = e, \mu$, the differential decay rates, $\frac{d\Gamma}{dq^2}$ and $\frac{d\Gamma}{dE_\tau}$, the forward-backward asymmetry $A_{FB}$ (defined in Sec. 3.3), and the ratio of the differential decay rates $B(q^2) = \frac{d\Gamma(B\to X_c \tau \bar{\nu}_\tau)/dq^2}{d\Gamma(B\to X_c \ell \bar{\nu}_\ell)/dq^2}$. While we add the NP effects at tree level, we include the perturbative $O(\alpha_s)$ and nonperturbative $(1/m_b^2)$ corrections in the SM contribution in all observables that we consider here. Adding the $O(\alpha_s)$ correction to the forward-backward asymmetry $A_{FB}$ is less trivial than other observables since one has to consider the tree-body and four-body decays separately. We first implement our analysis in a model-independent approach and consider the most general dimension-6 set of NP operators that contribute to the $b \to c\tau\bar{\nu}_\tau$ decay. We then consider several leptoquark models where in some of these models more than one NP coupling at a time is present.

The theoretical prediction of the inclusive decay rate is rather precise in the SM. The differential decay rate can be expanded systematically both in terms of perturbative and nonpertur-

bative QCD corrections. Perturbative QCD corrections of $O(\alpha_s)$ to the differential decay rate were calculated in [46, 47, 48, 49]. For our purpose, the calculations in [49] are more useful, where the corrections to the five hadronic structure functions are given and the formulas for the virtual and real gluon corrections are given separately. This allows us to calculate the correction to the phenomenological aspects of the inclusive B decay such as $q^2$ and $E_\tau$ distributions, the ratio of the differential decay rates $B(q^2) = \frac{d\Gamma(B\to X_c\tau\bar{\nu}_\tau)/dq^2}{d\Gamma(B\to X_c\ell\bar{\nu}_\ell)/dq^2}$ and the forward-backward asymmetry, $A_{FB}$.

Nonperturbative corrections to the inclusive semileptonic decay, which is an expansion in $\Lambda_{QCD}/m_b$, are calculated in the context of operator product expansion (OPE) and heavy quark effective theory (HQET); see [50, 51, 52, 53], and [54]. Here $m_b$ is the heavy quark mass (the bottom quark) and $\Lambda_{QCD}$ is the nonperturbative scale parameter of the strong interactions. In the limit $m_b \to \infty$, we recover the free quark decay and the $\Lambda_{QCD}/m_b$ correction vanishes. The leading order nonperturbative correction is of order $\Lambda^2_{QCD}/m^2_b$ and is parametrized by two hadronic matrix elements, $\lambda_1$ and $\lambda_2$, which are related to the kinetic energy and the spin interaction energy of the $b$ quark in the $B$ meson, respectively. We will elaborate more on nonperturbative corrections in the next chapter where we include these corrections in the NP parts.

Higher order $O(\alpha_s^2)$ corrections to the total rate are known in the SM, but it turns out that even at order $O(\alpha_s)$, the radiative corrections to $B \to X_c\tau^-\bar{\nu}_\tau$ and $B \to X_c\ell^-\bar{\nu}_\ell$ are correlated and cancel out largely in the ratio of the decay rates $R(X_c) = \frac{\Gamma(B\to X_c\tau\bar{\nu}_\tau)}{\Gamma(B\to X_c\ell\bar{\nu}_\ell)}$ [55]. So we only consider the order $O(\alpha_s)$ correction in the ratios of the total/differential decay rates as well as in the definition of the forward-backward asymmetry. The second order QCD corrections to semileptonic $b \to c$ inclusive transitions, not considered here, can be important for the rates and the absolute differential rates [55, 56] and so the ratios should be considered cleaner probes of new physics.

For the SM predictions for $R(D^{(*)})$ in this chapter, we use the results of the fits given by [10] and [13] for $R(D) = 0.299 \pm 0.003$ and $R(D^*) = 0.255 \pm 0.004$ respectively. The experimental averages of $R(D)$ and $R(D^*)$ measurements evaluated by the Heavy-Flavor Averaging Group are

[9]

$$R(D)_{exp} = 0.407 \pm 0.039 \pm 0.024, \tag{3.1}$$

$$R(D^*)_{exp} = 0.304 \pm 0.013 \pm 0.007. \tag{3.2}$$

The combined analysis of $R(D)$ and $R(D^*)$, taking into account measurement correlations, finds that the deviation is at the level of $4.1\,\sigma$ from the SM prediction [9]. In our calculations, we construct the ratios of the experimental results (3.1) and (3.2) to the phenomenological SM predictions,

$$\begin{aligned} R(D)^{Ratio} &= \frac{R(D)_{exp}}{R(D)_{SM}} = 1.36 \pm 0.15, \\ R(D^*)^{Ratio} &= \frac{R(D^*)_{exp}}{R(D^*)_{SM}} = 1.19 \pm 0.06. \end{aligned} \tag{3.3}$$

We use the values in Eq. (3.3) to find the allowed parameter space of the NP models. By taking one operator at a time, we fix the size of the operators by fitting to the measurements in Eq. (3.3) and then we make predictions for several observables in the inclusive decay.

This chapter is organized as follows: The effective Hamiltonian of the NP interactions and helicity amplitudes of the inclusive B decay are presented in Sec. 3.2. In Sec. 3.3, the power correction and the radiative correction of order $O(\alpha_s)$ are discussed. The model-independent phenomenological analysis of individual new-physics couplings is considered in Sec. 3.4, and leptoquark models are considered in Sec. 3.5. And finally we conclude in Sec. 3.6.

## 3.2 Formalism

### 3.2.1 Effective Hamiltonian

The effective Hamiltonian of the NP operators for the quark-level transition $b \to c\tau^-\bar{\nu}_\tau$ can be written in the form

$$\begin{aligned}\mathcal{H}_{eff} &= \frac{G_F V_{cb}}{\sqrt{2}}\Big\{\Big[\bar{c}\gamma_\mu(1-\gamma_5)b + g_L\bar{c}\gamma_\mu(1-\gamma_5)b + g_R\bar{c}\gamma_\mu(1+\gamma_5)b\Big]\bar{\tau}\gamma^\mu(1-\gamma_5)\nu_\tau \\ &+\Big[g_S\bar{c}b + g_P\bar{c}\gamma_5 b\Big]\bar{\tau}(1-\gamma_5)\nu_\tau + \Big[g_T\bar{c}\sigma^{\mu\nu}(1-\gamma_5)b\Big]\bar{\tau}\sigma_{\mu\nu}(1-\gamma_5)\nu_\tau + H.c.\Big\},\end{aligned} \tag{3.4}$$

where $G_F$ is the Fermi constant, $V_{cb}$ is the CKM matrix element, and we use $\sigma_{\mu\nu} = i[\gamma_\mu, \gamma_\nu]/2$. When $g_L = g_R = g_S = g_P = g_T = 0$, the above equation produces the SM effective Hamiltonian. Here, we consider only the active neutrinos which are left chiral. In the presence of new physics, in general, the $\tau$ lepton can be associated with any neutrino flavor. To allow for lepton universality violation, we assume NP to dominantly affect the third generation leptons.

### 3.2.2 Decay process

In this section we present the calculations of the inclusive B decay at the free quark level with new-physics contributions. The process under consideration is

$$b(p_b) \to \tau^-(p_\tau) + \bar{\nu}_\tau(p_{\bar{\nu}_\tau}) + c(p_c).$$

The differential decay rate is

$$d\Gamma = \frac{1}{2m_b}\frac{G_F^2|V_{cb}|^2}{4}\sum_{\lambda_c}\sum_{\lambda_\tau}|\mathcal{M}_{\lambda_c}^{\lambda_\tau}|^2 d\Phi_3, \tag{3.5}$$

where $d\Phi_3$ is the three-body phase space which can be written as

$$d\Phi_3 = \frac{\sqrt{\lambda(m_b^2, m_c^2, q^2)}}{256\pi^3 m_b^2}\left(1 - \frac{m_\tau^2}{q^2}\right) dq^2 d(\cos\theta_\tau), \tag{3.6}$$

with

$$q = p_b - p_c, \tag{3.7}$$

$$\lambda(a,b,c) = a^2 + b^2 + c^2 - 2ab - 2ac - 2bc\,. \tag{3.8}$$

The angle $\theta_\tau$ is defined as the angle between the momenta of the $\tau$ lepton and the $b$ quark in the dilepton rest frame.

The helicity amplitude $\mathcal{M}_{\lambda_c}^{\lambda_\tau}$ is written as [57]

$$\mathcal{M}_{\lambda_c}^{\lambda_\tau} = H_{\lambda_c,\lambda=0}^{SP} L^{\lambda_\tau} + \sum_{\lambda} \eta_\lambda H_{\lambda_c,\lambda}^{VA} L_\lambda^{\lambda_\tau} + \sum_{\lambda,\lambda'} \eta_\lambda \eta_{\lambda'} H_{\lambda_c,\lambda,\lambda'}^{(T)\lambda_b} L_{\lambda,\lambda'}^{\lambda_\tau}. \tag{3.9}$$

Here, ($\lambda$, $\lambda'$) indicate the helicity of the virtual vector boson, $\lambda_c$ and $\lambda_\tau$ are the helicities of the $c$ quark and the $\tau$ lepton, respectively, and $\eta_\lambda = 1$ for $\lambda = t$ and $\eta_\lambda = -1$ for $\lambda = 0, \pm 1$. The explicit expressions for the hadronic ($H_{\lambda_c}$) and leptonic ($L^{\lambda_\tau}$) helicity amplitudes are presented in Appendix B.

### 3.3 QCD correction to differential decay rates and forward-backward asymmetry

From the twofold decay distribution (3.5), one may obtain expressions for various observables at the free quark level. These expressions in terms of hadronic helicity amplitudes are presented in Appendix D.

Here we shortly discuss the inclusion of QCD corrections to the differential rates. In [49], the hadronic tensor of the transition $b \to c$ is parametrized in terms of five hadronic structure functions. The QCD corrections to these structure functions are calculated to $O(\alpha_s)$ and generic BLM ($\alpha_s^n \beta_0^{n-1}$) order, and numerical results are given in the massless lepton case. This correction con-

sists of two parts: loop correction, which is the virtual part and has the same kinematics as the three-body decay, and the real gluon emission (four-body decay) which has an infrared divergence that cancels out with the divergence in the loop contribution.

Here, using the results of [49], we add the $O(\alpha_s)$ correction to the differential decay rates and forward-backward asymmetry in the case where the final lepton is massive. To add the $O(\alpha_s)$ correction, one should find the appropriate integration intervals for the three-body (four-body) decay in the case of loop correction (real gluon emission). Since the correction to the triple differential distribution for $b \to c l \bar{\nu}_l$ is given as a function of the lepton energy, it is more convenient to introduce the definitions of the forward and backward terms in the forward-backward asymmetry ($A_{FB}$) [Eq. (3.12)] in terms of the lepton energy rather than the $\tau$ scattering angle $\theta_\tau$. Therefore, the integration is done over the lepton energy rather than the angle $\theta_\tau$.

In Appendix C, we find the relation between the $\tau$ energy $E_\tau$, which is defined in the $b$ quark's rest frame, and the angle $\theta_\tau$ defined in the dilepton's rest frame. A comprehensive study of decay kinematics is given in [58].

For the energy $E_\tau$ in four-body decay we find (see Appendix C)

$$E_\tau = \frac{1}{4m_b q^2}\left[(m_b^2 + q^2 - r^2)(m_\tau^2 + q^2) - (q^2 - m_\tau^2)\sqrt{\lambda(m_b^2, q^2, r^2)}\cos(\theta_\tau)\right], \tag{3.10}$$

where $q^2$ and $r^2$ are the invariant masses of the dilepton and the charm-quark/gluon systems, respectively. For three-body decay $r^2$ reduces to $m_c^2$. From the above equation we can find the bounds on the $\tau$ energy by $\cos(\theta_\tau) = \pm 1$,

$$E_\tau^{\pm} = \frac{1}{4m_b q^2}\left[(m_b^2 + q^2 - r^2)(m_\tau^2 + q^2) \pm (q^2 - m_\tau^2)\sqrt{\lambda(m_b^2, q^2, r^2)}\right]. \tag{3.11}$$

Using this equation we can easily calculate the forward-backward asymmetry by performing the integration over $E_\tau$ instead of $\cos(\theta_\tau)$. We therefore define the forward-backward asymmetry in

| Parameter | Value |
|---|---|
| $m_b$ | $4.71 \pm 0.05\ GeV$ |
| $\delta m_{bc}$ | $3.40 \pm 0.02\ GeV$ |
| $\lambda_1$ | $-0.30\ GeV^2 \pm 25\%$ |
| $\lambda_2$ | $0.12\ GeV^2 \pm 25\%$ |
| $\alpha_s$ | $0.218^{+0.065}_{-0.040}$ |

**Table 3.1:** Parameters used in numerical results.

the case of four-body decay as

$$A_{FB} = \frac{\int (\int_{E_\tau^-}^{E_\tau^0} \frac{d\Gamma}{dq^2 dr^2 dE_\tau} dE_\tau - \int_{E_\tau^0}^{E_\tau^+} \frac{d\Gamma}{dq^2 dr^2 dE_\tau} dE_\tau) dr^2}{\frac{d\Gamma}{dq^2}}, \tag{3.12}$$

where $E_\tau^0 = \frac{(m_b^2+q^2-r^2)(m_\tau^2+q^2)}{4m_b q^2}$. Note that the integration over $r^2$ appears only in the case of the four-body decay.

## 3.4 Model-independent analysis of individual new-physics couplings

In this section we consider one NP coupling at a time. Constraints on NP parameters are considered from the existing measurements of $R(D)$ and $R(D^*)$ mesons and from the $B_c$ lifetime. The $B_c$ measurement does not have any significant effect on the constraints except for the $g_P$ coupling. (In general, NP couplings are taken to be complex. Nevertheless, in the numerical analysis of $R(X_c)$, Fig. 3.1 and Tables 3.3 and 3.4, we take these couplings to be real for simplicity.)

We require the NP couplings to reproduce the measurements of $R_D^{Ratio}$ and $R_{D^*}^{Ratio}$ within the $3\sigma$ range. The coupling $g_S(g_P)$ only contributes to $R_D^{Ratio}(R_{D^*}^{Ratio})$ while the other couplings contribute to both channels. The constraint due to $B_c$ has been considered before in [38, 36, 37]. Here we follow the same procedure and use an upper limit of $\mathcal{B}(B_c \to \tau^- \bar{\nu}_\tau) \leq 30\%$, and we take $f_{B_c} = 0.434(15)$ GeV from lattice QCD [40], to impose this constraint on the NP coupling $g_P$. For numerical inputs we use the $1S$ mass scheme for the quark masses (see [59, 60] and [54]). We use the parameters as given in [54], and they are presented in Table 3.1.

The SM prediction for the ratio of decay rates becomes

$$R(X_c)_{SM} = \frac{\mathcal{B}(B \to X_c \tau \bar{\nu})}{\mathcal{B}(B \to X_c \ell \bar{\nu})} = 0.221 \pm 0.005, \tag{3.13}$$

which is comparable with the central value of $R(X_c)_{SM} = 0.222$ given in [37] and $R(X_c)_{SM} = 0.223$ in [54, 61] where they add in addition the $O(\alpha_s^2)$ correction to the total rate.

Power correction of order $1/m_b^3$ to this decay rate has been calculated in [62]. Taking into account this correction will result in a reduction of $\sim 7\%$ in $R(X_c)$ which is a noticeable effect. Nevertheless, in order to be consistent throughout this work we do not consider this correction for our numerical study and we present all observables calculated up to the same perturbative and nonperturbative order.

We now consider the effect of NP models on the total inclusive decay rate. There is an ALEPH measurement [63]

$$\mathcal{B}(b \to X \tau^- \bar{\nu}_\tau)_{exp} = (2.43 \pm 0.32) \times 10^{-2}, \tag{3.14}$$

where $X = X_c + X_u$ are all possible states from $b \to c$ and $b \to u$ transitions. In some part of our analysis we will use the above measurement as an experimental input. When we do that we will set the ALEPH measurement to the inclusive rate for $\mathcal{B}(B \to X_c \tau^- \bar{\nu}_\tau)$. The ALEPH measurement represents the inclusive decays of a mixture of $b$ hadrons and in the leading order in the heavy quark expansion all $b$ hadrons have the same width. Moreover, we will neglect the small $b \to X_u \tau^- \bar{\nu}_\tau$ transition.

Using the world average for the semileptonic branching ratio into the light lepton [9],

$$\mathcal{B}(B \to X_c \ell^- \bar{\nu}_\ell)_{exp} = (10.65 \pm 0.16) \times 10^{-2}, \tag{3.15}$$

we can find for the ratio

$$R(X_c)_{exp} = 0.228 \pm 0.030. \tag{3.16}$$

In Fig. 3.1 we plot the effect of the new physics scenarios on the ratio of total inclusive decay rates

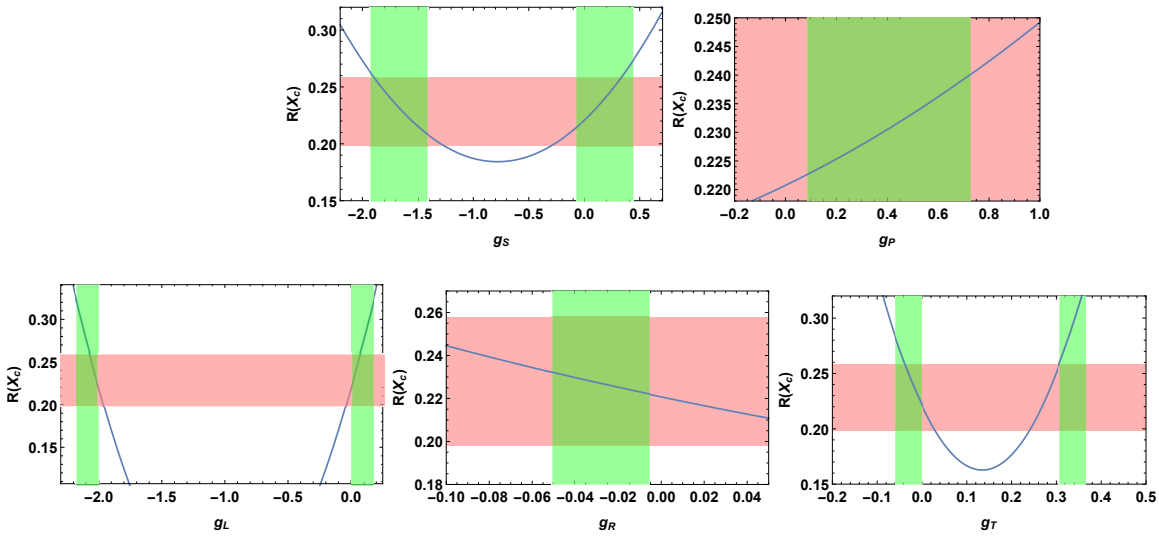


**Figure 3.1:** The effect of real NP couplings on the ratio of total decay rates $R(X_c)$ (blue lines). The pink shaded areas are the allowed regions within $1\sigma$ of the central value for $R(X_c)_{exp}$ and the green shaded areas are constraints on the couplings due to measurements of $R(D)$ and $R(D^*)$ and the branching ratio of $B_c$.

$R(X_c)$ (blue lines) by taking the NP couplings to be real. The pink shaded areas show the allowed range of measured $R(X_c)$, within $1\sigma$ using (3.16) and the green shaded areas are constraints (on the couplings) due to the measurements of $R(D)$ and $R(D^*)$ within a $3\sigma$ interval and the branching ratio of $B_c$. As we can see from the figure, for the $g_S$, $g_L$ and $g_T$ couplings, the experimental ($1\sigma$) bounds on $R(X_c)$ can reduce the allowed parameter space for the NP couplings. This effect is more pronounced for the $g_L$ and $g_T$ couplings where a significant part of the allowed coupling values are excluded by $R(X_c)$. The allowed values of the couplings are given in Table 3.2. On the other hand if the ALEPH result is not used as an input, large deviations from the SM are possible for the inclusive rate. As an illustration, in Tables 3.3 and 3.4 we present maximum and minimum values of $R(D^{(*)})$ in each model by considering the measurements of $R(D^{(*)})$ and the branching ratio of $B_c$ as constraints, and we compare them with the corresponding values when we add the inclusive measurement as another constraint.

Now we consider differential rates and we first consider effects of perturbative and non-perturbative corrections to the differential rates in the SM. In Fig. 3.2 we plot the differential distributions, $\frac{1}{\Gamma_0}\frac{d\Gamma}{dq^2}$ and $\frac{1}{\Gamma_0}\frac{d\Gamma}{dE_\tau}$, the ratio of the differential decay rate $B = \frac{d\Gamma(B\to X_c\tau\bar{\nu}_\tau)/dq^2}{d\Gamma(B\to X_c\ell\bar{\nu}_\ell)/dq^2}$, and

| Coupling | Allowed value |
|---|---|
| $g_S$ | $(-1.89, -1.42)$ and $(-0.07, 0.33)$ |
| $g_P$ | $(0.09, 0.73)$ |
| $g_L$ | $(-2.07, -2.01)$ and $(0.01, 0.07)$ |
| $g_R$ | $(-0.05, -0.01)$ |
| $g_T$ | $(-0.04, 0)$ |

**Table 3.2:** Allowed values of the coupling constants taken from Fig. 3.1.

| | Max/Min Values<br>Without (With) Inclusive Constraint<br>$g_S$ or $g_P$ | Max/Min Values<br>Without (With) Inclusive Constraint<br>$g_L$ |
|---|---|---|
| $R(D)^{Ratio}$ | 1.83/0.90 (1.75/0.90)<br>*at* $g_S$ = –1.92 or 0.43 / –1.42 or –0.07<br>($g_S$ = –1.89/–1.42 or –0.07 ) | 1.38/1.01 (1.14/1.01)<br>*at* $g_L = -2.17$ or 0.17 / $-2$ or 0.005<br>($g_L = -2.07$ or 0.07 / $-2$ or 0.005) |
| $R(D)$ | 0.545/0.269 (0.523/0.269)<br>*at* $g_S$ = –1.92 or 0.43 / -1.42 or -0.07<br>($g_S$ = –1.89/–1.42 or –0.07) | 0.410/0.301 (0.340/0.301)<br>*at* $g_L = -2.17$ or 0.17 / $-2$ or 0.005<br>($g_L = -2.07$ or 0.07 / $-2$ or 0.005) |
| $R(D^*)^{Ratio}$ | 1.10/1.01 (1.10/1.01)<br>*at* $g_P$ = 0.726/0.087<br>($g_P$ = 0.726/0.087) | 1.38/1.01 (1.14/1.01)<br>*at* $g_L = -2.17$ or 0.17 / $-2$ or 0.005<br>($g_L = -2.07$ or 0.07 / $-2$ or 0.005) |
| $R(D^*)$ | 0.281/0.257 (0.281/0.257)<br>*at* $g_P$ = 0.726/0.087<br>($g_P$ = 0.726/0.087) | 0.351/0.257 (0.290/0.257)<br>*at* $g_L = -2.17$ or 0.17 / $-2$ or 0.005<br>($g_L = -2.07$ or 0.07 / $-2$ or 0.005) |

**Table 3.3:** Comparing maximum and minimum values of $R(D^{(*)})$ by using measurements of $R(D^{(*)})$ and the branching ratio of $B_c$ without (with) adding the inclusive measurement as a constraint.

| | Max/Min Values<br>Without (With) Inclusive Constraint<br>$g_R$ | Max/Min Values<br>Without (With) Inclusive Constraint<br>$g_T$ |
|---|---|---|
| $R(D)^{Ratio}$ | 0.99/0.90 (0.99/0.90)<br>$at\ g_R = -0.006/-0.05$<br>$(g_R = -0.006/-0.05)$ | 1.41/0.95 (1.00/0.97)<br>$at\ g_T = 0.365/-0.058$<br>$(g_T = -0.002/-0.038)$ |
| $R(D)$ | 0.295/0.269 (0.295/0.269)<br>$at\ g_R = -0.006/-0.05$<br>$(g_R = -0.006/-0.05)$ | 0.421/0.283 (0.298/0.288)<br>$at\ g_T = 0.365/-0.058$<br>$(g_T = -0.002/-0.038)$ |
| $R(D^*)^{Ratio}$ | 1.09/1.01 (1.09/1.01)<br>$at\ g_R = -0.05/-0.006$<br>$(g_R = -0.05/-0.006)$ | 1.38/1.01 (1.23/1.01)<br>$at\ g_T = 0.365$ or $-0.058$ / $0.309$ or $-0.002$<br>$(g_T = -0.038/-0.002)$ |
| $R(D^*)$ | 0.278/0.257 (0.278/0.257)<br>$at\ g_R = -0.05/-0.006$<br>$(g_R = -0.05/-0.006)$ | 0.351/0.257 (0.314/0.257)<br>$at\ g_T = 0.365$ or $-0.058$ / $0.309$ or $-0.002$<br>$(g_T = -0.038/-0.002)$ |

**Table 3.4:** Comparing maximum and minimum values of $R(D^{(*)})$ by using measurements of $R(D^{(*)})$ and the branching ratio of $B_c$ without (with) adding the inclusive measurement as a constraint.

the forward-backward asymmetry $A_{FB}$ in Eq. (3.12) in the SM at leading and next-to-leading order and with the $1/m_b^2$ correction. We normalize these observables to $\Gamma_0$ where

$$\Gamma_0 = \frac{G_F^2 |V_{cb}|^2 m_b^5}{192\pi^3}. \tag{3.17}$$

As shown, the radiative correction to $B$ and $A_{FB}$ is not as effective as in the case of $d\Gamma/dq^2$ or $d\Gamma/dE_\tau$. In general, we expect higher order perturbative corrections to affect the $q^2$ and the $E_\tau$ distributions by larger amounts compared to the $B$ and the $A_{FB}$ observables which involve ratios of differential quantities. The $1/m_b^2$ correction has a considerable effect on all observables except the ratio of differential branching ratios, $B$. In this observable the power correction becomes noticeable only close to the end point region. In general however, one should be careful when interpreting the power corrections locally as the OPE breaks down near the end points.

In Figures 3.3 - 3.6 we present the effects of different NP couplings on the observables $\frac{1}{\Gamma_0}\frac{d\Gamma}{dq^2}$, $\frac{1}{\Gamma_0}\frac{d\Gamma}{dE_\tau}$, $B$, and $A_{FB}$ by considering one coupling at a time. In these plots, the SM uncertainties to the observables are shown as error bars. To calculate these uncertainties we use the numerical values in Table 3.1 and propagate the uncertainties for each observable. To account for $O(\alpha_s^2)$ corrections

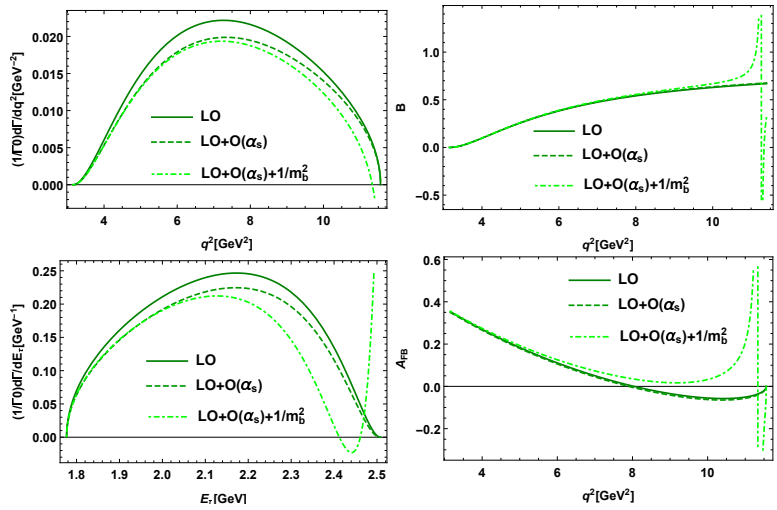


**Figure 3.2:** The differential decay rates $(1/\Gamma_0)d\Gamma/dq^2$ and $(1/\Gamma_0)d\Gamma/dE_\tau$, the ratio of the differential decay rates $B$, and forward-backward asymmetry $A_{FB}$ at leading (solid line), next-to-leading (dashed line) and next-to-leading order with $1/m_b^2$ correction (dashed-dotted line) for the process $B \to X_c\tau^-\bar{\nu}_\tau$.

for each observable, we use the calculations in [55] where the $O(\alpha_s)$ and $O(\alpha_s^2)$ orders contribute to the total decay rate with the amount of about 10% and 6% of the leading order, respectively. Therefore, we assume the unknown higher order contributions in the differential distributions to follow the same ratios. We estimate the errors due to $O(\alpha_s^2)$ corrections to be $\pm 70\%$ of the $O(\alpha_s)$ correction and add this estimate as an uncertainty to the differential decay rates. For the two observables $B$ and $A_{FB}$, we see that these uncertainties are considerably smaller.

Except for the $g_P$ coupling which is tightly constrained by $B_c$, we see that NP models can have considerable effects on these observables in general. In particular we see that $A_{FB}$ can have zero crossings and take negative values unlike the SM for some NP couplings.

## 3.5 Leptoquark model results

In this section we introduce leptoquark models that can be the origin of the general couplings in the effective Hamiltonian (3.4). In the last chapter we considered these models in detail. To be self-contained, here we briefly describe how these models generate the couplings in the effective Hamiltonian (3.4). The Lagrangian that generates the contributions to $b \to c\tau^-\bar{\nu}_\tau$ is given by

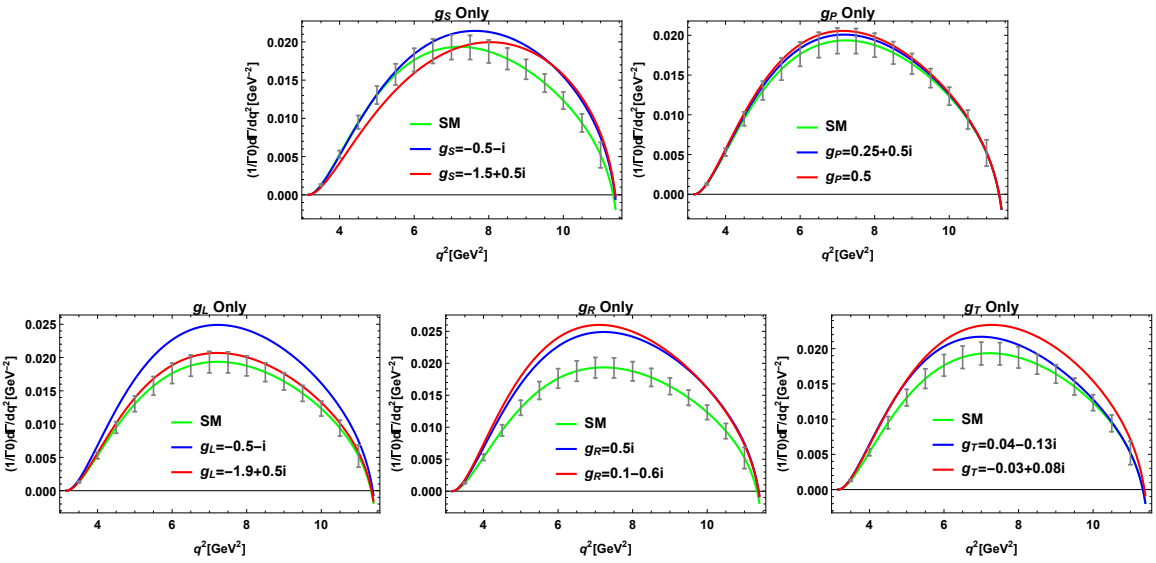


**Figure 3.3:** The effect of individual new-physics couplings on the $B \to X_c \tau^- \bar{\nu}_\tau$ differential decay rate $(1/\Gamma_0) d\Gamma/dq^2$, including the QCD $O(\alpha_s)$ and $1/m_b^2$ correction in the SM contribution only. Each plot shows the observable in the Standard Model and for two allowed values of the new-physics couplings.

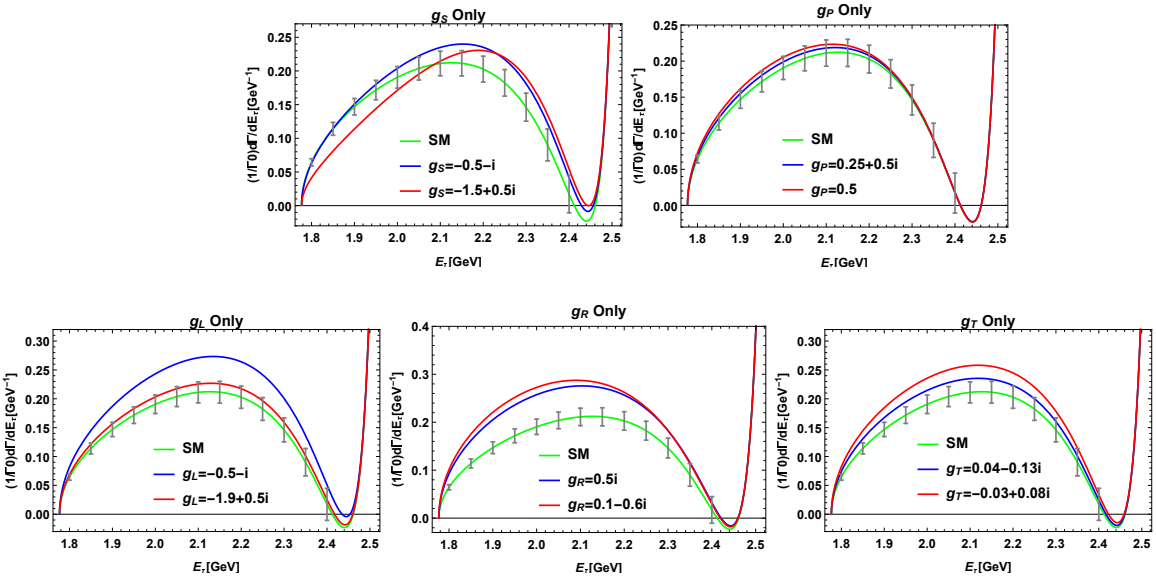


**Figure 3.4:** The effect of individual new-physics couplings on the $B \to X_c \tau^- \bar{\nu}_\tau$ differential decay rate $(1/\Gamma_0) d\Gamma/dE_\tau$, including the QCD $O(\alpha_s)$ and $1/m_b^2$ correction in the SM contribution only. Each plot shows the observable in the Standard Model and for two allowed values of the new-physics couplings.

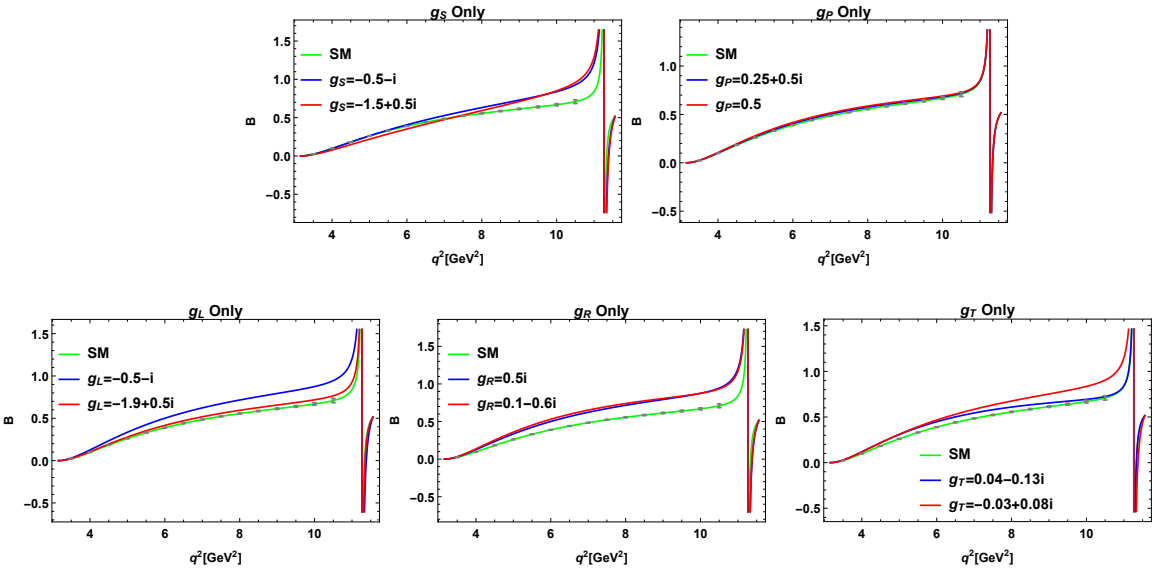


**Figure 3.5:** The effect of individual new-physics couplings on the $B$ ratio, including the QCD $O(\alpha_s)$ and $1/m_b^2$ correction in the SM contribution only. Each plot shows the observable in the Standard Model and for two allowed values of the new-physics couplings.

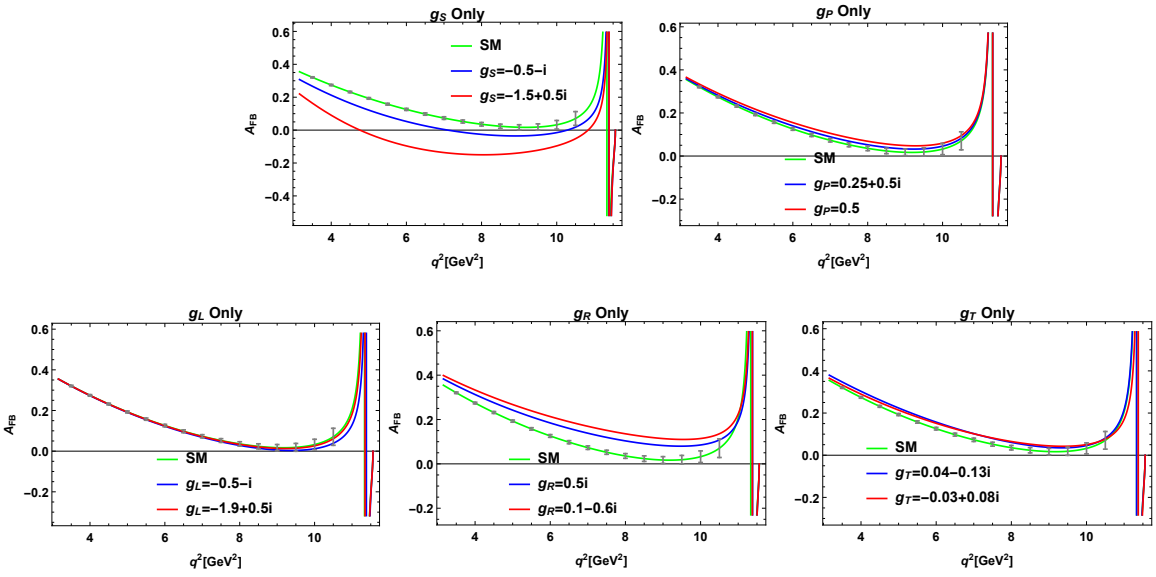


**Figure 3.6:** The effect of individual new-physics couplings on the $B \to X_c \tau^- \bar{\nu}_\tau$ forward-backward asymmetry $A_{FB}$, including the QCD $O(\alpha_s)$ and $1/m_b^2$ correction in the SM contribution only. Each plot shows the observable in the Standard Model and for two allowed values of the new-physics couplings.

$$
\begin{aligned}
\mathcal{L}^{\rm LQ} &= \mathcal{L}^{\rm LQ}_{F=0} + \mathcal{L}^{\rm LQ}_{F=-2}\,, \\
\mathcal{L}^{\rm LQ}_{F=0} &= (h^{ij}_{1L}\bar{Q}_{iL}\gamma^\mu L_{jL} + h^{ij}_{1R}\bar{d}_{iR}\gamma^\mu \ell_{jR})U_{1\mu} + h^{ij}_{3L}\bar{Q}_{iL}\vec{\sigma}\gamma^\mu L_{jL}\cdot\vec{U}_{3\mu} \\
&\quad + (h^{ij}_{2L}\bar{u}_{iR}L_{jL} + h^{ij}_{2R}\bar{Q}_{iL}i\sigma_2\ell_{jR})R_2 + h.c., \\
\mathcal{L}^{\rm LQ}_{F=-2} &= (g^{ij}_{1L}\bar{Q}^c_{iL}i\sigma_2 L_{jL} + g^{ij}_{1R}\bar{u}^c_{iR}\ell_{jR})S_1 + (g^{ij}_{3L}\bar{Q}^c_{iL}i\sigma_2\vec{\sigma}L_{jL})\cdot\vec{S}_3 \\
&\quad + (g^{ij}_{2L}\bar{d}^c_{iR}\gamma_\mu L_{jL} + g^{ij}_{2R}\bar{Q}^c_{iL}\gamma_\mu\ell_{jR})V^\mu_2 + h.c.\,. \qquad (3.18)
\end{aligned}
$$

After integrating out the LQs and performing the convenient Fierz transformations we find that these models can generate scalar $(g_S, g_P)$; vector $(g_L)$; and tensor $(g_T)$ couplings as follows:

- The $\boldsymbol{S}_3$ and $\boldsymbol{U}_3$ triplet scalar and vector leptoquarks generate the vector coupling $g_L$.
- The $U_1$ singlet vector leptoquark generates scalar $(g_S, g_P)$ and vector $(g_L)$ couplings.
- The $R_2$ doublet scalar leptoquark generates scalar $(g_S, g_P)$ and tensor $(g_T)$ couplings.
- The $S_1$ singlet scalar leptoquark generates scalar $(g_S, g_P)$, vector $(g_L)$ and tensor $(g_T)$ couplings.

The leptoquark Lagrangian generates these couplings in the following way:

$$
\begin{aligned}
g_S &= \frac{\sqrt{2}}{4G_F V_{cb}}\sum_{k=1}^{3} V_{k3}\left[-\frac{2g^{kl}_{2L}g^{23*}_{2R}}{M^2_{V_2}} - \frac{2h^{2l}_{1L}h^{k3*}_{1R}}{M^2_{U_1}} - \frac{g^{kl}_{1L}g^{23*}_{1R}}{2M^2_{S_1}} - \frac{h^{2l}_{2L}h^{k3*}_{2R}}{2M^2_{R_2}}\right], \qquad (3.19)\\
g_P &= \frac{\sqrt{2}}{4G_F V_{cb}}\sum_{k=1}^{3} V_{k3}\left[-\frac{2g^{kl}_{2L}g^{23*}_{2R}}{M^2_{V_2}} - \frac{2h^{2l}_{1L}h^{k3*}_{1R}}{M^2_{U_1}} + \frac{g^{kl}_{1L}g^{23*}_{1R}}{2M^2_{S_1}} + \frac{h^{2l}_{2L}h^{k3*}_{2R}}{2M^2_{R_2}}\right], \qquad (3.20)\\
g_L &= \frac{\sqrt{2}}{4G_F V_{cb}}\sum_{k=1}^{3} V_{k3}\left[\frac{g^{kl}_{1L}g^{23*}_{1L}}{2M^2_{S_1}} - \frac{g^{kl}_{3L}g^{23*}_{3L}}{2M^2_{S_3}} + \frac{h^{2l}_{1L}h^{k3*}_{1L}}{M^2_{U_1}} - \frac{h^{2l}_{3L}h^{k3*}_{3L}}{M^2_{U_3}}\right], \qquad (3.21)\\
g_R &= 0, \qquad (3.22)\\
g_T &= \frac{\sqrt{2}}{4G_F V_{cb}}\sum_{k=1}^{3} V_{k3}\left[\frac{g^{kl}_{1L}g^{23*}_{1R}}{8M^2_{S_1}} - \frac{h^{2l}_{2L}h^{k3*}_{2R}}{8M^2_{R_2}}\right], \qquad (3.23)
\end{aligned}
$$

where $g^{ij}$ and $h^{ij}$ are the leptoquark couplings with $i(j)$ indicating the generation of quarks (leptons) and $M$'s are leptoquark masses with the subscripts corresponding to the leptoquark type. One should run these couplings down to the $b$ quark mass scale as they are defined at the leptoquark mass scale ($\sim 1\,TeV$). Here $V_{k3}$ corresponds to the CKM matrix element, with 3 referring to the bottom quark. We neglect the CKM-suppressed contributions from $k = 1$ and $k = 2$.

The leptoquark couplings can also be constrained by $b \to s\nu\bar{\nu}$ decays, so we also consider the exclusive $B \to K^{(*)}\nu\bar{\nu}$ decays in our analysis. Following Ref. [28], the $b \to s\nu_j\bar{\nu}_i$ process can be described by the effective Hamiltonian,

$$H_{eff} = \frac{4G_F}{\sqrt{2}} V_{tb}V_{ts}^* \left[ \left( \delta_{ij} C_L^{(\mathrm{SM})} + C_L^{ij} \right) O_L^{ij} + C_R^{ij} O_R^{ij} \right] , \tag{3.24}$$

where the left-handed and right-handed operators are defined as

$$\begin{aligned} O_L^{ij} &= (\bar{s}_L \gamma^\mu b_L)(\bar{\nu}_{jL} \gamma_\mu \nu_{iL}) , \\ O_R^{ij} &= (\bar{s}_R \gamma^\mu b_R)(\bar{\nu}_{jL} \gamma_\mu \nu_{iL}) . \end{aligned} \tag{3.25}$$

The SM Wilson coefficient $C_L^{(\mathrm{SM})}$ receives contributions from the box and the $Z$-penguin diagrams, which yield

$$C_L^{(\mathrm{SM})} = \frac{\alpha}{2\pi \sin^2\theta_W} X(m_t^2/M_W^2) , \tag{3.26}$$

where the loop function $X(x_t)$ can be found e.g. in Ref. [45]. Leptoquarks produce contributions to $C_L^{ij}$ which, to leading order, are equal to [28]

$$C_L^{ij} = -\frac{1}{2\sqrt{2}G_F V_{tb}V_{ts}^*} \left[ \frac{g_{1L}^{3i} g_{1L}^{2j*}}{2M_{S_1}^2} + \frac{g_{3L}^{3i} g_{3L}^{2j*}}{2M_{S_3}^2} - \frac{2h_{3L}^{2i} h_{3L}^{3j*}}{M_{U_3}^2} \right] . \tag{3.27a}$$

Now we obtain the common coefficients for the $b \to c\tau\bar{\nu}_l$ and $b \to s\nu_\tau\bar{\nu}_l$ processes,

$$C_L^{l3} = -\frac{1}{2\sqrt{2}G_F V_{tb}V_{ts}^*}\left[\frac{g_{1L}^{3l}g_{1L}^{23*}}{2M_{S_1}^2} + \frac{g_{3L}^{3l}g_{3L}^{23*}}{2M_{S_3}^2} - \frac{2h_{3L}^{2l}h_{3L}^{33*}}{M_{U_3}^2}\right]. \tag{3.28a}$$

Hence, for $l = 3$ we obtain

$$\frac{\mathcal{B}_K^{\text{SM+NP}}}{\mathcal{B}_K^{\text{SM}}} = \frac{\mathcal{B}_{K^*}^{\text{SM+NP}}}{\mathcal{B}_{K^*}^{\text{SM}}} = \left|\frac{3C_L^{(\text{SM})} + C_L^{33}}{3C_L^{(\text{SM})}}\right|^2, \tag{3.29}$$

while for $l = 1, 2$ we have

$$\frac{\mathcal{B}_K^{\text{SM+NP}}}{\mathcal{B}_K^{\text{SM}}} = \frac{\mathcal{B}_{K^*}^{\text{SM+NP}}}{\mathcal{B}_{K^*}^{\text{SM}}} = \left|\frac{C_L^{l3}}{3C_L^{(\text{SM})}}\right|^2. \tag{3.30}$$

Now we apply leptoquark models to the inclusive decay $B \to X_c\tau^-\bar{\nu}_\tau$. In leptoquark models in general, we can have all neutrino generations coupled to the $\tau$ lepton as NP effects. We impose the constraints on all the leptoquark couplings simultaneously from the experimental measurements of $R(D)$ and $R(D^*)$ within a $3\,\sigma$ confidence level, as well as $\tau_{B_c}$ and $\mathcal{B}(B \to K^{(*)}\nu\bar{\nu})$. Then, we substitute the allowed values of the couplings in the calculations of $R_D^{Ratio}$, $R_{D^*}^{Ratio}$, and $R_{X_c}^{Ratio}$ to demonstrate the allowed regions of these observables in the presence of each leptoquark model. The results are presented in Fig. 3.7.

Since in leptoquark models in general, there can be multiple NP couplings present (as opposed to model independent scenarios where one coupling at a time is considered), in Figs. 3.8 - 3.12, we present the effect of different leptoquark models ($S_1$, $R_2$, $U_1$, $\boldsymbol{S}_3$, $\boldsymbol{U}_3$) for some allowed values of the model parameters on the inclusive decay $B \to X_c\tau^-\bar{\nu}_\tau$ observables. $\boldsymbol{S}_3$ and $\boldsymbol{U}_3$ models are tightly constrained and only small effects are possible, while other models can have large effects on the considered observables. This can be seen in the correlation plots in the $R_{X_c}^{Ratio} - R_D^{Ratio}$ and $R_{X_c}^{Ratio} - R_{D^*}^{Ratio}$ planes where in the $\boldsymbol{S}_3$ and $\boldsymbol{U}_3$ models we see small deviations of the $R$ values from

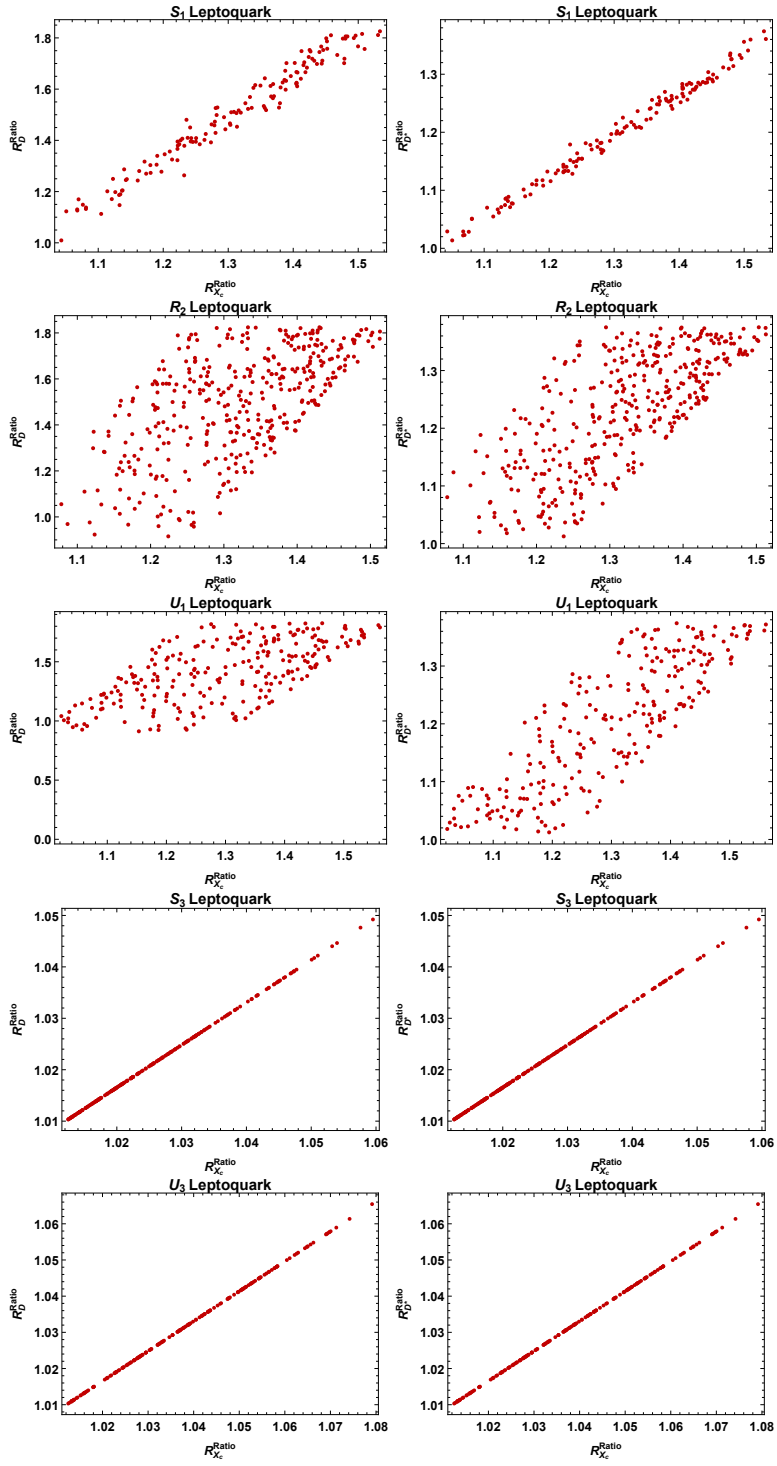


**Figure 3.7:** The allowed regions in the $R_{X_c}^{Ratio} - R_D^{Ratio}$ and $R_{X_c}^{Ratio} - R_{D^*}^{Ratio}$ planes for each leptoquark model where the couplings are constrained by measurements of $R(D)$ and $R(D^*)$, the branching ratio of $B_c \to \tau^- \bar{\nu}_\tau$, and are consistent with the upper bounds on $\mathcal{B}(B \to K^{(*)} \nu \bar{\nu})$ at 90% C.L.

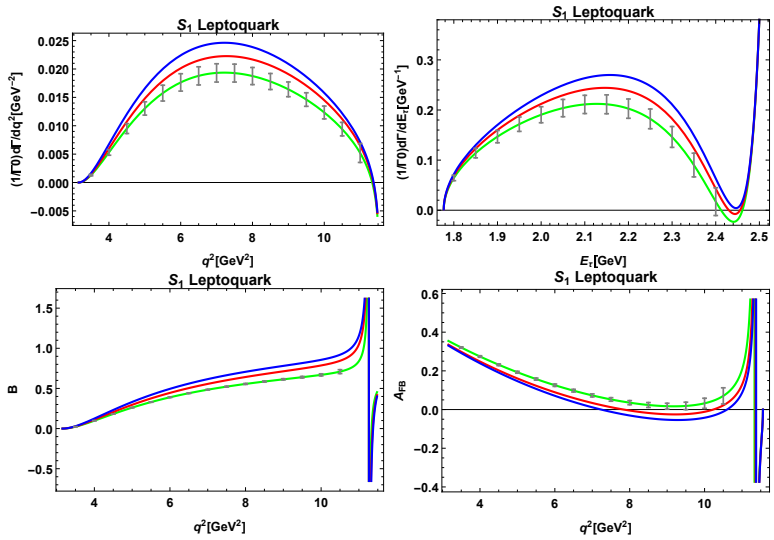


**Figure 3.8:** The effects of the $S_1$ leptoquark model on the differential decay rates $(1/\Gamma_0)d\Gamma/dq^2$, $(1/\Gamma_0)d\Gamma/dE_\tau$; the ratio of differential rates $B$; and the forward-backward asymmetry $(A_{FB})$ of $B \to X_c\tau^-\bar{\nu}_\tau$. Each plot shows the observable in the Standard Model and for two allowed values of the NP couplings. The red curves correspond to $g_{1L}^{33}g_{1R}^{23*} = 0.203 + 0.121i$, $g_{1L}^{32}g_{1R}^{23*} = 1.100 - 0.385i$, $g_{1L}^{31}g_{1R}^{23*} = 0.270 + 0.149i$, $g_{1L}^{33}g_{1L}^{23*} = -0.015 + 0.014i$, $g_{1L}^{32}g_{1L}^{23*} = -0.027 - 0.031i$, $g_{1L}^{31}g_{1L}^{23*} = -0.054 - 0.009i$, and the blue curves correspond to $g_{1L}^{33}g_{1R}^{23*} = 0.420 - 0.369i$, $g_{1L}^{32}g_{1R}^{23*} = -0.818 - 0.253i$, $g_{1L}^{31}g_{1R}^{23*} = 0.711 + 0.761i$, $g_{1L}^{33}g_{1L}^{23*} = 0.095 + 0.002i$, $g_{1L}^{32}g_{1L}^{23*} = -0.042 - 0.110i$, $g_{1L}^{31}g_{1L}^{23*} = -0.003 - 0.022i$, while the green curves correspond to the Standard Model.

the SM predictions while large deviations are possible with the other leptoquarks. The differential distributions can have different shapes from the SM and $A_{FB}$ can have zero crossings and take negative values for certain leptoquark models. The pattern of deviations from the SM can also be different for the different leptoquark models. Hence the careful measurements of these observables can point to the presence of leptoquarks and give clues to their structures.

## 3.6 Conclusions

Recent measurements of $R(D^{(*)})$ that show large deviation from the SM might be providing hints of lepton nonuniversal NP. The underlying transition in these decays $b \to c\tau^-\bar{\nu}_\tau$ can also be probed in other decays and in this chapter we considered one such process which is the inclusive decay $B \to X_c\tau^-\bar{\nu}_\tau$. Inclusive decays suffer from less hadronic uncertainties than exclusive decays and so these decays offer good tests of the SM. In this chapter we considered NP effects in the

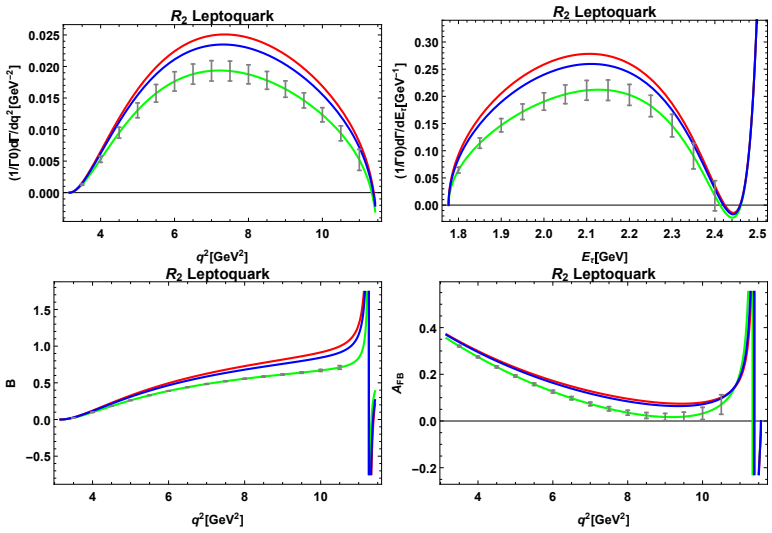


**Figure 3.9:** The effects of the $R_2$ leptoquark model on the differential decay rates $(1/\Gamma_0)d\Gamma/dq^2$, $(1/\Gamma_0)d\Gamma/dE_\tau$; the ratio of differential rates $B$; and the forward-backward asymmetry $(A_{FB})$ of $B \longrightarrow X_c\tau^-\bar{\nu}_\tau$. Each plot shows the observable in the Standard Model and for two allowed values of the NP couplings. The red curves correspond to $h_{2L}^{23}h_{2R}^{33*} = 0.106 - 0.958i$, $h_{2L}^{22}h_{2R}^{33*} = -0.218 - 0.546i$, $h_{2L}^{21}h_{2R}^{33*} = 0.493 - 0.134i$, and the blue curves correspond to $h_{2L}^{23}h_{2R}^{33*} = -0.141 + 0.104i$, $h_{2L}^{22}h_{2R}^{33*} = -0.814 - 0.647i$, $h_{2L}^{21}h_{2R}^{33*} = -0.324 - 0.140i$, respectively, while the green curves correspond to the Standard Model.

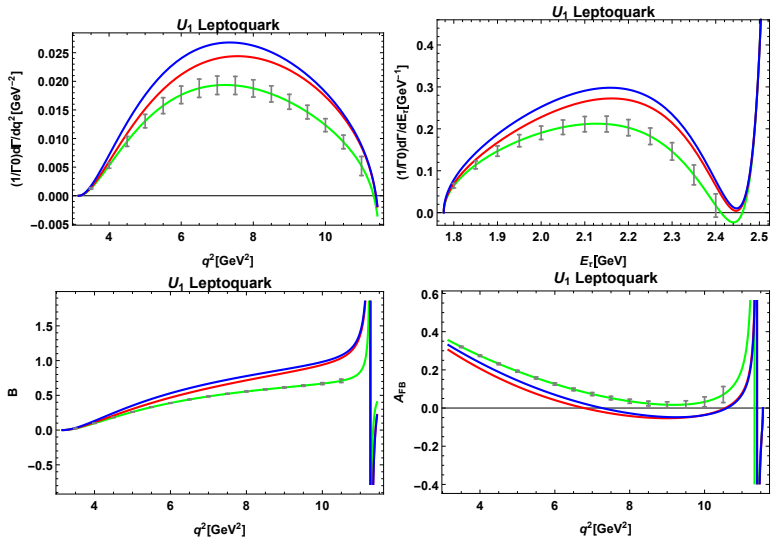


**Figure 3.10:** The effects of the $U_1$ leptoquark model on the differential decay rates $(1/\Gamma_0)d\Gamma/dq^2$, $(1/\Gamma_0)d\Gamma/dE_\tau$; the ratio of differential rates $B$; and the forward-backward asymmetry $(A_{FB})$ of $B \to X_c\tau^-\bar{\nu}_\tau$. Each plot shows the observable in the Standard Model and for two allowed values of the NP couplings. The red curves correspond to $h_{1L}^{23}h_{1R}^{33*} = -0.127 - 0.395i$, $h_{1L}^{22}h_{1R}^{33*} = 0.077 + 0.043i$, $h_{1L}^{21}h_{1R}^{33*} = -0.040 + 0.034i$, $h_{1L}^{23}h_{1L}^{33*} = -1.523 - 0.394i$, $h_{1L}^{22}h_{1L}^{33*} = 0.247 + 0.473i$, $h_{1L}^{21}h_{1L}^{33*} = 0.226 + 1.261i$, and the blue curves correspond to $h_{1L}^{23}h_{1R}^{33*} = 0.017 - 0.028i$, $h_{1L}^{22}h_{1R}^{33*} = -0.115 + 0.017i$, $h_{1L}^{21}h_{1R}^{33*} = -0.238 - 0.041i$, $h_{1L}^{23}h_{1L}^{33*} = -1.22 + 0.301i$, $h_{1L}^{22}h_{1L}^{33*} = 0.730 - 0.039i$, $h_{1L}^{21}h_{1L}^{33*} = -1.327 + 0.357i$, respectively, while the green curves correspond to the Standard Model.

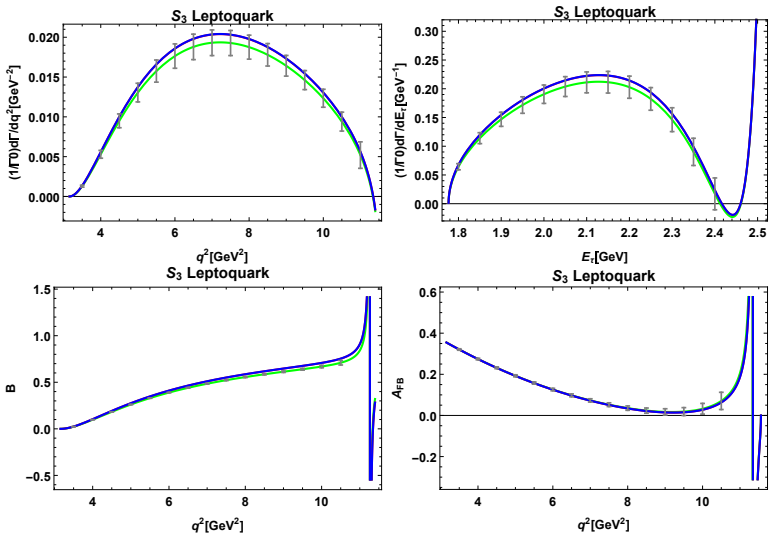


**Figure 3.11:** The effects of the $S_3$ leptoquark model on the differential decay rates $(1/\Gamma_0)d\Gamma/dq^2$, $(1/\Gamma_0)d\Gamma/dE_\tau$; the ratio of differential rates $B$; and the forward-backward asymmetry $(A_{FB})$ of $B \to X_c\tau^-\bar{\nu}_\tau$. Each plot shows the observable in the Standard Model and for two allowed values of the NP couplings. The red curves correspond to $g_{3L}^{33}g_{3L}^{23*} = -0.062 - 0.028i$, $g_{3L}^{32}g_{3L}^{23*} = 0.031 - 0.005i$, $g_{3L}^{31}g_{3L}^{23*} = 0.013 - 0.003i$, and the blue curves correspond to $g_{3L}^{33}g_{3L}^{23*} = -0.062 - 0.028i$, $g_{3L}^{32}g_{3L}^{23*} = 0.003 - 0.031i$, $g_{3L}^{31}g_{3L}^{23*} = 0.052 - 0.054i$, respectively, while the green curves correspond to the Standard Model.

inclusive decay $B \to X_c\tau^-\bar{\nu}_\tau$ with the NP parameters constrained by the $R(D^{(*)})$ measurements. We first adopted a model independent approach where the NP is expressed in terms of higher dimensional operators with various Lorentz structures. Considering one NP operator at a time, we considered the effect of NP on the inclusive decay. In the SM, the inclusive decays were calculated to perturbative $O(\alpha_s)$, and nonperturbative $1/m_b^2$ corrections. Several observables including rates as well as differential distributions were discussed with a particular focus on the ratio of rates $R(X_c) = \frac{\mathcal{B}[B\to X_c\tau^-\bar{\nu}_\tau]}{\mathcal{B}[B\to X_c\ell^-\bar{\nu}_\ell]}$. ALEPH has a measurement of $b \to X\tau^-\bar{\nu}_\tau$ which we converted into a measurement of $B \to X_c\tau^-\bar{\nu}_\tau$ under certain assumptions. Using this as an input we showed that this measurement further constrained the NP couplings introduced to address the $R(D^{(*)})$ anomalies. Not including the ALEPH measurement we found that large deviations from the SM in $R(X_c)$ are possible with the present $R(D^{(*)})$ measurements. This highlights the importance of a precise measurement of the inclusive rate as a sensitive probe of NP. We then considered explicit models of NP with leptoquarks and for various models of leptoquarks studied their effects in the

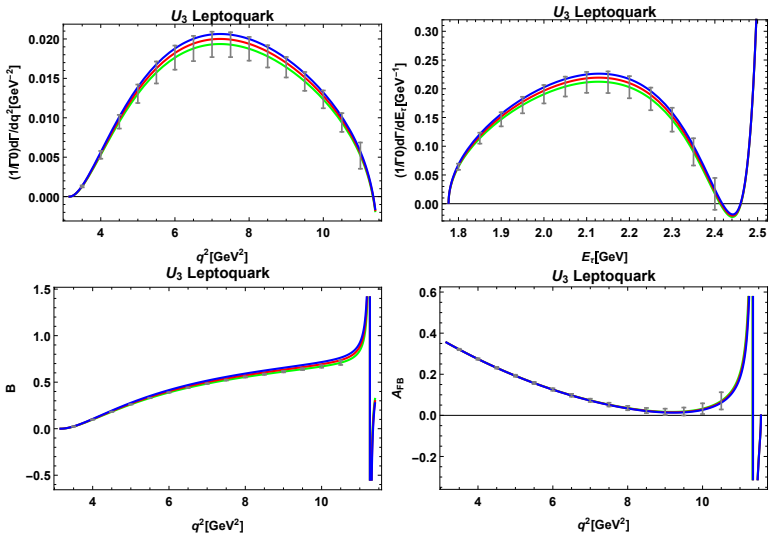


**Figure 3.12:** The effects of the $\boldsymbol{U}_3$ leptoquark model on the differential decay rates $(1/\Gamma_0)d\Gamma/dq^2$, $(1/\Gamma_0)d\Gamma/dE_\tau$; the ratio of differential rates $B$; and the forward-backward asymmetry $(A_{FB})$ of $B \to X_c\tau^-\bar{\nu}_\tau$. Each plot shows the observable in the Standard Model and for two allowed values of the NP couplings. The red curves correspond to $h_{3L}^{23}h_{3L}^{33*} = -0.019{+}0.002i$, $h_{3L}^{22}h_{3L}^{33*} = 0.011{-}0.007i$, $h_{3L}^{21}h_{3L}^{33*} = 0.026 - 0.012i$, and the blue curves correspond to $h_{3L}^{23}h_{3L}^{33*} = -0.037 + 0.005i$, $h_{3L}^{22}h_{3L}^{33*} = 0.015 + 0.002i$, $h_{3L}^{21}h_{3L}^{33*} = -0.003 - 0.019i$, respectively, while the green curves correspond to the Standard Model.

inclusive decay. We found that large deviations are possible in certain models of leptoquarks and the patterns of these deviations are different for different models. Therefore, careful measurements in the inclusive decay can not only point to the presence of leptoquarks but can give clues about their structure.

# CHAPTER 4

# NEW PHYSICS IN INCLUSIVE SEMILEPTONIC B DECAY INCLUDING NONPERTURBATIVE CORRECTIONS

## 4.1 Introduction

In the previous chapter we discussed the effects of new physics (NP) operators in the inclusive semileptonic B decay. There, we considered NP contributions at tree level and nonperturbative corrections of order $O(1/m_b^2)$ were included only in the SM part. In this chapter which is based on Ref. [64], we carry out the calculations of nonpertubative effects for all NP Dirac structures and present the effect of these corrections numerically. In particular, we study the effect of these corrections on the lepton flavor universality observable $R(X_c) = \frac{\mathcal{B}(\bar{B}\to X_c\tau^-\bar{\nu}_\tau)}{\mathcal{B}(\bar{B}\to X_c\ell^-\bar{\nu}_\ell)}$ and compare the results for this observable with and without power corrections in the NP contributions. We will see that the order of these corrections are at the percent level and in the parameter region of our interest, they are mostly noticeable in the scalar and tensor parts.

This chapter is organized as follows: In section 4.2, we briefly describe the inclusive $B$ decay process and present the results of our calculations. In section 4.3, we present the numerical results and in section 4.4, we finish this chapter with a conclusion.

## 4.2 Inclusive B decay

The inclusive semileptonic $B$ decay rate can be calculated systematically by an expansion in terms of perturbative and nonperturbative corrections. The leading terms in this expansion

reproduce the free quark decay rate while higher order terms are written as double expansions in terms of short distance perturbative effect which is an expansion in $\alpha_s$, and long distance nonperturbative effect which is an expansion in $\Lambda_{QCD}/m_b$.

Nonperturbative corrections are calculated in the context of operator product expansion (OPE) and heavy quark effective theory (HQET). The techniques to calculate these corrections are known well (see e.g. [50, 51, 52, 53, 54, 65, 66]). The expansion is basically written in terms of operators with increasing dimensions where the higher dimension operators are suppressed by powers of $1/m_b$. A convenient method to calculate these corrections to arbitrary order in $1/m_b$, is presented in [67]. In this chapter, we extend the SM results by adding the scalar, pseudo-scalar, vector and tensor currents as NP effects. We consider the effective Hamiltonian,

$$\begin{aligned}\mathcal{H}_{eff} &= \frac{G_F V_{cb}}{\sqrt{2}}\Big\{\Big[\bar{c}\gamma_\mu(1-\gamma_5)b + g_L\bar{c}\gamma_\mu(1-\gamma_5)b + g_R\bar{c}\gamma_\mu(1+\gamma_5)b\Big]\bar{\tau}\gamma^\mu(1-\gamma_5)\nu_\tau \\ &\quad + \Big[g_S\bar{c}b + g_P\bar{c}\gamma_5 b\Big]\bar{\tau}(1-\gamma_5)\nu_\tau + \Big[g_T\bar{c}\sigma^{\mu\nu}(1-\gamma_5)b\Big]\bar{\tau}\sigma_{\mu\nu}(1-\gamma_5)\nu_\tau + h.c.\Big\},\end{aligned} \tag{4.1}$$

where $G_F$ is the Fermi constant and $V_{cb}$ is the Cabibbo-Kobayashi-Maskawa (CKM) matrix element. When $g_S = g_P = g_L = g_R = g_T = 0$, the above equation produces the SM effective Hamiltonian.

To calculate the differential decay rate for $\bar{B} \to X_c\tau^-\bar{\nu}_\tau$, we use the optical theorem to find the imaginary part of the time ordered products of the charged currents,

$$\int d^4x e^{-iq.x}\langle B|T\{O^\dagger(x), O(0)\}|B\rangle, \tag{4.2}$$

where $O$ consists of SM and NP currents,

$$O = (1+g_L)\bar{c}\gamma^\mu(1-\gamma_5)b + g_R\bar{c}\gamma^\mu(1+\gamma_5)b + g_S\bar{c}b + g_P\bar{c}\gamma_5 b + g_T\bar{c}\sigma^{\mu\nu}(1-\gamma_5)b. \tag{4.3}$$

The time ordered product can then be written as an operator product expansion where a

series of operators with increasing dimensions appear. Then, using the heavy quark effective theory, we can separate the residual momentum of the heavy quark in the hadron (which is of order $\Lambda_{QCD}$) and define the matrix elements of the nonrenomalizable operators in the operator expansion. This procedure leads to the determination of hadronic form factors. After contracting with the leptonic currents, we can calculate the three-fold differential decay rate $\frac{d\Gamma}{dq^2 dE_\tau dE_\nu}$. Here the kinematic variable $q^2$ is the dilepton invariant mass and $E_\tau$ and $E_\nu$ are the energies of the $\tau$ lepton and the corresponding neutrino in the rest frame of the $B$ meson. The explicit expression of the three-fold decay distribution in terms of the invariant quantities is provided in Appendix E. The leading order result is the free quark decay distribution and the first nonperturbative correction appears at order $\Lambda^2_{QCD}/m_b^2$. This correction is proportional to two hadronic parameters $\lambda_1$ and $\lambda_2$ (or $\mu_\pi^2$ and $\mu_G^2$) which correspond to the kinetic energy and the spin interaction energy of the $b$ quark in the hadron, respectively.

After integrating over the energies of the charged lepton and the neutrino, we can find the $q^2$ distribution as [64],

$$\begin{aligned}\frac{d\Gamma}{d\hat{q}^2} =& N(\hat{q}^2)\Big[(|1+g_L|^2+|g_R|^2)\frac{d\Gamma}{d\hat{q}^2}\Big|_{SM} + \mathrm{Re}(g_R^*(1+g_L))\frac{d\Gamma}{d\hat{q}^2}\Big|_{LR} + |g_S|^2\frac{d\Gamma}{d\hat{q}^2}\Big|_{S} \\ &+ \mathrm{Re}(g_S^*(1+g_L+g_R))\frac{d\Gamma}{d\hat{q}^2}\Big|_{SLR} + |g_P|^2\frac{d\Gamma}{d\hat{q}^2}\Big|_{P} + \mathrm{Re}(g_P^*(1+g_L-g_R))\frac{d\Gamma}{d\hat{q}^2}\Big|_{PLR} \\ &+ |g_T|^2\frac{d\Gamma}{d\hat{q}^2}\Big|_{T} + \mathrm{Re}((1+g_L)g_T^*)\frac{d\Gamma}{d\hat{q}^2}\Big|_{LT} + \mathrm{Re}(g_R g_T^*)\frac{d\Gamma}{d\hat{q}^2}\Big|_{RT}\Big], \end{aligned} \tag{4.4}$$

where $N(\hat{q}^2) = \frac{G_F^2|V_{cb}|^2 m_b^5 (1-\hat{m}_\tau^2/\hat{q}^2)^2}{96\pi^3\sqrt{\lambda(1,\hat{q}^2,\rho^2)}}$ and $\lambda(a,b,c) = a^2+b^2+c^2-2ab-2ac-2bc$. The various terms on the right hand side of the above equation are presented in the following, with subscripts that correspond to contributions of SM, NP and interference terms,

$$\left.\frac{d\Gamma}{d\hat{q}^2}\right|_{SM} = \left(1+\frac{\lambda_1}{2m_b^2}\right)\lambda(1,\hat{q}^2,\rho^2)\Big\{\big[(1-\rho)^2+\hat{q}^2(1+\rho)-2(\hat{q}^2)^2\big]$$
$$+\frac{\hat{m}_\tau^2}{\hat{q}^2}\big[2(1-\rho)^2-\hat{q}^2(1+\rho)-(\hat{q}^2)^2\big]\Big\}+\frac{3\lambda_2}{2m_b^2}\Big\{\big[(1-\rho)^3(1-5\rho)-\hat{q}^2(1-\rho)^2(1+5\rho)$$
$$-3(\hat{q}^2)^2(5+6\rho+5\rho^2)+25(\hat{q}^2)^3(1+\rho)-10(\hat{q}^2)^4\big]$$
$$+\frac{\hat{m}_\tau^2}{\hat{q}^2}\big[2(1-\rho)^3(1-5\rho)-\hat{q}^2(5-9\rho-21\rho^2+25\rho^3)$$
$$+3(\hat{q}^2)^2(1+2\rho+5\rho^2)+5(\hat{q}^2)^3(1+\rho)-5(\hat{q}^2)^4\big]\Big\}, \tag{4.5}$$

$$\left.\frac{d\Gamma}{dq^2}\right|_{LR} = -12\sqrt{\rho}\hat{q}^2\left(1+\frac{\lambda_1}{2m_b^2}\right)\lambda(1,\hat{q}^2,\rho^2)+4\sqrt{\rho}\frac{3\lambda_2}{2m_b^2}\Big\{\big[2(1-\rho)^3-3\hat{q}^2(1-\rho)^2$$
$$+12(\hat{q}^2)^2(1+\rho)-7(\hat{q}^2)^3\big]+\frac{4\hat{m}_\tau^2}{\hat{q}^2}\big[(1-\rho)^3-3\hat{q}^2\rho(1-\rho)-3\rho(\hat{q}^2)^2+(\hat{q}^2)^3\big]\Big\}, \tag{4.6}$$

$$\left.\frac{d\Gamma}{d\hat{q}^2}\right|_{S} = \frac{3\hat{q}^2}{4}((1+\sqrt{\rho})^2-\hat{q}^2)\Big[\left(1+\frac{\lambda_1}{2m_b^2}\right)\lambda(1,\hat{q}^2,\rho^2)$$
$$+\frac{3\lambda_2}{2m_b^2}\Big((1-\sqrt{\rho})^2(1+6\sqrt{\rho}+5\rho)-2\hat{q}^2(1-2\sqrt{\rho}+5\rho)+5(\hat{q}^2)^2\Big)\Big], \tag{4.7}$$

$$\left.\frac{d\Gamma}{d\hat{q}^2}\right|_{SLR} = \frac{3\hat{m}_\tau}{2}(1-\sqrt{\rho})((1+\sqrt{\rho})^2-\hat{q}^2)\Big[\left(1+\frac{\lambda_1}{2m_b^2}\right)\lambda(1,\hat{q}^2,\rho^2)$$
$$+\frac{3\lambda_2}{2m_b^2}\Big((1-\sqrt{\rho})^2(1+6\sqrt{\rho}+5\rho)-2\hat{q}^2(1-2\sqrt{\rho}+5\rho)+5(\hat{q}^2)^2\Big)\Big], \tag{4.8}$$

$$\left.\frac{d\Gamma}{d\hat{q}^2}\right|_P = \frac{3\hat{q}^2}{4}((1-\sqrt{\rho})^2-\hat{q}^2)\Big[\Big(1+\frac{\lambda_1}{2m_b^2}\Big)\lambda(1,\hat{q}^2,\rho^2) + \frac{3\lambda_2}{2m_b^2}\Big((1+\sqrt{\rho})^2(1-6\sqrt{\rho}+5\rho)-2\hat{q}^2(1+2\sqrt{\rho}+5\rho)+5(\hat{q}^2)^2\Big)\Big], \tag{4.9}$$

$$\left.\frac{d\Gamma}{d\hat{q}^2}\right|_{PLR} = \frac{3\hat{m}_\tau}{2}(1+\sqrt{\rho})((1-\sqrt{\rho})^2-\hat{q}^2)\Big[\Big(1+\frac{\lambda_1}{2m_b^2}\Big)\lambda(1,\hat{q}^2,\rho^2) + \frac{3\lambda_2}{2m_b^2}\Big((1+\sqrt{\rho})^2(1-6\sqrt{\rho}+5\rho)-2\hat{q}^2(1+2\sqrt{\rho}+5\rho)+5(\hat{q}^2)^2\Big)\Big], \tag{4.10}$$

$$\begin{aligned}\left.\frac{d\Gamma}{d\hat{q}^2}\right|_T = 8(1+\frac{2\hat{m}_\tau^2}{\hat{q}^2})\Big[\Big(1+\frac{\lambda_1}{2m_b^2}\Big)\Big(&2(1-\rho)^4-5\hat{q}^2(1-\rho)^2(1+\rho)+(\hat{q}^2)^2(3+2\rho+3\rho^2)\\ &+(\hat{q}^2)^3(1+\rho)-(\hat{q}^2)^4\Big)+\frac{3\lambda_2}{2m_b^2}\Big(2(-1+\rho)^3(3+5\rho)+\hat{q}^2(3+17\rho+5\rho^2-25\rho^3)\\ &+(\hat{q}^2)^2(3+14\rho+15\rho^2)+5(\hat{q}^2)^3(1+\rho)-5(\hat{q}^2)^4\Big)\Big],\end{aligned} \tag{4.11}$$

$$\begin{aligned}\left.\frac{d\Gamma}{d\hat{q}^2}\right|_{LT} = 36\hat{m}_\tau\sqrt{\rho}\Big[&\Big(1+\frac{\lambda_1}{2m_b^2}\Big)\Big((-1+\rho)^3+\hat{q}^2(1+2\rho-3\rho^2)+(\hat{q}^2)^2(1+3\rho)-(\hat{q}^2)^3\Big)\\ &+\frac{\lambda_2}{2m_b^2}\Big((1-\rho)^2(1+15\rho)+\hat{q}^2(3+10\rho-45\rho^2)+(\hat{q}^2)^2(19+45\rho)-15(\hat{q}^2)^3\Big)\Big],\end{aligned} \tag{4.12}$$

$$\begin{aligned}\left.\frac{d\Gamma}{d\hat{q}^2}\right|_{RT} = -36\hat{m}_\tau\Big[&\Big(1+\frac{\lambda_1}{2m_b^2}\Big)\Big((-1+\rho)^3-\hat{q}^2(-3+2\rho+\rho^2)-(\hat{q}^2)^2(3+\rho)+(\hat{q}^2)^3\Big)\\ &+\frac{\lambda_2}{2m_b^2}\Big((1-\rho)^2(5+11\rho)+\hat{q}^2(1-18\rho-15\rho^2)-(\hat{q}^2)^2(13+3\rho)+7(\hat{q}^2)^3\Big)\Big].\end{aligned} \tag{4.13}$$

| Parameter ($1S$ scheme) | Value [30] | Parameter (kinetic scheme) | Value [75] |
|---|---|---|---|
| $m_b^{1S}$ | $4.691 \pm 0.037\ GeV$ | $m_b^{kin}$ | $4.561 \pm 0.021\ GeV$ |
| $\lambda_1$ | $-0.362 \pm 0.067\ GeV^2$ | $m_c$ | $1.092 \pm 0.020\ GeV$ |
| $\rho_1$ | $0.043 \pm 0.048\ GeV^3$ | $\mu_\pi^2$ | $0.464 \pm 0.067\ GeV^2$ |
| $\tau_1$ | $0.161 \pm 0.122\ GeV^3$ | $\rho_D^3$ | $0.175 \pm 0.040\ GeV^3$ |
| $\tau_3$ | $0.213 \pm 0.102\ GeV^3$ | $\mu_G^2$ | $0.333 \pm 0.061\ GeV^2$ |

**Table 4.1:** Values of the parameters used for the numerical results. The correlation matrices are taken from the references mentioned in the table.

Here we have defined the normalized quantities, $\hat{q}^2 = q^2/m_b^2$, $\rho = m_c^2/m_b^2$ and $\hat{m}_\tau = m_\tau/m_b$. Note that there is no scalar-pseudoscalar and (pseudo)scalar-tensor interference terms in the $q^2$ distribution. For $g_S = g_P = g_L = g_R = g_T = 0$, we reproduce the SM results and for $g_S = g_P = g_L = g_R = 0$ we reproduce the results given in [68].

## 4.3 Numerical Results

In this section, we present the numerical results of our calculations in two mass schemes for the quarks masses: the $1S$ mass scheme [59, 60] and the kinetic scheme [69, 70, 71, 72]. In the $1S$ scheme, we follow [73, 74] to write the rate in terms of the nonperturbative parameters, $m_b$, $\lambda_1$ at $O(1/m_b^2)$ and $\rho_1$, $\tau_1$ and $\tau_3$ at $O(1/m_b^3)$, and we use the numerical results of the fit together with the correlations between the parameters from Ref. [30]. In the kinetic scheme the nonperturbative parameters are $m_b$ and $m_c$, $\mu_\pi^2$ and $\mu_G^2$ at $O(1/m_b^2)$ and $\rho_D^3$ at $O(1/m_b^3)$. The numerical values of these parameters together with their correlation matrix are presented in Refs. [72, 75]. We present the numerical inputs in table 4.1. The correlation matrices of these parameters are taken from the references mentioned in the table and we do not repeat them here.

In our numerical results we also include the $O(1/m_b^3)$ correction in SM which is derived in [62]. Besides nonperturbative effects, we include the $O(\alpha_s)$ perturbative corrections in SM calculated in [47, 49]. The effects of higher order perturbative corrections are very small in the observables where the ratio of rates are calculated [55, 76], so we include only $O(\alpha_s)$ corrections.

We find for the ratio of branching ratios in SM, $R(X_c)_{SM} = \frac{\mathcal{B}(B\to X_c\tau^-\bar{\nu}_\tau)_{SM}}{\mathcal{B}(B\to X_c\ell^-\bar{\nu}_\ell)_{SM}}$, in the $1S$ scheme,

$$R(X_c)^{1S}_{SM} = 0.216 \pm 0.003\,, \tag{4.14}$$

and in the kinetic scheme,

$$R(X_c)^{kin}_{SM} = 0.213 \pm 0.004\,. \tag{4.15}$$

Adding the NP effects, we can find in the $1S$ scheme,

$$\begin{aligned}\frac{R(X_c)^{1S}}{R(X_c)^{1S}_{SM}} \simeq\ & 1 + 1.147\big(|g_L|^2 + |g_R|^2 + 2\,\mathrm{Re}(g_L)\big) + 0.031|g_P|^2 + 0.327|g_S|^2 + 12.637|g_T|^2 \\ & - 0.714\,\mathrm{Re}((1+g_L)g_R^*) + 0.096\,\mathrm{Re}((1+g_L-g_R)g_P^*) + 0.493\,\mathrm{Re}((1+g_L+g_R)g_S^*) \\ & + 5.514\,\mathrm{Re}(g_R g_T^*) - 3.402\,\mathrm{Re}((1+g_L)g_T^*),\end{aligned} \tag{4.16}$$

and similarly in the kinetic scheme,

$$\begin{aligned}\frac{R(X_c)^{kin}}{R(X_c)^{kin}_{SM}} \simeq\ & 1 + 1.266\big(|g_L|^2 + |g_R|^2 + 2\,\mathrm{Re}(g_L)\big) + 0.042|g_P|^2 + 0.351|g_S|^2 + 13.969|g_T|^2 \\ & - 0.744\,\mathrm{Re}((1+g_L)g_R^*) + 0.120\,\mathrm{Re}((1+g_L-g_R)g_P^*) + 0.525\,\mathrm{Re}((1+g_L+g_R)g_S^*) \\ & + 6.094\,\mathrm{Re}(g_R g_T^*) - 3.462\,\mathrm{Re}((1+g_L)g_T^*).\end{aligned} \tag{4.17}$$

There is a measurement of the inclusive rate by ALEPH [63],

$$\mathcal{B}(b \to X\tau^-\bar{\nu}_\tau)_{exp} = (2.43 \pm 0.32) \times 10^{-2}\,, \tag{4.18}$$

where $X = X_c + X_u$ are all possible states from $b \to c$ and $b \to u$ transitions. This measurement is dominated by the $b \to c$ mode since $\frac{|V_{ub}|}{|V_{cb}|} = 0.083 \pm 0.006$, as measured by LHCb [77]. On the other hand the $b \to u$ mode has a larger phase space compared to the $b \to c$ mode. We estimate the contribution of the $b \to u$ mode to this measurement by,

$$\mathcal{B}(b \to X\tau^-\bar{\nu}_\tau)_{exp} \approx \mathcal{B}(b \to X_c\tau^-\bar{\nu}_\tau)_{exp}(1 + \frac{|V_{ub}|^2}{|V_{cb}|^2} \times 2.8), \tag{4.19}$$

where the factor 2.8 is due to the larger phase space in the $b \to u$ mode. This estimation which is consistent with the one given in [37] leads to,

$$\mathcal{B}(b \to X_c\tau^-\bar{\nu}_\tau)_{exp} = (2.38 \pm 0.32) \times 10^{-2}. \tag{4.20}$$

Note that the ALEPH measurement represents the inclusive weak decay for a mixture of $b$ hadrons and to leading order in the heavy quark expansion, all $b$ hadrons have the same width. So this measurement can be considered as the branching ratio for each individual $b$ hadron.

Using the world average for the semileptonic branching ratio into the light lepton [30], $\mathcal{B}(B \to X_c\ell^-\bar{\nu}_\ell)_{exp} = (10.65 \pm 0.16) \times 10^{-2}$, we can find an experimental value for the ratio,

$$R(X_c)_{exp} = 0.223 \pm 0.030. \tag{4.21}$$

In Fig. (4.1) we present the results (in the $1S$ scheme) for the observable $R(X_c)$ when we turn on one NP coupling at a time. We consider two cases: the first case is when the NP contribution is considered only at parton level (dashed red curves), and the second case is when we add the subleading $1/m_b$ corrections to these NP contributions (solid red curves). The gray and brown bands correspond to the uncertainties of this observable when we vary the values of the parameters within their uncertainties. The green bands are the constraints on the couplings when we consider the measurements of $R(D^{(*)})$ within $3\sigma$. For the $g_P$ coupling, it is well known that the $B_c$ lifetime leads to a strong constraint [36, 37, 38]. We use $\mathcal{B}(B_c \to \tau^-\bar{\nu}_\tau) \leq 30\%$ as in [15], to include this constraint on the $g_P$ coupling which is included in the green band in the plot. The pink band, is the value of $R(X_c)_{exp}$ within $1\sigma$.

In the parameter space of interest, adding the $1/m_b$ corrections to the NP contributions causes a change of $R(X_c)$ that is numerically at the percent level. This change is mostly noticeable in the $g_S$

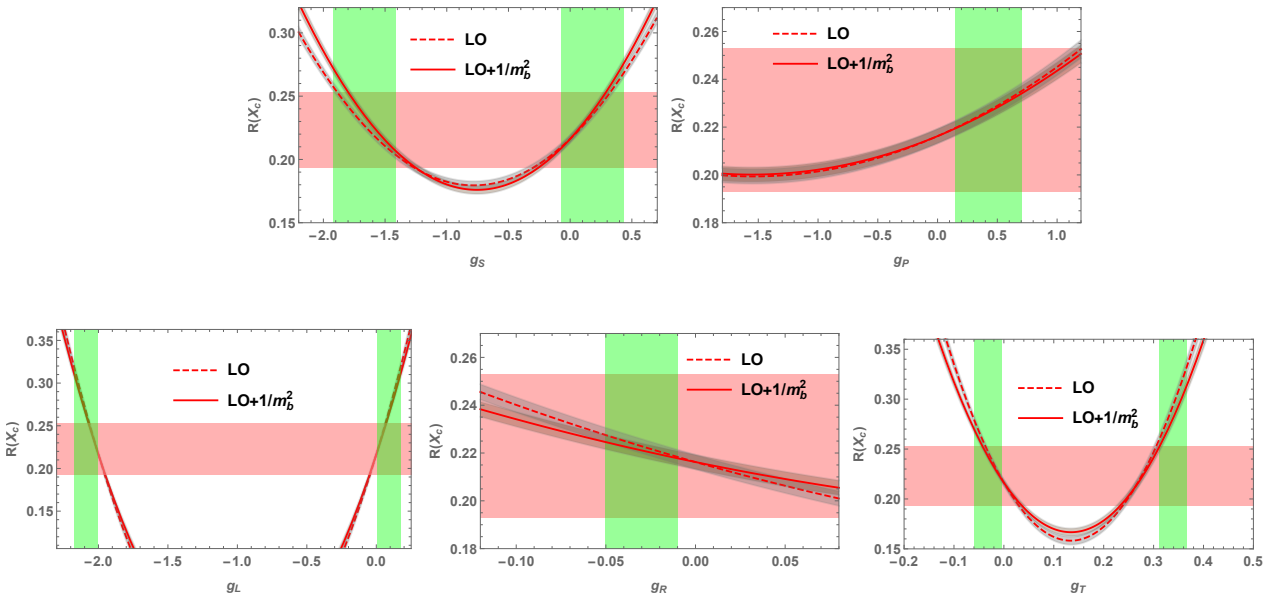


**Figure 4.1:** The ratio of decay rates $R(X_c)$ (in $1S$ scheme) when one coupling at a time is present. The dashed red curves correspond to the case when the NP contribution is added at parton level while the solid red curves correspond to the case when power corrections are included in the NP contributions. Green bands are the constraints on the couplings due to $R(D^{(*)})_{exp}$ within $3\sigma$ and $B_c$ lifetime. The pink band is $R(X_c)_{exp}$ within $1\sigma$.

and $g_T$ case where the maximum correction, in the parameter space that is favored by $R(D^{(*)})$, is $\approx 5\%$.

## 4.4 Conclusions

Recent measurements of $R(D^{(*)})$ show large deviations from SM predictions and this could be a signal of nonuniversal NP. The quark level transition in this observable is $b \to c\tau^-\bar{\nu}_\tau$ and we can probe this transition in other decay modes such as the inclusive decay $B \to X_c\tau\nu_\tau$. In the last chapter, we studied this decay mode when we add all possible NP Dirac structures to it. There, we considered the NP contributions at tree level. In this chapter, we extended this study by including the effects of $1/m_b$ corrections in the NP Dirac structures. We presented the results of our calculations for the differential decay rate $\frac{d\Gamma}{dq^2}$ as well as the three-fold decay distribution and presented some numerical results of the effects of these power corrections on the observable $R(X_c)$. By constraining the NP parameters by the existing $R(D^{(*)})$ measurements, we presented the favored parameter region by these measurements to illustrate if the power corrections in the

NP part are important. We found that, in the parameter range of interest, these corrections are generically at the percent level (except for the $g_P$ coupling which is very small) and the maximum effect of these corrections is in the $g_S$ and $g_T$ part which is $\approx 5\%$.

# CHAPTER 5

# CP VIOLATION IN $\bar{B}^0 \to D^{*+}\mu^-\bar{\nu}_\mu$

## 5.1 Introduction

The observed anomalies in the semileptonic $B \to D^{(*)}\ell\nu_\ell$ transition have caused a lot of activity in the field and there are numerous works in the literature that examine the nature of the new physics (NP) required to explain these anomalies. These include both model-independent and model-dependent analyses. Therefore, there are many possibilities for the NP. In this chapter which is based on Ref. [78], we focus on the CP-violating observables as a means of differentiating the NP scenarios. More specifically, we focus on CP violating triple products (TP) [79, 80, 81, 82, 83] that appear in the angular distribution of the decay $\bar{B}^0 \to D^{*+}(\to D^0\pi^+)\mu^-\bar{\nu}_\mu$.

Generically, triple products take the form $\mathbf{v}_1 \cdot (\mathbf{v}_2 \times \mathbf{v}_3)$ where $\mathbf{v}_i$ can be the polarization or momentum of the final state particles. These terms are kinematical effects and hence they require an interference of two amplitudes with different Lorentz structures. This fact will help distinguish different NP explanations of the $R(D^{(*)})$ anomalies. An important feature of TPs is that they do not require hadronic (CP conserving) phases. This is in contrast to direct CP violation where besides weak phase differences, one also needs strong phase differences which are usually very hard to calculate or estimate. This is particularly useful in our case where the only hadronic transition is $\bar{B} \to D^*$ and therefore the hadronic phase remains the same among different amplitudes. So the main CP-violating effects in $\bar{B}^0 \to D^{*+}(\to D^0\pi^+)\mu^-\bar{\nu}_\mu$ appear as CP-violating asymmetries in the

angular distributions (TPs).

In this chapter we present the calculation of the full angular distribution of the decay $\bar{B}^0 \to D^{*+}(\to D^0\pi^+)\mu^-\bar{\nu}_\mu$ and investigate how the CP-violating angular asymmetries help us distinguish various NP models. To do so, we begin in Sec. 5.2 with a derivation of the angular distribution both in the SM and with the addition of NP. In Sec. 5.3, we consider several LQ models and the implications of the CP-violating angular asymmetries for these models and finally we conclude in Sec. 5.4.

## 5.2 Angular Analysis

In this section we discuss the kinematics of the decay $\bar{B} \to D^*(\to D\pi)\ell^-\bar{\nu}_\ell$ and define the angular observables in the process using transversity amplitudes. The total decay amplitude for this process can be expressed as a sum over several pairs of effective two-body decays. Here we begin by examining the SM contribution and then continue to discuss NP parts.

### 5.2.1 Transversity amplitudes: SM

The decay $\bar{B} \to D^*\ell^-\bar{\nu}_\ell$ is considered to be $\bar{B} \to D^*W^{*-}$, where the on-shell $D^*$ decays to $D\pi$ and the off-shell $W^{*-}$ decays to $\ell^-\bar{\nu}_\ell$. Its amplitude is given by

$$\mathcal{M}_{(m;n)}(B \to D^*W^*) \;=\; \epsilon^{*\mu}_{D^*}(m) M_{\mu\nu} \epsilon^{*\nu}_{W^*}(n)\,, \tag{5.1}$$

where $\epsilon^\mu_{V^*}(m)$ is the polarization of a vector particle ($D^*$ or $W^*$). Here $m, n = \pm 1, 0$ and $t$ represent the transverse, longitudinal and timelike polarizations, respectively. (Only the off-shell $W^{*-}$ has a timelike polarization.)

In the $B$-meson rest frame we write the polarizations of the two vector particles as

$$\begin{aligned} \epsilon^\mu_{D^*}(\pm) &= (0, 1, \pm i, 0)/\sqrt{2}\,,\ \epsilon^\mu_{D^*}(0) = (k_z, 0, 0, k_0)/m_{D^*}\,, \\ \epsilon^\mu_{W^*}(\pm) &= (0, 1, \mp i, 0)/\sqrt{2}\,,\ \epsilon^\mu_{W^*}(0) = -(q_z, 0, 0, q_0)/\sqrt{q^2}\,,\ \epsilon^\mu_{W^*}(t) = q^\mu/\sqrt{q^2}\,, \end{aligned} \tag{5.2}$$

where $k^\mu = (k_0, 0, 0, k_z)$ and $q^\mu = (q_0, 0, 0, q_z)$ are the four momenta of the $D^*$ and $W^*$, respectively, both written in the rest frame of the $B$. The polarization vectors of the off-shell $W^*$ satisfy the following orthonormality and completeness relations:

$$\begin{aligned} \epsilon^{*\mu}_{W^*}(m)\epsilon_{W^*\mu}(m') &= g_{mm'} , \\ \sum_{m,m'} \epsilon^{*\mu}_{W^*}(m)\epsilon^{\nu}_{W^*}(m')g_{mm'} &= g^{\mu\nu} , \end{aligned} \tag{5.3}$$

where $g_{mm'} = \mathrm{diag}(+,-,-,-)$ for $m = t, \pm, 0$. For the on-shell $D^*$, these relations are

$$\begin{aligned} \epsilon^{*\mu}_{D^*}(m)\epsilon_{D^*\mu}(m') &= -\delta_{mm'} , \\ \sum_{m,m'} \epsilon^{*\mu}_{D^*}(m)\epsilon^{\nu}_{D^*}(m')\delta_{mm'} &= -g^{\mu\nu} + \frac{k^\mu k^\nu}{m^2_{D^*}} . \end{aligned} \tag{5.4}$$

Since the $B$ meson has spin 0, of the 12 combinations of $D^*$ and $W^*$ polarizations, only 4 are allowed, producing the following helicity amplitudes:

$$\begin{aligned} \mathcal{M}_{(+;+)}(B \to D^*W^*) &= \mathcal{A}_+ , \\ \mathcal{M}_{(-;-)}(B \to D^*W^*) &= \mathcal{A}_- , \\ \mathcal{M}_{(0;0)}(B \to D^*W^*) &= \mathcal{A}_0 , \\ \mathcal{M}_{(0;t)}(B \to D^*W^*) &= \mathcal{A}_t . \end{aligned} \tag{5.5}$$

One may also go to the transversity basis by writing the amplitudes involving transverse polarizations as

$$\mathcal{A}_{||,\perp} = (\mathcal{A}_+ \pm \mathcal{A}_-)/\sqrt{2} . \tag{5.6}$$

The full amplitude for the decay process $B \to D^*(\to D\pi)\ell^-\bar{\nu}_\ell$ can now be expressed as

$$\begin{aligned}
&\mathcal{M}(B \to D^*(\to D\pi)W^*(\to \ell^-\bar{\nu}_\ell)) \qquad (5.7)\\
&\quad \propto \sum_{m,m'=\pm,0} \epsilon^{\sigma}_{D^*}(m)(p_D)_\sigma \, g_{mm'} \, \epsilon^{*\rho}_{D^*}(m') \, M_{\rho\nu} \sum_{n,n'=t,\pm,0} \epsilon^{*\nu}_{W^*}(n') \, g_{n'n} \, \epsilon^{\mu}_{W^*}(n) \, (\bar{u}_\ell \gamma_\mu P_L v_{\bar{\nu}_\ell}) \, .
\end{aligned}$$

Here we have made explicit use of the fact that $\epsilon^{\sigma}_{D^*}(p_{D^*})_\sigma = \epsilon^{\sigma}_{D^*}(p_D + p_\pi)_\sigma = 0$, so that $A(D^* \to D\pi) \propto \epsilon^{\sigma}_{D^*}(p_D - p_\pi)_\sigma = 2\epsilon^{\sigma}_{D^*}(p_D)_\sigma$. In the above amplitude, one can project out the relevant helicity components to obtain

$$\begin{aligned}
&\mathcal{M}(B \to D^*(\to D\pi)W^*(\to \ell^-\bar{\nu}_\ell))\\
&\quad \propto \sum_{m,m'=\pm,0} \sum_{n,n'=t,\pm,0} \epsilon^{\sigma}_{D^*}(m)(p_D)_\sigma \, g_{mm'} \, \mathcal{M}_{(m',n')}(B \to D^*W^*) \, g_{n'n} \, \epsilon^{\mu}_{W^*}(n) \, (\bar{u}_\ell \gamma_\mu P_L v_{\bar{\nu}_\ell})\\
&\quad \propto - \sum_{m=\pm,0} \sum_{n=t,\pm,0} g_{nn} \mathcal{H}_{D^*}(m) \, \mathcal{M}_{(m,n)}(B \to D^*W^*) \, \mathcal{L}_{W^*}(n) \, , \qquad (5.8)
\end{aligned}$$

where

$$\mathcal{H}_{D^*}(m) = \epsilon_{D^*}(m) \cdot p_D \, , \; \mathcal{L}_{W^*}(n) = \epsilon^{\mu}_{W^*}(n)(\bar{u}_\ell \gamma_\mu P_L v_{\bar{\nu}_\ell}) \, . \qquad (5.9)$$

The notation of Eq. (5.8) can be simplified by defining a timelike polarization for the $D^*$: $\mathcal{H}_{D^*}(t) \equiv \mathcal{H}_{D^*}(0)$. In this case, the helicities of Eq. (5.5) become $\mathcal{M}_{(m;m)}(B \to D^*W^*) = \mathcal{A}_m$ and

$$\mathcal{M}(B \to D^*(\to D\pi)W^*(\to \ell^-\bar{\nu}_\ell)) \;\; \propto \;\; - \sum_{m=t,\pm,0} g_{mm} \, \mathcal{A}_m \, \mathcal{H}_{D^*}(m) \, \mathcal{L}_{W^*}(m) \, . \qquad (5.10)$$

Written in this form, the differential decay rate can now be constructed from the helicity amplitudes and the Lorentz-invariant quantities $\mathcal{H}_{D^*}$ and $\mathcal{L}_{W^*}$. The spin-summed square of the amplitude is

$$|\mathcal{M}|^2 \;\; \propto \sum_{m,m'=t,\pm,0} g_{mm} g_{m'm'} \left(\mathcal{A}_m \mathcal{A}^*_{m'}\right) \left(\mathcal{H}_{D^*}(m)\mathcal{H}^*_{D^*}(m')\right) \sum_{\text{spins}} \mathcal{L}_{W^*}(m)\mathcal{L}^*_{W^*}(m') \, . \qquad (5.11)$$

The leptonic part of the above squared amplitude is given in the appendix in Eq. (F.2).

### 5.2.2 New Physics

From Eq. (5.10), we see that, in the SM, the decay amplitude can be written as the product of a hadronic piece $\mathcal{H}_{D^*}(m)$, a leptonic piece $\mathcal{L}_{W^*}(m)$, and a helicity amplitude $\mathcal{A}_m$, summed over all helicities $m$. As we will see, this same structure holds in the presence of NP. We can consider separately the NP leptonic and hadronic contributions. We begin with the leptonic piece.

In the SM, we have $\bar{B} \to D^* W^{*-}$, where the $W^{*-}$ decays to $\ell^- \bar{\nu}_\ell$ via a $(V-A)$ interaction. If NP is present, there are several possible differences. First, there may also be scalar and/or tensor interactions. Second, the decay products may include a $\bar{\nu}$ of a flavour other than $\ell$. In what follows, we assume that neutrinos are left-handed, as in the SM. Regarding the $\bar{\nu}$ flavour, technically we should write $\bar{\nu}_i$ and sum over all possibilities for $i$ (since the $\bar{\nu}$ is undetected). However, this makes the notation cumbersome, and does not change the physics. For this reason, for notational simplicity, we continue to write $\bar{\nu}_\ell$, though the reader should be aware that other $\bar{\nu}$ flavours are possible. Thus, in the presence of NP, the relevant two-body processes to consider are $\bar{B} \to D^* N^{*-} (\to \ell^- \bar{\nu}_\ell)$, where $N = S-P, V-A, T$ represent left-handed scalar, vector and tensor interactions, respectively. In what follows, we label these $SP$, $VA$ and $T$. (The $VA$ contribution includes that of the SM.)

Turning to the hadronic piece, we note that the underlying decay is $b \to c\ell^-\bar{\nu}$. For each of the leptonic $SP$, $VA$ and $T$ Lorentz structures, we introduce NP contributions to the $b \to c$ transition. The effective Hamiltonian is

$$\begin{aligned}\mathcal{H}_{eff} &= \frac{G_F V_{cb}}{\sqrt{2}} \Big\{ \left[ (1+g_L)\, \bar{c}\gamma_\mu(1-\gamma_5)b + g_R\, \bar{c}\gamma_\mu(1+\gamma_5)b \right] \bar{\ell}\gamma^\mu(1-\gamma_5)\nu_\ell \\ &+ \left[ g_S\, \bar{c}b + g_P\, \bar{c}\gamma_5 b \right] \bar{\ell}(1-\gamma_5)\nu_\ell + g_T\, \bar{c}\sigma^{\mu\nu}(1-\gamma_5)b\bar{\ell}\sigma_{\mu\nu}(1-\gamma_5)\nu_\ell + h.c. \Big\} \,. \quad (5.12)\end{aligned}$$

### 5.2.3 Transversity amplitudes: NP

Including all possible contributions (SM + NP), the amplitude for the process can be expressed as

$$\begin{aligned}\mathcal{M}^{\text{SM+NP}} \propto & \sum_{m,m'=\pm,0} \epsilon^{\nu}_{D^*}(m)(p_D)_\nu \, g_{mm'} \, \epsilon^{*\mu}_{D^*}(m') \, M^{SP}_{\mu} \, (\bar{u}_\ell P_L v_{\bar{\nu}_\ell}) \\ & + \sum_{m,m'} \epsilon^{\sigma}_{D^*}(m)(p_D)_\sigma \, g_{mm'} \, \epsilon^{*\rho}_{D^*}(m') \, M^{VA}_{\rho\nu} \sum_{n,n'} \epsilon^{*\nu}_{VA}(n') \, g_{n'n} \, \epsilon^{\mu}_{VA}(n) \, (\bar{u}_\ell \gamma_\mu P_L v_{\bar{\nu}_\ell}) \\ & + \sum_{m,m'} \epsilon^{\beta}_{D^*}(m)(p_D)_\beta \, g_{mm'} \, \epsilon^{*\rho}_{D^*}(m') \, M^{T}_{\rho,\sigma\alpha} \\ & \quad \times \sum_{n,n'} \epsilon^{*\sigma}_{T}(n') \, g_{n'n} \, \epsilon^{\mu}_{T}(n) \sum_{p,p'} \epsilon^{*\alpha}_{T}(p') \, g_{p'p} \, \epsilon^{\nu}_{T}(p) \, (\bar{u}_\ell \sigma_{\mu\nu} P_L v_{\bar{\nu}_\ell}) \, . \end{aligned} \tag{5.13}$$

The vector part is identical to the SM with the SM coupling replaced by possible NP couplings in the hadronic amplitudes.

As in the vector-current case, we can define hadronic amplitudes by contracting the currents with polarization vectors of the intermediate states. The scalar, vector, and tensor amplitudes are

$$\begin{aligned} \mathcal{M}^{SP}_{(m)}(B \to D^* SP^*) &= \epsilon^{*\mu}_{D^*}(m) \, M^{SP}_{\mu} \, , \\ \mathcal{M}^{VA}_{(m;n)}(B \to D^* VA^*) &= \epsilon^{*\mu}_{D^*}(m) \, M^{VA}_{\mu\nu} \, \epsilon^{*\nu}_{VA}(n) \, , \\ \mathcal{M}^{T}_{(m;n,p)}(B \to D^* T^*) &= i\epsilon^{*\rho}_{D^*}(m) \, M^{T}_{\rho,\sigma\alpha} \, \epsilon^{*\sigma}_{T}(n) \, \epsilon^{*\alpha}_{T}(p) \, . \end{aligned} \tag{5.14}$$

Using the above definitions we can now rewrite the total amplitude of Eq. (5.13) as

$$\begin{aligned}\mathcal{M}^{\text{SM+NP}} \propto & - \sum_{m=\pm,0} \mathcal{H}_{D^*}(m) \left\{ \mathcal{M}^{SP}_{(m)} \, \mathcal{L}_{SP} + \sum_{n=t,\pm,0} g_{nn} \, \mathcal{M}^{VA}_{(m;n)} \, \mathcal{L}_{VA}(n) \right. \\ & \left. + \sum_{n,p=t,\pm,0} g_{nn} \, g_{pp} \, \mathcal{M}^{T}_{(m;n,p)} \, \mathcal{L}_{T}(n,p) \right\} , \end{aligned} \tag{5.15}$$

where the leptonic amplitudes have been defined as

$$\begin{aligned}
\mathcal{L}_{SP} &= \bar{u}_\ell P_L v_{\bar{\nu}_\ell} \,, \\
\mathcal{L}_{VA}(n) &= \epsilon^\mu_{VA}(n)\, \bar{u}_\ell \gamma_\mu P_L v_{\bar{\nu}_\ell} \,, \\
\mathcal{L}_T(n,p) &= -i\epsilon^\mu_T(n)\, \epsilon^\nu_T(p)\, (\bar{u}_\ell \sigma_{\mu\nu} P_L v_{\bar{\nu}_\ell}) \,.
\end{aligned} \tag{5.16}$$

Since the decaying $B$ meson is a pseudoscalar, conservation of angular momentum leads to the relationships $m = 0$ for the scalar part, $m = n$ for the vector part and $m = n + p$ for the tensor part. In addition, since the tensor current is antisymmetric under the interchange of $n$ and $p$, the amplitudes corresponding to $n = p$ automatically vanish. Thus, similar to Eq. (5.5), the non-zero helicity amplitudes in the full angular distribution are given by

$$\begin{aligned}
\mathcal{M}^{SP}_{(0)}(B \to D^* SP^*) &= \mathcal{A}_{SP} \,, \\
\mathcal{M}^{VA}_{(+;+)}(B \to D^* VA^*) &= \mathcal{A}_+ \,, \\
\mathcal{M}^{VA}_{(-;-)}(B \to D^* VA^*) &= \mathcal{A}_- \,, \\
\mathcal{M}^{VA}_{(0;0)}(B \to D^* VA^*) &= \mathcal{A}_0 \,, \\
\mathcal{M}^{VA}_{(0;t)}(B \to D^* VA^*) &= \mathcal{A}_t \,, \\
\mathcal{M}^{T}_{(+;+,0)}(B \to D^* T^*) = \mathcal{M}^{T}_{(+;+,t)}(B \to D^* T^*) &= \mathcal{A}_{+,T} \,, \\
\mathcal{M}^{T}_{(0;-,+)}(B \to D^* T^*) = \mathcal{M}^{T}_{(0;0,t)}(B \to D^* T^*) &= \mathcal{A}_{0,T} \,, \\
\mathcal{M}^{T}_{(-;0,-)}(B \to D^* T^*) = \mathcal{M}^{T}_{(-;-,t)}(B \to D^* T^*) &= \mathcal{A}_{-,T} \,.
\end{aligned} \tag{5.17}$$

Using the definitions for the $B \to D^*$ form factors given in Refs. [28, 84], we can find these

hadronic helicity amplitudes as,

$$
\begin{aligned}
\mathcal{A}_{SP} &= -g_P \frac{\sqrt{\lambda(m_B^2, m_{D^*}^2, q^2)}}{m_b + m_c} A_0(q^2) \,, \\
\mathcal{A}_+ &= (1 + g_L - g_R)\,(m_B + m_{D^*}) A_1(q^2) - (1 + g_L + g_R) \frac{\sqrt{\lambda(m_B^2, m_{D^*}^2, q^2)}}{m_B + m_{D^*}} V(q^2) \,, \\
\mathcal{A}_- &= (1 + g_L - g_R)\,(m_B + m_{D^*}) A_1(q^2) + (1 + g_L + g_R) \frac{\sqrt{\lambda(m_B^2, m_{D^*}^2, q^2)}}{m_B + m_{D^*}} V(q^2) \,, \\
\mathcal{A}_0 &= -(1 + g_L - g_R) \frac{(m_B + m_{D^*})(m_B^2 - m_{D^*}^2 - q^2)}{2 m_{D^*} \sqrt{q^2}} A_1(q^2) \\
&\quad + (1 + g_L - g_R) \frac{\lambda(m_B^2, m_{D^*}^2, q^2)}{2 m_{D^*} (m_B + m_{D^*}) \sqrt{q^2}} A_2(q^2) \,, \\
\mathcal{A}_t &= -(1 + g_L - g_R) \frac{\sqrt{\lambda(m_B^2, m_{D^*}^2, q^2)}}{\sqrt{q^2}} A_0(q^2) \,, \\
\mathcal{A}_{0,T} &= g_T \frac{1}{2 m_{D^*} (m_B^2 - m_{D^*}^2)} \Big( (m_B^2 - m_{D^*}^2)(m_B^2 + 3 m_{D^*}^2 - q^2) T_2(q^2) - \lambda(m_B^2, m_{D^*}^2, q^2) T_3(q^2) \Big) \,, \\
\mathcal{A}_{\pm,T} &= g_T \frac{\sqrt{\lambda(m_B^2, m_{D^*}^2, q^2)} T_1(q^2) \pm (m_B^2 - m_{D^*}^2) T_2(q^2)}{\sqrt{q^2}} \,,
\end{aligned}
\tag{5.18}
$$

where $\lambda(a, b, c) = a^2 + b^2 + c^2 - 2ab - 2ac - 2bc$.

The differential decay rate is proportional to the spin-summed amplitude squared. We have

$$
\begin{aligned}
\left| \mathcal{M}^{\text{SM+NP}} \right|^2 &= |\mathcal{M}_{SP}|^2 + |\mathcal{M}_{VA}|^2 + |\mathcal{M}_T|^2 \\
&\quad + 2\text{Re}\left[ \mathcal{M}_{SP} \mathcal{M}_{VA}^* + \mathcal{M}_{SP} \mathcal{M}_T^* + \mathcal{M}_{VA} \mathcal{M}_T^* \right] \,.
\end{aligned}
\tag{5.19}
$$

The individual terms are given by

1.

$$|\mathcal{M}_{SP}|^2 \propto \sum_{m,m'=\pm,0} \mathcal{M}^{SP}_{(m)}\, \mathcal{M}^{SP*}_{(m')}\, \mathcal{H}_{D^*}(m)\, \mathcal{H}^*_{D^*}(m) \sum_{\text{spins}} \mathcal{L}_{SP}\, \mathcal{L}^*_{SP}\,,$$
$$= |\mathcal{A}_{SP}|^2\, |\mathcal{H}_{D^*}(0)|^2 \sum_{\text{spins}} \mathcal{L}_{SP}\, \mathcal{L}^*_{SP}\,. \tag{5.20}$$

2. $|\mathcal{M}_{VA}|^2$ is given in Eq. (5.11).

3.

$$|\mathcal{M}_T|^2 \propto \sum_{m,m'=\pm,0} \left(\mathcal{H}_{D^*}(m)\, \mathcal{H}^*_{D^*}(m')\right) \sum_{n,n',p,p'=t,\pm,0} g_{nn}\, g_{n'n'}\, g_{pp}\, g_{p'p'}$$
$$\times \left(\mathcal{M}^{T}_{(m;n,p)}\, \mathcal{M}^{T*}_{(m';n',p')}\right) \sum_{\text{spins}} \mathcal{L}_T(n,p)\, \mathcal{L}^*_T(n',p')\,. \tag{5.21}$$

4.

$$\mathcal{M}_{SP}\mathcal{M}^*_{VA} \propto \sum_{m=\pm,0} \mathcal{H}_{D^*}(0)\, \mathcal{H}^*_{D^*}(m) \sum_{n=t,\pm,0} g_{nn}\, \mathcal{M}^{SP}_{(0)}$$
$$\times\, \mathcal{M}^{VA*}_{(m;n)} \sum_{\text{spins}} \mathcal{L}_{SP}\, \mathcal{L}^*_{VA}(n)\,. \tag{5.22}$$

5.

$$\mathcal{M}_{SP}\mathcal{M}^*_{T} \propto \sum_{m=\pm,0} \mathcal{H}_{D^*}(0)\, \mathcal{H}^*_{D^*}(m) \sum_{n,p=t,\pm,0} g_{nn}\, g_{pp}\, \mathcal{M}^{SP}_{(0)}$$
$$\times\, \mathcal{M}^{T*}_{(m;n,p)} \sum_{\text{spins}} \mathcal{L}_{SP}\, \mathcal{L}^*_T(n,p)\,. \tag{5.23}$$

6.

$$\mathcal{M}_{VA}\, \mathcal{M}^*_{T} \propto \sum_{m,m'=\pm,0} \mathcal{H}_{D^*}(m)\, \mathcal{H}^*_{D^*}(m') \sum_{n,n',p'=t,\pm,0} g_{nn}\, g_{n'n'}\, g_{p'p'}\, \mathcal{M}^{VA}_{(m;n)}$$
$$\times\, \mathcal{M}^{T*}_{(m';n',p')} \sum_{\text{spins}} \mathcal{L}_{VA}(n)\, \mathcal{L}^*_T(n',p')\,. \tag{5.24}$$

The leptonic contributions to $\left|\mathcal{M}^{\text{SM+NP}}\right|^2$ are given in the Appendix F.

For the vector currents we introduced the transversity amplitudes above. In the same manner we can define the transversity amplitudes for the tensor currents as,

$$\begin{aligned}\mathcal{A}_{||,T} &= (\mathcal{A}_{+,T} + \mathcal{A}_{-,T})/\sqrt{2}\,, \\ \mathcal{A}_{\perp,T} &= (\mathcal{A}_{+,T} - \mathcal{A}_{-,T})/\sqrt{2}\,. \end{aligned} \tag{5.25}$$

In what follows, we will present the angular distribution in the transversity basis where the amplitudes are $\mathcal{A}_{SP}$, $\mathcal{A}_0$, $\mathcal{A}_t$, $\mathcal{A}_{||}$, $\mathcal{A}_\perp$, $\mathcal{A}_{0,T}$, $\mathcal{A}_{||,T}$ and $\mathcal{A}_{\perp,T}$.

### 5.2.4 Angular Distribution

In the previous subsection, we computed the square of the full amplitude for $\bar{B} \to D^*(\to D\pi)\ell^-\bar{\nu}_\ell$. Using the results from appendix F, this can be expressed as a function of the final-state momenta. In this section, we obtain the angular distribution of the decay.

To this end, we use the formalism of helicity angles defined in the rest frames of the intermediate particles, as shown in Fig. 5.1. We have chosen the $z$-axis to align with the direction of the $D^*$ in the rest frame of the $B$. With this choice of alignment, the helicity angles $\theta^*$ and $\pi - \theta_\ell$ respectively measure the polar angles of the $D$ and the charged lepton in the rest frames of their parent particles ($D^*$ and $N^*$, respectively), and $\chi$ is the azimuthal angle between the decay planes of the two intermediate states. For the CP-conjugate decay, the helicity angles are defined in the same way. Thus, in comparing the decay and the CP-conjugate decay, $\bar{\theta}^* = \theta^*$, $\bar{\theta}_\ell = \theta_\ell$, and $\bar{\chi} = \chi$.

Using the above definitions we can express the four momenta of the $D$ and the $\ell^-$ in the rest frames of their respective parent particles as follows:

$$\begin{aligned} p_D^\mu &= (E_D, |\vec{p}_D|\sin\theta^*, 0, |\vec{p}_D|\cos\theta^*)\,, \\ p_\ell^\mu &= (E_\ell, |\vec{p}_\ell|\sin\theta_\ell\cos\chi, |\vec{p}_\ell|\sin\theta_\ell\sin\chi, -|\vec{p}_\ell|\cos\theta_\ell)\,, \end{aligned} \tag{5.26}$$

where $E_X$ and $\vec{p}_X$ ($X = D, \ell$) represent the energy and the three-momentum of $X$ in its parent rest

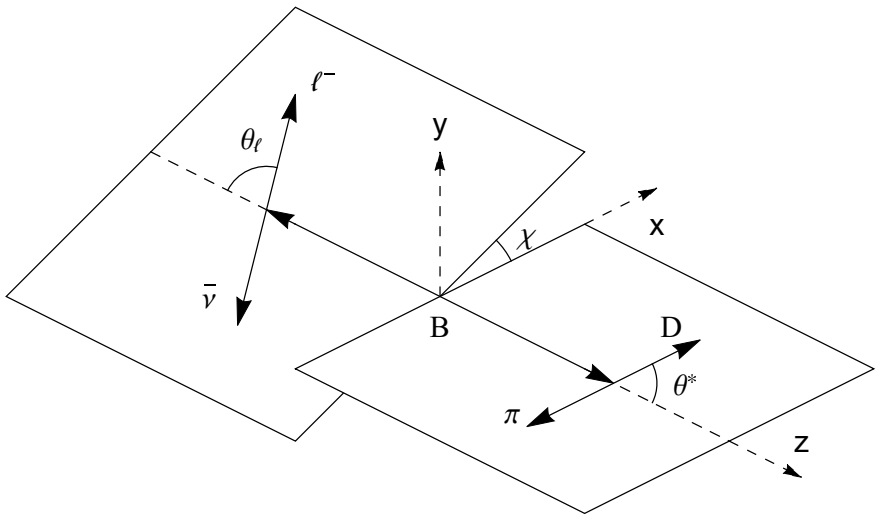


**Figure 5.1:** Definition of the angles in the $\bar{B} \to D^*(\to D\pi)\ell^-\bar{\nu}_\ell$ distribution.

frame. The complete angular distribution can then be written as [78]

$$\frac{d^4\Gamma}{dq^2\, d(\cos\theta_\ell)\, d(\cos\theta^*)\, d\chi} = \frac{3}{8\pi}\frac{G_F^2|V_{cb}|^2(q^2-m_\ell^2)^2|\vec{p}_{D^*}|}{2^8\pi^3 m_B^2 q^2} \times \mathcal{B}(D^* \to D\pi)\left(N_1 + \frac{m_\ell}{\sqrt{q^2}}N_2 + \frac{m_\ell^2}{q^2}N_3\right), \quad (5.27)$$

where $q = p_\ell + p_{\bar{\nu}_\ell}$, and $|\vec{p}_{D^*}| = \sqrt{\lambda(m_B^2, m_{D^*}^2, q^2)}/(2m_B)$, with $\lambda(a,b,c) = a^2+b^2+c^2-2ab-2ac-2bc$, is the 3-momentum of $D^*$ in the $B$-meson rest frame. For $N_1$, $N_2$ and $N_3$, the angular functions associated with the various (combinations of) helicity amplitudes are given in Tables 5.1, 5.2 and 5.3, respectively.

### 5.2.5 CP Violation and Triple Products

The components in the angular distribution that particularly interest us are those whose coefficients are $\mathrm{Im}(\mathcal{A}_i\mathcal{A}_j^*)$, where $\mathcal{A}_{i,j}$ are two different helicity amplitudes. These are the terms that are used to generate CP-violating asymmetries. Note that they are all proportional to $\sin\chi$ or $\sin 2\chi = 2\sin\chi\cos\chi$ and they change sign under the transformation $\chi \to -\chi$.

As we mentioned earlier, technically, these angular components are not, by themselves,

| Amplitude in $N_1$ | Angular Function |
|---|---|
| $\lvert\mathcal{A}_0\rvert^2$ | $4\sin^2\theta_\ell\cos^2\theta^*$ |
| $\lvert\mathcal{A}_\perp\rvert^2$ | $2\sin^2\theta^*(\cos^2\chi+\cos^2\theta_\ell\sin^2\chi)$ |
| $\lvert\mathcal{A}_\parallel\rvert^2$ | $2\sin^2\theta^*(\cos^2\theta_\ell\cos^2\chi+\sin^2\chi)$ |
| $\lvert\mathcal{A}_{\parallel,T}\rvert^2$ | $32\sin^2\theta_\ell\sin^2\theta^*\cos^2\chi$ |
| $\lvert\mathcal{A}_{\perp,T}\rvert^2$ | $32\sin^2\theta_\ell\sin^2\theta^*\sin^2\chi$ |
| $\lvert\mathcal{A}_{0,T}\rvert^2$ | $64\cos^2\theta_\ell\cos^2\theta^*$ |
| $\lvert\mathcal{A}_{SP}\rvert^2$ | $4\cos^2\theta^*$ |
| $\mathrm{Re}(\mathcal{A}_\parallel\mathcal{A}_\perp^*)$ | $-4\cos\theta_\ell\sin^2\theta^*$ |
| $\mathrm{Re}(\mathcal{A}_0\mathcal{A}_\parallel^*)$ | $-\sqrt{2}\sin 2\theta_\ell\sin 2\theta^*\cos\chi$ |
| $\mathrm{Re}(\mathcal{A}_0\mathcal{A}_\perp^*)$ | $2\sqrt{2}\sin\theta_\ell\sin 2\theta^*\cos\chi$ |
| $\mathrm{Re}(\mathcal{A}_{\parallel,T}\mathcal{A}_{SP}^*)$ | $8\sqrt{2}\sin\theta_\ell\sin 2\theta^*\cos\chi$ |
| $\mathrm{Re}(\mathcal{A}_{0,T}\mathcal{A}_{\parallel,T}^*)$ | $16\sqrt{2}\sin 2\theta_\ell\sin 2\theta^*\cos\chi$ |
| $\mathrm{Re}(\mathcal{A}_{0,T}\mathcal{A}_{SP}^*)$ | $32\cos\theta_\ell\cos^2\theta^*$ |
| $\mathrm{Im}(\mathcal{A}_\perp\mathcal{A}_0^*)$ | $-\sqrt{2}\sin 2\theta_\ell\sin 2\theta^*\sin\chi$ |
| $\mathrm{Im}(\mathcal{A}_\parallel\mathcal{A}_\perp^*)$ | $2\sin^2\theta_\ell\sin^2\theta^*\sin 2\chi$ |
| $\mathrm{Im}(\mathcal{A}_{SP}\mathcal{A}_{\perp,T}^*)$ | $-8\sqrt{2}\sin\theta_\ell\sin 2\theta^*\sin\chi$ |
| $\mathrm{Im}(\mathcal{A}_0\mathcal{A}_\parallel^*)$ | $-2\sqrt{2}\sin\theta_\ell\sin 2\theta^*\sin\chi$ |

**Table 5.1:** Terms in the $N_1$ part of the angular distribution.

CP-violating observables. Suppose that the helicity amplitudes $\mathcal{A}_i$ and $\mathcal{A}_j$ had the same weak phase but different strong phases. $\mathrm{Im}(\mathcal{A}_i\mathcal{A}_j^*)$ would then be nonzero, but this would not indicate CP violation, since the weak-phase difference vanishes. This would be a *fake* signal. Suppose instead that $\mathcal{A}_i$ and $\mathcal{A}_j$ had the same strong phase but different weak phases. $\mathrm{Im}(\mathcal{A}_i\mathcal{A}_j^*)$ would again be nonzero, and in this case it would be a *true* CP-violating signal. In order to distinguish true and fake signals, one must compare the same quantity in the decay and the CP-conjugate decay. For a true signal, the angular component will be the same in both decays. This is because, in going from process to antiprocess, the weak phases change sign and the azimuthal angle $\chi \to -\chi$. A fake signal will be indicated if the angular component changes sign. Thus, in the general case, to obtain a true CP-violating signal, one must add the angular distributions for the decay and the CP-conjugate decay. (Even though we are adding the distributions, these are referred to as CP-violating asymmetries.)

Now, as argued in the introduction, in the case of $\bar{B} \to D^*(\to D\pi)\ell^-\bar{\nu}_\ell$, the SM and NP

| Amplitude in $N_2$ | Angular Function |
|---|---|
| $\mathrm{Re}(\mathcal{A}_0\mathcal{A}^*_{0,T})$ | $-32\cos^2\theta^*$ |
| $\mathrm{Re}(\mathcal{A}_{0,T}\mathcal{A}^*_t)$ | $32\cos\theta_\ell\cos^2\theta^*$ |
| $\mathrm{Re}(\mathcal{A}_0\mathcal{A}^*_{SP})$ | $-8\cos\theta_\ell\cos^2\theta^*$ |
| $\mathrm{Re}(\mathcal{A}_t\mathcal{A}^*_{SP})$ | $8\cos^2\theta^*$ |
| $\mathrm{Re}(\mathcal{A}_\parallel\mathcal{A}^*_{\perp,T})$ | $16\cos\theta_\ell\sin^2\theta^*$ |
| $\mathrm{Re}(\mathcal{A}_{\parallel,T}\mathcal{A}^*_\perp)$ | $16\cos\theta_\ell\sin^2\theta^*$ |
| $\mathrm{Re}(\mathcal{A}_\parallel\mathcal{A}^*_{\parallel,T})$ | $-16\sin^2\theta^*$ |
| $\mathrm{Re}(\mathcal{A}_\perp\mathcal{A}^*_{\perp,T})$ | $-16\sin^2\theta^*$ |
| $\mathrm{Re}(\mathcal{A}_0\mathcal{A}^*_{\perp,T})$ | $-8\sqrt{2}\sin\theta_\ell sin2\theta^*\cos\chi$ |
| $\mathrm{Re}(\mathcal{A}_{0,T}\mathcal{A}^*_\perp)$ | $-8\sqrt{2}\sin\theta_\ell\sin 2\theta^*\cos\chi$ |
| $\mathrm{Re}(\mathcal{A}_{\parallel,T}\mathcal{A}^*_t)$ | $8\sqrt{2}\sin\theta_\ell\sin 2\theta^*\cos\chi$ |
| $\mathrm{Re}(\mathcal{A}_\parallel\mathcal{A}^*_{SP})$ | $-2\sqrt{2}\sin\theta_\ell\sin 2\theta^*\cos\chi$ |
| $\mathrm{Im}(\mathcal{A}_0\mathcal{A}^*_{\parallel,T})$ | $8\sqrt{2}\sin\theta_\ell\sin 2\theta^*\sin\chi$ |
| $\mathrm{Im}(\mathcal{A}_\parallel\mathcal{A}^*_{0,T})$ | $-8\sqrt{2}\sin\theta_\ell\sin 2\theta^*\sin\chi$ |
| $\mathrm{Im}(\mathcal{A}_t\mathcal{A}^*_{\perp,T})$ | $-8\sqrt{2}\sin\theta_\ell\sin 2\theta^*\sin\chi$ |
| $\mathrm{Im}(\mathcal{A}_\perp\mathcal{A}^*_{SP})$ | $-2\sqrt{2}\sin\theta_\ell\sin 2\theta^*\sin\chi$ |

**Table 5.2:** Terms in the $N_2$ part of the angular distribution. These are suppressed by $m_\ell/\sqrt{q^2}$.

contributions all basically have the same strong phase. That is, there is no strong-phase difference between any pair of transversity amplitudes. In this case, the angular components whose coefficients are $\mathrm{Im}(\mathcal{A}_i\mathcal{A}^*_j)$ *are* signals of CP violation.

In Tables 5.1, 5.2 and 5.3, one finds, respectively, four, three and four of these CP-violating observables. However, one must be careful here. These do not all involve different factors of $\mathrm{Im}(\mathcal{A}_i\mathcal{A}^*_j)$ – some combinations of helicity amplitudes appear in more than one Table. Also, these observables involve only three angular functions, so there can be a number of different contributions to a single observable. In addition, the angular components listed in the three Tables are not all the same size. Compared to Table 5.1, the observables in Tables 5.2 and 5.3 are suppressed by $m_\ell/\sqrt{q^2}$ and $m_\ell^2/q^2$, respectively. Typically, one has $q^2 = O(m_B^2)$, so these suppression factors are significant. However, if the angular distribution can be measured in that region of phase space where $q^2 = O(m_\ell^2)$, useful information can be obtained from the CP-violating observables in these Tables. Finally, the helicity amplitudes all get contributions from the NP operators in Eq. (5.12), so if a particular NP operator is nonzero, several helicity amplitudes may be affected.

| Amplitude in $N_3$ | Angular Function |
|---|---|
| $\lvert\mathcal{A}_t\rvert^2$ | $4\cos^2\theta^*$ |
| $\lvert\mathcal{A}_0\rvert^2$ | $4\cos^2\theta_\ell\cos^2\theta^*$ |
| $\lvert\mathcal{A}_\perp\rvert^2$ | $2\sin^2\theta_\ell\sin^2\theta^*\sin^2\chi$ |
| $\lvert\mathcal{A}_\parallel\rvert^2$ | $2\sin^2\theta_\ell\sin^2\theta^*\cos^2\chi$ |
| $\lvert\mathcal{A}_{\parallel,T}\rvert^2$ | $32\sin^2\theta^*(\cos^2\theta_\ell\cos^2\chi+\sin^2\chi)$ |
| $\lvert\mathcal{A}_{\perp,T}\rvert^2$ | $32\sin^2\theta^*(\cos^2\chi+\cos^2\theta_\ell\sin^2\chi)$ |
| $\lvert\mathcal{A}_{0,T}\rvert^2$ | $64\sin^2\theta_\ell\cos^2\theta^*$ |
| $\mathrm{Re}(\mathcal{A}_0\mathcal{A}_t^*)$ | $-8\cos\theta_\ell\cos^2\theta^*$ |
| $\mathrm{Re}(\mathcal{A}_0\mathcal{A}_\parallel^*)$ | $\sqrt{2}\sin 2\theta_\ell\sin 2\theta^*\cos\chi$ |
| $\mathrm{Re}(\mathcal{A}_\parallel\mathcal{A}_t^*)$ | $-2\sqrt{2}\sin\theta_\ell\sin 2\theta^*\cos\chi$ |
| $\mathrm{Re}(\mathcal{A}_{0,T}\mathcal{A}_{\perp,T}^*)$ | $32\sqrt{2}\sin\theta_\ell\sin 2\theta^*\cos\chi$ |
| $\mathrm{Re}(\mathcal{A}_{0,T}\mathcal{A}_{\parallel,T}^*)$ | $-16\sqrt{2}\sin 2\theta_\ell\sin 2\theta^*\cos\chi$ |
| $\mathrm{Re}(\mathcal{A}_{\parallel,T}\mathcal{A}_{\perp,T}^*)$ | $-64\cos\theta_\ell\sin^2\theta^*$ |
| $\mathrm{Im}(\mathcal{A}_\parallel\mathcal{A}_\perp^*)$ | $-2\sin^2\theta_\ell\sin^2\theta^*\sin 2\chi$ |
| $\mathrm{Im}(\mathcal{A}_t\mathcal{A}_\perp^*)$ | $2\sqrt{2}\sin\theta_\ell\sin 2\theta^*\sin\chi$ |
| $\mathrm{Im}(\mathcal{A}_\perp\mathcal{A}_0^*)$ | $\sqrt{2}\sin 2\theta_\ell\sin 2\theta^*\sin\chi$ |

**Table 5.3:** Terms in the $N_3$ part of the angular distribution. These are suppressed by $m_\ell^2/q^2$.

In Table 5.4 we present all the information about the CP-violating angular observables: the contributing helicity amplitudes, the angular functions, the suppression factor, and the NP couplings probed. This allows us to interpret possible future measurements.

For example, suppose that the angular distribution is measured using the full data set. In this case, the measurements are dominated by the unsuppressed contributions of Table 5.1. This angular distribution contains both CP-conserving and CP-violating pieces, and both can be affected by NP. We focus on the CP-violating observables of Table 5.4.

- Suppose that the angular distribution is found to include the component $\sin 2\theta_\ell\sin 2\theta^*\sin\chi$. This indicates that $\mathrm{Im}(\mathcal{A}_\perp\mathcal{A}_0^*)\neq 0$, which implies that $g_R\neq 0$, and that it has a different (weak) phase than $(1+g_L)$. In this case, one expects to also observe nonzero coefficients for the other two angular functions in Table 5.4, $\sin^2\theta_\ell\sin^2\theta^*\sin 2\chi$ and $\sin\theta_\ell\sin 2\theta^*\sin\chi$.

- The third angular function, $\sin\theta_\ell\sin 2\theta^*\sin\chi$, receives an additional contribution from $\mathrm{Im}(\mathcal{A}_{SP}\mathcal{A}_{\perp,T}^*)$. But if it has been established that $g_R\neq 0$, one cannot tell if $g_P$ and $g_T$ are

| Not suppressed | Coupling | Angular Function |
|---|---|---|
| $\mathrm{Im}(\mathcal{A}_\perp \mathcal{A}_0^*)$ | $\mathrm{Im}[(1+g_L+g_R)(1+g_L-g_R)^*]$ | $-\sqrt{2}\sin 2\theta_\ell \sin 2\theta^* \sin\chi$ |
| $\mathrm{Im}(\mathcal{A}_\parallel \mathcal{A}_\perp^*)$ | $\mathrm{Im}[(1+g_L-g_R)(1+g_L+g_R)^*]$ | $2\sin^2\theta_\ell \sin^2\theta^* \sin 2\chi$ |
| $\mathrm{Im}(\mathcal{A}_{SP} \mathcal{A}_{\perp,T}^*)$ | $\mathrm{Im}(g_P g_T^*)$ | $-8\sqrt{2}\sin\theta_\ell \sin 2\theta^* \sin\chi$ |
| $\mathrm{Im}(\mathcal{A}_0 \mathcal{A}_\parallel^*)$ | $\mathrm{Im}[(1+g_L-g_R)(1+g_L+g_R)^*]$ | $-2\sqrt{2}\sin\theta_\ell \sin 2\theta^* \sin\chi$ |
| Suppressed by $m_\ell/\sqrt{q^2}$ | Coupling | Angular Function |
| $\mathrm{Im}(\mathcal{A}_0 \mathcal{A}_{\parallel,T}^*)$ | $\mathrm{Im}[(1+g_L-g_R)g_T^*]$ | $8\sqrt{2}\sin\theta_\ell \sin 2\theta^* \sin\chi$ |
| $\mathrm{Im}(\mathcal{A}_\parallel \mathcal{A}_{0,T}^*)$ | $\mathrm{Im}[(1+g_L-g_R)g_T^*]$ | $-8\sqrt{2}\sin\theta_\ell \sin 2\theta^* \sin\chi$ |
| $\mathrm{Im}(\mathcal{A}_t \mathcal{A}_{\perp,T}^*)$ | $\mathrm{Im}[(1+g_L-g_R)g_T^*]$ | $-8\sqrt{2}\sin\theta_\ell \sin 2\theta^* \sin\chi$ |
| $\mathrm{Im}(\mathcal{A}_\perp \mathcal{A}_{SP}^*)$ | $\mathrm{Im}[(1+g_L+g_R)g_P^*]$ | $-2\sqrt{2}\sin\theta_\ell \sin 2\theta^* \sin\chi$ |
| Suppressed by $m_\ell^2/q^2$ | Coupling | Angular Function |
| $\mathrm{Im}(\mathcal{A}_\parallel \mathcal{A}_\perp^*)$ | $\mathrm{Im}[(1+g_L-g_R)(1+g_L+g_R)^*]$ | $-2\sin^2\theta_\ell \sin^2\theta^* \sin 2\chi$ |
| $\mathrm{Im}(\mathcal{A}_t \mathcal{A}_\perp^*)$ | $\mathrm{Im}[(1+g_L+g_R)(1+g_L-g_R)^*]$ | $2\sqrt{2}\sin\theta_\ell \sin 2\theta^* \sin\chi$ |
| $\mathrm{Im}(\mathcal{A}_\perp \mathcal{A}_0^*)$ | $\mathrm{Im}[(1+g_L+g_R)(1+g_L-g_R)^*]$ | $\sqrt{2}\sin 2\theta_\ell \sin 2\theta^* \sin\chi$ |

**Table 5.4:** The CP-violating terms in the angular distribution, their corresponding NP couplings, and the angular functions to which they contribute.

also nonzero. This is where the CP-conserving observables come into play. From Table 5.1, we see that both $|\mathcal{A}_{SP}|^2$ and $|\mathcal{A}_{\perp,T}|^2$ can be determined from the angular distribution, so in principle we will know if they are nonzero (though we will have no information about their phases).

- If it is found that the coefficients of the first two angular functions are $\simeq 0$, this implies that $g_R \simeq 0$ (or that its phase is the same as that of $(1+g_L)$). In this case, the measurement of a nonzero coefficient of the third angular function will point clearly to $\mathrm{Im}(\mathcal{A}_{SP}\mathcal{A}_{\perp,T}^*) \neq 0$.

Finally, suppose that the angular analysis reveals no unsuppressed CP-violating observables. To probe other such observables, it will now be necessary to reconstruct the angular distribution for the data with $q^2 = O(m_\ell^2)$. If this is possible, one can see if the angular function $\sin\theta_\ell \sin 2\theta^* \sin\chi$ has a nonzero coefficient in the data suppressed by $m_\ell/\sqrt{q^2}$. If it does, this indicates that $g_T$ or $g_P$ (or both) is nonzero. As noted above, one can perform a cross-check by measuring CP-conserving observables. In particular, from Table 5.1, we see that the angular distribution can give us information about new tensor and scalar interactions.

## 5.3 Leptoquarks as New-Physics Models

In the previous section, we derived the angular distribution for $\bar{B} \to D^*(\to D\pi)\ell^-\bar{\nu}_\ell$ in the presence of NP. This applies to $\ell = e, \mu, \tau$. In this section, we examine the leptoquark (LQ) models that can generate nonzero CP-violating observables in $\bar{B}^0 \to D^{*+}\mu^-\bar{\nu}_\mu$.

In the SM, the decay $b \to c\ell^-\bar{\nu}$ is due to the tree-level exchange of a $W$. In order to generate a significant discrepancy with the SM, the NP contributions to this decay must also take place at tree level. This can occur in the presence of leptoquarks [28, 85, 86].

Below we examine whether CP-violating observables can be generated with LQs. Specifically, we determine which of the NP parameters $g_{L,R,S,P,T}$ [Eq. (5.12)] can be generated. Here, our main goal is to examine the implications of the measurement of CP-violating observables in $\bar{B}^0 \to D^{*+}\mu^-\bar{\nu}_\mu$. As such, these LQ models are not complete. That is, there may be constraints from other measurements that are not taken into account here. For example, because $R^{\mu/e}_{D^*}/(R^{\mu/e}_{D^*})_{\rm SM} = 1.00\pm0.05$, any NP that contributes to $b \to c\mu^-\bar{\nu}_\mu$ must equally affect $b \to ce^-\bar{\nu}_e$. But it is well known that a LQ that couples to both $\mu$ and $e$ will be constrained by $\mu \to e\gamma$ and $b \to se\mu$ [87]. Should a CP-violating observable be measured in $\bar{B}^0 \to D^{*+}\mu^-\bar{\nu}_\mu$ suggesting the presence of LQs, these constraints must be taken into account at the model-building stage. Now we discuss the implications of CP violation for LQ models of our interest.

In previous chapters, we discussed how LQs contribute to the decay $\bar{B}^0 \to D^{(*)}\ell^-\bar{\nu}_\ell$. Here we repeat the discussion to be self-contained. There are ten models in which the LQ couples to SM particles through dimension $\leq 4$ operators [35]. These include five spin-0 and five spin-1 LQs. Six of these can contribute to $b \to c\mu^-\bar{\nu}_\mu$ [28]. Three have fermion-number-conserving couplings and three have fermion-number-violating couplings. The interaction Lagrangian that generates the

contributions to $b \to c\mu^-\bar{\nu}_\mu$ is given by

$$\begin{aligned}
\mathcal{L}^{\rm LQ} &= \mathcal{L}^{\rm LQ}_{F=0} + \mathcal{L}^{\rm LQ}_{F=-2}\,, \\
\mathcal{L}^{\rm LQ}_{F=0} &= (h^{ij}_{1L}\bar{Q}_{iL}\gamma^\mu L_{jL} + h^{ij}_{1R}\bar{d}_{iR}\gamma^\mu \ell_{jR})U_{1\mu} + h^{ij}_{3L}\bar{Q}_{iL}\vec{\sigma}\gamma^\mu L_{jL}\cdot\vec{U}_{3\mu} \\
&\quad + (h^{ij}_{2L}\bar{u}_{iR}L_{jL} + h^{ij}_{2R}\bar{Q}_{iL}i\sigma_2\ell_{jR})R_2 + h.c., \\
\mathcal{L}^{\rm LQ}_{F=-2} &= (g^{ij}_{1L}\bar{Q}^c_{iL}i\sigma_2 L_{jL} + g^{ij}_{1R}\bar{u}^c_{iR}\ell_{jR})S_1 + (g^{ij}_{3L}\bar{Q}^c_{iL}i\sigma_2\vec{\sigma}L_{jL})\cdot\vec{S}_3 \\
&\quad + (g^{ij}_{2L}\bar{d}^c_{iR}\gamma_\mu L_{jL} + g^{ij}_{2R}\bar{Q}^c_{iL}\gamma_\mu\ell_{jR})V^\mu_2 + h.c.
\end{aligned} \tag{5.28}$$

Here $Q$ and $L$ represent left-handed quark and lepton $SU(2)_L$ doublets, respectively; $u$, $d$ and $\ell$ represent right-handed up-type quark, down-type quark and charged lepton $SU(2)_L$ singlets, respectively. The indices $i$ and $j$ are the quark and lepton generations and $\psi^c = C\bar{\psi}^T$ is a charge-conjugated field.

For all six models, we integrate out the LQ to form four-fermion operators. We then perform Fierz transformations to put these operators in the form of Eq. (5.12). In this way, we determine which LQs contribute to which $g_{L,R,S,P,T}$ coefficients.

In Table 5.5 we summarize the contributions of all the LQs to the $g_{L,R,S,P,T}$ coefficients of Eq. (5.12).

| Model | $g_L$ | $g_R$ | $g_S$ | $g_P$ | $g_T$ |
|---|---|---|---|---|---|
| $U_1$ | $\frac{1}{2}h^{22}_{1L}h^{32*}_{1L}$ | 0 | $-h^{22}_{1L}h^{32*}_{1R}$ | $-h^{22}_{1L}h^{32*}_{1R}$ | 0 |
| $U_3$ | $-\frac{1}{2}h^{22}_{3L}h^{32*}_{3L}$ | 0 | 0 | 0 | 0 |
| $R_2$ | 0 | 0 | $\frac{1}{4}h^{22}_{2L}h^{32*}_{2R}$ | $-\frac{1}{4}h^{22}_{2L}h^{32*}_{2R}$ | $\frac{1}{16}h^{22}_{2L}h^{32*}_{2R}$ |
| $S_1$ | $-\frac{1}{4}g^{32}_{1L}g^{22*}_{1L}$ | 0 | $\frac{1}{4}g^{32}_{1L}g^{22*}_{1R}$ | $-\frac{1}{4}g^{32}_{1L}g^{22*}_{1R}$ | $-\frac{1}{16}g^{32}_{1L}g^{22*}_{1R}$ |
| $S_3$ | $\frac{1}{4}g^{32}_{3L}g^{22*}_{3L}$ | 0 | 0 | 0 | 0 |
| $V_2$ | 0 | 0 | $-g^{22*}_{2R}g^{32}_{2L}$ | $-g^{22*}_{2R}g^{32}_{2L}$ | 0 |

**Table 5.5:** Contributions of the various LQs to the $g_{L,R,S,P,T}$ coefficients of Eq. (5.12). All entries must be multiplied by $1/(\sqrt{2}G_F V_{cb}M^2_{\rm LQ})$.

### 5.3.1 CP Violation

As shown in Table 5.4, the CP-violating observables involve any pair of $\{(1+g_L), g_R, g_P, g_T\}$. Above we have seen that most LQ models contribute to $g_L$. It must be pointed out that, in $b \to c\mu^-\bar{\nu}_\mu$, $g_L$ cannot be large. This is because it is the coefficient of the $(V-A)\times(V-A)$ operator $\bar{c}\gamma_\mu(1-\gamma_5)b\bar{\mu}\gamma^\mu(1-\gamma_5)\nu_\mu$, which is related by $SU(2)_L\times U(1)_Y$ to the $b \to s\mu^+\mu^-$ operator $\bar{s}\gamma_\mu(1-\gamma_5)b\bar{\mu}\gamma^\mu(1-\gamma_5)\mu$ [88]. In order to explain the anomalies in the $b \to s\mu^+\mu^-$ observables, we require [89]

$$g_L = \frac{\alpha}{2\pi}(-0.68 \pm 0.12) = O(10^{-3}) \ . \tag{5.29}$$

In $(1+g_L)$, this is negligible.

Most NP models proposed to explain the $R_{D^{(*)}}$ and $R_{J/\psi}$ experimental data contribute only to $g_L$ (in $b \to c\tau^-\bar{\nu}_\tau$). As such, they predict no CP-violating effects. Should a nonzero CP-violating observable be measured, this would rule out these models, or at least force them to be modified.

Conclusions about the type of NP present depend on which nonzero observables are measured:

- If the angular distribution is found to include the components $\sin 2\theta_\ell \sin 2\theta^* \sin\chi$ and $\sin^2\theta_\ell \sin^2\theta^* \sin 2\chi$ (the top two entries in Table 5.4), this requires a nonzero $g_R$. This can only arise in a $W'$ model, and so excludes all LQ models.

- If the $\sin 2\theta_\ell \sin 2\theta^* \sin\chi$ and $\sin^2\theta_\ell \sin^2\theta^* \sin 2\chi$ components do not appear in the angular distribution, but $\sin\theta_\ell \sin 2\theta^* \sin\chi$ (the third entry in Table 5.4) does, this indicates that $g_P$ and $g_T$ are nonzero, and that they have a relative phase. This can only occur in a model with two LQs. $g_T$ can come from a $R_2$ or $S_1$ LQ, while $g_P$ can be due to a $U_1$, $R_2$, $S_1$ or $V_2$ LQ (but the two LQs must be different).

- If none of the above three angular functions are present in the angular distribution, this implies that $g_R$ and one of $g_P$ and $g_T$ are zero (or that there is no phase difference). There can still be a CP-violating observable in the data suppressed by $m_\ell/\sqrt{q^2}$ (entries 5-8 in Table

5.4). If this is found to be nonzero, this indicates that one of $g_T$ or $g_P$ (or both, if they have the same phase) is nonzero. The $g_P$ option is particularly interesting. The $U_1$ LQ is a very popular NP choice (for example, see Ref. [90]), and it can generate $g_P$, but not $g_T$. If this is the only nonzero CP-violating observable found, this would be strong support for the $U_1$ LQ.

- There is also information from the CP-conserving observables. The full angular distribution has components proportional to $|\mathcal{A}_{\parallel,T}|^2$, $|\mathcal{A}_{\perp,T}|^2$, $|\mathcal{A}_{0,T}|^2$ and $|\mathcal{A}_{SP}|^2$. Measurements of these quantities also gives information about which of $g_T$ and/or $g_P$ is or is not nonzero.

## 5.4 Conclusions

At the present time, the anomalies in the measurements of $R_{D^{(*)}}$ and $R_{J/\psi}$ suggest the presence of new physics in $b \to c\tau^-\bar{\nu}$ decays. A number of different NP explanations have been proposed, as well as several methods for differentiating these NP models. In this chapter, we explored the possibility of using CP-violating observables to distinguish the various NP scenarios.

The angular distribution in $\bar{B}^0 \to D^{*+}(\to D^0\pi^+)\tau^-\bar{\nu}_\tau$ can be used to provide CP-violating asymmetries. Now, the reconstruction of this angular distribution requires the knowledge of the 3-momentum of the $\tau$. The problem here is that $\vec{p}_\tau$ cannot be measured since its decay products include $\nu_\tau$, which is undetected. Thus, while our ultimate goal is to compute the complete angular distribution, including information related to the decay products of the $\tau$, here we took a first step by focusing on the decay $\bar{B}^0 \to D^{*+}\mu^-\bar{\nu}_\mu$. Here $\vec{p}_\mu$ is measurable, so the angular distribution can be constructed. In addition, NP that contributes to $b \to c\tau^-\bar{\nu}$ may well also affect $b \to c\mu^-\bar{\nu}$.

In the SM, the hadronic $b \to c$ current is purely LH. In the presence of NP, there can be additional contributions to this LH current, parametrized by $g_L$, as well as other Lorentz structures: RH ($g_R$), scalar ($g_S$), pseudoscalar ($g_P$) and tensor ($g_T$) currents. We computed the angular distribution of $\bar{B} \to D^*\ell^-\bar{\nu}_\ell$ in terms of the helicity amplitudes $A_i$, both in the SM and with NP. We identified the CP-violating angular asymmetries, proportional to $\mathrm{Im}[A_iA_j^*]$, and showed how all CP-violating observables depend on any pair of $\{(1+g_L), g_R, g_P, g_T\}$.

We then examined various LQ models that contribute to $b \to c\mu^-\bar{\nu}_\mu$. While LQ models do

not contribute to $g_R$, they can contribute to all other couplings, namely $g_L$, $g_P$ and $g_T$.

The most popular explanations of the $B$ anomalies involve NP that contributes only to $g_L$. Should any nonzero CP-violating observable be measured, this would rule out these models, or at least require them to be modified. In addition, there are CP-violating asymmetries that depend on $(1 + g_L)$-$g_R$, $g_P$-$g_T$, $(1 + g_L + g_R)$-$g_P$ and $(1 + g_L - g_R)$-$g_T$ interference. By measuring all of these, along with the CP-conserving components of the angular distribution, it will be possible to distinguish several LQ models.

# CHAPTER 6

# B ANOMALIES AND THE MUON $(g-2)$

## 6.1 Introduction

So far, we have been mainly concerned with $B$ anomalies and the new-physics effects in $B$ decays. Another anomaly in low energy measurements that has persisted for a long time is the muon $(g-2)$. In this chapter which is based on Ref. [91], we explain all the $B$-meson and the muon $(g-2)$ anomalies in a concrete model: a two-Higgs-doublet model (2HDM) extended to include TeV-scale leptoquarks and a light scalar $S$ with mass $m_S \sim 10-200$ MeV. We find solutions that depend on only a small number of parameters and show that these explanations motivate interesting new searches, particularly for rare meson decays to diphoton final states and Higgs boson decays to four photons.

The anomalous magnetic moment of the muon is a longstanding anomaly in particle physics. A recent evaluation of the standard model (SM) prediction [92] finds a $3.7\,\sigma$ discrepancy with the experimental measurement [93]:

$$(g-2)_\mu^{exp} - (g-2)_\mu^{\rm SM} = 27.4(2.7)(2.6)(6.3)\times 10^{-10}\,, \tag{6.1}$$

where the first two uncertainties are theoretical and the last is experimental.

The $B$ anomalies that we have been concerned with so far, were in the charged current (CC) processes, $b \to c\tau^-\bar{\nu}_\tau$. There are also many measurements in the neutral current (NC) processes $(b \to s\ell^+\ell^-)$ that show deviations from SM predictions. Similar to $R(D^{(*)})$, the lepton universality ratio $R_K \equiv \mathcal{B}(B^+ \to K^+\mu^+\mu^-)/\mathcal{B}(B^+ \to K^+e^+e^-)$ [94, 95] has been precisely measured by LHCb [96], which finds

$$R_K^{\rm exp} = 0.846\,^{+0.060\ +0.016}_{-0.054\ -0.014}\,,\ 1 \le q^2 \le 6.0\ {\rm GeV}^2\,, \tag{6.2}$$

where $q^2 = m^2_{\ell^+\ell^-}$. This is lower than the SM prediction $R_K^{\rm SM} = 1.00 \pm 0.01$ [97] by $2.5\sigma$. The related ratio $R_{K^*} \equiv \mathcal{B}(B^0 \to K^{*0}\mu^+\mu^-)/\mathcal{B}(B^0 \to K^{*0}e^+e^-)$ has been measured by LHCb to be [98]

$$R_{K^*}^{\rm exp} = \begin{cases} 0.66\,^{+0.11}_{-0.07} \pm 0.03\,, & 0.045 \le q^2 \le 1.1\,{\rm GeV}^2 \text{ (low } q^2\text{)} \\ 0.69\,^{+0.11}_{-0.07} \pm 0.05\,, & 1.1 \le q^2 \le 6.0\,{\rm GeV}^2 \text{ (central } q^2\text{)}\,. \end{cases} \tag{6.3}$$

These are also lower than the SM predictions [97] $R_{K^*}^{\rm SM} = 0.906 \pm 0.028$ (low $q^2$) and $R_{K^*}^{\rm SM} = 1.00 \pm 0.01$ (central $q^2$) by $2.3\sigma$ and $2.5\sigma$, respectively. Taken together, the general consensus is that these $B$ decay branching ratios differ significantly from SM predictions, and theoretical hadronic uncertainties [99, 100, 101] alone may not explain the data.

An interesting question, then, is whether the $B$ anomalies have a common explanation in terms of new physics. Early work on the simultaneous explanation of the CC and NC anomalies [88, 102, 103, 104] has been followed by many model calculations; an incomplete list can be found in Refs. [105, 106, 107, 108, 109, 110, 111, 112, 113, 114, 115, 116, 89, 117, 118, 119, 120, 121, 122, 123, 124, 125, 126, 127, 41, 128, 90, 129, 130, 131, 132, 133, 134]. Remarkably, there appears to be a rather simple explanation for both the CC and NC anomalies in terms of a single vector leptoquark $U$ with SM quantum numbers $(3, 1, \frac{2}{3})$ that couples dominantly to left-handed quarks and leptons. For a mass $m_U \sim 1$ TeV and $O(1)$ couplings to the third generation, the $U$ leptoquark can explain the $R(D^{(*)})$ and $R(K^{(*)})$ anomalies, at least for the central $q^2$ data. Weak-scale states do not fully resolve the low $q^2$ discrepancy, since a larger effect is required to modify the larger SM widths near the photon pole, but the $U$ leptoquark does also reduce the discrepancy for the low $q^2$ data to roughly $1.7\sigma$ [89].

However, the $U$ leptoquark does not resolve the $(g-2)_\mu$ anomaly; it contributes at one-loop, but this contribution is too small. We must therefore introduce additional particles if we are also to explain the $(g-2)_\mu$ discrepancy. To do this, we consider a weakly coupled light scalar particle $S$ with mass $m_S \sim 10 - 200$ MeV that is an extension of the standard Type II 2HDM model. The scalar $S$, which we will often refer to as the dark Higgs boson, couples to both leptons and quarks, but with couplings that are suppressed both by Yukawa couplings and a small mixing parameter $\sin\theta$.

At the one-loop level, its contribution to $(g-2)_\mu$ is too small to resolve the anomaly. However, motivated by the leptoquark solution to the $B$ anomalies, we note that leptoquarks (as well as other TeV-scale particles) will generically induce an $S\gamma\gamma$ coupling, and this can resolve the $(g-2)_\mu$ anomaly through a two-loop Barr-Zee diagram (Fig. 6.4). In this way, the solutions to the $(g-2)_\mu$ and $B$ anomalies proposed here are connected. As an aside, for values of $m_S$ just below $2m_\mu$, this model can also completely remove the discrepancy in the low $q^2$ of $R_{K^*}$ measurement, following a possibility noted previously in Ref. [135].

In addition to resolving longstanding anomalies, the proposed explanation predicts new signals. In particular, given the light state $S$ and its couplings to electrons and photons, the model predicts new meson decays, such as $B \to KS$ and $K \to \pi S$, followed by $S \to e^+e^-, \gamma\gamma$, leading to di-lepton and di-photon signals that could be discovered in current and near-future experiments. The model also predicts exotic Higgs boson decays $h \to SS \to \gamma\gamma\gamma\gamma$, which may appear in detectors as a contribution to the $h \to \gamma\gamma$ signal.

This chapter is organized as follows. In Sec. 6.2, we present the model, including the new fields and the relevant model parameters. In Sec. 6.3, we determine the parameter values that resolve the $(g-2)_\mu$ anomaly. In Sec. 6.4, we then discuss constraints on the model from hadronic physics and show that a resolution to the $(g-2)_\mu$ and $B$ constraints exists in a viable region of parameter space. The interesting implications for exotic $B$, $K$, and Higgs boson decays are discussed in Sec. 6.5. In Sec. 6.6, we conclude this chapter with a short summary.

## 6.2 The Model

Our model is an extension of the Type II 2HDM. The Type II 2HDM contains two Higgs doublets $H_u$ and $H_d$, which get vacuum expectation values (vevs) $v_u$ and $v_d$ and give mass to the up-type and down-type fermions, respectively. We extend this by adding a singlet scalar $\phi$, which

couples to the Higgs doublets through the portal interactions [91]

$$V_{\text{portal}} = A\,(H_u^\dagger H_d + H_d^\dagger H_u)\phi + \left[\lambda_u H_u^\dagger H_u + \lambda_d H_d^\dagger H_d + \lambda_{ud}(H_u^\dagger H_d + H_d^\dagger H_u)\right]\phi\phi\,, \tag{6.4}$$

where CP conservation is assumed. In this extension, we consider parameters such that $H_u$ and $H_d$ get vevs, but $\phi$ doesn't. After electroweak symmetry breaking, then, the trilinear scalar couplings mix the new scalar with the Higgs bosons of the 2HDM, and the quartic scalar couplings contribute to new Higgs boson decays $h \to \phi\phi$ and to the mass of the $\phi$.

More precisely, to determine the physical states of the theory, we minimize the full Higgs potential and diagonalize the mass matrices; for details, see Appendix G. In the end, the physical states include the SM-like Higgs boson $h$ and the heavy Higgs bosons $H$, $A$, and $H^\pm$ of the 2HDM, but also a new real scalar, the dark Higgs boson $S$, with Lagrangian [91]

$$\mathcal{L}_S = \frac{1}{2}(\partial_\mu S)^2 - \frac{1}{2}m_S^2 S^2 - \sin\theta\tan\beta\sum_{f=d,l}\frac{m_f}{v}\bar{f}fS - \sin\theta'\cot\beta\sum_{f=u}\frac{m_f}{v}\bar{f}fS - \frac{1}{4}\kappa S F_{\mu\nu}F^{\mu\nu}, \tag{6.5}$$

where $v \simeq 246$ GeV and $\tan\beta = v_u/v_d$. The couplings to fermions are inherited from the mixing of the dark Higgs boson with the 2HDM Higgs bosons: they are suppressed by Yukawa couplings, and the down-type couplings are enhanced by $\tan\beta$, while the up-type couplings are suppressed by $\cot\beta$. In addition, they are modified by the mixing angles $\sin\theta$ and $\sin\theta'$. For weak portal interactions $A \ll m_h$ and large $\tan\beta$, these mixing angles can be written in terms of the physical Higgs boson masses. As shown in Appendix G, the results are

$$\sin\theta \approx -\frac{vA}{m_H^2}\,, \quad \sin\theta' \approx -\frac{2vA}{m_h^2}\left(1 - \frac{m_h^2}{2m_H^2}\right). \tag{6.6}$$

The last term of Eq. (6.5) is an $S\gamma\gamma$ coupling governed by the parameter $\kappa$, which has dimensions of inverse mass. This coupling is generically induced by heavy states, such as leptoquarks, as will be discussed in Sec. 6.3.

Finally, as discussed in Sec. 6.1, we add a vector leptoquark $U$ with SM quantum numbers $(3, 1, \frac{2}{3})$ and Lagrangian

$$\mathcal{L}_U = -\frac{1}{4}F^U_{\mu\nu}F^{U\mu\nu} - m_U^2 U_\mu U^\mu - \left[h^U_{ij}\left(\bar{Q}_{iL}\gamma^\mu L_{jL}\right)U_\mu + \text{H.c.}\right] - g m_U S U_\mu U^\mu \,. \tag{6.7}$$

The $U$ leptoquark's couplings to left-handed quarks and leptons resolve the $B$ meson anomalies. The leptoquark's couplings to right-handed quarks and leptons are constrained to be small [136]. We have also included the leptoquark's couplings to $S$. This interaction is allowed by all symmetries, but will not play an important role in any of the phenomenology discussed below. As we will discuss later, we consider the $U$ leptoquark coupling to photons to be the same as the one between the $W$ boson and photons. Since the leptoquark is colored, it couples to gluons also [137]. This coupling leads to their pair production at high energies but it does not affect our phenomenology here.

In summary, the model we consider consists of a 2HDM model extended to include a light dark Higgs boson $S$ and a leptoquark $U$. The leptoquark's couplings $h^U_{ij}$ are chosen to resolve the $B$ anomalies [41]. In addition to these, the parameters of the theory that are most relevant for the phenomenology we discuss below are

$$m_S, \tan\beta, \sin\theta, m_H, \kappa \,, \tag{6.8}$$

where $\tan\beta$, $\sin\theta$, and $m_H$ fully determine $\sin\theta'$ and the $S$ couplings to fermions, and $\kappa$ determines the $S$ couplings to photons. We will be primarily interested in the parameter ranges $m_S \sim 10 - 200$ MeV, moderate to large $\tan\beta \sim 10 - 60$, small mixing angles $\sin\theta \sim 0.005$, $m_H \sim 1$ TeV, and $\kappa \sim (1\,\text{TeV})^{-1}$.

### 6.3 Resolving the Muon Magnetic Moment Anomaly

Given a 2HDM extended to include a dark Higgs boson $S$ and a vector leptoquark $U$ through the Lagrangian terms of Eqs. (6.5) and (6.7), respectively, we can now calculate the beyond-the-SM

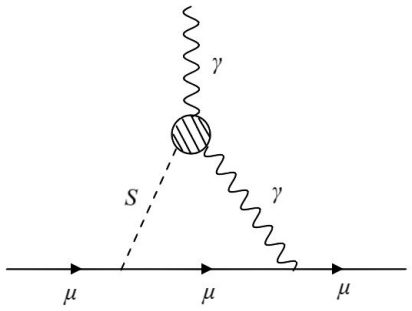


**Figure 6.1:** Contribution of the effective $S\gamma\gamma$ coupling to $(g-2)_\mu$.

contributions to $(g-2)_\mu$.

### 6.3.1 Dark Higgs Boson Contribution from Effective $S\gamma\gamma$ Coupling

Let us first consider the dark Higgs boson contribution from the $S\gamma\gamma$ effective coupling shown in Fig. 6.1. This contribution is dominated by the log-enhanced term [138]

$$\Delta(g-2)_\mu^{S\gamma\gamma} \approx \frac{1}{4\pi^2}\sin\theta\tan\beta\frac{m_\mu^2}{v}\kappa\ln\left(\frac{\Lambda}{m_S}\right)\,, \tag{6.9}$$

where $\Lambda$ is the cutoff scale, which we may take to be of the order of the mass of the particles that induce the effective $S\gamma\gamma$ coupling. Parameters required to resolve the $(g-2)_\mu$ anomaly are presented in Fig. 6.2. For dark Higgs mixing angle $\sin\theta \sim 0.005$ and $\tan\beta \sim 10-60$, we see that the effective coupling required is $\kappa \sim (1\,\text{TeV})^{-1}$. In our calculations we also include the contribution to the lepton anomalous magnetic moment at the one-loop level, which has been calculated to be [139]

$$\delta a_\ell^{(\text{1-loop})} = \frac{g_\ell^2}{8\pi^2}\int_0^1 dz\frac{(1+z)(1-z)^2}{(1-z)^2+r^{-2}z}\,, \tag{6.10}$$

where $r = m_\ell/m_S$ and, in our case, $g_\ell = \sin\theta\tan\beta(m_\ell/v)$.

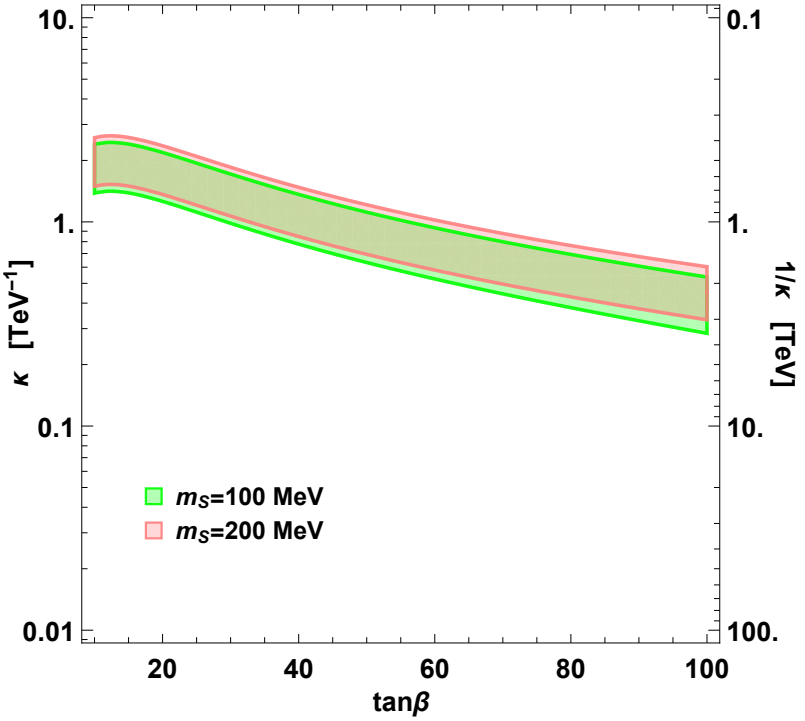


**Figure 6.2:** The region of the $(\tan\beta, \kappa)$ plane where an effective $S\gamma\gamma$ coupling induces a Barr-Zee contribution to $(g-2)_\mu$ that enhances the theoretical prediction to be within $1\sigma$ of the measured value. The sub-dominant 1-loop contribution from a virtual $S$ has also been included. We fix $\sin\theta = 0.005$, $\Lambda = 2$ TeV, and show results for $m_S = 100$ MeV and 200 MeV, as indicated.

### 6.3.2 Dark Higgs Boson Contribution from $S\gamma\gamma$ Coupling Induced by $V$ Leptoquarks

How could such values of $\kappa$ be induced? As an example, motivated by the effectiveness of leptoquarks for explaining the $B$ anomalies, we consider adding $N_{\rm LQ}$ vector leptoquarks $V_i$, $i = 1, \ldots, N_{\rm LQ}$, with Lagrangians

$$\mathcal{L}_{V_i} = -\frac{1}{4} F^{V_i}_{\mu\nu} F^{V_i \mu\nu} - m^2_{V_i} V_{i\mu} V^\mu_i - \left[ h^V_{jk} \left( \bar{Q}_{jR} \gamma^\mu L_{kR} \right) V_{i\mu} + \text{H.c.} \right] - g_{V_i} m_{V_i} S V_{i\mu} V^\mu_i \,, \tag{6.11}$$

where for simplicity we add only leptoquarks with SM quantum numbers $(3, 1, \frac{5}{3})$ and assume that their couplings to right-handed quarks and leptons are identical.

Assuming small couplings $h^V_{jk}$, the leading way in which these $V_i$ leptoquarks contribute to $(g-2)_\mu$ is by inducing an $S\gamma\gamma$ coupling, which then contributes through a Barr-Zee diagram. The Barr-Zee contribution to $(g-2)_\mu$ with a $W$ boson in the loop has been calculated in Ref. [140] in the context of 2HDMs. As leptoquarks are not gauge bosons, there might be ambiguities in the leptoquark two loop contribution. For an $O(1)$ estimate of this contribution, we model the effect of this leptoquark loop by the $W$ loop. We find that the leptoquark contributions to $(g-2)_\mu$ are always positive, that is, in the right direction, and they induce an effective $S\gamma\gamma$ coupling parameter

$$\kappa = \frac{\alpha_{\rm EM}}{4\pi} \sum_{i=1}^{N_{\rm LQ}} \frac{N^c Q^2 g_{V_i}}{m_{V_i}} F_W(4 m^2_{V_i}/m^2_S) \,, \tag{6.12}$$

where $\alpha_{\rm EM} \simeq 1/137$, $N^c = 3$ and $Q = \frac{5}{3}$ are the number of colors and electric charge of the leptoquarks $V_i$, respectively, $g_{V_i}$ parameterizes the $SV_iV_i$ coupling in Eq. (6.7), and $F_W$ is a loop function defined in Ref. [141].

For large leptoquark masses $m_{V_i} \gg m_S$, the loop function is $F_W \simeq 7$. In the simple case where we have $N_{\rm LQ}$ copies of degenerate leptoquarks with mass $m_{V_i} = m_{\rm LQ}$ and coupling $g_{V_i} = g_V$, Eq. (6.12) reduces to

$$\kappa \simeq 0.034 \frac{N_{\rm LQ}\, g_V}{m_{\rm LQ}} \,. \tag{6.13}$$

Setting $g_V = 3$ and requiring $\kappa \approx \text{TeV}^{-1}$, the mass and number of leptoquarks required to resolve

the $(g-2)_\mu$ anomaly are related by $m_{\rm LQ} \approx N_{\rm LQ}\,(100\text{ GeV})$. The required parameters are shown graphically in Fig. 6.3.

We see that it is not difficult to induce an effective $S\gamma\gamma$ coupling large enough to resolve the $(g-2)_\mu$ anomaly. For the $\tan\beta = 60$ case shown, with even just $N_{\rm LQ} = 5$ leptoquarks with mass $m_{\rm LQ} = 2$ TeV, which is currently viable, one can reduce the discrepancy in $(g-2)_\mu$ to $1\sigma$. Alternatively, one can achieve the same result with $N_{\rm LQ} = 10$ leptoquarks with mass $m_{\rm LQ} = 4$ TeV, which is likely challenging even for searches at the High Luminosity LHC. For the $\tan\beta = 40$ case shown, one requires roughly twice as many leptoquarks, but the number is still not very large. Generically, One might be able to directly see leptoquarks. First generation scalar leptoquarks have been excluded below 1435 GeV and 1400 GeV in LHC pair production searches by CMS [142] and ATLAS [143], respectively. Higher energy hadron [144, 145] and lepton [146, 147, 148] colliders may be able to extend the search.

In our model, the assumed new physics that is necessarily light is the dark Higgs boson $S$. This will have interesting observable consequences, as we discuss in Sec. 6.5.

### 6.3.3 $U$ Leptoquark Contribution

In addition to the contributions to $(g-2)_\mu$ mediated by the dark Higgs boson and independent of the $U$ leptoquark, there are also the contributions that depend on the $U$ leptoquark shown in Fig. 6.4. These include the two-loop Barr-Zee contribution from a $S\gamma\gamma$ coupling mediated by the $U$ leptoquark, similar to those discussed above for $V$ leptoquarks in Sec. 6.3.2, and also two one-loop contributions independent of the dark Higgs boson.

The two-loop Barr-Zee diagram's contribution is as discussed above. The contribution of a single $U$ leptoquark with mass $\sim$ TeV is not sufficient to raise the theoretical prediction for $(g-2)_\mu$ to the experimental value.

In addition, however, there are the one-loop contributions from the coupling of $U$ to the muon and down-type quarks, $h^U_{i\mu}\bar{d}_{iL}\gamma^\nu\mu_L U_\nu$, where $i = d, s, b$. These contributions to $(g-2)_\mu$

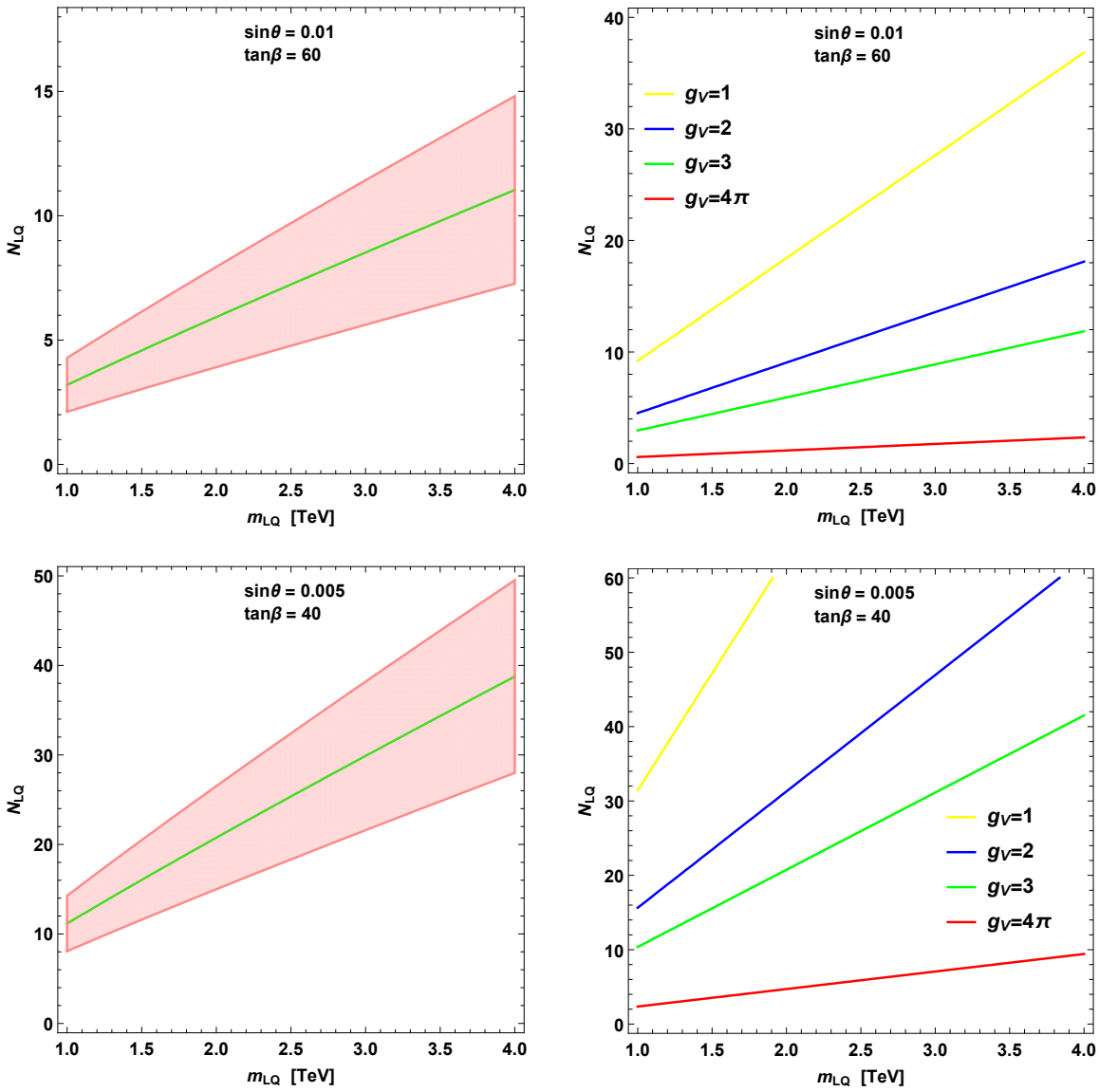


**Figure 6.3:** The region of the $(m_{\rm LQ}, N_{\rm LQ})$ plane where $N_{\rm LQ}$ vector leptoquarks $V_i$ with mass $m_{\rm LQ}$ and SM quantum numbers $(3, 1, \frac{5}{3})$ induce an effective $S\gamma\gamma$ coupling that resolves the $(g-2)_\mu$ anomaly. In all panels, we set $m_S = 100$ MeV. In the upper and lower panels, we fix $(\sin\theta, \tan\beta) = (0.01, 60)$ and $(0.005, 40)$, respectively. For the left panels, we set $g_V = 3$ and show the bands where the $(g-2)_\mu$ discrepancy is reduced to $1\sigma$. For the right panels, we consider the several values of $g_V$ indicated and plot the lines on which the theoretical prediction for $(g-2)_\mu$ exactly matches its experimentally measured value. (In the upper and lower right panels, the induced couplings are $\kappa \simeq (3.2\ \text{TeV})^{-1}$ and $(0.9\ \text{TeV})^{-1}$, respectively.)

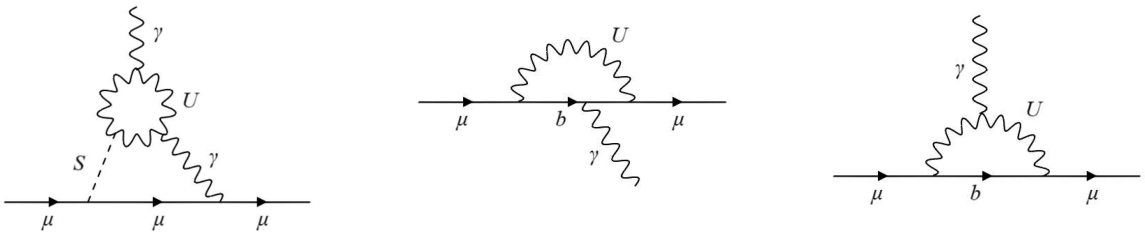


**Figure 6.4:** $U$ leptoquark contributions to $(g-2)_\mu$. Left: two-loop Barr-Zee diagram involving also the dark Higgs boson $S$. Center and right: one-loop diagrams that are independent of the dark Higgs boson.

are [149]

$$\Delta(g-2)^U_\mu = \sum_{i=d,s,b} -\frac{N^c (h^U_{i\mu})^2}{16\pi^2}\left(\frac{4m_\mu^2}{3m_U^2}Q_i - \frac{5m_\mu^2}{3m_U^2}Q_U\right), \tag{6.14}$$

where $N^c = 3$ is the number of colors, and $Q_i = -\frac{1}{3}$ and $Q_U = -\frac{2}{3}$ are the electric charges of the down-type quarks and the $U$ leptoquark. Substituting these charges and the value for the muon mass, we find

$$\Delta(g-2)^U_\mu = \sum_{i=d,s,b} -1.4\times10^{-10}(h^U_{i\mu})^2\left(\frac{\text{TeV}}{m_U}\right)^2 . \tag{6.15}$$

This contribution is of the wrong sign to explain the $(g-2)_\mu$ anomaly and depends on the couplings $h^U_{i\mu}$. In particular, the couplings $h^U_{b\mu}$ and $h^U_{s\mu}$ contribute to $b \to s\mu^+\mu^-$ and are used to explain the $R(K^*)$ and $b \to s\mu^+\mu^-$ anomalies [41, 90]. As we show in the next section, however, the couplings $h_{i\mu}$ have small enough values that we can ignore the one-loop contribution to $(g-2)_\mu$. In summary, then, the $U$ leptoquark contributions to $(g-2)_\mu$ are negligible in our model and do not modify our discussion about the $V$ leptoquark requirements to resolve the $(g-2)_\mu$ anomaly.

## 6.4 Resolving the $B$ Anomalies and Hadronic Constraints

### 6.4.1 The $U$ Leptoquark and $B$ Anomalies

The couplings of the $U$ leptoquark in Eq. (6.7) can resolve all the $B$ anomalies. Let us start with the $b \to s\mu^+\mu^-$ anomalies, which include the $R_K$ and $R_{K^*}$ measurements. The procedure to fit for new physics is the following. The $b \to s\mu^+\mu^-$ transitions are defined via an effective

Hamiltonian with vector and axial vector operators:

$$\begin{aligned} H_{\rm eff} &= -\frac{\alpha G_F}{\sqrt{2}\pi} V_{tb} V_{ts}^* \sum_{a=9,10} \left( C_a O_a + C'_a O'_a \right) , \\ O_{9(10)} &= [\bar{s}\gamma_\mu P_L b][\bar{\mu}\gamma^\mu(\gamma_5)\mu] , \end{aligned} \tag{6.16}$$

where the $V_{ij}$ are elements of the Cabibbo-Kobayashi-Maskawa (CKM) matrix, and the primed operators are obtained by replacing $L$ with $R$. The Wilson coefficients include both SM and new physics contributions: $C_a = C_{a,\,\rm SM} + C_{a,\,\rm NP}$. One now fits to the data to extract $C_{a,\rm NP}$. There are several scenarios that give a good fit to the data, and the results of recent fits can be found in Refs. [136, 137, 150, 151, 152, 153]. One of the popular solutions is $C^{\mu\mu}_{9,\,\rm NP} = -C^{\mu\mu}_{10,\,\rm NP}$, which can arise from the tree-level exchange of the $U$ leptoquark in Eq. (6.7). Following the results of Ref. [136], fitting to the $b \to s\mu^+\mu^-$ data constrains the central values of the $U$ couplings to satisfy

$$h^U_{b\mu}\, h^U_{s\mu} = 8 \times 10^{-4} . \tag{6.17}$$

The framework to explain all the $B$ anomalies, including both the CC and the NC anomalies, involves the $U$ leptoquark coupling to the third generation quarks and leptons in the gauge basis with $O(1)$ coupling, $h^U_{b\tau} \sim 1$ [41]. As one moves from the gauge to the mass basis, for the quarks and leptons, the couplings $h^U_{b\mu}$ and $h^U_{s\mu}$ are generated. Hence one has the hierarchy $h^U_{b\tau} \sim 1 > h^U_{b\mu} > h^U_{s\mu} > h^U_{d\mu}$. Using the allowed values of $h^U_{b\mu} \sim 0.1 - 0.6$ [41] and Eq. (6.17), we see the one-loop $U$ contribution to $(g-2)^U_\mu$ in Eq. (6.15) cannot resolve the $(g-2)_\mu$ discrepancy. The $(g-2)_\mu$ anomaly therefore requires additional new physics, such as the $S$ boson discussed in Sec. 6.3 .

### 6.4.2 Hadronic Constraints

In this model the $S$ boson inherits its couplings from the Higgs boson, and so necessarily couples to both leptons and hadrons. The lepton couplings, specifically the muon coupling, are desired to resolve the $(g-2)_\mu$ anomaly. Here we begin to examine the implications of the hadronic couplings, which may either constrain the model or lead to predictions of interesting new signals.

Particularly stringent are constraints on FCNC processes, since couplings like $bsS$ are induced through a penguin loop. Integrating out the $W$-top loop induces the effective $bsS$ vertex [154]

$$\mathcal{L}_{bs} = \frac{\sin\theta'}{v\tan\beta}\frac{3\sqrt{2}G_F m_t^2 V_{ts}^* V_{tb}}{16\pi^2} m_b \bar{s} P_R b S + \text{H.c.}\,, \tag{6.18}$$

where the factor $\frac{\sin\theta'}{v\tan\beta}$ comes from the top quark coupling to $S$. By the same loop process, but replacing $b$ and $s$ quarks by $s$ and $d$ quarks, respectively, the $sdS$ vertex is also generated. Note that the FCNC amplitude depends on the mixing angle $\sin\theta'$ in Eq. (6.6), which is suppressed by $m_h^2$, while the $(g-2)_\mu$ in Eq. (6.9) is controlled by the mixing angle $\sin\theta$ in Eq. (6.6), which is suppressed by $m_H^2$. If a higher value of $m_H$ is compensated by a larger value of the mixing parameter $A$ to keep the same $\sin\theta$, then $\sin\theta'$ can become too large and be inconsistent with FCNC data.

The FCNC interactions will induce two-body decays $B \to K^{(*)}S$ and $K \to \pi S$. To determine the signature of these processes, it is important to determine how the $S$ decays. For $m_S \sim 10 - 200$ MeV, the possible decays are $S \to e^+e^-, \gamma\gamma$. In Figs. 6.5 and 6.6, we show the $S$ lifetime and branching fraction to $e^+e^-$, respectively. We see that for most of the parameters of interest, the $S$ flight distance (excluding the boost factor) is $c\tau_0 \sim 1$ mm, and so the $S$ decay is effectively prompt. We also see that the dominant decay is to di-photons, with $BR(S \to e^+e^-) \sim 10^{-5} - 10^{-3}$ in the parameter region of interest.

We now determine the rates for the two-body decays $B \to K^{(*)}S$ and $K \to \pi S$. For the two-body decays $B \to K^{(*)}S$ we have [155, 156]

$$BR(B \to KS) = \frac{g_{bs}^2 f_0^2(m_S^2)(m_B^2 - m_K^2)^2 |\vec{p}_K|\tau_B}{32\pi m_B^2 (m_b - m_s)^2} \tag{6.19}$$

and

$$BR(B \to K^*S) = \frac{g_{bs}^2 A_0^2(m_S^2)|\vec{p}_{K^*}|^3\tau_B}{8\pi(m_b + m_s)^2}\,, \tag{6.20}$$

where $m_b$ and $m_s$ are the bottom and strange quark masses, respectively, $f_0$ and $A_0$ are form factors, which are taken from Refs. [157, 158], and $g_{bs}$ is the flavor-changing $b \to s$ coupling

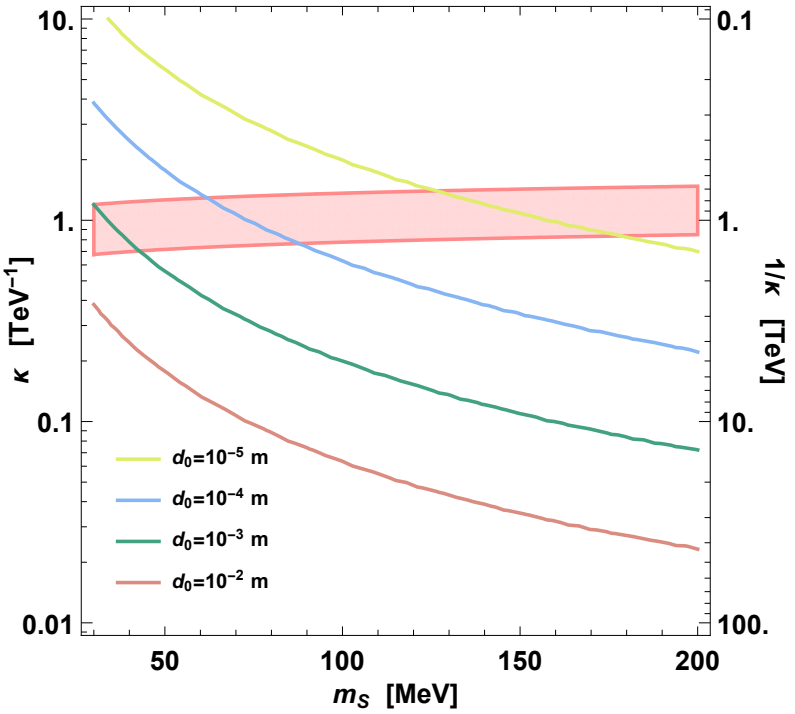


**Figure 6.5:** Contours of constant flight distance (excluding the boost factor) ($d_0 = c\tau_0$) of the light scalar $S$ in the $(m_S, \kappa)$ plane. We fix $\sin\theta = 0.005$ and $\tan\beta = 40$. In the pink shaded region, the $(g-2)_\mu$ anomaly is reduced to $1\sigma$.

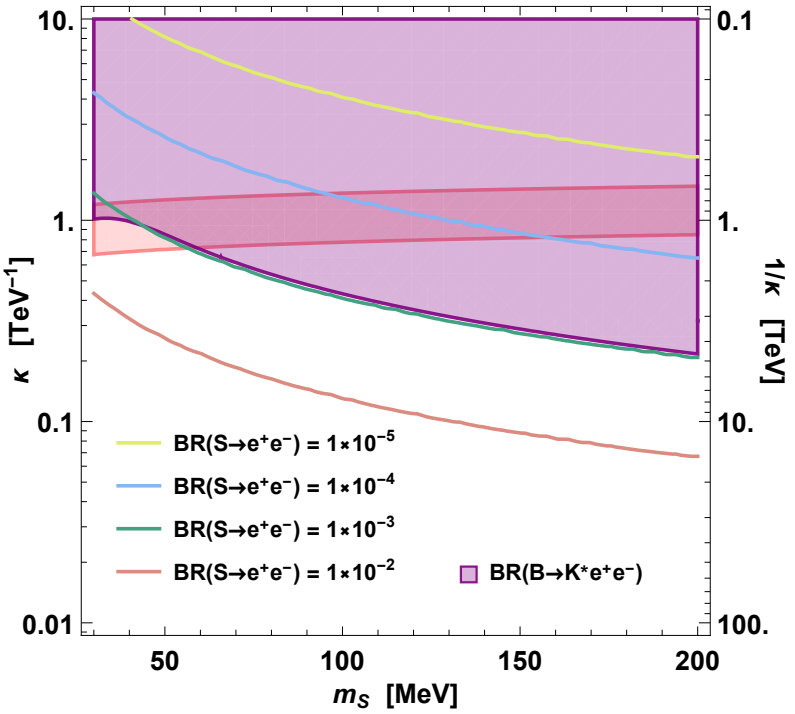


**Figure 6.6:** Contours of constant branching fraction $BR(S \to e^+e^-)$ in the $(m_S, \kappa)$ plane. We fix $\sin\theta = 0.005$ and $\tan\beta = 40$. In the pink shaded region, the $(g-2)_\mu$ anomaly is reduced to $1\sigma$, and in the purple shaded region, $BR(B \to K^* e^+ e^-)$ is within $1\sigma$ of its measured value.

| Observable | New scalar contribution $\sin\theta = 0.005$, $\tan\beta = 40$ | Existing constraints/measurements |
|---|---|---|
| $BR(B \to KS)$ | $1.7 \times 10^{-4}$ | $< 10\%$ |
| $BR(B \to K^* S)$ | $1.7 \times 10^{-4}$ | $< 10\%$ |
| $BR(B_s \to \mu^+\mu^-)$ | $4.2 \times 10^{-14}$ | $(3.0 \pm 0.4) \times 10^{-9}$ |
| $BR(B_s \to \gamma\gamma)$ | $7.4 \times 10^{-11}$ | $< 3.1 \times 10^{-6}$ |
| $\Delta M_{B_s}^{NS}$ | $-2.5 \times 10^{-17}$ GeV | $< 1.7 \times 10^{-12}$ GeV |
| $\Delta M_K^{NS}$ | $-6.3 \times 10^{-24}$ GeV | $< 5.9 \times 10^{-18}$ GeV |
| $BR(K^+ \to \mu^+ \nu e^+ e^-)$ | $3.3 \times 10^{-14}$ | $(7.81 \pm 0.23) \times 10^{-8}$ |
| $BR(K^\pm \to \pi^\pm e^+ e^-)$ | $8.7 \times 10^{-11}$ | $(3.11 \pm 0.12) \times 10^{-7}$ |
| $BR(K_S \to \gamma\gamma)$ | $3.3 \times 10^{-16}$ | $(2.63 \pm 0.17) \times 10^{-6}$ |
| $BR(K_L \to \gamma\gamma)$ | $3.2 \times 10^{-14}$ | $(5.47 \pm 0.04) \times 10^{-4}$ |
| $\delta(g-2)_e$ | $6.3 \times 10^{-14}$ | $(-87 \pm 36) \times 10^{-14}$ |

**Table 6.1:** Values of the contribution of the new scalar $S$ to various meson observables. We fix the dark scalar mass to $m_S = 100$ MeV. References for the experimental constraints are given in the text.

with the normalization $\mathcal{L}_{bs} = g_{bs}\bar{s}P_R bS$. Given the prompt $S$ decays to $e^+e^-$ and $\gamma\gamma$, we have $BR(B \to K^{(*)}e^+e^-)$ dominantly coming from $BR(B \to K^{(*)}S)BR(S \to e^+e^-)$ and $BR(B \to K^{(*)}\gamma\gamma)$ dominated by $BR(B \to K^{(*)}S)BR(S \to \gamma\gamma)$. One can extend this to $K$ decays also.

We now discuss constraints from $B$ and $K$ decays on this model. In this subsection, we will consider a variety of non-leading constraints and show that they are far from excluding the favored parameter space of this model. These observables are listed in Table 6.1 and are the following:

- $B$ Total Decay Width: In the first two rows of Table 6.1, we require that $BR(B \to K^{(*)}S)$ not exceed the uncertainty in the SM prediction of the width of the $B$ meson, which we take to be around 10% [159].

- $B_s$ Decay: The process $B_s \to \mu^+\mu^-$ is mediated by an $s$-channel dark Higgs boson $S$, where the matrix element is $\mathcal{M}_{B_s \to \mu^+\mu^-} = \frac{g_{bs}g_\mu}{m_{B_s}^2 - m_S^2}(\bar{s}P_R b)\,(\bar{\mu}\mu)$. We use `flavio` [160] to calculate the contribution of the light scalar $S$ to this decay mode. The branching ratio of this decay is measured to be $(3.0 \pm 0.4) \times 10^{-9}$ [35]. The process $B_s \to \gamma\gamma$ is also mediated by an $s$-channel $S$. The SM prediction for $BR(B_s \to \gamma\gamma)$ is around $5 \times 10^{-7}$ [161], and there exists an experimental upper bound of $3.1 \times 10^{-6}$ [35] for this observable. The branching ratio of

the decay in terms of the effective $S\gamma\gamma$ coupling $\kappa$ is

$$BR(B_s \to \gamma\gamma) = \frac{|g_{bs}|^2|\kappa|^2}{64\pi} \frac{f_{B_s}^2 m_{B_s}^7}{m_b^2 (m_{B_s}^2 - m_S^2)^2} \tau_{B_s} \ . \tag{6.21}$$

- $B_s$ and $K$ Mixing: In the SM, the $B_s$ mass difference is $\Delta M_{B_s}^{\rm SM} = (17.4 \pm 2.6)$ ps$^{-1}$ [41]. We require that the new scalar contribution not exceed the SM uncertainty. The expression for the mass difference due to the new scalar is [162, 156]

$$\Delta M_{B_s}^{\rm NS} = -\frac{5}{24} \frac{g_{bs}^2}{m_{B_s}^2 - m_S^2} f_B^2 m_{B_s} \ . \tag{6.22}$$

  We use a similar equation for the $K - \bar{K}$ mixing mass difference and use the experimental value $\Delta M_K^{\rm exp} = (52.93 \pm 0.09) \times 10^8$ s$^{-1}$ [35].

- $K$ Decay: The rare decay $K^+ \to \mu^+ \nu e^+ e^-$ has been measured by the NA48/2 Collaboration to be $BR(K^+ \to \mu^+ \nu e^+ e^-) = (7.81 \pm 0.23) \times 10^{-8}$ [163], where the measurement is restricted to the kinematic region with $m_{e^+e^-} \geq 140$ MeV. To study this decay mode, we calculate the branching ratio of the decay $K \to \mu \nu_\mu S$, where the scalar particle $S$ is radiated off the muon leg [164]. The total branching ratio is then determined through

$$BR(K^+ \to \mu^+ \nu_\mu e^+ e^-) = BR(K^+ \to \mu^+ \nu_\mu S) BR(S \to e^+ e^-) \ . \tag{6.23}$$

  The $K^\pm \to \pi^\pm e^+ e^-$ mode also has been measured by the NA48/2 Collaboration to be $BR(K^\pm \to \pi^\pm e^+ e^-) = (3.11 \pm 0.12) \times 10^{-7}$ [165]. For this process we find the two-body decay rate $K^\pm \to \pi^\pm S$, and the branching ratio of the desired process is determined by

$$BR(K^\pm \to \pi^\pm e^+ e^-) = BR(K^\pm \to \pi^\pm S) BR(S \to e^+ e^-) \ . \tag{6.24}$$

- $K_{S,L}$ Decays: The decays $K_{S,L} \to \gamma\gamma$ are mediated through $s$-channel dark Higgs bosons $S$,

just as in the case $B_s \to \gamma\gamma$ discussed above. The new contributions to these decay modes and their Particle Data Group values [35] are presented in Table 6.1.

- Last, although not a hadronic constraint, we also list the model prediction for $(g-2)_e$. Just as there is a Barr-Zee contribution to $(g-2)_\mu$, there is an analogous Barr-Zee contribution to $(g-2)_e$. In contrast to the muon case, the measured value for $(g-2)_e$ is smaller than the SM prediction, and so our model's contribution to $(g-2)_e$ is in the wrong direction. However, as can be seen in Table 6.1, the contribution to $(g-2)_e$ is very small, and does not significantly worsen the agreement between theory and experiment.

We see that none of the constraints listed in Table 6.1 is a significant constraint on the model. In the next section, we will consider the leading constraints, which do constrain parts of the model parameter space, but also provide interesting predictions for signals that could be seen in the near future.

## 6.5 New Signals of the Model

### 6.5.1 $B \to K^{(*)} e^+ e^-$

As noted above, the model contributes to the decay $B \to K^{(*)} e^+ e^-$ with branching fraction $BR(B \to K^{(*)} e^+ e^-) = BR(B \to K^{(*)} S) BR(S \to e^+ e^-)$. The region of the $(m_S, \kappa)$ parameter space that is consistent with the measured value of $BR(B \to K^{(*)} e^+ e^-) = (3.1^{+0.9\ +0.2}_{-0.8\ -0.3} \pm 0.2) \times 10^{-7}$ [166] is shown in Fig. 6.6, along with the region in which the $(g-2)_\mu$ anomaly is resolved. We see that the existing constraint on $BR(B \to K^{(*)} e^+ e^-)$ excludes the very lowest values of $m_S \sim 10$ MeV, but most of the parameter space is allowed. Future measurements of $BR(B \to K^{(*)} e^+ e^-)$ with increased sensitivity may therefore see a deviation predicted by this model. There is also a measurement of the inclusive $B \to X_s e^+ e^-$ decay [167] for $0.1 < m^2_{e^+e^-} < 2.0\ \text{GeV}^2$, but this is outside the $m_S$ range we consider and so cannot be used to constrain our model.

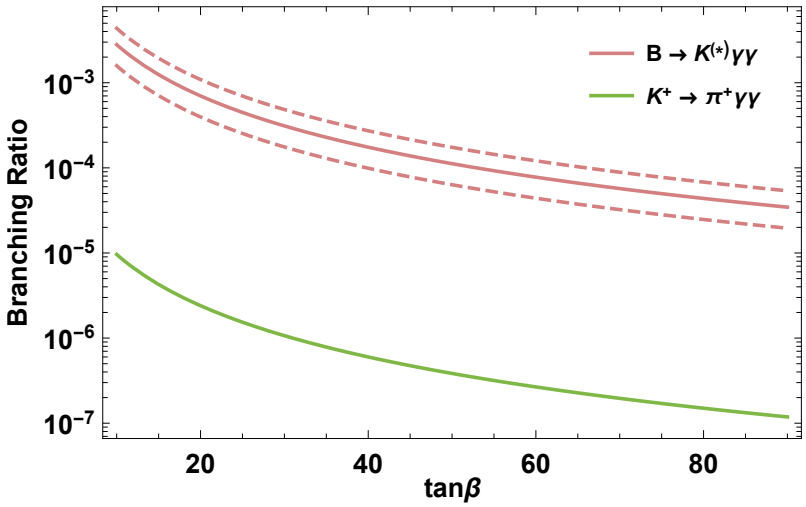


**Figure 6.7:** The values of the branching fractions for the decays $B \to K^{(*)}\gamma\gamma$ and $K^+ \to \pi^+\gamma\gamma$. The branching fractions for $B \to K\gamma\gamma$ and $B \to K^*\gamma\gamma$ are essentially identical. The dashed bands correspond to the $2\sigma$ variations of the $B \to K^{(*)}$ form factors. We fix $\sin\theta = 0.005$ and $m_S = 100$ MeV.

### 6.5.2 $B \to K^{(*)}\gamma\gamma$

As the $S$ decays almost always to di-photons, another important signal for the $S$ state is from $B \to K^{(*)}\gamma\gamma$ decays. In Fig. 6.7 we show the predictions for $B \to K^{(*)}\gamma\gamma$. The predictions depend on the $B \to K^{(*)}$ form factors $f_0$ and $A_0$ mentioned above. We show the range of the predictions as we vary the form factors within $2\sigma$ of the quoted uncertainty. It should be noted that the form factors are not from first principle QCD calculations, and so one should keep that in mind when discussing uncertainties in the form factors. The predictions for $B \to K\gamma\gamma$ and $B \to K^*\gamma\gamma$ are almost identical, and range from roughly $1 \times 10^{-4}$ to $3 \times 10^{-4}$ for $\tan\beta = 40$.

Because the $\gamma\gamma$ comes from a light $S$, for a sufficiently low $m_S$, the two $\gamma$ may be collinear and look like a single $\gamma$. One of the $\gamma$ may also be soft, in which case again the $2\gamma$ will look like a single $\gamma$. Hence, experimentally one should check the $B \to K^{(*)}\gamma$ signal carefully to look for signs of a di-photon resonance. We should also point out that our predictions for the $B \to K^*\gamma\gamma$ rates should be considered as ballpark estimates, as one can choose a more general 2HDM model to relax the branching ratio predictions. If the mass of the $S$ is close to the $\pi^0$ mass, the final states

for $B \to K^{(*)}\pi^0$ and $B \to K^{(*)}S$, with both $\pi^0$ and $S$ decaying to $\gamma\gamma$, are the same, and one will have to consider carefully adding the two contributions. As nonleptonic decays are very difficult to calculate it will be difficult to detect the presence of the $S$ particle in this case or obtain constraints on the model from the $B \to K^{(*)}\pi^0$ measurement. In the SM, the non-resonant decay $B \to X_s\gamma\gamma$ has a branching ratio around $4\times10^{-7}$ [161], where the photons are required to have an energy greater than 100 MeV. Also, in Ref. [168], a study of the short distance effects in $B \to K^{(*)}\gamma\gamma$ decays, together with the resonant contributions, is presented. At present, the observed $B \to K^{(*)}\gamma\gamma$ signals come only from known resonances, but analyses of the currently unexplored non-resonant regions could yield signals of the dark Higgs boson $S$.

### 6.5.3 $K \to \pi\gamma\gamma$

In Fig. 6.7 we also show the predicted branching ratios for $K^+ \to \pi^+\gamma\gamma$. For $\tan\beta = 40$, the prediction is approximately $6\times10^{-7}$. If the $S$ mass is near the $\pi^0$ mass, the $K^+ \to \pi^+\gamma\gamma$ decay will be swamped by the $K^+ \to \pi^+\pi^0$ decay, which has a branching ratio of about 21% [35]. Away from the $\pi^0$ resonance, there is a measurement of the non-resonant $K^+ \to \pi^+\gamma\gamma$ decay with branching ratio $(1.01 \pm 0.06) \times 10^{-6}$ [35], but this measurement is obtained by combining measurements made for di-photon invariant masses above the range of $S$ masses we consider. The predictions of this model could be tested by future measurements with this sensitivity, but for di-photon masses between 10 and 200 MeV.

For the neutral kaons, the model predictions for $\sin\theta = 0.005$, $\tan\beta = 40$, and $m_S = 100$ MeV are $BR(K_L \to \pi^0 S) = 4\times10^{-7}$ and $BR(K_S \to \pi^0 S) = 4\times10^{-9}$. The much smaller branching ratio for $K_S$ is largely due to the $K_S$ having a much shorter lifetime than $K_L$, while the $K^+$ and $K_L$ lifetimes are of the same order. The measured branching ratios are $BR(K_L \to \pi^0\gamma\gamma) = (1.273\pm0.033)\times10^{-6}$ and $BR(K_S \to \pi^0\gamma\gamma) = (4.9\pm1.8)\times10^{-8}$ [35]. Again, the model predictions are not far from current sensitivities and predict a sharp signal with di-photon mass equal to $m_S$.

### 6.5.4 $h \to \gamma\gamma\gamma\gamma$ and Implications for $h \to \gamma\gamma$

The model discussed here may also modify Higgs boson decays through the process $h \to SS$, followed by $S \to \gamma\gamma$.[1] Since the SM Higgs boson is much heavier than the scalar $S$, the two photons from $S$ decay are boosted and highly collimated. Therefore, the decay $h \to S(\to \gamma\gamma)S(\to \gamma\gamma)$ contributes to the $h \to \gamma\gamma$ signal [169]. We can calculate the couplings appearing in the $\frac{1}{2}g_{hSS}hSS$ interaction in terms of the parameters of the potential and mixing parameters. The resulting branching ratio is

$$BR(h \to SS) = \frac{g_{hSS}^2}{32\pi m_h \Gamma_h}\sqrt{1 - \frac{4m_S^2}{m_h^2}} \ . \tag{6.25}$$

The signal strengths measured by CMS and ATLAS are $\mu^{\gamma\gamma} = 1.18^{+0.17}_{-0.14}$ [170] and $\mu^{\gamma\gamma} = 1.06^{+0.14}_{-0.12}$ [171], respectively. By a naive combination of these two measurements, we find $\mu^{\gamma\gamma} = 1.11 \pm 0.10$. (We averaged the CMS and ATLAS measurements to $\mu^{\gamma\gamma} = 1.18 \pm 0.16$ and $\mu^{\gamma\gamma} = 1.06 \pm 0.13$, respectively.)

In the parameter region of our interest in the model, we can find values for parameters of the potential such that the addition of the process $h \to SS \to \gamma\gamma\gamma\gamma$ to the SM rate of $h \to \gamma\gamma$ does not exceed the measured signal strength. As an example, for $\sin\theta = 0.005$ and $\tan\beta = 40$, and taking $m_{du} = 200$ GeV, $\lambda_1 = 0.6$, $\lambda_2 = 0.3$, $\lambda_{345} = 2.8$, $\lambda_d = -0.3$, $\lambda_u = 0.0005$, and $\lambda_{ud} = 0.005$, the signal strength becomes $\mu^{\gamma\gamma} \approx 1.08$. Of course, this also implies that as the experimental constraints on $\mu^{\gamma\gamma}$ become more precise, a deviation from the SM expectation may appear.

## 6.6 Conclusions

In this chapter, we have proposed a concrete model that resolves both the $(g-2)_\mu$ and $B$ meson anomalies, which are currently among the leading discrepancies between SM predictions and experimental data. The model is a Type II 2HDM model, such as the Higgs sector of the minimal supersymmetric model, extended to include a light dark Higgs boson $S$, a leptoquark $U$, and additional leptoquarks $V$. The $U$ leptoquark resolves the $B$ anomalies, and the $V$ leptoquarks

[1] The model also predicts heavy Higgs boson decays $H \to SS$, but the branching ratio for this is very small, of the order of $10^{-6}$.

generate a $S\gamma\gamma$ coupling. This coupling induces a two-loop Barr-Zee contribution to $(g-2)_\mu$, which is shown in Fig. 6.1.

For dark Higgs mass $m_S \sim 100$ MeV and dark Higgs mixing angle $\sin\theta \sim 0.005$, $\tan\beta \sim 40$, and $N_{\rm LQ} \sim 10$ $V$ leptoquarks with masses at the TeV scale, the correction resolves the $(g-2)_\mu$ anomaly. The introduction of a new light scalar $S$ has many possible effects on SM meson phenomenology. We have checked that all current bounds on $K$ and $B$ properties, as well as the current constraint on $(g-2)_e$, are respected for the parameters that solve the $(g-2)_\mu$ and $B$ meson anomalies; see Table 6.1.

In the near future, however, there are measurements that could uncover beyond-the-SM effects and provide evidence for this model. In particular, the dark Higgs boson is light enough to be produced in meson decays, and it then decays through $S \to e^+e^-, \gamma\gamma$. The $S$ boson has $c\tau \sim 0.01 - 1$ mm, and so for most model parameters the decay is indistinguishable from prompt, yielding interesting new di-electron events from $B \to K^{(*)}e^+e^-$ with $m_{e^+e^-} = m_S$ and di-photon signals from $B \to K^{(*)}\gamma\gamma$ and $K \to \pi\gamma\gamma$ with $m_{\gamma\gamma} = m_S$. The branching ratios for some of these modes are shown in Figs. 6.6 and 6.7. In all cases, the predicted branching ratios are not far from current sensitivities, although current measurements typically explore ranges of $m_{e^+e^-}$ and $m_{\gamma\gamma}$ outside the considered range of $m_S$. As examples, the model predicts values $BR(B \to K^{(*)}\gamma\gamma) \sim 10^{-4}$ and $BR(K^+ \to \pi^+\gamma\gamma), BR(K_L \to \pi^0\gamma\gamma) \sim 10^{-6}$. Provided the $S$ is not too degenerate with the neutral pion $\pi^0$, these signals could be observed above background in the near future, for example, at Belle II, providing a motivation to look for these exotic di-photon modes and an avenue for testing this model. More generally, these decay modes test many models where the $(g-2)_\mu$ anomaly is resolved by a two-loop Barr-Zee contribution generated by a light $S$ with an $S\gamma\gamma$ coupling.

In addition, there are potentially observable contributions to exotic Higgs decays $h \to SS \to \gamma\gamma\gamma\gamma$, which, given that the $S$ is very light, typically lead to signals indistinguishable from $h \to \gamma\gamma$. For typical energies of the photons in the boosted $S \to \gamma\gamma$ decay, $E_\gamma = 30$ GeV, the opening angle of the photons is approximately $0.2^\circ$. Taking the distance from the beam to the electromagnetic

calorimeter to be $\sim$ 1.2 m (which is the case for CMS), the separation of the photons would become $\sim$ 4 mm which is too small. On the other hand, CMS has a silicon tracker with a mass of about a tenth of a radiation length. So for four 30 GeV photons, there is a 40% chance that one of the photons pair produces in the silicon and we might be able to distinguish each photon.

In all decay modes with photons in the final states, while the main signals are the ones with two photons in the final states, one or both of these photons can convert internally to $e^+e^-$ Dalitz pairs which can be searched for in experiments.

# CHAPTER 7

# CONCLUSIONS

There are a lot of opportunities in exploring beyond the Standard Model (SM) physics in hadronic systems that contain heavy quarks. The ideal hadrons for this purpose are the ones that contain the $b$ quark which is the heaviest quark that can hadronize. Interestingly, there has been many measurements of the $B$-meson decays that deviate from their SM predictions. These measurements are grouped into two main categories: charged current decays $B \to D^{(*)}\ell\nu_\ell$, and neutral current decays $B \to K^{(*)}\ell^+\ell^-$. The theoretically clean observables related to these decay modes are $R(D^{(*)}) = \frac{\mathcal{B}(B\to D^{(*)}\tau\nu)}{\mathcal{B}(B\to D^{(*)}\ell\nu)}$ and $R(K^{(*)}) = \frac{\mathcal{B}(B\to K^{(*)}\mu^+\mu^-)}{\mathcal{B}(B\to K^{(*)}e^+e^-)}$, where $\ell = e, \mu$. $R(D^{(*)})$ has been measured by BaBar [2, 3], Belle [4, 5, 6, 14] and LHCb [7, 8]. The average of these measurements deviate from the SM predictions by $\sim 3.1\,\sigma$ [9]. $R(K^{(*)})$ has been measured by LHCb [96, 98] where these measurements deviate from the SM predictions by $\sim 2.5\,\sigma$. These deviations point to the lepton flavor universality violation which is absent in the SM. These anomalies have been our main focus in this dissertation. We have studied new physics (NP) effects in the decay mode $\Lambda_b \to \Lambda_c\tau\nu_\tau$. This decay mode is important in diagnosing the $R(D^{(*)})$ anomalies since it has the same quark level transition, $b \to c\tau\nu_\tau$. We have calculated various differential decay distributions including all possible NP Lorentz structures that can contribute to this decay mode. Taking the allowed values of the couplings from $R(D^*)$ measurements, we have studied how $R(\Lambda_c)$ as well as the differential observables, deviate from their SM predictions. We have explored how future measurements of $R(\Lambda_c)$ can help differentiate NP models responsible for the $R(D^{(*)})$ anomalies. We have also studied the leptoquark models that can explain these anomalies and how they can affect various observables related to the decay mode $\Lambda_b \to \Lambda_c\tau\nu_\tau$.

Another decay mode that has the same quark level transition as $R(D^{(*)})$ is the inclusive decay $B \to X_c \ell \nu_\ell$. We have studied this decay mode in the presence of all possible NP Lorentz structures, both model-independently and with all possible leptoquark models that can contribute to this decay mode. We have also carried out the calculation of non-perturbative corrections to this decay mode both in the SM and when all possible NP Lorentz structures are included. This calculation leads to a more precise prediction for this decay mode when NP is added to SM.

An important component of particle physics is CP violation as it is known that the observed amount of CP violation is not enough to explain the baryon asymmetry of the universe. As a consequence, we should look for new sources of CP violation. We have studied the angular distribution of the decay $\bar{B}^0 \to D^{*+}(\to D\pi)\mu^- \bar{\nu}_\mu$ in search of CP violating triple products. These triple products are constructed with the momenta and/or polarizations of the final state particles. Observation of CP violation in the angular distribution of this decay mode is a definite sign of NP, since in the SM, we do not expect any CP violation in this decay mode. We can also use this angular distribution to distinguish various NP models. We have used the angular distribution of this decay mode to determine which couplings are necessary to produce certain (CP conserving or CP violating) angular terms. This can also be used to distinguish different explicit NP models. We have used this angular distributions to study various leptoquark models some of which are very plausible candidates to address the $R(D^{(*)})$ and $R(K^{(*)})$ anomalies.

Finally, in the last chapter, we have presented a study of the muon $(g-2)$ anomaly and its possible connection with the $B$ anomalies. $(g-2)_\mu$ is a longstanding anomaly in particle physics and there has been a lot of efforts to address it with new physics models. Here, we introduced a simplified model to resolve this anomaly together with the $B$-meson anomalies. The model consists of a weakly coupled light scalar particle $S$ in the framework of the two Higgs doublet model (2HDM) of type II. This scalar particle which is usually called the dark Higgs boson, couples to both leptons and quarks through its mixing with the neutral Higgses of the 2HDM. This means that

these couplings are further suppressed by mixing angles when we compare them with the neutral Higgses couplings to fermions in the 2HDM. In this model, the light scalar further couples to two photons ($S\gamma\gamma$). In general, this coupling can be induced by the coupling between $S$ and TeV scale charged particles and here we have considered leptoquarks as these heavy particles. The effective $S\gamma\gamma$ coupling can then contribute to the $(g-2)_\mu$ through a two-loop Barr-Zee diagram and this contribution can resolve the $(g-2)_\mu$ anomaly. In this model, we see that to explain the $(g-2)_\mu$ anomaly, we need a large coupling between the light scalar $S$ and two photons and this leads to interesting signals in the $B$ and $K$, as well as the SM Higgs decays to photons.

# LIST OF REFERENCES

[1] W. Detmold, C. Lehner, and S. Meinel, "$\Lambda_b \to p\ell^-\bar{\nu}_\ell$ and $\Lambda_b \to \Lambda_c\ell^-\bar{\nu}_\ell$ form factors from lattice QCD with relativistic heavy quarks," *Phys. Rev.* **D92** no. 3, (2015) 034503, arXiv:1503.01421 [hep-lat].

[2] **BaBar** Collaboration, J. P. Lees *et al.*, "Evidence for an excess of $\bar{B} \to D^{(*)}\tau^-\bar{\nu}_\tau$ decays," *Phys. Rev. Lett.* **109** (2012) 101802, arXiv:1205.5442 [hep-ex].

[3] **BaBar** Collaboration, J. P. Lees *et al.*, "Measurement of an Excess of $\bar{B} \to D^{(*)}\tau^-\bar{\nu}_\tau$ Decays and Implications for Charged Higgs Bosons," *Phys. Rev.* **D88** no. 7, (2013) 072012, arXiv:1303.0571 [hep-ex].

[4] **Belle** Collaboration, M. Huschle *et al.*, "Measurement of the branching ratio of $\bar{B} \to D^{(*)}\tau^-\bar{\nu}_\tau$ relative to $\bar{B} \to D^{(*)}\ell^-\bar{\nu}_\ell$ decays with hadronic tagging at Belle," *Phys. Rev.* **D92** no. 7, (2015) 072014, arXiv:1507.03233 [hep-ex].

[5] **Belle** Collaboration, Y. Sato *et al.*, "Measurement of the branching ratio of $\bar{B}^0 \to D^{*+}\tau^-\bar{\nu}_\tau$ relative to $\bar{B}^0 \to D^{*+}\ell^-\bar{\nu}_\ell$ decays with a semileptonic tagging method," *Phys. Rev.* **D94** no. 7, (2016) 072007, arXiv:1607.07923 [hep-ex].

[6] **Belle** Collaboration, S. Hirose *et al.*, "Measurement of the $\tau$ lepton polarization and $R(D^*)$ in the decay $\bar{B} \to D^*\tau^-\bar{\nu}_\tau$," *Phys. Rev. Lett.* **118** no. 21, (2017) 211801, arXiv:1612.00529 [hep-ex].

[7] **LHCb** Collaboration, R. Aaij *et al.*, "Measurement of the ratio of branching fractions $\mathcal{B}(\bar{B}^0 \to D^{*+}\tau^-\bar{\nu}_\tau)/\mathcal{B}(\bar{B}^0 \to D^{*+}\mu^-\bar{\nu}_\mu)$," *Phys. Rev. Lett.* **115** no. 11, (2015) 111803, arXiv:1506.08614 [hep-ex]. [Erratum: Phys. Rev. Lett.115,no.15,159901(2015)].

[8] **LHCb** Collaboration, R. Aaij *et al.*, "Measurement of the ratio of the $B^0 \to D^{*-}\tau^+\nu_\tau$ and $B^0 \to D^{*-}\mu^+\nu_\mu$ branching fractions using three-prong $\tau$-lepton decays," *Phys. Rev. Lett.* **120** no. 17, (2018) 171802, arXiv:1708.08856 [hep-ex].

[9] **HFLAV** Collaboration, Y. Amhis *et al.*, "Averages of $b$-hadron, $c$-hadron, and $\tau$-lepton properties as of summer 2016," *Eur. Phys. J.* **C77** no. 12, (2017) 895, arXiv:1612.07233 [hep-ex].

[10] D. Bigi and P. Gambino, "Revisiting $B \to D\ell\nu$," *Phys. Rev.* **D94** no. 9, (2016) 094008, arXiv:1606.08030 [hep-ph].

[11] F. U. Bernlochner, Z. Ligeti, M. Papucci, and D. J. Robinson, "Combined analysis of semileptonic $B$ decays to $D$ and $D^*$: $R(D^{(*)})$, $|V_{cb}|$, and new physics," *Phys. Rev.* **D95** no. 11, (2017) 115008, arXiv:1703.05330 [hep-ph]. [erratum: Phys. Rev.D97,no.5,059902(2018)].

[12] D. Bigi, P. Gambino, and S. Schacht, "$R(D^*)$, $|V_{cb}|$, and the Heavy Quark Symmetry relations between form factors," *JHEP* **11** (2017) 061, arXiv:1707.09509 [hep-ph].

[13] S. Jaiswal, S. Nandi, and S. K. Patra, "Extraction of $|V_{cb}|$ from $B \to D^{(*)}\ell\nu_\ell$ and the Standard Model predictions of $R(D^{(*)})$," *JHEP* **12** (2017) 060, arXiv:1707.09977 [hep-ph].

[14] **Belle** Collaboration, A. Abdesselam *et al.*, "Measurement of $\mathcal{R}(D)$ and $\mathcal{R}(D^*)$ with a semileptonic tagging method," arXiv:1904.08794 [hep-ex].

[15] A. Datta, S. Kamali, S. Meinel, and A. Rashed, "Phenomenology of $\Lambda_b \to \Lambda_c \tau \overline{\nu}_\tau$ using lattice QCD calculations," *JHEP* **08** (2017) 131, arXiv:1702.02243 [hep-ph].

[16] T. Gutsche, M. A. Ivanov, J. G. Körner, V. E. Lyubovitskij, P. Santorelli, and N. Habyl, "Semileptonic decay $\Lambda_b \to \Lambda_c \tau^- \bar{\nu}_\tau$ in the covariant confined quark model," *Phys. Rev.* **D91** no. 7, (2015) 074001, arXiv:1502.04864 [hep-ph]. [Erratum: Phys. Rev.D91,no.11,119907(2015)].

[17] S. Shivashankara, W. Wu, and A. Datta, "$\Lambda_b \to \Lambda_c \tau \bar{\nu}_\tau$ Decay in the Standard Model and with New Physics," *Phys. Rev.* **D91** no. 11, (2015) 115003, arXiv:1502.07230 [hep-ph].

[18] R. Dutta, "$\Lambda_b \to (\Lambda_c,\ p)\ \tau\ \nu$ decays within standard model and beyond," *Phys. Rev.* **D93** no. 5, (2016) 054003, arXiv:1512.04034 [hep-ph].

[19] R. N. Faustov and V. O. Galkin, "Semileptonic decays of $\Lambda_b$ baryons in the relativistic quark model," *Phys. Rev.* **D94** no. 7, (2016) 073008, arXiv:1609.00199 [hep-ph].

[20] X.-Q. Li, Y.-D. Yang, and X. Zhang, "$\Lambda_b \to \Lambda_c \tau \overline{\nu}_\tau$ decay in scalar and vector leptoquark scenarios," *JHEP* **02** (2017) 068, arXiv:1611.01635 [hep-ph].

[21] P. Böer, A. Kokulu, J.-N. Toelstede, and D. van Dyk, "Angular Analysis of $\Lambda_b \to \Lambda_c(\to \Lambda\pi)\ell\bar{\nu}$," arXiv:1907.12554 [hep-ph].

[22] A. Ray, S. Sahoo, and R. Mohanta, "Probing new physics in semileptonic $\Lambda_b$ decays," *Phys. Rev.* **D99** no. 1, (2019) 015015, arXiv:1812.08314 [hep-ph].

[23] F. U. Bernlochner, Z. Ligeti, D. J. Robinson, and W. L. Sutcliffe, "Precise predictions for $\Lambda_b \to \Lambda_c$ semileptonic decays," *Phys. Rev.* **D99** no. 5, (2019) 055008, arXiv:1812.07593 [hep-ph].

[24] T. Gutsche, M. A. Ivanov, J. G. Körner, V. E. Lyubovitskij, P. Santorelli, and C.-T. Tran, "Analyzing lepton flavor universality in the decays $\Lambda_b \to \Lambda_c^{(*)}(\frac{1}{2}^{\pm}, \frac{3}{2}^{-}) + \ell\ \bar{\nu}_\ell$," *Phys. Rev.* **D98** no. 5, (2018) 053003, arXiv:1807.11300 [hep-ph].

[25] E. Di Salvo, F. Fontanelli, and Z. J. Ajaltouni, "Detailed Study of the Decay $\Lambda_b \to \Lambda_c \tau \bar{\nu}_\tau$," *Int. J. Mod. Phys.* **A33** no. 29, (2018) 1850169, arXiv:1804.05592 [hep-ph].

[26] K. Azizi and J. Y. Süngü, "Semileptonic $\Lambda_b \to \Lambda_c \ell \bar{\nu}_\ell$ Transition in Full QCD," *Phys. Rev.* **D97** no. 7, (2018) 074007, arXiv:1803.02085 [hep-ph].

[27] J. Zhu, B. Wei, J.-H. Sheng, R.-M. Wang, Y. Gao, and G.-R. Lu, "Probing the R-parity violating supersymmetric effects in $B_c \to J/\psi \ell^- \bar{\nu}_\ell, \eta_c \ell^- \bar{\nu}_\ell$ and $\Lambda_b \to \Lambda_c \ell^- \bar{\nu}_\ell$ decays," *Nucl. Phys.* **B934** (2018) 380–395, arXiv:1801.00917 [hep-ph].

[28] Y. Sakaki, M. Tanaka, A. Tayduganov, and R. Watanabe, "Testing leptoquark models in $\bar{B} \to D^{(*)} \tau \bar{\nu}$," *Phys. Rev.* **D88** no. 9, (2013) 094012, arXiv:1309.0301 [hep-ph].

[29] S. Fajfer, J. F. Kamenik, and I. Nisandzic, "On the $B \to D^* \tau \bar{\nu}_\tau$ Sensitivity to New Physics," *Phys. Rev.* **D85** (2012) 094025, arXiv:1203.2654 [hep-ph].

[30] **Heavy Flavor Averaging Group** Collaboration, Y. Amhis *et al.*, "Averages of $b$-hadron, $c$-hadron, and $\tau$-lepton properties as of summer 2016," *Eur. Phys. J.* **C77** (2017) 895, arXiv:1612.07233 [hep-ex]. updated results and plots available at https://hflav.web.cern.ch.

[31] C.-H. Chen and C.-Q. Geng, "Lepton angular asymmetries in semileptonic charmful B decays," *Phys. Rev.* **D71** (2005) 077501, arXiv:hep-ph/0503123 [hep-ph].

[32] T. Bhattacharya, V. Cirigliano, S. D. Cohen, A. Filipuzzi, M. Gonzalez-Alonso, M. L. Graesser, R. Gupta, and H.-W. Lin, "Probing Novel Scalar and Tensor Interactions from (Ultra)Cold Neutrons to the LHC," *Phys. Rev.* **D85** (2012) 054512, arXiv:1110.6448 [hep-ph].

[33] J. G. Korner and G. A. Schuler, "Exclusive Semileptonic Heavy Meson Decays Including Lepton Mass Effects," *Z. Phys.* **C46** (1990) 93.

[34] T. Feldmann and M. W. Y. Yip, "Form Factors for $\Lambda_b \to \Lambda$ Transitions in SCET," *Phys. Rev.* **D85** (2012) 014035, arXiv:1111.1844 [hep-ph]. [Erratum: Phys. Rev.D86,079901(2012)].

[35] **Particle Data Group** Collaboration, M. Tanabashi *et al.*, "Review of Particle Physics," *Phys. Rev.* **D98** no. 3, (2018) 030001.

[36] R. Alonso, B. Grinstein, and J. Martin Camalich, "Lifetime of $B_c^-$ Constrains Explanations for Anomalies in $B \to D^{(*)} \tau \nu$," *Phys. Rev. Lett.* **118** no. 8, (2017) 081802, arXiv:1611.06676 [hep-ph].

[37] A. Celis, M. Jung, X.-Q. Li, and A. Pich, "Scalar contributions to $b \to c(u)\tau\nu$ transitions," *Phys. Lett.* **B771** (2017) 168–179, arXiv:1612.07757 [hep-ph].

[38] X.-Q. Li, Y.-D. Yang, and X. Zhang, "Revisiting the one leptoquark solution to the $R(D^{(*)})$ anomalies and its phenomenological implications," *JHEP* **08** (2016) 054, arXiv:1605.09308 [hep-ph].

[39] M. Beneke and G. Buchalla, "The $B_c$ Meson Lifetime," *Phys. Rev.* **D53** (1996) 4991–5000, arXiv:hep-ph/9601249 [hep-ph].

[40] **HPQCD** Collaboration, B. Colquhoun, C. T. H. Davies, R. J. Dowdall, J. Kettle, J. Koponen, G. P. Lepage, and A. T. Lytle, "B-meson decay constants: a more complete picture from full lattice QCD," *Phys. Rev.* **D91** no. 11, (2015) 114509, arXiv:1503.05762 [hep-lat].

[41] B. Bhattacharya, A. Datta, J.-P. Guévin, D. London, and R. Watanabe, "Simultaneous Explanation of the $R_K$ and $R_{D^{(*)}}$ Puzzles: a Model Analysis," *JHEP* **01** (2017) 015, arXiv:1609.09078 [hep-ph].

[42] **BaBar** Collaboration, J. P. Lees *et al.*, "Search for $B \to K^{(*)}\nu\bar{\nu}$ and invisible quarkonium decays," *Phys. Rev.* **D87** no. 11, (2013) 112005, arXiv:1303.7465 [hep-ex].

[43] **Belle** Collaboration, O. Lutz *et al.*, "Search for $B \to h^{(*)}\nu\bar{\nu}$ with the full Belle $\Upsilon(4S)$ data sample," *Phys. Rev.* **D87** no. 11, (2013) 111103, arXiv:1303.3719 [hep-ex].

[44] A. J. Buras, J. Girrbach-Noe, C. Niehoff, and D. M. Straub, "$B \to K^{(*)}\nu\bar{\nu}$ decays in the Standard Model and beyond," *JHEP* **02** (2015) 184, arXiv:1409.4557 [hep-ph].

[45] A. J. Buras, "Weak Hamiltonian, CP violation and rare decays," in *Probing the standard model of particle interactions. Proceedings, Summer School in Theoretical Physics, NATO Advanced Study Institute, 68th session, Les Houches, France, July 28-September 5, 1997. Pt. 1, 2*, pp. 281–539. 1998. arXiv:hep-ph/9806471 [hep-ph].

[46] A. Czarnecki, M. Jezabek, and J. H. Kuhn, "Radiative corrections to $b \to c\tau\bar{\nu}_\tau$ ," *Phys. Lett.* **B346** (1995) 335–341, arXiv:hep-ph/9411282 [hep-ph].

[47] M. Jezabek and L. Motyka, "Tau lepton distributions in semileptonic B decays," *Nucl. Phys.* **B501** (1997) 207–223, arXiv:hep-ph/9701358 [hep-ph].

[48] M. Trott, "Improving extractions of $|V_{cb}|$ and $m_b$ from the hadronic invariant mass moments of semileptonic inclusive B decay," *Phys. Rev.* **D70** (2004) 073003, arXiv:hep-ph/0402120 [hep-ph].

[49] V. Aquila, P. Gambino, G. Ridolfi, and N. Uraltsev, "Perturbative corrections to semileptonic b decay distributions," *Nucl. Phys.* **B719** (2005) 77–102, arXiv:hep-ph/0503083 [hep-ph].

[50] S. Balk, J. G. Korner, D. Pirjol, and K. Schilcher, "Inclusive semileptonic B decays in QCD including lepton mass effects," *Z. Phys.* **C64** (1994) 37–44, arXiv:hep-ph/9312220 [hep-ph].

[51] L. Koyrakh, "Nonperturbative corrections to the heavy lepton energy distribution in the inclusive decays $H(b) \to \tau\bar{\nu}X$," *Phys. Rev.* **D49** (1994) 3379–3384, arXiv:hep-ph/9311215 [hep-ph].

[52] A. F. Falk, Z. Ligeti, M. Neubert, and Y. Nir, "Heavy quark expansion for the inclusive decay $\bar{B} \to \tau\bar{\nu}X$," *Phys. Lett.* **B326** (1994) 145–153, arXiv:hep-ph/9401226 [hep-ph].

[53] B. Blok, L. Koyrakh, M. A. Shifman, and A. I. Vainshtein, "Differential distributions in semileptonic decays of the heavy flavors in QCD," *Phys. Rev.* **D49** (1994) 3356, arXiv:hep-ph/9307247 [hep-ph]. [Erratum: Phys. Rev.D50,3572(1994)].

[54] Z. Ligeti and F. J. Tackmann, "Precise predictions for $B \to X_c \tau \bar{\nu}$ decay distributions," *Phys. Rev.* **D90** no. 3, (2014) 034021, arXiv:1406.7013 [hep-ph].

[55] S. Biswas and K. Melnikov, "Second order QCD corrections to inclusive semileptonic $b \to X_c \ell \bar{\nu}_\ell$ decays with massless and massive lepton," *JHEP* **02** (2010) 089, arXiv:0911.4142 [hep-ph].

[56] M. E. Luke, M. J. Savage, and M. B. Wise, "Charm mass dependence of the $O(\alpha_s^2 n(f))$ correction to inclusive $B \to X(c) e \bar{\nu}_e$ decay," *Phys. Lett.* **B345** (1995) 301–306, arXiv:hep-ph/9410387 [hep-ph].

[57] M. Tanaka and R. Watanabe, "New physics in the weak interaction of $\bar{B} \to D^{(*)} \tau \bar{\nu}$," *Phys. Rev.* **D87** no. 3, (2013) 034028, arXiv:1212.1878 [hep-ph].

[58] E. Byckling and K. Kajantie, *Particle Kinematics*. University of Jyvaskyla, Jyvaskyla, Finland, 1971. http://www-spires.fnal.gov/spires/find/books/www?cl=QC794.6.K5B99.

[59] A. H. Hoang, Z. Ligeti, and A. V. Manohar, "B decay and the Upsilon mass," *Phys. Rev. Lett.* **82** (1999) 277–280, arXiv:hep-ph/9809423 [hep-ph].

[60] A. H. Hoang, Z. Ligeti, and A. V. Manohar, "B decays in the upsilon expansion," *Phys. Rev.* **D59** (1999) 074017, arXiv:hep-ph/9811239 [hep-ph].

[61] M. Freytsis, Z. Ligeti, and J. T. Ruderman, "Flavor models for $\bar{B} \to D^{(*)} \tau \bar{\nu}$," *Phys. Rev.* **D92** no. 5, (2015) 054018, arXiv:1506.08896 [hep-ph].

[62] T. Mannel, A. V. Rusov, and F. Shahriaran, "Inclusive semitauonic $B$ decays to order $\bar{O}(\Lambda_{QCD}^3/m_b^3)$," *Nucl. Phys.* **B921** (2017) 211–224, arXiv:1702.01089 [hep-ph].

[63] **ALEPH** Collaboration, R. Barate *et al.*, "Measurements of $BR(b \to \tau^- \bar{\nu}_\tau X)$ and $BR(b \to \tau^- \bar{\nu}_\tau D^{*\pm} X)$ and upper limits on $BR(B^- \to \tau^- \bar{\nu}_\tau)$ and $BR(b \to s \nu \bar{\nu})$," *Eur. Phys. J.* **C19** (2001) 213–227, arXiv:hep-ex/0010022 [hep-ex].

[64] S. Kamali, "New physics in inclusive semileptonic $B$ decays including nonperturbative corrections," *Int. J. Mod. Phys.* **A34** no. 06n07, (2019) 1950036, arXiv:1811.07393 [hep-ph].

[65] A. V. Manohar and M. B. Wise, "Inclusive semileptonic B and polarized $\Lambda_b$ decays from QCD," *Phys. Rev.* **D49** (1994) 1310–1329, arXiv:hep-ph/9308246 [hep-ph].

[66] A. F. Falk, M. E. Luke, and M. J. Savage, "Nonperturbative contributions to the inclusive rare decays $B \to X_s \gamma$ and $B \to X_s l^+ l^-$," *Phys. Rev.* **D49** (1994) 3367–3378, arXiv:hep-ph/9308288 [hep-ph].

[67] B. M. Dassinger, T. Mannel, and S. Turczyk, "Inclusive semi-leptonic B decays to order $1/m_b^4$," *JHEP* **03** (2007) 087, arXiv:hep-ph/0611168 [hep-ph].

[68] P. Colangelo and F. De Fazio, "Tension in the inclusive versus exclusive determinations of $|V_{cb}|$: a possible role of new physics," *Phys. Rev.* **D95** no. 1, (2017) 011701, arXiv:1611.07387 [hep-ph].

[69] D. Benson, I. I. Bigi, T. Mannel, and N. Uraltsev, "Imprecated, yet impeccable: On the theoretical evaluation of $\Gamma(B \to X_c \ell \nu)$," *Nucl. Phys.* **B665** (2003) 367–401, arXiv:hep-ph/0302262 [hep-ph].

[70] P. Gambino and N. Uraltsev, "Moments of semileptonic B decay distributions in the $1/m_b$ expansion," *Eur. Phys. J.* **C34** (2004) 181–189, arXiv:hep-ph/0401063 [hep-ph].

[71] P. Gambino, "B semileptonic moments at NNLO," *JHEP* **09** (2011) 055, arXiv:1107.3100 [hep-ph].

[72] A. Alberti, P. Gambino, K. J. Healey, and S. Nandi, "Precision Determination of the Cabibbo-Kobayashi-Maskawa Element $V_{cb}$," *Phys. Rev. Lett.* **114** no. 6, (2015) 061802, arXiv:1411.6560 [hep-ph].

[73] C. W. Bauer, Z. Ligeti, M. Luke, and A. V. Manohar, "B decay shape variables and the precision determination of |V(cb)| and m(b)," *Phys. Rev.* **D67** (2003) 054012, arXiv:hep-ph/0210027 [hep-ph].

[74] C. W. Bauer, Z. Ligeti, M. Luke, A. V. Manohar, and M. Trott, "Global analysis of inclusive B decays," *Phys. Rev.* **D70** (2004) 094017, arXiv:hep-ph/0408002 [hep-ph].

[75] S. Bhattacharya, S. Nandi, and S. Kumar Patra, "$b \to c\tau\nu_\tau$ Decays: A Catalogue to Compare, Constrain, and Correlate New Physics Effects," arXiv:1805.08222 [hep-ph].

[76] S. Kamali, A. Rashed, and A. Datta, "New physics in inclusive $B \to X_c \ell \bar{\nu}$ decay in light of $R(D^{(*)})$ measurements," *Phys. Rev.* **D97** no. 9, (2018) 095034, arXiv:1801.08259 [hep-ph].

[77] **LHCb** Collaboration, R. Aaij *et al.*, "Determination of the quark coupling strength $|V_{ub}|$ using baryonic decays," *Nature Phys.* **11** (2015) 743–747, arXiv:1504.01568 [hep-ex].

[78] B. Bhattacharya, A. Datta, S. Kamali, and D. London, "CP Violation in $\bar{B}^0 \to D^{*+}\mu^-\bar{\nu}_\mu$," *JHEP* **05** (2019) 191, arXiv:1903.02567 [hep-ph].

[79] G. Valencia, "Angular correlations in the decay $B \to VV$ and CP violation," *Phys. Rev. D* **39** (Jun, 1989) 3339–3345. https://link.aps.org/doi/10.1103/PhysRevD.39.3339.

[80] A. Datta and D. London, "Triple-product correlations in $B \to V_1 V_2$ decays and new physics," *Int. J. Mod. Phys.* **A19** (2004) 2505–2544, arXiv:hep-ph/0303159 [hep-ph].

[81] W. Bensalem, A. Datta, and D. London, "New physics effects on triple product correlations in Lambda(b) decays," *Phys. Rev.* **D66** (2002) 094004, arXiv:hep-ph/0208054 [hep-ph].

[82] M. Duraisamy and A. Datta, "The Full $B \to D^* \tau^- \bar{\nu}_\tau$ Angular Distribution and CP violating Triple Products," *JHEP* **09** (2013) 059, arXiv:1302.7031 [hep-ph].

[83] M. Gronau and J. L. Rosner, "Triple product asymmetries in $K$, $D_{(s)}$ and $B_{(s)}$ decays," *Phys. Rev.* **D84** (2011) 096013, arXiv:1107.1232 [hep-ph].

[84] M. Beneke and T. Feldmann, "Symmetry breaking corrections to heavy to light B meson form-factors at large recoil," *Nucl. Phys.* **B592** (2001) 3–34, arXiv:hep-ph/0008255 [hep-ph].

[85] I. Doršner, S. Fajfer, N. Košnik, and I. Nišandžić, "Minimally flavored colored scalar in $\bar{B} \to D^{(*)} \tau \bar{\nu}$ and the mass matrices constraints," *JHEP* **11** (2013) 084, arXiv:1306.6493 [hep-ph].

[86] B. Dumont, K. Nishiwaki, and R. Watanabe, "LHC constraints and prospects for $S_1$ scalar leptoquark explaining the $\bar{B} \to D^{(*)} \tau \bar{\nu}$ anomaly," *Phys. Rev.* **D94** no. 3, (2016) 034001, arXiv:1603.05248 [hep-ph].

[87] A. Crivellin, D. Müller, A. Signer, and Y. Ulrich, "Correlating lepton flavor universality violation in $B$ decays with $\mu \to e\gamma$ using leptoquarks," *Phys. Rev.* **D97** no. 1, (2018) 015019, arXiv:1706.08511 [hep-ph].

[88] B. Bhattacharya, A. Datta, D. London, and S. Shivashankara, "Simultaneous Explanation of the $R_K$ and $R(D^{(*)})$ Puzzles," *Phys. Lett.* **B742** (2015) 370–374, arXiv:1412.7164 [hep-ph].

[89] A. K. Alok, B. Bhattacharya, A. Datta, D. Kumar, J. Kumar, and D. London, "New Physics in $b \to s\mu^+\mu^-$ after the Measurement of $R_{K^*}$," *Phys. Rev.* **D96** no. 9, (2017) 095009, arXiv:1704.07397 [hep-ph].

[90] J. Kumar, D. London, and R. Watanabe, "Combined Explanations of the $b \to s\mu^+\mu^-$ and $b \to c\tau^-\bar{\nu}$ Anomalies: a General Model Analysis," *Phys. Rev.* **D99** no. 1, (2019) 015007, arXiv:1806.07403 [hep-ph].

[91] A. Datta, J. L. Feng, S. Kamali, and J. Kumar, "Resolving the $(g-2)_\mu$ and $B$ Anomalies with Leptoquarks and a Dark Higgs Boson," *Phys. Rev.* **D101** no. 3, (2020) 035010, arXiv:1908.08625 [hep-ph].

[92] **RBC, UKQCD** Collaboration, T. Blum, P. A. Boyle, V. Gülpers, T. Izubuchi, L. Jin, C. Jung, A. Jüttner, C. Lehner, A. Portelli, and J. T. Tsang, "Calculation of the hadronic vacuum polarization contribution to the muon anomalous magnetic moment," *Phys. Rev. Lett.* **121** no. 2, (2018) 022003, arXiv:1801.07224 [hep-lat].

[93] **Muon g-2** Collaboration, G. W. Bennett *et al.*, "Final Report of the Muon E821 Anomalous Magnetic Moment Measurement at BNL," *Phys. Rev.* **D73** (2006) 072003, arXiv:hep-ex/0602035 [hep-ex].

[94] G. Hiller and F. Kruger, "More model-independent analysis of $b \to s$ processes," *Phys. Rev.* **D69** (2004) 074020, arXiv:hep-ph/0310219 [hep-ph].

[95] G. Hiller and M. Schmaltz, "$R_K$ and future $b \to s\ell\ell$ physics beyond the standard model opportunities," *Phys. Rev.* **D90** (2014) 054014, arXiv:1408.1627 [hep-ph].

[96] **LHCb** Collaboration, R. Aaij *et al.*, "Search for lepton-universality violation in $B^+ \to K^+\ell^+\ell^-$ decays," *Phys. Rev. Lett.* **122** no. 19, (2019) 191801, arXiv:1903.09252 [hep-ex].

[97] M. Bordone, G. Isidori, and A. Pattori, "On the Standard Model predictions for $R_K$ and $R_{K^*}$," *Eur. Phys. J.* **C76** no. 8, (2016) 440, arXiv:1605.07633 [hep-ph].

[98] **LHCb** Collaboration, R. Aaij *et al.*, "Test of lepton universality with $B^0 \to K^{*0}\ell^+\ell^-$ decays," *JHEP* **08** (2017) 055, arXiv:1705.05802 [hep-ex].

[99] S. Descotes-Genon, L. Hofer, J. Matias, and J. Virto, "On the impact of power corrections in the prediction of $B \to K^*\mu^+\mu^-$ observables," *JHEP* **12** (2014) 125, arXiv:1407.8526 [hep-ph].

[100] J. Lyon and R. Zwicky, "Resonances gone topsy turvy - the charm of QCD or new physics in $b \to s\ell^+\ell^-$?," arXiv:1406.0566 [hep-ph].

[101] S. Jäger and J. Martin Camalich, "Reassessing the discovery potential of the $B \to K^*\ell^+\ell^-$ decays in the large-recoil region: SM challenges and BSM opportunities," *Phys. Rev.* **D93** no. 1, (2016) 014028, arXiv:1412.3183 [hep-ph].

[102] R. Alonso, B. Grinstein, and J. Martin Camalich, "Lepton universality violation and lepton flavor conservation in $B$-meson decays," *JHEP* **10** (2015) 184, arXiv:1505.05164 [hep-ph].

[103] A. Greljo, G. Isidori, and D. Marzocca, "On the breaking of Lepton Flavor Universality in $B$ decays," *JHEP* **07** (2015) 142, arXiv:1506.01705 [hep-ph].

[104] L. Calibbi, A. Crivellin, and T. Ota, "Effective Field Theory Approach to $b \to s\ell\ell'$, $B \to K^{(*)}\nu\overline{\nu}$ and $B \to D^{(*)}\tau\nu$ with Third Generation Couplings," *Phys. Rev. Lett.* **115** (2015) 181801, arXiv:1506.02661 [hep-ph].

[105] W. Altmannshofer, P. S. Bhupal Dev, and A. Soni, "$R_{D^{(*)}}$ anomaly: A possible hint for natural supersymmetry with $R$-parity violation," *Phys. Rev.* **D96** no. 9, (2017) 095010, arXiv:1704.06659 [hep-ph].

[106] B. Capdevila, A. Crivellin, S. Descotes-Genon, J. Matias, and J. Virto, "Patterns of New Physics in $b \to s\ell^+\ell^-$ transitions in the light of recent data," *JHEP* **01** (2018) 093, arXiv:1704.05340 [hep-ph].

[107] W. Altmannshofer, P. Stangl, and D. M. Straub, "Interpreting Hints for Lepton Flavor Universality Violation," *Phys. Rev.* **D96** no. 5, (2017) 055008, arXiv:1704.05435 [hep-ph].

[108] G. D'Amico, M. Nardecchia, P. Panci, F. Sannino, A. Strumia, R. Torre, and A. Urbano, "Flavour anomalies after the $R_{K^*}$ measurement," *JHEP* **09** (2017) 010, arXiv:1704.05438 [hep-ph].

[109] G. Hiller and I. Nisandzic, "$R_K$ and $R_{K^*}$ beyond the standard model," *Phys. Rev.* **D96** no. 3, (2017) 035003, arXiv:1704.05444 [hep-ph].

[110] L.-S. Geng, B. Grinstein, S. Jäger, J. Martin Camalich, X.-L. Ren, and R.-X. Shi, "Towards the discovery of new physics with lepton-universality ratios of $b \to s\ell\ell$ decays," *Phys. Rev.* **D96** no. 9, (2017) 093006, arXiv:1704.05446 [hep-ph].

[111] M. Ciuchini, A. M. Coutinho, M. Fedele, E. Franco, A. Paul, L. Silvestrini, and M. Valli, "On Flavourful Easter Eggs for New Physics Hunger and Lepton Flavour Universality Violation," *Eur. Phys. J.* **C77** no. 10, (2017) 688, arXiv:1704.05447 [hep-ph].

[112] A. Celis, J. Fuentes-Martin, A. Vicente, and J. Virto, "Gauge-invariant implications of the LHCb measurements on lepton-flavor nonuniversality," *Phys. Rev.* **D96** no. 3, (2017) 035026, arXiv:1704.05672 [hep-ph].

[113] D. Bečirević and O. Sumensari, "A leptoquark model to accommodate $R_K^{\rm exp} < R_K^{\rm SM}$ and $R_{K^*}^{\rm exp} < R_{K^*}^{\rm SM}$," *JHEP* **08** (2017) 104, arXiv:1704.05835 [hep-ph].

[114] S. Di Chiara, A. Fowlie, S. Fraser, C. Marzo, L. Marzola, M. Raidal, and C. Spethmann, "Minimal flavor-changing $Z'$ models and muon $g-2$ after the $R_{K^*}$ measurement," *Nucl. Phys.* **B923** (2017) 245–257, arXiv:1704.06200 [hep-ph].

[115] F. Sala and D. M. Straub, "A New Light Particle in $B$ Decays?," *Phys. Lett.* **B774** (2017) 205–209, arXiv:1704.06188 [hep-ph].

[116] D. Ghosh, "Explaining the $R_K$ and $R_{K^*}$ anomalies," *Eur. Phys. J.* **C77** no. 10, (2017) 694, arXiv:1704.06240 [hep-ph].

[117] A. K. Alok, D. Kumar, J. Kumar, and R. Sharma, "Lepton flavor non-universality in the B-sector: a global analyses of various new physics models," arXiv:1704.07347 [hep-ph].

[118] W. Wang and S. Zhao, "Implications of the $R_K$ and $R_{K^*}$ anomalies," *Chin. Phys.* **C42** no. 1, (2018) 013105, arXiv:1704.08168 [hep-ph].

[119] C. Bonilla, T. Modak, R. Srivastava, and J. W. F. Valle, "$U(1)_{B_3-3L_\mu}$ gauge symmetry as a simple description of $b \to s$ anomalies," *Phys. Rev.* **D98** no. 9, (2018) 095002, arXiv:1705.00915 [hep-ph].

[120] D. Bardhan, P. Byakti, and D. Ghosh, "Role of Tensor operators in $R_K$ and $R_{K^*}$," *Phys. Lett.* **B773** (2017) 505–512, arXiv:1705.09305 [hep-ph].

[121] A. Crivellin, D. Müller, and T. Ota, "Simultaneous explanation of $R(D^{(*)})$ and $b \to s\mu^+\mu^-$: the last scalar leptoquarks standing," *JHEP* **09** (2017) 040, arXiv:1703.09226 [hep-ph].

[122] S. Fajfer and N. Košnik, "Vector leptoquark resolution of $R_K$ and $R_{D^{(*)}}$ puzzles," *Phys. Lett.* **B755** (2016) 270–274, arXiv:1511.06024 [hep-ph].

[123] M. Bauer and M. Neubert, "Minimal Leptoquark Explanation for the $R_{D^{(*)}}$ , $R_K$ , and $(g-2)_\mu$ Anomalies," *Phys. Rev. Lett.* **116** no. 14, (2016) 141802, arXiv:1511.01900 [hep-ph].

[124] R. Barbieri, G. Isidori, A. Pattori, and F. Senia, "Anomalies in $B$-decays and $U(2)$ flavour symmetry," *Eur. Phys. J.* **C76** no. 2, (2016) 67, arXiv:1512.01560 [hep-ph].

[125] D. Das, C. Hati, G. Kumar, and N. Mahajan, "Towards a unified explanation of $R_{D^{(*)}}$, $R_K$ and $(g-2)_\mu$ anomalies in a left-right model with leptoquarks," *Phys. Rev.* **D94** (2016) 055034, arXiv:1605.06313 [hep-ph].

[126] S. M. Boucenna, A. Celis, J. Fuentes-Martin, A. Vicente, and J. Virto, "Phenomenology of an $SU(2) \times SU(2) \times U(1)$ model with lepton-flavour non-universality," *JHEP* **12** (2016) 059, arXiv:1608.01349 [hep-ph].

[127] D. Bečirević, S. Fajfer, N. Košnik, and O. Sumensari, "Leptoquark model to explain the $B$-physics anomalies, $R_K$ and $R_D$," *Phys. Rev.* **D94** no. 11, (2016) 115021, arXiv:1608.08501 [hep-ph].

[128] C.-H. Chen, T. Nomura, and H. Okada, "Excesses of muon $g-2$, $R_{D^{(*)}}$, and $R_K$ in a leptoquark model," *Phys. Lett.* **B774** (2017) 456–464, arXiv:1703.03251 [hep-ph].

[129] M. Blanke and A. Crivellin, "$B$ Meson Anomalies in a Pati-Salam Model within the Randall-Sundrum Background," *Phys. Rev. Lett.* **121** no. 1, (2018) 011801, arXiv:1801.07256 [hep-ph].

[130] A. Crivellin, C. Greub, D. Müller, and F. Saturnino, "Importance of Loop Effects in Explaining the Accumulated Evidence for New Physics in B Decays with a Vector Leptoquark," *Phys. Rev. Lett.* **122** no. 1, (2019) 011805, arXiv:1807.02068 [hep-ph].

[131] A. Crivellin and F. Saturnino, "Explaining the Flavor Anomalies with a Vector Leptoquark (Moriond 2019 update)," in *54th Rencontres de Moriond on QCD and High Energy Interactions (Moriond QCD 2019) La Thuile, Italy, March 23-30, 2019*. 2019. arXiv:1906.01222 [hep-ph].

[132] S.-P. Li and X.-Q. Li, "Probing New Physics Signals with Symmetry-Restored Yukawa Textures," arXiv:1907.13555 [hep-ph].

[133] S.-P. Li, X.-Q. Li, Y.-D. Yang, and X. Zhang, "$R_{D^{(*)}}$, $R_{K^{(*)}}$ and neutrino mass in the 2HDM-III with right-handed neutrinos," *JHEP* **09** (2018) 149, arXiv:1807.08530 [hep-ph].

[134] O. Popov, M. A. Schmidt, and G. White, "$R_2$ as a single leptoquark solution to $R_{D^{(*)}}$ and $R_{K^{(*)}}$," *Phys. Rev.* **D100** no. 3, (2019) 035028, arXiv:1905.06339 [hep-ph].

[135] W. Altmannshofer, M. J. Baker, S. Gori, R. Harnik, M. Pospelov, E. Stamou, and A. Thamm, "Light resonances and the low-$q^2$ bin of $R_{K^*}$," *JHEP* **03** (2018) 188, arXiv:1711.07494 [hep-ph].

[136] A. Datta, J. Kumar, and D. London, "The $B$ Anomalies and New Physics in $b \to se^+e^-$," *Phys. Lett.* **B797** (2019) 134858, arXiv:1903.10086 [hep-ph].

[137] J. Aebischer, W. Altmannshofer, D. Guadagnoli, M. Reboud, P. Stangl, and D. M. Straub, "$B$-decay discrepancies after Moriond 2019," arXiv:1903.10434 [hep-ph].

[138] H. Davoudiasl and W. J. Marciano, "Tale of two anomalies," *Phys. Rev.* **D98** no. 7, (2018) 075011, arXiv:1806.10252 [hep-ph].

[139] C.-Y. Chen, H. Davoudiasl, W. J. Marciano, and C. Zhang, "Implications of a light "dark Higgs" solution to the $g_\mu - 2$ discrepancy," *Phys. Rev.* **D93** no. 3, (2016) 035006, arXiv:1511.04715 [hep-ph].

[140] V. Ilisie, "New Barr-Zee contributions to $(g-2)_\mu$ in two-Higgs-doublet models," *JHEP* **04** (2015) 077, arXiv:1502.04199 [hep-ph].

[141] W. J. Marciano, C. Zhang, and S. Willenbrock, "Higgs Decay to Two Photons," *Phys. Rev.* **D85** (2012) 013002, arXiv:1109.5304 [hep-ph].

[142] **CMS** Collaboration, A. M. Sirunyan *et al.*, "Search for pair production of first-generation scalar leptoquarks at $\sqrt{s} = 13$ TeV," *Phys. Rev. D* **99** no. 5, (2019) 052002, arXiv:1811.01197 [hep-ex].

[143] **ATLAS** Collaboration, V. W. S. Wong, "Searching for leptoquarks with the ATLAS detector," in *17th Conference on Flavor Physics and CP Violation*. 6, 2019. arXiv:1906.08983 [hep-ex].

[144] **FCC** Collaboration, A. Abada *et al.*, "FCC-hh: The Hadron Collider: Future Circular Collider Conceptual Design Report Volume 3," *Eur. Phys. J. ST* **228** no. 4, (2019) 755–1107.

[145] S. J. Oliveros, D. Summers, L. Cremaldi, J. Acosta, and D. Neuffer, "Exploration of a High Luminosity 100 TeV Proton Antiproton Collider," in *82nd Annual Meeting of the Southeastern Section of the American Physicsl Society (SESAPS 2015)*. 4, 2017. arXiv:1704.03891 [physics.acc-ph].

[146] "A Multi-TeV Linear Collider Based on CLIC Technology: CLIC Conceptual Design Report,".

[147] D. V. Neuffer and R. B. Palmer, "A High-Energy High-Luminosity $\mu^+ - \mu^-$ Collider," *Conf. Proc. C* **940627** (1995) 52–54.

[148] R. B. Palmer, "Muon Colliders," *Rev. Accel. Sci. Tech.* **7** (2014) 137–159.

[149] F. S. Queiroz and W. Shepherd, "New Physics Contributions to the Muon Anomalous Magnetic Moment: A Numerical Code," *Phys. Rev.* **D89** no. 9, (2014) 095024, arXiv:1403.2309 [hep-ph].

[150] K. Kowalska, D. Kumar, and E. M. Sessolo, "Implications for New Physics in $b \to s\mu\mu$ transitions after recent measurements by Belle and LHCb," arXiv:1903.10932 [hep-ph].

[151] A. K. Alok, A. Dighe, S. Gangal, and D. Kumar, "Continuing search for new physics in $b \to s\mu\mu$ decays: two operators at a time," *JHEP* **06** (2019) 089, arXiv:1903.09617 [hep-ph].

[152] M. Ciuchini, A. M. Coutinho, M. Fedele, E. Franco, A. Paul, L. Silvestrini, and M. Valli, "New Physics in $b \to s\ell^+\ell^-$ confronts new data on Lepton Universality," arXiv:1903.09632 [hep-ph].

[153] M. Alguero, B. Capdevila, S. Descotes-Genon, P. Masjuan, and J. Matias, "What $R_K$ and $Q_5$ can tell us about New Physics in $b \to s\ell\ell$ transitions?," *JHEP* **07** (2019) 096, arXiv:1902.04900 [hep-ph].

[154] B. Batell, M. Pospelov, and A. Ritz, "Multi-lepton Signatures of a Hidden Sector in Rare $B$ Decays," *Phys. Rev.* **D83** (2011) 054005, arXiv:0911.4938 [hep-ph].

[155] A. Datta, J. Liao, and D. Marfatia, "A light $Z'$ for the $R_K$ puzzle and nonstandard neutrino interactions," *Phys. Lett.* **B768** (2017) 265–269, arXiv:1702.01099 [hep-ph].

[156] A. Datta, J. Kumar, J. Liao, and D. Marfatia, "New light mediators for the $R_K$ and $R_{K^*}$ puzzles," *Phys. Rev.* **D97** no. 11, (2018) 115038, arXiv:1705.08423 [hep-ph].

[157] A. Bharucha, D. M. Straub, and R. Zwicky, "$B \to V\ell^+\ell^-$ in the Standard Model from light-cone sum rules," *JHEP* **08** (2016) 098, arXiv:1503.05534 [hep-ph].

[158] P. Ball and R. Zwicky, "New results on $B \to \pi, K, \eta$ decay formfactors from light-cone sum rules," *Phys. Rev.* **D71** (2005) 014015, arXiv:hep-ph/0406232 [hep-ph].

[159] A. Lenz, "Lifetimes and heavy quark expansion," *Int. J. Mod. Phys.* **A30** no. 10, (2015) 1543005, arXiv:1405.3601 [hep-ph]. [,63(2014)].

[160] D. M. Straub, "flavio: a Python package for flavour and precision phenomenology in the Standard Model and beyond," arXiv:1810.08132 [hep-ph].

[161] L. Reina, G. Ricciardi, and A. Soni, "QCD corrections to $b \to s\gamma\gamma$ induced decays: $B \to X_s\gamma\gamma$ and $B_s \to \gamma\gamma$," *Phys. Rev.* **D56** (1997) 5805–5815, arXiv:hep-ph/9706253 [hep-ph].

[162] D. Atwood, L. Reina, and A. Soni, "Phenomenology of two Higgs doublet models with flavor changing neutral currents," *Phys. Rev.* **D55** (1997) 3156–3176, arXiv:hep-ph/9609279 [hep-ph].

[163] G. Khoriauli, "Measurement of $BR(K^{\pm} \to \mu^{\pm}\nu_{\mu}e^{+}e^{-})$ with NA48/2 at CERN," *Journal of Physics: Conference Series* **800** no. 1, (2017) 012035. http://stacks.iop.org/1742-6596/800/i=1/a=012035.

[164] C. E. Carlson and B. C. Rislow, "New Physics and the Proton Radius Problem," *Phys. Rev.* **D86** (2012) 035013, arXiv:1206.3587 [hep-ph].

[165] **NA48/2** Collaboration, J. R. Batley *et al.*, "Precise measurement of the $K^{\pm} \to \pi^{\pm}e^{+}e^{-}$ decay," *Phys. Lett.* **B677** (2009) 246–254, arXiv:0903.3130 [hep-ex].

[166] **LHCb** Collaboration, R. Aaij *et al.*, "Measurement of the $B^0 \to K^{*0}e^{+}e^{-}$ branching fraction at low dilepton mass," *JHEP* **05** (2013) 159, arXiv:1304.3035 [hep-ex].

[167] **BaBar** Collaboration, J. P. Lees *et al.*, "Measurement of the $B \to X_s l^{+} l^{-}$ branching fraction and search for direct CP violation from a sum of exclusive final states," *Phys. Rev. Lett.* **112** (2014) 211802, arXiv:1312.5364 [hep-ex].

[168] G. Hiller and A. S. Safir, "Predictions for $B \to K\gamma\gamma$ decays," *JHEP* **02** (2005) 011, arXiv:hep-ph/0411344 [hep-ph].

[169] B. A. Dobrescu, G. L. Landsberg, and K. T. Matchev, "Higgs boson decays to CP odd scalars at the Tevatron and beyond," *Phys. Rev.* **D63** (2001) 075003, arXiv:hep-ph/0005308 [hep-ph].

[170] **CMS** Collaboration, A. M. Sirunyan *et al.*, "Measurements of Higgs boson properties in the diphoton decay channel in proton-proton collisions at $\sqrt{s}$ = 13 TeV," *JHEP* **11** (2018) 185, arXiv:1804.02716 [hep-ex].

[171] **ATLAS** Collaboration, "Measurements of Higgs boson properties in the diphoton decay channel using 80 fb$^{-1}$ of $pp$ collision data at $\sqrt{s}$ = 13 TeV with the ATLAS detector," Tech. Rep. ATLAS-CONF-2018-028, CERN, Geneva, Jul, 2018. http://cds.cern.ch/record/2628771.

[172] P. R. Auvil and J. J. Brehm, "Wave Functions for Particles of Higher Spin," *Phys. Rev.* **145** no. 4, (1966) 1152.

[173] B. Batell, N. Lange, D. McKeen, M. Pospelov, and A. Ritz, "Muon anomalous magnetic moment through the leptonic Higgs portal," *Phys. Rev.* **D95** no. 7, (2017) 075003, arXiv:1606.04943 [hep-ph].

[174] M. Carena, I. Low, and C. E. M. Wagner, "Implications of a Modified Higgs to Diphoton Decay Width," *JHEP* **08** (2012) 060, arXiv:1206.1082 [hep-ph].

# APPENDICES

# APPENDIX A

# HELICITY SPINORS AND POLARIZATION VECTORS

In this appendix, we give explicit expressions for the spinors and polarization vectors used to calculate the helicity amplitudes for the decay $\Lambda_b \to \Lambda_c \tau \bar{\nu}_\tau$.

## A.1 $\Lambda_b$ rest frame

To calculate the hadronic helicity amplitudes, we work in the $\Lambda_b$ rest frame and take the three-momentum of the $\Lambda_c$ along the $+z$ direction and the three-momentum of the virtual vector boson along the $-z$ direction. The baryon spinors are then given by [172]

$$\begin{aligned} \bar{u}_2(\pm\tfrac{1}{2}, p_{\Lambda_c}) &= \sqrt{E_{\Lambda_c} + m_{\Lambda_c}} \left( \chi^\dagger_\pm, \frac{\mp|\mathbf{p}_{\Lambda_c}|}{E_{\Lambda_c} + m_{\Lambda_c}} \chi^\dagger_\pm \right) , \\ u_1(\pm\tfrac{1}{2}, p_{\Lambda_b}) &= \sqrt{2m_{\Lambda_b}} \begin{pmatrix} \chi_\pm \\ 0 \end{pmatrix} , \end{aligned} \tag{A.1}$$

where $\chi_+ = \begin{pmatrix} 1 \\ 0 \end{pmatrix}$ and $\chi_- = \begin{pmatrix} 0 \\ 1 \end{pmatrix}$ are the usual Pauli two-spinors. The polarization vectors of the virtual vector boson are,

$$\begin{aligned} \epsilon^{\mu*}(t) &= \frac{1}{\sqrt{q^2}} (q_0; 0, 0, -|\mathbf{q}|) , \\ \epsilon^{\mu*}(\pm 1) &= \frac{1}{\sqrt{2}} (0; \pm 1, -i, 0) , \\ \epsilon^{\mu*}(0) &= \frac{1}{\sqrt{q^2}} (|\mathbf{q}|; 0, 0, -q_0) , \end{aligned} \tag{A.2}$$

where $q^\mu = (q_0; 0, 0, -|\mathbf{q}|)$ is the four-momentum of the virtual vector boson in the $\Lambda_b$ rest frame. We have

$$q_0 = \frac{1}{2m_{\Lambda_b}}(m^2_{\Lambda_b} - m^2_{\Lambda_c} + q^2)\,, \tag{A.3}$$

$$|\mathbf{q}| = |\mathbf{p}_{\Lambda_c}| = \frac{1}{2m_{\Lambda_b}}\sqrt{Q_+Q_-}\,, \tag{A.4}$$

where

$$Q_\pm = (m_{\Lambda_b} \pm m_{\Lambda_c})^2 - q^2. \tag{A.5}$$

## A.2 Dilepton rest frame

In the calculation of the lepton helicity amplitudes, we work in the rest frame of the virtual vector boson, which is equal to the rest frame of the $\tau\bar{\nu}_\tau$ dilepton system. We define the angle $\theta_\tau$ as the angle between the three-momenta of the $\tau$ and the $\Lambda_c$ in this frame.

The lepton spinors for $\mathbf{p}_\tau$ pointing in the $+z$ direction and $\mathbf{p}_{\bar{\nu}_\tau}$ pointing in the $-z$ direction are

$$\begin{aligned}
\bar{u}_\tau(\pm\tfrac{1}{2}, p_\tau) &= \sqrt{E_\tau + m_\tau}\left(\chi^\dagger_\pm, \frac{\mp|\mathbf{p}_\tau|}{E_\tau + m_\tau}\chi^\dagger_\pm\right), \\
v_{\bar{\nu}_\tau}(\tfrac{1}{2}, p_{\bar{\nu}_\tau}) &= \sqrt{E_\nu}\begin{pmatrix} \chi_+ \\ -\chi_+ \end{pmatrix}.
\end{aligned} \tag{A.6}$$

We then rotate these about the $y$ axis by the angle $\theta_\tau$ so that after the rotation, the three-momentum of the $\Lambda_c$ points in the $+z$ direction. The two-spinors transform as

$$\begin{aligned}
\chi'_\pm &= e^{-i\theta_\tau\sigma_2/2}\chi_\pm \\
&= \begin{pmatrix} \cos(\theta_\tau/2) & -\sin(\theta_\tau/2) \\ \sin(\theta_\tau/2) & \cos(\theta_\tau/2) \end{pmatrix}\chi_\pm,
\end{aligned} \tag{A.7}$$

and

$$\chi'^{\dagger}_{\pm} = \chi^{\dagger}_{\pm}\begin{pmatrix} \cos(\theta_\tau/2) & \sin(\theta_\tau/2) \\ -\sin(\theta_\tau/2) & \cos(\theta_\tau/2) \end{pmatrix}, \tag{A.8}$$

and the full lepton spinors after the rotation are

$$\begin{aligned}
\bar{u}_\tau(+\tfrac{1}{2}, p_\tau) &= \sqrt{E_\tau + m_\tau}\left(\cos(\theta_\tau/2), \sin(\theta_\tau/2), \frac{-|\mathbf{p}_\tau|}{E_\tau + m_\tau}\cos(\theta_\tau/2), \frac{-|\mathbf{p}_\tau|}{E_\tau + m_\tau}\sin(\theta_\tau/2)\right), \\
\bar{u}_\tau(-\tfrac{1}{2}, p_\tau) &= \sqrt{E_\tau + m_\tau}\left(-\sin(\theta_\tau/2), \cos(\theta_\tau/2), \frac{-|\mathbf{p}_\tau|}{E_\tau + m_\tau}\sin(\theta_\tau/2), \frac{|\mathbf{p}_\tau|}{E_\tau + m_\tau}\cos(\theta_\tau/2)\right), \\
v_{\bar{\nu}_\tau}(\tfrac{1}{2}, p_{\bar{\nu}_\tau}) &= \sqrt{E_\nu}\begin{pmatrix} \cos(\theta_\tau/2) \\ \sin(\theta_\tau/2) \\ -\cos(\theta_\tau/2) \\ -\sin(\theta_\tau/2) \end{pmatrix}.
\end{aligned} \tag{A.9}$$

The polarization vectors of the virtual vector boson in this frame are

$$\begin{aligned}
\epsilon^{\mu*}(t) &= (1; 0, 0, 0), \\
\epsilon^{\mu*}(\pm 1) &= \frac{1}{\sqrt{2}}(0; \pm 1, -i, 0), \\
\epsilon^{\mu*}(0) &= (0; 0, 0, -1).
\end{aligned} \tag{A.10}$$

The three-momentum and energy of the $\tau$ lepton in this frame can be written as

$$\begin{aligned}
|\mathbf{p}_\tau| &= \sqrt{q^2}\, v^2/2, \\
E_\tau &= |\mathbf{p}_\tau| + m_\tau^2/\sqrt{q^2},
\end{aligned} \tag{A.11}$$

where

$$v = \sqrt{1 - \frac{m_\tau^2}{q^2}}. \tag{A.12}$$

# APPENDIX B

## HELICITY AMPLITUDES

In general for the process $B \to X_c \tau^- \bar{\nu}_\tau$, the scalar-type, vector/axial-vector-type, and tensor-type hadronic helicity amplitudes are defined as

$$\begin{aligned} H^{SP}_{\lambda_c,\lambda=0} &= H^{S}_{\lambda_c,\lambda=0} + H^{P}_{\lambda_c,\lambda=0}, \\ H^{S}_{\lambda_c,\lambda=0} &= g_S \langle X_c | \bar{c} b | B \rangle , \\ H^{P}_{\lambda_c,\lambda=0} &= g_P \langle X_c | \bar{c} \gamma_5 b | B \rangle , \end{aligned} \tag{B.1}$$

$$\begin{aligned} H^{VA}_{\lambda_c,\lambda} &= H^{V}_{\lambda_c,\lambda} - H^{A}_{\lambda_c,\lambda}, \\ H^{V}_{\lambda_c,\lambda} &= (1 + g_L + g_R)\, \epsilon^{*\mu}(\lambda) \langle X_c | \bar{c} \gamma_\mu b | B \rangle , \\ H^{A}_{\lambda_c,\lambda} &= (1 + g_L - g_R)\, \epsilon^{*\mu}(\lambda) \langle X_c | \bar{c} \gamma_\mu \gamma_5 b | B \rangle , \end{aligned} \tag{B.2}$$

and

$$\begin{aligned} H^{(T)\lambda_b}_{\lambda_c,\lambda,\lambda'} &= H^{(T1)\lambda_b}_{\lambda_c,\lambda,\lambda'} - H^{(T2)\lambda_b}_{\lambda_c,\lambda,\lambda'}, \\ H^{(T1)\lambda_b}_{\lambda_c,\lambda,\lambda'} &= g_T\, \epsilon^{*\mu}(\lambda) \epsilon^{*\nu}(\lambda') \langle X_c | \bar{c} i \sigma_{\mu\nu} b | B \rangle , \\ H^{(T2)\lambda_b}_{\lambda_c,\lambda,\lambda'} &= g_T\, \epsilon^{*\mu}(\lambda) \epsilon^{*\nu}(\lambda') \langle X_c | \bar{c} i \sigma_{\mu\nu} \gamma_5 b | B \rangle , \end{aligned} \tag{B.3}$$

where $\epsilon^\mu$ is the polarization vector of the virtual vector boson. The leptonic amplitudes are defined as

$$\begin{aligned} L^{\lambda_\tau} &= \langle \tau \bar{\nu}_\tau | \, \bar{\tau}(1-\gamma_5)\nu_\tau \, |0\rangle \,, \\ L^{\lambda_\tau}_{\lambda} &= \epsilon^\mu(\lambda) \, \langle \tau \bar{\nu}_\tau | \, \bar{\tau}\gamma_\mu(1-\gamma_5)\nu_\tau \, |0\rangle \,, \\ L^{\lambda_\tau}_{\lambda,\lambda'} &= -i\epsilon^\mu(\lambda)\epsilon^\nu(\lambda') \, \langle \tau \bar{\nu}_\tau | \, \bar{\tau}\sigma_{\mu\nu}(1-\gamma_5)\nu_\tau \, |0\rangle \,. \end{aligned} \tag{B.4}$$

When we consider the process as a free quark decay, we simply use the quark spinors without hadronic expectation values. So the matrix elements for the hadronic vector and axial vector currents will become

$$\langle X_c | \, \bar{c}\gamma^\mu b \, |B\rangle \;\rightarrow\; \bar{u}_c \gamma^\mu u_b, \tag{B.5}$$

$$\langle X_c | \, \bar{c}\gamma^\mu\gamma_5 b \, |B\rangle \;\rightarrow\; \bar{u}_c \gamma^\mu\gamma_5 u_b, \tag{B.6}$$

for the scalar and pseudoscalar currents

$$\begin{aligned} \langle X_c | \, \bar{c} b \, |B\rangle &\rightarrow \bar{u}_c u_b, \\ \langle X_c | \, \bar{c}\gamma_5 b \, |B\rangle &\rightarrow \bar{u}_c \gamma_5 u_b, \end{aligned} \tag{B.7}$$

and for the tensor currents

$$\begin{aligned} \langle X_c | \, \bar{c} i\sigma^{\mu\nu} b \, |B\rangle &\rightarrow \bar{u}_c i\sigma^{\mu\nu} u_b, \\ \langle X_c | \, \bar{c} i\sigma^{\mu\nu}\gamma_5 b \, |B\rangle &\rightarrow \bar{u}_c i\sigma^{\mu\nu}\gamma_5 u_b. \end{aligned} \tag{B.8}$$

The hadronic and leptonic helicity amplitudes of the process $b \rightarrow c\tau^-\bar{\nu}_\tau$ in the presence of scalar and pseudoscalar, vector and axial-vector, and tensor NP operators are below.

## B.1 Hadronic helicity amplitudes

Below, we present only the nonvanishing hadronic helicity amplitudes and use the definitions $Q_\pm = (m_b \pm m_c)^2 - q^2$.

The scalar and pseudoscalar helicity amplitudes associated with the new physics scalar and pseudoscalar interactions are

$$\begin{aligned} H^{SP}_{1/2,0} &= g_S\sqrt{Q_+} - g_P\sqrt{Q_-}\,, \\ H^{SP}_{-1/2,0} &= g_S\sqrt{Q_+} + g_P\sqrt{Q_-}\,. \end{aligned} \tag{B.9}$$

The parity-related amplitudes are

$$\begin{aligned} H^{S}_{\lambda_c,\lambda_{NP}} &= H^{S}_{-\lambda_c,-\lambda_{NP}}\,, \\ H^{P}_{\lambda_c,\lambda_{NP}} &= -H^{P}_{-\lambda_c,-\lambda_{NP}}\,. \end{aligned} \tag{B.10}$$

For the vector and axial-vector helicity amplitudes, we find

$$\begin{aligned} H^{VA}_{1/2,0} &= (1+g_L+g_R)\frac{\sqrt{Q_-}}{\sqrt{q^2}}(m_b+m_c) - (1+g_L-g_R)\frac{\sqrt{Q_+}}{\sqrt{q^2}}(m_b-m_c)\,, \\ H^{VA}_{1/2,+1} &= -(1+g_L+g_R)\sqrt{2Q_-} + (1+g_L-g_R)\sqrt{2Q_+}\,, \\ H^{VA}_{1/2,t} &= (1+g_L+g_R)\frac{\sqrt{Q_+}}{\sqrt{q^2}}(m_b-m_c) - (1+g_L-g_R)\frac{\sqrt{Q_-}}{\sqrt{q^2}}(m_b+m_c)\,, \\ H^{VA}_{-1/2,0} &= (1+g_L+g_R)\frac{\sqrt{Q_-}}{\sqrt{q^2}}(m_b+m_c) + (1+g_L-g_R)\frac{\sqrt{Q_+}}{\sqrt{q^2}}(m_b-m_c)\,, \\ H^{VA}_{-1/2,-1} &= -(1+g_L+g_R)\sqrt{2Q_-} - (1+g_L-g_R)\sqrt{2Q_+}\,, \\ H^{VA}_{-1/2,t} &= (1+g_L+g_R)\frac{\sqrt{Q_+}}{\sqrt{q^2}}(m_b-m_c) + (1+g_L-g_R)\frac{\sqrt{Q_-}}{\sqrt{q^2}}(m_b+m_c)\,. \end{aligned} \tag{B.11}$$

We also have the relations

$$\begin{aligned} H^V_{\lambda_c,\lambda_w} &= H^V_{-\lambda_c,-\lambda_w} \,, \\ H^A_{\lambda_c,\lambda_w} &= -H^A_{-\lambda_c,-\lambda_w} \,. \end{aligned} \tag{B.12}$$

The tensor helicity amplitudes are

$$\begin{aligned} H^{(T)-1/2}_{-1/2,t,0} &= -g_T\big[-\sqrt{Q_-}+\sqrt{Q_+}\big], \\ H^{(T)+1/2}_{+1/2,t,0} &= g_T\big[\sqrt{Q_-}+\sqrt{Q_+}\big], \\ H^{(T)-1/2}_{+1/2,t,+1} &= -g_T\frac{\sqrt{2}}{\sqrt{q^2}}\big[(m_b+m_c)\sqrt{Q_-}+(m_b-m_c)\sqrt{Q_+}\big], \\ H^{(T)+1/2}_{-1/2,t,-1} &= -g_T\frac{\sqrt{2}}{\sqrt{q^2}}\big[(m_b+m_c)\sqrt{Q_-}-(m_b-m_c)\sqrt{Q_+}\big], \\ H^{(T)-1/2}_{+1/2,0,+1} &= -g_T\frac{\sqrt{2}}{\sqrt{q^2}}\big[(m_b+m_c)\sqrt{Q_-}+(m_b-m_c)\sqrt{Q_+}\big], \\ H^{(T)+1/2}_{-1/2,0,-1} &= g_T\frac{\sqrt{2}}{\sqrt{q^2}}\big[(m_b+m_c)\sqrt{Q_-}-(m_b-m_c)\sqrt{Q_+}\big], \\ H^{(T)+1/2}_{+1/2,+1,-1} &= -g_T\big[\sqrt{Q_-}+\sqrt{Q_+}\big], \\ H^{(T)-1/2}_{-1/2,+1,-1} &= -g_T\big[\sqrt{Q_-}-\sqrt{Q_+}\big]. \end{aligned} \tag{B.13}$$

The other nonvanishing helicity amplitudes of tensor type are related to the above by

$$H^{(T)\lambda_b}_{\lambda_c,\lambda,\lambda'} = -H^{(T)\lambda_b}_{\lambda_c,\lambda',\lambda} \,. \tag{B.14}$$

## B.2 Leptonic helicity amplitudes

In the following, we define

$$v = \sqrt{1 - \frac{m_\tau^2}{q^2}}. \tag{B.15}$$

The scalar and pseudoscalar leptonic helicity amplitudes are

$$\begin{aligned} L^{+1/2} &= 2\sqrt{q^2}v, \\ L^{-1/2} &= 0, \end{aligned} \tag{B.16}$$

while the vector and axial-vector amplitudes are

$$\begin{aligned} L_{\pm1}^{+1/2} &= \pm\sqrt{2}m_\tau v \ \sin(\theta_\tau), \\ L_0^{+1/2} &= -2m_\tau v \ \cos(\theta_\tau), \\ L_t^{+1/2} &= 2m_\tau v, \\ L_{\pm1}^{-1/2} &= \sqrt{2q^2}v \ (1 \pm \cos(\theta_\tau)), \\ L_0^{-1/2} &= 2\sqrt{q^2}v \ \sin(\theta_\tau), \\ L_t^{-1/2} &= 0, \end{aligned} \tag{B.17}$$

and the tensor amplitudes are

$$\begin{aligned}
L^{+1/2}_{0,\pm 1} &= -\sqrt{2q^2}v\ \sin(\theta_\tau), \\
L^{+1/2}_{\pm 1,t} &= \mp\sqrt{2q^2}v\ \sin(\theta_\tau), \\
L^{+1/2}_{t,0} &= L^{+1/2}_{+1,-1} = -2\sqrt{q^2}v\ \cos(\theta_\tau), \\
L^{-1/2}_{0,\pm 1} &= \mp\sqrt{2}m_\tau v\ (1 \pm \cos(\theta_\tau)), \\
L^{-1/2}_{\pm 1,t} &= -\sqrt{2}m_\tau v\ (1 \pm \cos(\theta_\tau)), \\
L^{-1/2}_{t,0} &= L^{-1/2}_{+1,-1} = 2m_\tau v\ \sin(\theta_\tau).
\end{aligned} \tag{B.18}$$

Here we have the relation

$$L^{\lambda_\tau}_{\lambda,\lambda'} = -L^{\lambda_\tau}_{\lambda',\lambda}. \tag{B.19}$$

# APPENDIX C

## FOUR-BODY DECAY KINEMATICS

In this appendix we derive the expression for the lepton's energy in the $b$ quark rest frame $E_\ell$, in terms of the scattering angle in the dilepton's rest frame $\theta_\ell$. Consider the four-body decay

$$b(p_b) \rightarrow \ell^-(p_\ell) + \bar{\nu}_\ell(p_{\bar{\nu}_\ell}) + c(p_c) + g(p_g), \tag{C.1}$$

where $g$ is the real gluon. A four-body decay can be described in five invariants; here we present three of them which are relevant to our discussion. We have

$$r^2 = (p_c + p_g)^2 = (p_b - p_\ell - p_\nu)^2, \tag{C.2}$$

$$q^2 = (p_\ell + p_\nu)^2 = (p_b - p_g - p_c)^2, \tag{C.3}$$

$$s^2 = (p_b - p_\ell)^2 = (p_g + p_c + p_\nu)^2. \tag{C.4}$$

The expressions on the right-hand side above are written using 4-momentum conservation. By expanding Eq. (C.4) in the dilepton's rest frame we have

$$s^2 = m_b^2 + m_\ell^2 - 2E_b^{\ell\nu}E_\ell^{\ell\nu} + 2P_b^{\ell\nu}P_\ell^{\ell\nu}cos(\theta_\ell), \tag{C.5}$$

where $E_b^{\ell\nu}$, $E_\ell^{\ell\nu}$, $P_b^{\ell\nu}$ and $P_\ell^{\ell\nu}$ refer to the energies and momenta of the $b$ quark and the massive lepton in the dilepton's rest frame. In order to find for these values in terms of invariants we expand Eq. (C.2), and using Eq. (C.3) we find

$$E_b^{\ell\nu} = \frac{m_b^2 + q^2 - r^2}{2\sqrt{q^2}}. \tag{C.6}$$

One can also find

$$E_\ell^{\ell\nu} = \frac{m_\ell^2 + q^2}{2\sqrt{q^2}}. \tag{C.7}$$

Using the above expressions for energies we can easily find the corresponding momenta

$$P_b^{\ell\nu} = \frac{\sqrt{\lambda(m_b^2, q^2, r^2)}}{2\sqrt{q^2}}, \tag{C.8}$$

$$P_\ell^{\ell\nu} = \frac{q^2 - m_\ell^2}{2\sqrt{q^2}}, \tag{C.9}$$

where $\lambda$ is defined as $\lambda(a, b, c) = a^2 + b^2 + c^2 - 2ab - 2ac - 2bc$. Finally by expanding Eq. (C.4) again, but this time in the $b$ quark's rest frame, and using Eq. (C.5) we find the expression for the lepton's energy as

$$E_\ell = \frac{1}{4m_b q^2}\left[(m_b^2 + q^2 - r^2)(m_\ell^2 + q^2) - (q^2 - m_\ell^2)\sqrt{\lambda(m_b^2, q^2, r^2)}cos(\theta_\ell)\right]. \tag{C.10}$$

In the case of three-body decay $b(p_b) \to \ell^-(p_\ell) + \bar{\nu}_\ell(p_{\bar{\nu}_\ell}) + c(p_c)$, $r^2$ reduces to $m_c^2$.

# APPENDIX D

## RESULTS FOR VARIOUS OBSERVABLES

For the twofold distribution $\frac{d\Gamma}{dq^2 dE_\ell}$, one finds from Eqs. (3.5) and (3.3)

$$\begin{aligned}\frac{d\Gamma}{dq^2 dE_\ell} &= \frac{G_F^2 |V_{cb}|^2 q^2 (1 - m_\ell^2/q^2)}{256 m_b^2 \pi^3} \Bigg[ C_1^{VA} + \frac{m_\ell^2}{q^2} C_2^{VA} + C_3^{SP} \\ &\quad + C_4^T + \frac{m_\ell^2}{q^2} C_5^T + \frac{4m_\ell}{\sqrt{q^2}} C_6^{VA-SP} + \frac{8m_\ell}{\sqrt{q^2}} C_7^{VA-T} + C_8^{SP-T} \Bigg] \end{aligned} \tag{D.1}$$

where the $C$ terms are

$$
\begin{aligned}
C_1^{VA} &= (1+\cos\theta)^2|H^{VA}_{1/2,1}|^2 + (1-\cos\theta)^2|H^{VA}_{-1/2,-1}|^2 + 2\sin\theta^2|H^{VA}_{-1/2,0}|^2 + 2\sin\theta^2|H^{VA}_{1/2,0}|^2,\\
C_2^{VA} &= \sin\theta^2|H^{VA}_{1/2,1}|^2 + \sin\theta^2|H^{VA}_{-1/2,-1}|^2 + 2|H^{VA}_{1/2,t} + \cos\theta H^{VA}_{1/2,0}|^2\\
&\quad + 2|H^{VA}_{-1/2,t} + \cos\theta H^{VA}_{-1/2,0}|^2,\\
C_3^{SP} &= 2|H^{SP}_{1/2,0}|^2 + 2|H^{SP}_{-1/2,0}|^2,\\
C_4^{T} &= 8\cos\theta^2|H^{(T)1/2}_{1/2,0,t} + H^{(T)1/2}_{1/2,1,-1}|^2 + 4\sin\theta^2|H^{(T)1/2}_{-1/2,-1,t} + H^{(T)1/2}_{-1/2,0,-1}|^2\\
&\quad + 4\sin\theta^2|H^{(T)-1/2}_{1/2,t,1} + H^{(T)-1/2}_{1/2,0,1}|^2 + 8\cos\theta^2|H^{(T)-1/2}_{-1/2,0,t} + H^{(T)-1/2}_{-1/2,1,-1}|^2,\\
C_5^{T} &= 8\sin\theta^2|H^{(T)1/2}_{1/2,0,t} + H^{(T)1/2}_{1/2,1,-1}|^2 + 4(1-\cos\theta)^2|H^{(T)1/2}_{-1/2,-1,t} + H^{(T)1/2}_{-1/2,0,-1}|^2\\
&\quad + 4(1+\cos\theta)^2|H^{(T)-1/2}_{1/2,0,1} + H^{(T)-1/2}_{1/2,t,1}|^2 + 8\sin\theta^2|H^{(T)-1/2}_{-1/2,0,t} + H^{(T)-1/2}_{-1/2,1,-1}|^2,\\
C_6^{VA-SP} &= Re[(\cos\theta H^{VA}_{1/2,0} + H^{VA}_{1/2,t})H^{SP*}_{1/2,0}] + Re[(\cos\theta H^{VA}_{-1/2,0} + H^{VA}_{-1/2,t})H^{SP*}_{-1/2,0}],\\
C_7^{VA-T} &= (1+\cos\theta)Re[(H^{(T)-1/2}_{1/2,0,1} + H^{(T)-1/2}_{1/2,t,1})H^{VA*}_{1/2,1}] - (1-\cos\theta)\times\\
&\quad Re[(H^{(T)1/2}_{-1/2,-1,t} + H^{(T)1/2}_{-1/2,0,-1})H^{VA*}_{-1/2,-1}] - Re[(H^{(T)1/2}_{1/2,0,t} + H^{(T)1/2}_{1/2,1,-1})(H^{VA*}_{1/2,0} + \cos\theta H^{VA*}_{1/2,t})]\\
&\quad - Re[(H^{(T)-1/2}_{-1/2,0,t} + H^{(T)-1/2}_{-1/2,1,-1})(\cos\theta H^{VA*}_{-1/2,t} + H^{VA*}_{-1/2,0})],\\
C_8^{SP-T} &= -8\cos\theta Re[H^{SP*}_{1/2,0}(H^{(T)1/2}_{1/2,0,t} + H^{(T)1/2}_{1/2,1,-1})] - 8\cos\theta Re[H^{SP*}_{-1/2,0}(H^{(T)-1/2}_{-1/2,0,t} + H^{(T)-1/2}_{-1/2,1,-1})],
\end{aligned}
\tag{D.2}
$$

with

$$
\cos\theta = \frac{(m_b^2 - m_c^2 + q^2)(q^2 + m_\ell^2) - (4m_b q^2 E_\ell)}{\sqrt{Q_+Q_-}(q^2 - m_\ell^2)}. \tag{D.3}
$$

From relation (D.1), one can conveniently find the distribution for $q^2$ or $E_\ell$. Nonperturbative corrections to these distributions (for SM) are presented elsewhere (see [52], [54] and [50]) and we do not repeat them here.

The forward-backward asymmetry can be written as the sum of tree level $A_{FB}^{0}$ and nonperturbative $A_{FB}^{O(1/m_b^2)}$ terms,

$$A_{FB} = A_{FB}^{0} + A_{FB}^{O(1/m_b^2)}, \tag{D.4}$$

with

$$\begin{aligned} A_{FB}^{0} &= (\frac{d\Gamma}{dq^2})^{-1} \frac{G_F^2 |V_{cb}|^2}{512\pi^3} \frac{q^2\sqrt{Q_+Q_-}}{m_b^3}\Big(1-\frac{m_\ell^2}{q^2}\Big)^2\Bigg[B_1^{VA} + \frac{2m_\ell^2}{q^2}B_2^{VA} + \frac{4m_\ell^2}{q^2}B_3^{T} + \\ &\quad \frac{2m_\ell}{\sqrt{q^2}}B_4^{VA-SP} + \frac{4m_\ell}{\sqrt{q^2}}B_5^{VA-T} + 4B_6^{SP-T}\Bigg], \end{aligned} \tag{D.5}$$

where

$$\begin{aligned} B_1^{VA} &= |H_{1/2,1}^{VA}|^2 - |H_{-1/2,-1}^{VA}|^2, \\ B_2^{VA} &= \mathrm{Re}[H_{1/2,t}^{VA*}H_{1/2,0}^{VA} + H_{-1/2,t}^{VA*}H_{-1/2,0}^{VA}], \\ B_3^{T} &= |H_{1/2,0,1}^{(T)-1/2} + H_{1/2,t,1}^{(T)-1/2}|^2 - |H_{-1/2,-1,0}^{(T)1/2} + H_{-1/2,t,-1}^{(T)1/2}|^2, \\ B_4^{VA-SP} &= \mathrm{Re}[H_{1/2,0}^{SP*}H_{1/2,0}^{VA} + H_{-1/2,0}^{SP*}H_{-1/2,0}^{VA}], \\ B_5^{VA-T} &= \mathrm{Re}[H_{1/2,t}^{VA*}(H_{1/2,-1,1}^{(T)1/2} + H_{1/2,t,0}^{(T)1/2})] + \mathrm{Re}[H_{1/2,1}^{VA*}(H_{1/2,0,1}^{(T)-1/2} + H_{1/2,t,1}^{(T)-1/2})] \\ &\quad + \mathrm{Re}[H_{-1/2,t}^{VA*}(H_{-1/2,-1,1}^{(T)-1/2} + H_{-1/2,t,0}^{(T)-1/2})] - \mathrm{Re}[H_{-1/2,-1}^{VA*}(H_{-1/2,-1,0}^{(T)1/2} + H_{-1/2,t,-1}^{(T)1/2})], \\ B_6^{SP-T} &= \mathrm{Re}[H_{1/2,0}^{SP*}(H_{1/2,-1,1}^{(T)1/2} + H_{1/2,t,0}^{(T)1/2})] + \mathrm{Re}[H_{-1/2,0}^{SP*}(H_{-1/2,-1,1}^{(T)-1/2} + H_{-1/2,t,0}^{(T)-1/2})]. \end{aligned} \tag{D.6}$$

Also, the $O(1/m_b^2)$ correction is

$$
\begin{aligned}
A_{FB}^{O(1/m_b^2)} &= \Big(\frac{d\Gamma}{dq^2}\Big)^{-1}\frac{G_F^2|V_{cb}|^2(1-m_\ell^2/q^2)^2}{384\pi^3 m_b^5 q^2}\big\{\lambda_1[(m_\ell^2 m_b^2 - m_\ell^2 m_c^2 - (q^2)^2)(3(m_b^2-m_c^2)^2 \\
&\quad + q^2(2m_b^2 - 6m_c^2 + 3q^2))] + \lambda_2[9m_b^6 m_\ell^2 - 45(m_c^2-q^2)^2(m_c^2 m_\ell^2 + (q^2)^2) \\
&\quad + m_b^4(-63m_c^2 m_\ell^2 + 3q^2(2m_\ell^2 + 9q^2)) + 3m_b^2(33m_c^4 m_\ell^2 + 2m_c^2 q^2(-8m_\ell^2 + 3q^2) \\
&\quad + (q^2)^2(3m_\ell^2 + 14q^2))]\big\}. \qquad \text{(D.7)}
\end{aligned}
$$

## APPENDIX E

## THE THREE-FOLD DIFFERENTIAL DISTRIBUTION

In this appendix we present the three-fold differential rate for the inclusive decay in terms of invariant quantities. We write the distribution in the presence of all NP couplings in the form,

$$\begin{aligned}\frac{d^3\Gamma}{dx^3} = \frac{G_F^2|V_{cb}|^2}{8\pi^3}\Big\{&|1+g_L|^2\frac{d^3\Gamma}{dx^3}\Big|_{SM} + |g_R|^2\frac{d^3\Gamma}{dx^3}\Big|_{R} + |g_S|^2\frac{d^3\Gamma}{dx^3}\Big|_{S} + |g_P|^2\frac{d^3\Gamma}{dx^3}\Big|_{P} + |g_T|^2\frac{d^3\Gamma}{dx^3}\Big|_{T} \\ &+ Re((1+g_L)g_R^*)\frac{d^3\Gamma}{dx^3}\Big|_{LR} + Re((1+g_L+g_R)g_S^*)\frac{d^3\Gamma}{dx^3}|_{SLR} \\ &+ Re((1+g_L-g_R)g_P^*)\frac{d^3\Gamma}{dx^3}\Big|_{PLR} + Re((1+g_L)g_T^*)\frac{d^3\Gamma}{dx^3}\Big|_{LT} + Re(g_Rg_T^*)\frac{d^3\Gamma}{dx^3}\Big|_{RT} \\ &+ Re((g_S-g_P)g_T^*)\frac{d^3\Gamma}{dx^3}\Big|_{SPT}\Big\},\end{aligned} \tag{E.1}$$

where the three independent variables are usually taken to be $dx^3 = dq^2dE_\tau dE_\nu$ or $dx^3 = dq^2dE_\tau dq.v$, $v$ being the four velocity of the $B$ meson. Each contribution to the differential rate can be written as,

$$\frac{d^3\Gamma}{dx^3}\Big|_A = \frac{1}{\Delta_0}\frac{d^3\Gamma}{dx^3}\Big|_A^{(1)} + \frac{1}{\Delta_0^2}\frac{d^3\Gamma}{dx^3}\Big|_A^{(2)} + \frac{1}{\Delta_0^3}\frac{d^3\Gamma}{dx^3}\Big|_A^{(3)}. \tag{E.2}$$

Here we have defined $\Delta_0 = p^2 - m_c^2$ with $p = m_b v - q$. The contributions (E.2) to the decay distribution are given by the substitutions [65, 50],

$$\begin{aligned}
\frac{1}{\Delta_0} &\rightarrow \delta(p^2 - m_c^2) \\
\frac{1}{\Delta_0^2} &\rightarrow -\delta'(p^2 - m_c^2) \\
\frac{1}{\Delta_0^3} &\rightarrow \frac{1}{2}\delta''(p^2 - m_c^2).
\end{aligned} \tag{E.3}$$

In the following we present various contributions to this distribution.

The SM contribution is given as,

$$\left.\frac{d^3\Gamma}{dx^3}\right|_{SM}^{(1)} = \frac{4}{3m_b}\left[6m_b p\cdot p_\tau p_\nu\cdot v + (\lambda_1+3\lambda_2)(2p_\tau\cdot p_\nu - 5p_\tau\cdot v p_\nu\cdot v)\right] \tag{E.4}$$

$$\begin{aligned}
\left.\frac{d^3\Gamma}{dx^3}\right|_{SM}^{(2)} = \frac{4}{3m_b}\Big[&2(\lambda_1+3\lambda_2)(-2p\cdot p_\nu + 5p\cdot v p_\nu\cdot v)p\cdot p_\tau + 2m_b\lambda_1(2p\cdot v p_\tau\cdot v - 5p\cdot p_\tau)p_\nu\cdot v \\
&+ 6m_b\lambda_2(p\cdot v p_\tau\cdot p_\nu - p\cdot p_\nu p_\tau\cdot v)\Big]
\end{aligned} \tag{E.5}$$

$$\left.\frac{d^3\Gamma}{dx^3}\right|_{SM}^{(3)} = \frac{32\lambda_1}{3}\left[p\cdot p - (p\cdot v)^2\right]p\cdot p_\tau p_\nu\cdot v\ . \tag{E.6}$$

The $A = R$ contribution is derived from SM part by the substitutions $p_\tau \rightarrow p_\nu$ and $p_\nu \rightarrow p_\tau$,

$$\left.\frac{d^3\Gamma}{dx^3}\right|_{R}^{(i)} = \left.\frac{d^3\Gamma}{dx^3}\right|_{SM}^{(i)}(p_\tau \leftrightarrow p_\nu) \qquad i = 1, 2, 3. \tag{E.7}$$

For $A = S$ we have,

$$\left.\frac{d^3\Gamma}{dx^3}\right|_S^{(1)} = \frac{1}{2m_b^2}\left[2m_b^2(p\cdot v + m_c) + (m_b + m_c)(\lambda_1 + 3\lambda_2)\right] p_\tau \cdot p_\nu \tag{E.8}$$

$$\left.\frac{d^3\Gamma}{dx^3}\right|_S^{(2)} = -\frac{(\lambda_1 + 3\lambda_2)}{3m_b}\left[3m_b(p\cdot v + m_c) - 3m_c p\cdot v + 2p\cdot p - 5(p\cdot v)^2\right] p_\tau \cdot p_\nu \tag{E.9}$$

$$\left.\frac{d^3\Gamma}{dx^3}\right|_S^{(3)} = \frac{4\lambda_1}{3}(p\cdot v + m_c)\left[p\cdot p - (p\cdot v)^2\right] p_\tau \cdot p_\nu\,, \tag{E.10}$$

while the $A = P$ case can be derived from $A = S$ case by the substitution $m_c \to -m_c$,

$$\left.\frac{d^3\Gamma}{dx^3}\right|_P^{(i)} = \left.\frac{d^3\Gamma}{dx^3}\right|_S^{(i)} (m_c \to -m_c) \qquad i = 1, 2, 3. \tag{E.11}$$

For $A = T$ we find,

$$\begin{aligned}\left.\frac{d^3\Gamma}{dx^3}\right|_T^{(1)} = \frac{16}{3m_b}\Big[&6m_b(2p\cdot p_\nu p_\tau \cdot v + 2p\cdot p_\tau p_\nu \cdot v - p\cdot v p_\tau \cdot p_\nu) \\ &+ 5(\lambda_1 + 3\lambda_2)(p_\tau \cdot p_\nu - 4p_\tau \cdot v p_\nu \cdot v)\Big]\end{aligned} \tag{E.12}$$

$$\begin{aligned}\left.\frac{d^3\Gamma}{dx^3}\right|_T^{(2)} = -\frac{32}{3m_b}\Big[&(\lambda_1 + 3\lambda_2)(8p\cdot p_\tau p\cdot p_\nu - 2p\cdot p p_\tau \cdot p_\nu + 5(p\cdot v)^2 p_\tau \cdot p_\nu - 10p\cdot p_\nu p\cdot v p_\tau \cdot v \\ &- 10p\cdot p_\tau p\cdot v p_\nu \cdot v) + 2m_b(5\lambda_1 - 3\lambda_2)(p\cdot p_\nu p_\tau \cdot v + p\cdot p_\tau p_\nu \cdot v) \\ &- 3m_b(\lambda_1 - \lambda_2)p\cdot v p_\tau \cdot p_\nu - 8m_b\lambda_1 p\cdot v p_\tau \cdot v p_\nu \cdot v\Big]\end{aligned} \tag{E.13}$$

$$\left.\frac{d^3\Gamma}{dx^3}\right|_T^{(3)} = -\frac{128\lambda_1}{3}\left[p\cdot p - (p\cdot v)^2\right]\left[p\cdot v p_\tau \cdot p_\nu - 2p\cdot p_\nu p_\tau \cdot v - 2p\cdot p_\tau p_\nu \cdot v\right] \tag{E.14}$$

For $A = LR$,

$$\left.\frac{d^3\Gamma}{dx^3}\right|^{(1)}_{LR} = -\frac{4m_c}{m_b^2}\left(2m_b^2+\lambda_1+3\lambda_2\right)p_\tau\cdot p_\nu \tag{E.15}$$

$$\left.\frac{d^3\Gamma}{dx^3}\right|^{(2)}_{LR} = \frac{8m_c}{m_b}\Big[-(\lambda_1+3\lambda_2)p\cdot v p_\tau\cdot p_\nu + m_b(\lambda_1+\lambda_2)p_\tau\cdot p_\nu - 4m_b\lambda_2 p_\tau\cdot v p_\nu\cdot v\Big] \tag{E.16}$$

$$\left.\frac{d^3\Gamma}{dx^3}\right|^{(3)}_{LR} = -\frac{32m_c\lambda_1}{3}\Big[p\cdot p-(p\cdot v)^2\Big]p_\tau\cdot p_\nu \tag{E.17}$$

For $A = SLR$,

$$\left.\frac{d^3\Gamma}{dx^3}\right|^{(1)}_{SLR} = \frac{m_\tau}{m_b^2}\Big[2m_b^2(p\cdot p_\nu + m_c p_\nu\cdot v)+(\lambda_1+3\lambda_2)(p\cdot p_\nu - m_b p_\nu\cdot v)\Big] \tag{E.18}$$

$$\begin{aligned}\left.\frac{d^3\Gamma}{dx^3}\right|^{(2)}_{SLR} = &-\frac{2m_\tau}{3m_b}\Big[(\lambda_1+3\lambda_2)(-3p\cdot p_\nu p\cdot v+3m_b m_c p_\nu\cdot v-5m_c p\cdot v p_\nu\cdot v+2m_c p\cdot p_\nu)\\ &+m_b(5\lambda_1+3\lambda_2)p\cdot p_\nu - 2m_b(\lambda_1-3\lambda_2)p\cdot v p_\nu\cdot v\Big]\end{aligned} \tag{E.19}$$

$$\left.\frac{d^3\Gamma}{dx^3}\right|^{(3)}_{SLR} = \frac{8m_\tau\lambda_1}{3}\Big[p\cdot p-(p\cdot v)^2\Big]\left(p\cdot p_\nu + m_c p_\nu\cdot v\right) \tag{E.20}$$

For $A = PLR$ we have,

$$\left.\frac{d^3\Gamma}{dx^3}\right|^{(i)}_{PLR} = \left.\frac{d^3\Gamma}{dx^3}\right|^{(i)}_{SLR}(m_c\to -m_c)\qquad i=1,2,3. \tag{E.21}$$

For $A = LT$,

$$\left.\frac{d^3\Gamma}{dx^3}\right|^{(1)}_{LT} = -48m_\tau m_c\left(p_\nu\cdot v\right) \tag{E.22}$$

$$\left.\frac{d^3\Gamma}{dx^3}\right|^{(2)}_{LT} = -\frac{16m_\tau m_c}{m_b}\Big[(\lambda_1+3\lambda_2)(-2p\cdot p_\nu+5p\cdot v p_\nu\cdot v)-3m_b(\lambda_1-\lambda_2)p_\nu\cdot v\Big] \tag{E.23}$$

$$\left.\frac{d^3\Gamma}{dx^3}\right|^{(3)}_{LT} = -64m_\tau m_c\lambda_1\Big[p\cdot p-(p\cdot v)^2\Big](p_\nu\cdot v) \tag{E.24}$$

For $A = RT$,

$$\left.\frac{d^3\Gamma}{dx^3}\right|_{RT}^{(1)} = \frac{24m_\tau}{m_b^2}\left[2m_b^2 p\cdot p_\nu + (\lambda_1+3\lambda_2)(p\cdot p_\nu - m_b p_\nu\cdot v)\right] \tag{E.25}$$

$$\left.\frac{d^3\Gamma}{dx^3}\right|_{RT}^{(2)} = -\frac{16m_\tau}{m_b}\left[-3(\lambda_1+3\lambda_2)p\cdot p_\nu p\cdot v + m_b(5\lambda_1-\lambda_2)p\cdot p_\nu - 2m_b(\lambda_1+\lambda_2)p\cdot v p_\nu\cdot v\right] \tag{E.26}$$

$$\left.\frac{d^3\Gamma}{dx^3}\right|_{RT}^{(3)} = 64m_\tau\lambda_1\left[p\cdot p - (p\cdot v)^2\right](p\cdot p_\nu) \tag{E.27}$$

For $A = SPT$,

$$\left.\frac{d^3\Gamma}{dx^3}\right|_{SPT}^{(1)} = 8\left(p\cdot p_\nu p_\tau\cdot v - p\cdot p_\tau p_\nu\cdot v\right) \tag{E.28}$$

$$\left.\frac{d^3\Gamma}{dx^3}\right|_{SPT}^{(2)} = \frac{8}{3m_b}\left[5(\lambda_1+3\lambda_2)p\cdot v - m_b(5\lambda_1+3\lambda_2)\right]\left(p\cdot p_\nu p_\tau\cdot v - p\cdot p_\tau p_\nu\cdot v\right) \tag{E.29}$$

$$\left.\frac{d^3\Gamma}{dx^3}\right|_{SPT}^{(3)} = \frac{32\lambda_1}{3}\left[p\cdot p - (p\cdot v)^2\right]\left(p\cdot p_\nu p_\tau\cdot v - p\cdot p_\tau p_\nu\cdot v\right) \tag{E.30}$$

# APPENDIX F

# $\left|\mathcal{M}^{\rm SM+NP}\right|^2$ LEPTONIC CONTRIBUTIONS

Here we present the leptonic parts of the angular distribution,

1. $|\mathcal{M}_{SP}|^2$:

$$\sum_{spins} \mathcal{L}_{SP}\,\mathcal{L}^*_{SP} \;=\; \mathrm{Tr}[(\not{p}_\ell + \mathrm{m}_\ell)\mathrm{P_L}\not{p}_{\bar{\nu}}\mathrm{P_R}]\;, \tag{F.1}$$

where $q = p_\ell + p_{\bar{\nu}_\ell}$.

2. $|\mathcal{M}_{VA}|^2$:

$$\sum_{\rm spins} \mathcal{L}_{VA}(n)\mathcal{L}^*_{VA}(n') \;=\; \epsilon^{\mu}_{VA}(n)\,\epsilon^{*\nu}_{VA}(n')\,\mathrm{Tr}\left[\bar{u}_\ell\gamma_\mu P_L v_{\bar{\nu}_\ell}\bar{v}_{\bar{\nu}_\ell}\gamma_\nu P_L u_\ell\right]\;. \tag{F.2}$$

3. $|\mathcal{M}_T|^2$:

$$\begin{aligned}\sum_{\rm spins} \mathcal{L}_T(n,p)\,\mathcal{L}^*_T(n',p')^* \;=\; &\mathrm{Tr}\left[(\not{p}_\ell + m_\ell)\sigma_{\mu\nu}P_L\not{p}_{\bar{\nu}_\ell}\sigma_{\alpha\beta}P_R\right]\\ &\times \epsilon^{\mu}_T(n)\,\epsilon^{\nu}_T(p)\,\epsilon^{*\alpha}_T(n')\,\epsilon^{*\beta}_T(p')\;.\end{aligned} \tag{F.3}$$

4. $\mathcal{M}_{SP}\mathcal{M}^*_{VA}$:

$$\sum_{\rm spins} \mathcal{L}_{SP}\,\mathcal{L}^*_{VA}(n) \;=\; \mathrm{Tr}[(\not{p}_\ell + m_\ell)P_L\not{p}_{\bar{\nu}_\ell}\gamma_\mu P_L]\epsilon^{*\mu}_{VA}(n)\;. \tag{F.4}$$

5. $\mathcal{M}_{SP}\mathcal{M}_T^*$:

$$\sum_{\text{spins}} \mathcal{L}_{SP}\, \mathcal{L}_T^*(n,p) \;=\; i\mathrm{Tr}\left[(\not{p}_\ell + m_\ell)P_L \not{p}_{\bar{\nu}_\ell}\sigma_{\mu\nu}P_R\right]\epsilon_T^{*\mu}(n)\,\epsilon_T^{*\nu}(p)\;. \tag{F.5}$$

6. $\mathcal{M}_{VA}\,\mathcal{M}_T^*$:

$$\begin{aligned}\sum_{\text{spins}} \mathcal{L}_{VA}(n)\,\mathcal{L}_T^*(n',p') \;=\; & i\mathrm{Tr}\left[(\not{p}_\ell + m_\ell)\gamma_\mu P_L \not{p}_{\bar{\nu}_\ell}\sigma_{\alpha\beta}P_R\right] \\ & \times \epsilon_{VA}^{\mu}(n)\epsilon_T^{*\alpha}(n')\epsilon_T^{*\beta}(p')\;.\end{aligned} \tag{F.6}$$

## APPENDIX G

## CALCULATION OF $S$ COUPLINGS IN TERMS OF 2HDM MODEL PARAMETERS

We now explicitly calculate the parameters in the Lagrangian in Eq. (6.5), following the analysis of Ref. [173]. We start with the Type II 2HDM with the Yukawa couplings

$$-\mathcal{L}_Y = \bar{L}^0 Y_e^0 H_d e_R^0 + \bar{Q}^0 Y_d^0 H_d d_R^0 + \bar{Q}^0 Y_u^0 \tilde{H}_u U_R^0 + \text{H.c.} \tag{G.1}$$

Here the superscript means the quantities are in flavor space.

We write the scalar potential as

$$V(H_d, H_u, \phi) = V_{\text{2HDM}}(H_d, H_u) + V_\phi(\phi) + V_{\text{portal}}(H_d, H_u, \phi) \ , \tag{G.2}$$

where

$$\begin{aligned} V_{\text{2HDM}} &= m_{dd}^2 H_d^\dagger H_d + m_{uu}^2 H_u^\dagger H_u - m_{du}^2 (H_d^\dagger H_u + H_u^\dagger H_d) + \frac{\lambda_1}{2}(H_d^\dagger H_d)^2 + \frac{\lambda_2}{2}(H_u^\dagger H_u)^2 \\ &\quad + \lambda_3 (H_d^\dagger H_d)(H_u^\dagger H_u) + \lambda_4 (H_d^\dagger H_u)(H_u^\dagger H_d) + \frac{\lambda_5}{2}\left[(H_d^\dagger H_u)^2 + (H_u^\dagger H_d)^2\right] \qquad \text{(G.3)} \\ V_\phi &= B\phi + \frac{1}{2} m_0^2 \phi^2 + \frac{A_\phi}{2}\phi^3 + \frac{\lambda_\phi}{4}\phi^4 \qquad \text{(G.4)} \\ V_{\text{portal}} &= A\,(H_u^\dagger H_d + H_d^\dagger H_u)\phi + \left[\lambda_u H_u^\dagger H_u + \lambda_d H_d^\dagger H_d + \lambda_{ud}(H_u^\dagger H_d + H_d^\dagger H_u)\right]\phi\phi \ . \qquad \text{(G.5)} \end{aligned}$$

After each doublet obtains a vev, we write the neutral real components of the doublets as $H_i = v_i + \rho_i$, where $i = d, u$. After expanding the potential, the elements of the mass matrix of the

CP-even scalars in the $(\rho_d, \rho_u, \phi)$ basis are

$$M_{11}^2 = m_{du}^2 \tan\beta + \lambda_1 v^2 \cos^2\beta \tag{G.6}$$

$$M_{22}^2 = m_{du}^2 \cot\beta + \lambda_2 v^2 \sin^2\beta \tag{G.7}$$

$$M_{12}^2 = -m_{du}^2 + \lambda_{345} v^2 \cos\beta \sin\beta \tag{G.8}$$

$$M_{13}^2 = vA \sin\beta \tag{G.9}$$

$$M_{23}^2 = vA \cos\beta \tag{G.10}$$

$$M_{33}^2 = m_0^2 + v^2\lambda_d \cos\beta^2 + v^2\lambda_u \sin\beta^2 + 2v^2\lambda_{ud} \cos\beta \sin\beta\,, \tag{G.11}$$

where $\lambda_{345} = \lambda_3 + \lambda_4 + \lambda_5$, and $v_d$ and $v_u$ are the vevs of the two doublets $H_d$ and $H_u$, with $\tan\beta = v_u/v_d$ and $v_d^2 + v_u^2 = v^2 = (246\ \text{GeV})^2$.

We assume $A \ll v, m_{du}$, so we can consider the portal terms as small perturbations. In this case we diagonalize the mass matrix perturbatively where the non-perturbed mass matrix is the usual 2HDM mass matrix. We define the mixing matrix that diagonalizes the mass matrix as

$$\begin{pmatrix} \rho_d \\ \rho_u \\ \phi \end{pmatrix} \approx \begin{pmatrix} -\sin\alpha & \cos\alpha & \delta_{13} \\ \cos\alpha & \sin\alpha & \delta_{23} \\ \delta_{31} & \delta_{32} & 1 \end{pmatrix} \begin{pmatrix} h \\ H \\ S \end{pmatrix}, \tag{G.12}$$

where $\delta_{ij}$ are small mixing angles that mix the light scalar with the other two scalars of the 2HDM. When we diagonalize the mass matrix of the 2HDM, the parameter $\alpha$ satisfies the usual equation

$$\tan 2\alpha = \frac{2M_{12}^2}{M_{11}^2 - M_{22}^2}\,, \tag{G.13}$$

and the masses of the two $CP$-even Higgs bosons are given by

$$m_{h,H}^2 = \frac{1}{2}\left[M_{11}^2 + M_{22}^2 \mp \sqrt{(M_{11}^2 - M_{22}^2)^2 + 4(M_{12}^2)^2}\right]. \tag{G.14}$$

To determine expressions for the $\delta_{ij}$, we write the mass matrix as

$$M^2 = \begin{pmatrix} M_{11}^2 & M_{12}^2 & 0 \\ M_{12}^2 & M_{22}^2 & 0 \\ 0 & 0 & M_{33}^2 \end{pmatrix} + \begin{pmatrix} 0 & 0 & vA\sin\beta \\ 0 & 0 & vA\cos\beta \\ vA\sin\beta & vA\cos\beta & 0 \end{pmatrix}, \tag{G.15}$$

where the second matrix is considered as a small perturbation. Below, we use the shorthand notation $s_\beta = \sin\beta$ and $c_\beta = \cos\beta$.

We require the lighter Higgs $h$ to have SM-like couplings to gauge bosons and fermions, so that we have $\beta - \alpha = \pi/2$. Assuming $M_{33} \ll m_h, m_H$, and writing $\alpha = \beta - \pi/2$, we find that the small mixing parameters are

$$\begin{aligned} \delta_{13} &= -\frac{2vAs_\beta^3}{m_h^2}\left[\frac{m_h^2}{2m_H^2} + \cot^2\beta\left(1 - \frac{m_h^2}{2m_H^2}\right)\right] \\ \delta_{23} &= -\frac{2vA}{m_h^2}s_\beta^2 c_\beta\left[1 - \frac{m_h^2}{2m_H^2}(1 - \cot^2\beta)\right] \\ \delta_{31} &= \frac{vAs_{2\beta}}{m_h^2} \\ \delta_{32} &= -\frac{vAc_{2\beta}}{m_H^2}\,. \end{aligned} \tag{G.16}$$

In the Yukawa sector after rotating to the mass basis and defining the mass matrices of fermions, the interaction terms between the physical light scalar $S$ and the fermions become

$$-\mathcal{L}_{ffS} = \left(\frac{\delta_{13}}{vc_\beta}\bar{e}M_e e + \frac{\delta_{13}}{vc_\beta}\bar{d}M_d d + \frac{\delta_{23}}{vs_\beta}\bar{u}M_u u\right)S\,, \tag{G.17}$$

where the $M_f$'s are the diagonal mass matrices of the fermions. To better compare with SM Higgs couplings, we write these couplings as

$$-\mathcal{L}_{ffS} = \sum_{f=\ell,d,u}\xi_f\frac{m_f}{v}\bar{f}fS\,. \tag{G.18}$$

Then using the expressions for the mixing parameters in Eq. (G.16), we find that the couplings of the scalar $S$ to fermions are

$$\xi_{\ell,d} = -\frac{2vAs_\beta^2}{m_h^2}\tan\beta\left[\frac{m_h^2}{2m_H^2}+\cot^2\beta\left(1-\frac{m_h^2}{2m_H^2}\right)\right] \tag{G.19}$$

$$\xi_u = -\frac{2vAs_\beta^2}{m_h^2}\cot\beta\left[1-\frac{m_h^2}{2m_H^2}\left(1-\cot^2\beta\right)\right], \tag{G.20}$$

where the couplings to down-type quarks and leptons are enhanced by $\tan\beta$ and the couplings to up-type quarks are suppressed by $\cot\beta$. In the limit of large $\tan\beta$, we may take $\beta \to \pi/2$ and $\alpha \to 0$ so that $s_\beta \to 1$ in the equations above, and we can write the couplings purely in terms of $\tan\beta$.

We can find the couplings of $S$ to the weak gauge bosons by expanding the kinetic terms of the two scalar doublets. We find

$$-\mathcal{L}_{VVS} = \xi_V\frac{1}{v}\left(2m_W^2W_\mu^\dagger W^\mu + m_Z^2Z_\mu Z^\mu\right)S\,, \tag{G.21}$$

where the coupling is the same for both $W$ and $Z$,

$$\xi_{W,Z} = c_\beta\delta_{13}+s_\beta\delta_{23} = \frac{-2vAs_\beta^3c_\beta}{m_h^2}\left(1+\cot^2\beta\right)\,. \tag{G.22}$$

In the large $\tan\beta$ limit we write $\cos\beta \approx \cot\beta$ and $\sin\beta \to 1$ so that we can write this coupling in terms of $\cot\beta$ only:

$$\xi_{W,Z} = \frac{-2vA\cot\beta}{m_h^2}(1+\cot^2\beta)\,. \tag{G.23}$$

In summary we have the following couplings in terms of $\tan\beta$:

$$\xi_{\ell,d} = -\frac{2vA}{m_h^2}\tan\beta\left[\frac{m_h^2}{2m_H^2}+\cot^2\beta\left(1-\frac{m_h^2}{2m_H^2}\right)\right] \tag{G.24}$$

$$\xi_u = -\frac{2vA}{m_h^2}\cot\beta\left[1-\frac{m_h^2}{2m_H^2}(1-\cot^2\beta)\right] \tag{G.25}$$

$$\xi_{W,Z} = -\frac{2vA}{m_h^2}\cot\beta\,(1+\cot^2\beta)\ . \tag{G.26}$$

# APPENDIX H

## COUPLING TO TWO PHOTONS

To calculate the scalar coupling to two photons, we use expressions from Ref. [174], where the decay width for Higgs to two photons is given in terms of generic spin-1, spin-$\frac{1}{2}$, and spin-0 particles in the loop. Although the contribution to $S \to \gamma\gamma$ is dominated by the effective coupling $\kappa$ in the parameter region we are interested in, we include all other possible particles in the loop for completeness. In our case, there are only spin-1 and spin-$\frac{1}{2}$ particles in the loop, so the rate can be written as

$$\Gamma(S \to \gamma\gamma) = \frac{\alpha_{\rm EM}^2 m_S^3}{1024\pi^3}\left|\frac{4\pi}{\alpha_{\rm EM}}\kappa + \frac{g_{SVV}}{m_V^2}N_{c,V}Q_V^2 A_1(r_V) + \frac{2g_{Sf\bar{f}}}{m_f}N_{c,f}Q_f^2 A_{1/2}(r_f)\right|^2, \tag{H.1}$$

where $r_i = 4m_i^2/m_S^2$. $V$ and $f$ represent spin-1 and spin-$\frac{1}{2}$ particles, respectively, $Q$ and $N_c$ are the particle's electric charge and number of colors, and the expressions for $A_1$ and $A_{1/2}$ are given in Ref. [174].

VITA

**Saeed Kamali**

## Education

- 2013-present – PhD, High Energy and Particle Physics, University of Mississippi
- 2010-2012 – Master of Science in Physics, Sharif University of Technology
- 2006-2010 – Bachelor of Science in Physics, Shiraz University

## Research Experience

- 2019-2020 – Research Assistant. High Energy, Flavor Physics, B physics and Beyond the SM, University of Mississippi
- 2018-2019 – Research Assistant and Visiting Scholar at the University of California, Irvine
- 2016-2017 – Research Assistant. High Energy, Flavor Physics, B Physics and Beyond the Standard Model. University of Mississippi
- 2015-2016 – General Relativity, Quantum Gravity and Spin-Foam Formalism. University of Mississippi
- 2011-2012 – Implications of Bell's Theorem and Nonlocality in Quantum Mechanics. Sharif University of Technology

## Publications

- Bhubanjyoti Bhattacharya, Alakabha Datta, Saeed Kamali, David London. "A Measurable Angular Distribution for $\bar{B} \to D^* \tau^- \bar{\nu}_\tau$ Decays", [arXiv:2005.03032]

- Alakabha Datta, Jonathan L. Feng, Saeed Kamali, Jacky Kumar. "Resolving the $(g-2)_\mu$ and $B$ Anomalies with Leptoquarks and a Dark Higgs Boson", Phys. Rev. D101 (2020) 035010, [arXiv:1908.08625]

- Bhubanjyoti Bhattacharya, Alakabha Datta, Saeed Kamali, David London. "CP Violation in $\bar{B}^0 \to D^+\mu^-\bar{\nu}_\mu$", JHEP 05:191, 2019 [arXiv:1903.02567]

- Saeed Kamali. "New physics in inclusive semileptonic B decays including nonperturbative corrections" Int.J.Mod.Phys. A34 (2019) no.06n07, 1950036, [arXiv:1811.07393]

- Saeed Kamali, Ahmed Rashed, Alakabha Datta. "New Physics in Inclusive $B \to X_c\tau\bar{\nu}_\tau$ decay in light of $R(D^{(*)})$ measurements." Phys. Rev. D97 (2018) 095034, [arXiv: 1801.08259]

- Alakabha Datta, Saeed Kamali, Stefan Meinel, Ahmed Rashed. "Phenomenology of $\Lambda_b \to \Lambda_c\tau\bar{\nu}_\tau$ using lattice QCD calculations". JHEP, 08:131, 2017, [arXiv: 1702.02243]

**Honors**

- Awarded the 2018 Graduate Student Achievement Award, University of Mississippi

- Member of Phi-Kappa-Phi Honor Society

- Awarded the dissertation fellowship for spring 2018, University of Mississippi

- Awarded as the first rank student in physics department in the commencement, Shiraz University

**Talks**

- Spring 2019 – Physics and Astronomy Colloquium, University of Mississippi. Title: "Charge current anomalies and the inclusive semileptonic B decays"

- Fall 2019 – Physics and Astronomy Colloquium, University of Mississippi. Title: "The Muon (g-2) and B anomalies"

- Spring 2018 – Phenomenology Symposium (Awarded travel support). Title: “New Physics in Inclusive B decays in light of $R(D^{(*)})$ measurements”
- Fall 2015 – Physics Graduate Student Research Symposium, Department of Physics and Astronomy, University of Mississippi. Title: "An introduction to Loop Quantum Gravity"